JOURNAL OF THE

Electrochemical Society

Vol. 109, No. 7 July 1962

THE GLC PROGRAM OF PROGRESS

Technical teamwork with our chlor-alkali customers provides a base for continuing improvements in GLC anode performance.

Our program of progress gives GLC anode customers better results now than ever before —seeks still better results in the years ahead.

Share the rewards of this program by putting custom made GLC anodes to work now in your electrolytic cells.

We can then help you develop the technical information and specifications needed to improve cell efficiency and lower your operating costs.

will lower cell operating costs

PRODUCTS ELECTRODE GLC DIVISION YOU CAN TRUST

GREAT LAKES CARBON CORPORATION

18 EAST 48TH STREET, NEW YORK 17, N.Y. OFFICES IN PRINCIPAL CITIES

Manuscripts submitted to the Journal should be sent, in triplicate, to the Editorial Office at 30 East 42 St., New York 17, N. Y. They should conform to the revised Instructions to Authors published on pp. 131*C*-132*C* of the May issue. Manuscripts so submitted become the property of The Electrochemical Society and may not be published elsewhere, in whole or in part, unless permission is requested of and granted by the Editor.

The Electrochemical Society does not maintain a supply of reprints of papers appearing in its Journal. A photoprint copy of any particular paper, however, may be obtained by corresponding direct with the Engineering Societies Library, 345 E. 47 St., New York, N. Y.

Inquiries re positive microfilm copies of volumes should be addressed to University Microfilms, Inc., 313 N. First St., Ann Arbor, Mich.

Walter J. Johnson, Inc., 111 Fifth Ave, New York 3, N. Y., have reprint rights to out-of print volumes of the Journal, and also have available for sale back volumes and single issues, with the exception of the current calendar year. Anyone interested in securing back copies should correspond direct with them.

Journal of the Electrochemical Society

JULY 1962 **VOL. 109 • NO. 7**

CONTENTS

Published monthly by The Electrochemical Society, Inc., from Manchester, N.H.; **Executive Offices, Editorial Office** and **Circulation Dept.,** and **Advertising Office** at 30 East 42 St., New York 17, N. Y., combining the JOURNAL and TRANSACTIONS OF THE ELECTROCHEMICAL SOCIETY. Statements and opinions given in articles and papers in the JOURNAL OF THE ELECTROCHEMICAL SOCIETY are those of the contributors, and The Electrochemical Society assumes no responsibility for them. Subscription to members as part of membership service; subscription to nonmembers $24.00 plus $1.50 for postage outside U.S. and Canada. Single copies $1.70 to members, $2.25 to nonmembers.

Entered as second-class matter at the Post Office at Manchester, N. H., under the act of August 24, 1912.

Editorial

Annals of Science

ANNALS OF SCIENCE is a British publication (Taylor & Francis, Ltd., Red Lion Court, Fleet St., London E.C. 4; £3 3s yearly), "A Quarterly Review of the History of Science and Technology Since the Renaissance." Our attention was called to the *Annals* by Dr. Norman Hackerman, who mentioned especially two articles by C. A. Russell (University College, London) entitled "The Electrochemical Theory of Sir Humphry Davy, I. The Voltaic Pile and Electrolysis. II. Electrical Interpretations of Chemistry" [Vol. 15, 1-14, 15-25 (1959)]. The publication does not seem to be well known; it is nominally available in four libraries in New York City, was located after some search in the Rare Books Room of the New York Academy of Medicine Library. Why it should be in the Rare Books Room is not obvious, since it is neither rare nor unduly valuable. It is a leisurely journal, the 1959 numbers (for example) having been published in 1961.

Sir Humphry was a famous man in his lifetime, and is credited with many remarkable findings. He discovered nitrous oxide, laughing gas, and started a series of "inhalation parties." He made sodium and potassium by electrolysis, was well aware that two dissimilar metals acquired opposite electrical charges on contact, proposed the attachment of zinc strips to protect copper sheathing on ships' bottoms from corrosion. (The British Admiralty tried such installations and removed them, much to Davy's disgust, when it was found that this "cathodic protection" allowed fouling by marine organisms, which the copper was used to prevent). Davy's experiments were dependent on the use of chemical batteries, and at one time friends and admirers raised money to present him with a 2000-double-plate battery.

While Davy's discoveries became somewhat overshadowed with the passage of time and the advent of still more remarkable findings, many scientists think that he should have the title "father of electrochemistry."

Of equal interest, in the 1957-1958 issues of *Annals of Science* are four articles by S. G. Brush (Radiation Lab., Livermore, Calif.), "The Development of the Kinetic Theory of Gases, I. Herapath, II. Waterston, III. Clausius, IV. Maxwell." Herapath in 1816 attempted to revive the ancient Greek kinetic theory, was largely ignored. Waterston proposed the principle of equipartition of energy in a paper sent to the Royal Society in 1845, presented orally in 1846, then laid aside, and finally published in 1892. Clausius published a detailed kinetic theory in 1857, and in 1859 Maxwell published his famous and controversial theory of gas molecule velocity distribution, which assumed the equipartition principle and the independent treatment of velocities in different directions. Maxwell no doubt reached his conclusions intuitively, was extremely doubtful of the validity of his assumptions; in 1879 he expressed doubt that the average kinetic energy of molecules of different gases could be the same at a given temperature. As late as 1891 Lord Kelvin said that the equipartition principle "is not only unproved but untrue."—An excellent summary (as well as details of the derivations) is found in J. R. Partington's "An Advanced Treatise on Physical Chemistry, Vol. I" (Longmans, Green & Co., 1949).

Some of us like to read bits of scientific, chemical, and electrochemical history now and then, even if we are not authorities in the field. For this purpose the *Annals of Science* is to be recommended.

—CVK

NEWS FROM
BELL LABORATORIES

A simple, highly sensitive microwave amplifier

Bell Laboratories engineers have developed an extremely sensitive parametric amplifier which approaches the maser in sensitivity. Both will be used in experiments with Telstar, the Bell System's experimental communications satellite.

Heart of the parametric amplifier is a newly developed semiconductor diode with very low intrinsic noise. Previously, the sensitivity of such amplifiers at microwave frequencies was severely limited by the unwanted noise generated in their diodes. The new diode, no bigger than the eye-end of a needle, solved this problem.

Our engineers also devised new circuitry to stabilize precisely the output of the klystron (microwave generator) supplying power for the amplifier. To reduce further the intrinsic noise of the amplifier, they immersed the diode and its circuits in liquid nitrogen, utilizing a new cooling arrangement which economically maintains a low temperature for many days without attention.

The new amplifier fills a need in the communications field for a simple microwave amplifier of high sensitivity in applications for which the higher sensitivity of the maser does not justify its additional complication.

Bell Laboratories' Michael Chruney adjusts waveguide assembly (in circle) housing the diode. After adjustment the entire parametric amplifier will be immersed in liquid nitrogen in dewar at left. The new amplifier operates at 4170 megacycles (center of band) and provides an almost flat gain of 38 db over a 50-megacycle band with a noise figure of approximately 0.6 db.

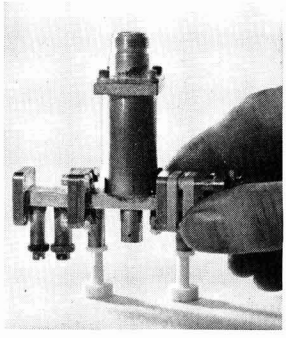

Close-up of the waveguide assembly, in which Bell Telephone Laboratories' newly developed diode is located.

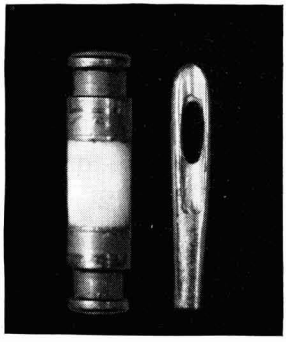

Heart of amplifier—a hermetically sealed gallium arsenide diode—is compared with eye of average-sized sewing needle.

BELL TELEPHONE LABORATORIES

World center of communications research and development

Dependable Supply–*EXTRAORDINARY* Purity

In all these Electronic Metals and Compounds from EAGLE-PICHER

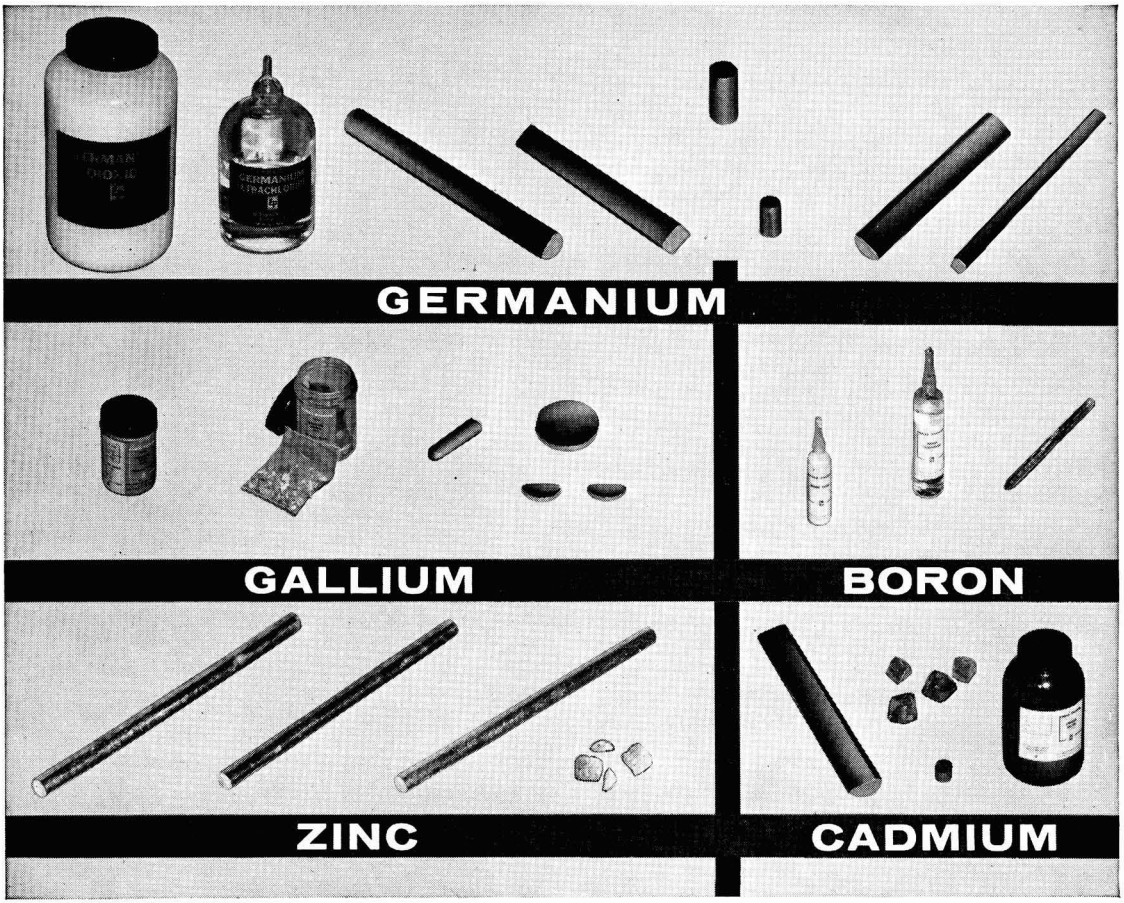

Yes, Eagle-Picher is the dependable source of all these products in pure metal and compound form.

This history of dependability started in 1935, when Eagle-Picher first separated Germanium from Zinc concentrates and paved the way for Gallium metal. As a result of constant purification and upgrading, for example, Eagle-Picher today supplies Germanium Dioxide with *minimum* purities of 99.999% and Gallium with purities as high as 99.99999%!

These extensive research activities are consistent with Eagle-Picher's dedicated objective—*continued* leadership as a dependable supplier for the rigid, precise demands of the semiconductor industry.

EAGLE-PICHER
ELECTRONIC METALS & COMPOUNDS

Germanium: *Intrinsic Metal • Dioxide • First Reduction Metal • Tetraiodide • Tetrachloride • Tetrabromide*

Gallium: *Metallic Crystals • Arsenide • Sesquioxide*

Boron: *Ultra High Purity • Tribromide • Oxide*

Zinc: *Ultra High Purity • Sulfide*

Cadmium: *Ultra High Purity • Sulfide*

FOR COMPLETE INFORMATION . . . CLIP and MAIL TODAY!
The Eagle-Picher Company • Chemicals & Metals Division • Dept. JES-762 • Cincinnati 1, Ohio
Gentlemen: Yes, I would like to have more information on Eagle-Picher Electronic Metals and Compounds.
Name_____
Firm_____
Address_____

EAGLE PICHER

Since 1843

EAGLE-PICHER

General Offices
Cincinnati 1, Ohio

Raney Type Transition Metals as Fuel Electrode Catalysts

H. Krupp, H. Rabenhorst, G. Sandstede, and G. Walter
Battelle-Institut e.V., Frankfurt (Main), Germany

and R. McJones
Cummins Engine Company, Inc., Columbus, Indiana

ABSTRACT

Porous metal electrodes incorporating Raney catalysts are prepared by powder techniques from transition metals of the first and eighth groups. Half-cell and fuel cell measurements are taken in various aqueous electrolytes at temperatures from 20° to 100°C. At 80°C in either 5*N* KOH or 5*N* H_2SO_4 electrolyte, both hydrogen and methanol yield current densities beyond 300 ma/cm². In 5*N* K_2CO_3 electrolyte, there are limiting current densities of the order of 10 ma/cm². Neither hexane nor methylcyclohexane display appreciable electrochemical oxidation under the conditions of this report. The methanol reaction appears to approach complete oxidation; this conclusion applies in both acid (CO_2-formation) and alkaline (carbonate formation) electrolyte as well as for both half-cell and fuel cell operation.

There is so far no satisfactory low-temperature hydrocarbon fuel electrode. On the other hand, electrochemical conversion at an appreciable rate of partially oxidized hydrocarbons such as methanol and glycol seems to be possible, but only in the case of methanol was complete oxidation reported (1). At least some of the reactions involved in the stepwise oxidation at the anode must be accelerated catalytically in order to achieve a sufficient reaction rate at low temperatures (below 200°C). The electrode must, therefore, contain catalysts accelerating, above all, the acceptance of electrons from the fuel by the anode.

The activity of a catalyst seems to be related to the number of crystallographically disoriented surface atoms. Defect structures are attained by several processes which are not discussed here. In the present investigations it was decided to use Raney catalysts because, on the one hand, they can be produced at room temperature so that recrystallization enhanced by elevated temperatures is avoided, and because, on the other hand, a relatively simple method of Raney electrode preparation was described by Justi (2-4). Raney catalysts are made by alloying the catalyst material with a base metal, for instance aluminum, which is subsequently dissolved from this alloy leaving the catalyst metal in a highly active state.

Justi has used Raney nickel electrodes, especially as hydrogen electrodes, with outstanding success. He also mentioned work with Raney electrodes based on copper, tungsten, molybdenum (for carbon monoxide oxidation), and palladium (as a pH electrode), but he did not discuss his results with these metals in detail. The present work must be regarded as an application, and possibly an extension, of Justi's technique.

The preparation of fuel electrodes from Raney copper, cobalt, nickel, rhodium, palladium, and platinum is described in the following along with the results obtained from tests with hydrogen, methanol, and hydrocarbon fuels.

Experimental Procedure

All electrode specimens were prepared in the form of porous disks by compressing a mixture of skeleton metal powder with powdered Raney alloy and subsequent dissolution of the base metal of the Raney alloy. In all cases the skeleton material and the catalytic substance of the Raney alloy were identical. The diameter of the disks was 1.2 cm. They were glued around the circumference into an electrode support ring made of Plexiglas. The projected surface area of the active part of the disk was 0.65 cm².

The Raney alloys were prepared by alloying the catalyst metal with aluminum. In order to achieve a high alloying rate without melting the components beforehand, the two metals were mixed in the form of powders and compressed into disks. The disks contained in individual crucibles were heated in an electric furnace until the alloying reaction started with conflagration at about 700°C. Owing to the heat of reaction, the temperature increased, causing the mixture to melt and to form a homogeneous alloy. Immediately after this reaction was completed, the alloy solidified; it was then removed from the furnace. It would not be possible, at least under mild conditions, to eliminate the aluminum from, in particular, the XAl compound where the catalyst metal X is compounded with aluminum at an atomic ratio of 1:1. The percentage of the catalytically active metal in the alloy, therefore, must be lower than the stoichiometric ratio of 1:1. It must, however, be above, say, 20 at. % because the alloy becomes too ductile for powdering below this limit.

For the preparation of the electrode disks, one part by volume of a pure metal powder, the skeleton material, was mixed with one part by volume of powdered Raney alloy. The mixture was subsequently compacted by pressing it into disks. Justi's

technique to achieve homoporosity by fractionation of the powders was not applied at this research stage.

The copper, cobalt, and nickel electrodes were prepared by compacting the powders at a pressure of 3,000 kg/cm², and sintering them at 400°C (Cu) and 600°C (Co, Ni). The platinum, palladium, and rhodium electrodes were left unsintered in order to prevent the formation of the stable compound XAl from the Raney alloy and the skeleton metal during the heat treatment. The unsintered electrodes were compacted at a pressure of 10,000 kg/cm², and at the same time two platinum screens were included with a view to increase the mechanical stability.

After cementation of the disks into a Plexiglas ring, the aluminum of the Raney alloy was dissolved by treating the electrode first with a dilute and then with a concentrated KOH solution, finally at a temperature of 80°C. The aluminum is not completely eliminated by this process. Further aluminum was dissolved anodically. A KOH solution was employed irrespective of whether the disks were used in alkaline or acid electrolytes because the dissolution rate of aluminum in acids is too large.

The electrodes were tested by taking current-potential plots using the half-cell system depicted in Fig. 1.

The test electrodes (porous disk cemented into a Plexiglas ring) were fixed in a Plexiglas holder providing a gas inlet. The electrical contact with the disk was established by two spring-type platinum wires to insure good contact. A platinum wire served as counter electrode. The electrode potential was measured against a calomel electrode using a Luggin capillary placed at a distance of 5 mm from the electrode surface, which gave a maximum measuring error of 50 mv. The ohmic polarization due to the ohmic resistances in the electrode and the electrolyte was not measured and consequently is still included in the potential values as reported. The measured potentials were not corrected for the diffusion potential between the electrolyte contained in the liquid junction ($5N$) and that at the reference electrode ($0.1N$); the involved error would not exceed 30 mv. The current was adjusted by means of a galvanostat. The measured amperages were converted into current densities by taking the projected surface area of the electrode to be 0.65 cm².

All electrodes were tested with gaseous hydrogen and methanol and some, in addition, with methylcyclohexane and hexane. The latter three fuels were admitted to the electrodes using nitrogen as a carrier gas. The electrode gas excess pressures totalled 0.5-1 atm. Reference runs were made using pure nitrogen.

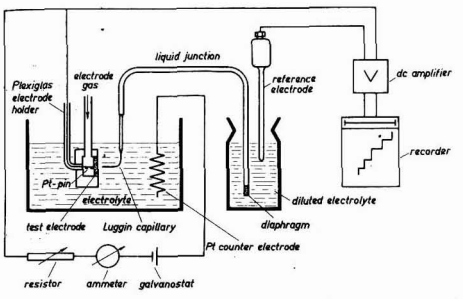

Fig. 1. Diagram of test stand for measuring current-potential plots.

In addition to the gaseous fuels, the tests included formaldehyde, formic acid, and methanol, dissolved in the electrolyte.

Alkaline, acid, and carbonate electrolytes have been employed as $5N$ solutions in water. The majority of the tests performed to date have been run at 80°C.

After the described chemical dissolution of aluminum, further aluminum was dissolved in the half-cell anodically. To this end the electrode was used as a hydrogen electrode. The electrode potential was increased stepwise to about 200 mv below the reversible oxygen potential. Although mainly hydrogen is oxidized during this process, part of the current is due to dissolving aluminum.

In the case of nickel, the electrode activity was much greater when electrochemical activation was used. For example a Raney nickel electrode using hydrogen in a half cell at −650 mv yielded current densities of 12 and 80 ma/cm², respectively, when the electrode was activated chemically in $5N$ KOH at 40°C for 24 hr or activated electrochemically for ½ hr in $5N$ KOH at 40°C with an electrode potential of +150 mv. Electrochemical activation was not necessary with the other metals of the eighth group tested.

The amount of hydrogen dissolved in the electrode was reduced substantially prior to tests with methanol or hexane by passing a nitrogen stream through the electrode. To accelerate this process, a potential was applied which was about 200 mv below the standard reversible oxidation potential of the corresponding electrode metal.

Current Density-Potential Plots

Most of the results are plotted in the form of current density-potential characteristics.

All reported potential values were obtained within a few minutes after adjustment of the current and remained constant during the measuring period up to several hours. Figure 2 depicts the results with hydrogen in KOH solution.

With all electrodes the open-circuit potential reached the reversible hydrogen potential. Deviations within ±30 mv are due to variations of the potential of the calomel reference electrode. The nickel electrode shows a distinct limiting current density beyond which the polarization as a function of the current deviates strongly from linearity. As the diagram shows, the platinum electrode has

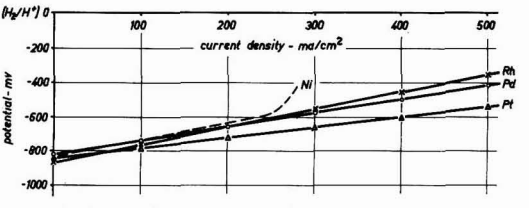

Fig. 2. Current density-potential plots of Raney electrodes with H_2 in $5N$ KOH at 80°C.

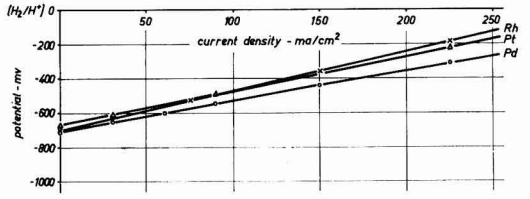

Fig. 3. Current density-potential plots of Raney electrodes with CH_3OH in 5*N* KOH at 80°C.

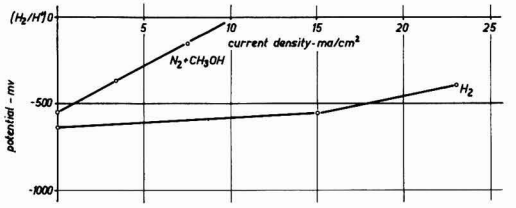

Fig. 4. Current density-potential plots of Raney palladium electrode with H_2 and CH_3OH in 5*N* K_2CO_3 at 80°C.

the smallest polarization. With palladium, platinum, and rhodium as hydrogen and methanol electrodes, the tests were not extended beyond current densities of about 500 ma/cm² and 300 ma/cm², respectively, so that the respective limiting current densities were not ascertained.

The results obtained with the sintered nickel electrode, using hydrogen as fuel were inferior to those reported by Justi, presumably because of the much smaller number of active pores. It is thus assumed that all electrodes investigated may be improved by employment of better techniques of powder metallurgy.

Figure 3 shows the results with methanol fuel in KOH solution.

Again the polarization increased linearly with the current. The open-circuit potential was about 100-150 mv smaller than that with hydrogen. Here palladium furnished the best results.

If the KOH electrolyte is replaced by K_2CO_3, very large polarizations are obtained both with hydrogen and methanol as fuels (see Fig. 4).

Large current densities were obtained not only

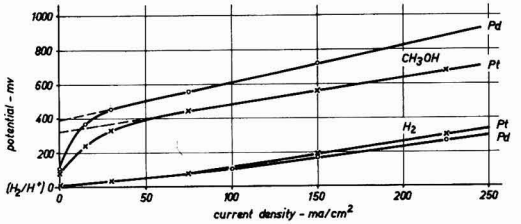

Fig. 5. Current density-potential plots of Raney electrodes in 5*N* H_2SO_4 at 100°C.

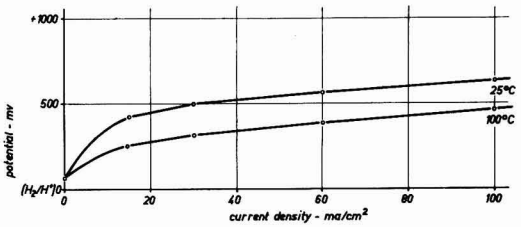

Fig. 6. Current density-potential plots of a Raney platinum electrode with CH_3OH in 5*N* H_2SO_4 as a function of temperature.

in KOH solution but also in H_2SO_4 solution with hydrogen and methanol as fuel (see Fig. 5 and 6).

With methanol, the polarization shows a peculiar nonlinearity at small current densities. With methanol in an acid solution, platinum proves to be superior to palladium as a catalyst. The open-circuit potential exceeds that of hydrogen by about 100 mv.

Figure 6 shows the temperature dependence of methanol oxidation as a function of the temperature between 25° and 100°C.

The above results are summarized in Table I together with results not illustrated so far. "Specific polarization" is defined as the slope of the curve potential *vs.* current density. For methanol in acid electrolyte, the slope is taken from the linear portion of the curve at large currents; in these cases the value of the open-circuit potential is complemented by the interception of the extrapolated linear part of the polarization curve with the ordinate. Copper and cobalt turned out to be unsatisfactory catalysts for methanol or hydrogen electrodes.

Table I. Open-circuit potential, specific polarization, and limiting current density with hydrogen and methanol, respectively, at 80°C

		H_2			CH_3OH		
Catalyst	Electrolyte	Open-circ. pot., mv	Spec. polar., ohm·cm²	Limit. curr. den., ma/cm²	Open-circ. pot., mv	Spec. polar., ohm·cm²	Limit. curr. den., ma/cm²
Cu	KOH	−780	3	10	—	—	zero
Cu	H_2SO_4	+20	24	10		not tested	
Co	KOH	−850	4	50	—	—	zero
Ni	KOH	−820	0.9	240	—	—	small
Pd	KOH	−820	0.8	>500	−710	1.8	>300
Pd	K_2CO_3	−640	5	15	−550	55	10
Pd	H_2SO_4	+10	1.1	>300	+100 (+380) *	2.3	>300
Rh	KOH	−860	1.0	>500	−700	2.3	>300
Pt	KOH	−840	0.6	>500	−670	2.0	>300
Pt	H_2SO_4	+10	1.2	>300	+80 (+320) *	1.5	>300

* Basis for calculation of the specific polarization.

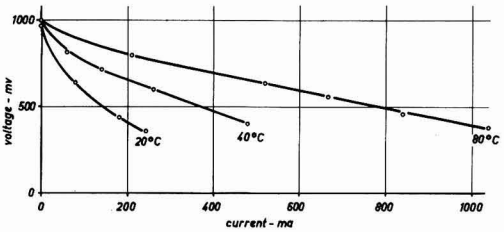

Fig. 7. Current-voltage plots of a fuel cell in 5*N* KOH as a function of temperature with methanol fuel (electrode area 12 cm²).

In addition, the following remarks may be made: (*A*) There was no appreciable electrochemical oxidation of hexane or methylcyclohexane with the described types of electrodes and under the described conditions. (*B*) Sintering of the noble metal electrodes destroys their activity with methanol and seriously affects their activity with hydrogen. (*C*) The current-potential plots with methanol are independent of whether the fuel is admitted as a vapor or dissolved in the electrolyte in excess concentrations. (*D*) In both KOH and H_2SO_4 solutions, formaldehyde and formic acid, dissolved in the electrolyte, are converted with current densities similar to those achieved with methanol.

Experiments with a Laboratory-Stage Alkaline Methanol Fuel Cell

A laboratory-stage methanol fuel cell was set up, using a palladium fuel electrode and a silver oxygen electrode of a projected surface area of 12 cm² each. The electrodes were spaced at 1 cm in an aqueous 5*N* KOH electrolyte to which methanol was added in amounts of 1 mole/l as a liquid admixture.

The current-voltage characteristic of the cell was plotted at 20°, 40°, and 80°C (Fig. 7).

It is apparent that, at the same voltage, the cell output rises about fourfold on increasing the temperature from 20° to 80°C. The characteristic does not change even after continuous operation for several weeks; the electrolyte had to be replaced several times during this period owing to the KOH consumption. The cell was used to examine the degree of conversion of, alternatively, methanol, formaldehyde, and formic acid.

Tests were run which showed that there was negligible activity of the methanol at the oxygen electrode.

A known amount of methanol was added to a cell, and the cell was operated until completely discharged. The total amount of current withdrawn was measured and compared to the calculated total current for complete oxidation to carbonate. The measured current corresponded to about 95% of the calculated current.

Methanol Oxidation Reactions

Various experimenters (1, 5-9) have found different reaction end products in methanol fuel cells. During the present program, several avenues have been followed in an attempt to investigate the course and the completeness of the methanol conversion.

In order to test their electrochemical activity, the supposed intermediates of the methanol oxidation were anodically oxidized in a half-cell arrangement. With formaldehyde as well as with formic acid large current densities were obtained at polarizations comparable to those observed with methanol. This holds for both an alkaline and an acid medium.

Another approach to the problem of the degree of oxidation is the chemical analysis of the electrolyte after extended operation. Therefore, the amounts of formaldehyde and formic acid were determined that were formed after a cell had been operated for 2 hr at, alternatively, 20° and 80°C from methanol owing to incomplete oxidation. The applied analytical procedure was based on the formation of an intensely colored complex of formaldehyde and chromotropic acid which was determined colorimetrically. Formic acid is reduced to formaldehyde by magnesium and sulfuric acid before its determination. Such a procedure was carried out for half-cells after 5000 coulombs had been withdrawn. In the case of alkaline electrolyte with a palladium electrode, the amounts of formaldehyde and formic acid totalled 5% of the converted electricity. With a rhodium electrode, they were about 10% thereof. In the case of an acid electrolyte, using a platinum electrode, the amount of formaldehyde was about 1%, and that of formic acid smaller than 0.1% of the converted electricity. There was no appreciable temperature effect.

The same analyses were conducted for the alkaline methanol fuel cell with a palladium electrode after 8000 coulombs had been withdrawn. The amounts of formaldehyde and formic acid corresponded to 1 and 3%, respectively, of the converted electricity.

Finally, at 20°C the laboratory stage alkaline fuel cell was operated on defined amounts of formaldehyde and formic acid in separate runs. Total current withdrawal was measured for each fuel and was found to be about 95% of the calculated current for complete oxidation in each case. This was in agreement with the tests run to determine fuel activity with methanol as the fuel.

These various findings lead to the conclusion that even at room temperatures methanol oxidation proceeds almost completely to carbonate or carbon dioxide on the Raney electrodes of the present study. This result appears to be independent of the electrolyte and of the half-cell *vs.* fuel cell operation.

Acknowledgments

The authors wish to acknowledge the valuable assistance of A. Köhling and K. Richter, members of Battelle-Institut, Frankfurt, and are particularly grateful to Cummins Engine Company for the active support of the research.

Manuscript received Nov. 30, 1961; final revised manuscript received March 23, 1962. This paper was prepared for delivery before the Detroit Meeting, Oct. 1-5, 1961.

Any discussion of this paper will appear in a Discussion Section to be published in the June 1963 JOURNAL.

REFERENCES

1. O. Block, M. Prigent, and J. C. Balaceanu, Paper presented at the Indianapolis Meeting, Electrochemical Society 1961.
2. E. Justi *et al.*, "High Drain H_2—Diffusion Electrodes," Franz Steiner Verlag, Wiesbaden (1960).
3. E. Justi and A. Winsel, paper presented at the Indianapolis Meeting, Electrochemical Society, 1961.
4. M. Dittman, E. Justi, and A. Winsel, paper presented at the Chicago Meeting, Am. Chem. Soc., 1961 (on oxygen electrodes made of silver).
5. M. J. Schlatter, *ibid.*
6. J. F. Yeager, paper presented at the Indianapolis Meeting, Electrochemical Society, 1961.
7. W. Vielstich, *ibid.*
8. L. R. Griffith, 15th Annual Power Sources Conference, 1961.
9. J. E. Wynn, 14th Annual Power Sources Conference, 1960.

Determination of the Internal Resistance of Leclanche Cells by Square-Wave Method

Aladar Tvarusko

The Carl F. Norberg Research Center, The Electric Storage Battery Company, Yardley, Pennsylvania

ABSTRACT

The internal resistance of Leclanché dry cells was studied on shelf and during discharge by means of a square-wave technique. A constant-current square-wave signal was passed through the cell on test, and the potential variation across the cell displayed on a high-sensitivity oscilloscope with differential input. The instantaneous voltage drop in the oscilloscope pattern, caused by the leading edge of the constant current square wave, indicated the internal resistance of the Leclanché cells. The internal resistance is independent of the amplitude and frequency of the applied square-wave current and of the momentary d-c current. The type of manganese dioxide used in the cathode mix and the composition of the electrolyte influenced the internal resistance of D-size Leclanché cells, both undischarged and during 4-ohm continuous discharge.

In the past, both steady-state and transient measuring methods using either alternating or direct current were investigated for determining the internal resistance of dry cells. Results obtained by these methods were inconsistent. One of the simplest and least accurate methods is the d-c steady-state method in which the resistance is calculated from the potential drop at a certain current drain (1-4). Several d-c transient methods were developed (5-8). Generally, the a-c steady-state methods use various types of impedance bridges to separate the resistive (real) and reactive (imaginary) part of the impedance. Various arrangements were used by the several authors (9-18). The a-c transient method is represented by Brodd's (19) current pulse method.

Impedance of an electrical circuit consists of two parts: resistive and reactive. The resistive part is frequency independent while the reactive part varies with the frequency. The reactive part can include inductance or capacitance or both. In the case of Leclanché cells with relatively short leads, the inductance is negligible, and only the capacitive reactance and the pure resistive component have a role in the impedance.

In general, the separation of the resistive and reactive components of the impedance by the a-c bridge methods is a fairly lengthy operation or complicated instrumentation is involved, *e.g.*, the use of double-servo-controlled a-c bridge (20). During the changes taking place in the discharge and storage of cells, not only the resistive part can change but also the reactive part. Brodd's pulse method (19) yielded only the resistive part of the impedance, whereas the square-wave current method gives information concerning the reactive part of the impedance as well as the resistive part. Very recently however, a pulse method was described (21) to measure parameters of the electrical double layer, namely, the reactive part of the impedance. Various square-wave techniques have been utilized previously for electrochemical studies (22-25).

In this modification of the method developed at this laboratory (25), a constant-current square-wave signal was passed through the test cell and the potential variation across the cell displayed on an oscilloscope. The instantaneous voltage drop in the oscilloscope pattern, caused by the leading edge of the constant-current square wave, represents the internal resistance of the Leclanché cell. Results concerning the reactive part of the impedance will be described in a later article.

Experimental

The block diagram of the circuit used to measure the internal resistance of Leclanché cells is shown in Fig. 1. The Leclanché cell A, was connected in series with a noninductive resistor B. This converted the constant-voltage output of the square-wave generator C, to constant current, since the value of resistor B is much larger than the sum of the impedances in the constant-current circuit loop (C-A-G-F). The voltage response of the square-wave current across the Leclanché cell was measured through oscilloscope probes (5X)D, with a high-

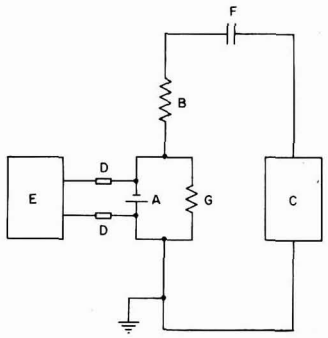

Fig. 1. Block diagram of the circuit: A, Leclanché cell; B, resistor; C, square-wave generator; D, oscilloscope probe (5X); E, oscilloscope; F, blocking capacitor; G, discharging resistor.

sensitivity differential input oscilloscope E, equipped with a Robot recorder camera. A capacitor F was used in series with the dry cell to prevent the discharge of the dry cell through the square-wave generator. Resistor G, in parallel with the cell, was used for discharging the Leclanché cell.

The use of matched oscilloscope probes and shielded cables together with the differential input of the oscilloscope minimized stray pick-up and noise. Ground loops were avoided by grounding the measuring circuitry only at one point. The shielding of the oscilloscope probes was grounded through the oscilloscope.

A Hickok Model 710 sine-square-wave generator was used with a rise time of less than 0.1 μsec for a range of 20 cycles to 1 Mc frequency. The square-wave current limiting resistor was 4200 ohm except for the study of internal resistance as a function of the square-wave current. The voltage used was 42.0v peak-to-peak. The blocking capacitor was 16 μF. The oscilloscope was a Tektronix Model 502 with a passband of d.c. to 100 kc at the most frequently used sensitivities and a rise time of 3.5 μsec.

Square waves of a certain base frequency can be represented by the Fourier series of sine waves of its fundamental and odd numbered harmonics. The leading edge of the square wave represents the high-frequency harmonics. If the inductance of the sample and leads is negligible, the instantaneous voltage drop of the signal corresponds to the resistive part of the impedance only. Knowing the square-wave current amplitude and the measured instantaneous voltage drop (times oscilloscope probes' attenuator factor 5X) the R is simply calculated from Ohm's law. When discharging the Leclanché cell, the resistor G is in parallel with the cell, and R is calculated with the help of Kirchoff's law.

All the Leclanché cells investigated were pasted-type D-size dry cells. In order to study the effect of the type of MnO_2 on the course of the internal resistance curves, MnO_2 of different origins was used. African ore (Ghana) represented the naturally occurring manganese dioxide. The African ore was also blended with a synthetic hydrous MnO_2 (4% alkali and 10% water content). The x-ray diffraction pattern of this synthetic MnO_2 had weak intensity γ-MnO_2 and very weak pyrolusite and cryptomelane peaks. The two electrolytic MnO_2 samples (sources A and B) were γ-MnO_2. The MnO_2: carbon black ratio was 8:1 for all cells. The electrolyte in the core was the same for all compositions with the exception of the African ore, synthetic MnO_2 mix which contained 20% less $ZnCl_2$ and 10% less NH_4Cl than the others. The same paste composition was used for all Leclanché cells except for the electrolytic MnO_2 from source B. The paste for this cell contained 120% more $ZnCl_2$ and 25% more NH_4Cl than the other one.

Results and Discussion

The internal resistance of the Leclanché cells was measured by a constant square-wave current. It was of interest to investigate the internal resistance as a function of the applied square-wave current amplitude. The current was varied from 1 to 20 ma peak-to-peak, and no change was observed in the internal resistance of the cell. The internal resistance is thus independent of the square-wave current amplitude, *i.e.*, it obeys Ohm's law. A current of 10 ma was subsequently chosen to obtain a convenient voltage drop.

The frequency dependence of the internal resistance was investigated in the frequency range of 20-10,000 cps. The internal resistance of Leclanché cells, R_i was thus found to be independent of the frequency as shown in Fig. 2. This frequency independence of the R_i was found for all the Leclanché cell compositions investigated.

The very slight deviation at low frequencies is due to the difficult readability of the voltage drop (where large vertical deflection factors are needed), while at high frequencies it is due to the distortion of the leading edge. The internal resistance of D-size Leclanché cells is in the range 0.1-0.4 ohm, according to the composition. These low values necessitated the use of the most sensitive range of the oscilloscope's vertical amplifier (200 μv/cm). At this range the passband of the amplifier is d.c. to 100 kc. The fifth odd harmonic component of the 10 kc square-wave signal is cut out by the amplifier, whereas the forty-ninth odd harmonic component of the 1 kc square-wave signal is carried over. The readability of the instantaneous voltage drop is good at 1 kc also. All the measurements were done at 1 kc.

Dry cells are made as uniformly as is practically possible. A certain deviation in the composition, as-

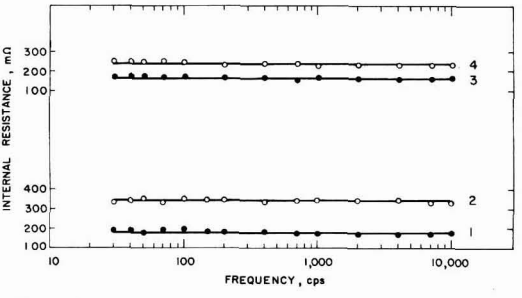

Fig. 2. Internal resistance of Leclanché cells as a function of frequency. Curve 1, African ore; curve 2, African ore, synthetic MnO_2; curve 3, electrolytic MnO_2, source B; curve 4, electrolytic MnO_2, source A.

Table I. Internal resistance of undischarged Leclanché cells (D-size) and its deviation

Type of MnO_2	Number of cells	R_{Mean}, ohm	Δ_{Max}, ohm	
African ore	15	0.18	+0.03	−0.01
Electrolytic MnO_2, source A	12	0.21	+0.06	−0.04
Electrolytic MnO_2, source B	12	0.16	+0.02	−0.01

sembly, etc., is unavoidable. This naturally shows up in the internal resistance values also. The arithmetical mean of at least 12 undischarged D-size Leclanché cells per lot, and the maximum deviation from it can be seen in Table I. The reproducibility of the internal resistance values for individual cells is good (±0.01 ohm).

On replacing part of the African ore in the core with a synthetic hydrous MnO_2, the internal resistance of the undischarged Leclanché cell was markedly increased (curve 2 *vs.* curve 1, Fig. 2). The slightly lower salt concentration in the mix electrolyte cannot be responsible alone for this marked resistance increase. Therefore, it is safe to assume that the synthetic MnO_2 in the core contributed largely to the internal resistance increase. Leclanché cells made with electrolytic MnO_2, source B, had a paste of significantly higher salt concentration which was mainly responsible for the internal resistance decrease of these cells (curve 3).

The internal resistance of Leclanché cells of various compositions was investigated also during discharge. Three cells or more were discharged for each composition to insure proper validity of results. Momentary current drains did not affect the internal resistance of cells except at very high current drains where it increased due to changes taking place which cannot be ascertained at this time. This confirms the results of Brodd (19), Fukuda *et al.* (14), and Panzer *et al.* (8) and is contrary to the studies reporting the dependence of the "internal resistance" of Leclanché cells on current drain (1, 4, 6, 14, 15). In the latter cases, the "internal resistance" includes not only the pure resistance, R_i, of Leclanché cells but also other types of polarization.

The internal resistance of Leclanché cells changes during discharge due to the current producing and secondary reactions. The internal resistance change for Leclanché cells containing African ore during 4 ohm continuous discharge can be seen in Fig. 3. The internal resistance of the cells having African ore only increased constantly, and the curve (No. 1) can be separated into two parts having slightly different slopes. Cells with synthetic hydrous MnO_2 and African ore produced a curve of an entirely different character. This curve was duplicated several times. The rapid internal resistance increase in the very beginning of the discharge and the nearly horizontal portion of the curve can be attributed to the presence of the synthetic MnO_2. In the second half of the discharge the synthetic MnO_2 had lost its influence, and the curve resembles that of cells with natural ore mixes. The voltage values on the individual

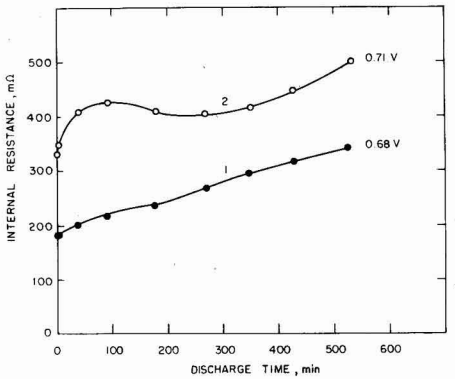

Fig. 3. Internal resistance of Leclanché cells containing natural ores discharged continuously through 4 ohm. Curve 1, African ore; curve 2, African ore, synthetic hydrous MnO_2.

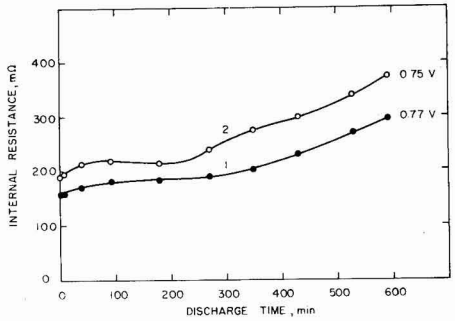

Fig. 4. Internal resistance of Leclanché cells having electrolytic MnO_2 discharged continuously through 4 ohm. Curve 1, electrolytic MnO_2, source B; curve 2, electrolytic MnO_2, source A.

curves represent the closed-circuit voltages at the cut-off time.

In the manganese dioxides of the above cells the amount of γ-MnO_2 was much less than in electrolytic MnO_2, as judged by the intensity of the γ-MnO_2 peaks in the x-ray diffraction patterns. The amount of γ-MnO_2 seems to influence the first portion of the internal resistance curve. African ore has a fair amount of γ-MnO_2, and its internal resistance curve for cells can be characterized by two slightly deviating slopes. The internal resistance curves of electrolytic MnO_2 (dominantly γ-MnO_2) can be separated into two parts with distinctly different slopes (Fig. 4). This is more evident in Leclanché cells (MnO_2, source B, curve 1) with a paste of much higher zinc chloride content (lower *p*H).

The two distinct slopes and the initial portion of the curves for the latter and other Leclanché cells represent various reactions taking place in the cells. With a paste of higher *p*H, the course of the internal resistance curve (No. 2) deviates from that previously described (No. 1) mainly in the 250-450 min range.

The previously described square-wave current method to determine the internal resistance naturally is not limited to Leclanché cells but can be applied to other electrochemical systems and their half-cells.

Acknowledgment

The author is indebted to Mr. B. Romvári for helpful discussions, and to the Ray-O-Vac Company, Madison, Wisconsin, for supplying the special Leclanché cells.

Manuscript received Oct. 18, 1961; revised manuscript received Feb. 1, 1962. This paper was prepared for delivery before the Detroit Meeting, October 1-5, 1961.

Any discussion of this paper will appear in a Discussion Section to be published in the June 1963 JOURNAL.

REFERENCES

1. C. Drotschmann, "Moderne Primärbatterien," pp. 68-72, Nikolaus Branz, Berlin-Schoeneberg (1951).
2. D. L. Ordway, *Trans. Electrochem. Soc.*, **17**, 341 (1910).
3. G. W. Vinal, "Primary Batteries," pp. 133-4, John Wiley & Sons, Inc., New York (1950).
4. N. K. Chaney, *Trans. Electrochem. Soc.*, **29**, 183 (1916).
5. H. Steinwehr, *Elektrotechnik*, **2**, 91 (1948).
6. R. Glicksman and C. K. Morehouse, *This Journal*, **102**, 273 (1955).
7. K. Kordesch and A. Marko, *ibid.*, **107**, 480 (1960).
8. R. E. Panzer, W. S. Harris, and W. C. Spindler, Paper presented at the Detroit Meeting of The Electrochemical Society, 1961.
9. H. D. Holler, *This Journal*, **97**, 271 (1950).
10. H. E. Lawson and F. J. Kirkman, *Trans. Electrochem. Soc.*, **70**, 441 (1936).
11. N. C. Cahoon, *ibid.*, **92**, 159 (1947).
12. C. Drotschmann, "Elektrochemie und Elektrotechnik im Batteriebau," V. Teil, pp. 77-88, Nikolaus Branz, Berlin (1953).
13. J. J. Coleman, *Trans. Electrochem. Soc.*, **90**, 545 (1946).
14. M. Fukuda, T. Hirai, and H. Manabe, *J. Electrochem. Soc., Japan*, **27**, 247 (1959); Overseas Edition, **27**, E 108 (1959).
15. J. Euler, *Z. Elektrochem.*, **60**, 1056 (1956).
16. C. Drotschmann, ref. (1), pp. 72-79.
17. J. Euler and K. Dehmelt, *Z. Elektrochem.*, **61**, 1200 (1957).
18. R. J. Brodd and H. J. DeWane, Paper presented at the Columbus Meeting of the Electrochemical Society, 1959.
19. R. J. Brodd, *This Journal*, **106**, 471 (1959).
20. C. O. Anderson, F. Möhl, and E. Stenhagen, *Acta Chem. Scand.*, **12**, 415 (1958).
21. J. S. Riney, G. M. Schmid, and N. Hackerman, *Rev. Sci. Instr.*, **32**, 588 (1961).
22. U. Bertocci, G. Bianchi, and C. Guerci, *Ann. Chim. (Rome)*, **44**, 44 (1954).
23. R. J. Brodd and N. Hackerman, *This Journal*, **104**, 704 (1957).
24. J. J. McMullen and N. Hackerman, *ibid.*, **106**, 341 (1959).
25. B. D. Cahan and P. Rüetschi, *ibid.*, **106**, 543 (1959).

Oxidation Studies on 304 Stainless Steel

E. A. Gulbransen and K. F. Andrew

Research Laboratories, Westinghouse Electric Corporation, Pittsburgh, Pennsylvania

ABSTRACT

The kinetics of oxidation of 304 stainless steel are studied between 500° and 1150°C at 0.1 atm for reaction times up to 6 hr. At 500°C about 2.3 $\mu g/cm^2$ of oxide are formed in a time period of 6 hr. The rate of increase after 6 hr is 0.1 $\mu g/cm^2/hr$. At 800°C a transition is observed in the rate of oxidation with the kinetics changing from the parabolic rate law to the linear rate law. This transition occurred for a weight gain of 9 $\mu g/cm^2$. At 900°C and for weight gains above 90 $\mu g/cm^2$ the parabolic rate law again was found to hold. A second transition is found in the kinetics of oxidation at 1150°C. This transition we relate to the vapor pressure of iron and chromium which acts to speed up the transfer of metal atoms through the oxide scale. A comparison of the kinetics of oxidation is made with the heat-resistant Kanthal alloys and with pure chromium.

This paper presents a systematic study of the kinetics of oxidation of 304 stainless steel between 500° and 1150°C at 0.1 atm and for reaction times up to 6 hr. Since 304 stainless steel is being used as a high-temperature material, one of the objectives of this work is to study the conditions under which the alloy fails in oxidation. Failure occurs when a rapid oxidation reaction develops in which diffusion processes are no longer rate controlling. For some metals and alloys failure is due to poor adhesion of the oxide. With other metals the oxide may volatilize. For those metals which form nonvolatile and adherent oxide films, failure may result from vaporization of the metal through the oxide film. This type of failure has been observed in the oxidation of chromium (1) and several heat resistant alloys (2-3).

From a thermodynamic point of view oxidation and corrosion are functions of the chemical potentials of the components in the environment and the chemical potentials of the metallic components in the alloy. The chemical potential of an alloying component is a function of the activity of the metal in the alloy. From a kinetic point of view the rate of oxidation or corrosion depends in part on the nature and properties of the oxide or corrosion film formed on the alloy.

Since both gaseous oxidation and corrosion in high-temperature water atmospheres depends on the same metallurgical factors in the alloy, a study of the kinetics of oxidation may help our interpretation of corrosion in water atmospheres.

Since the chemical activity of metal atoms in an alloy and the characteristics of the oxide film can be controlled by alloying additions (4), it is possible to

predict the oxidation and corrosion behavior of alloys.

Experimental

Apparatus.—The vacuum microbalance reaction system was used (5-6) for all of the measurements. The sensitivity of the microbalance was 0.83 μg per 0.001 cm. Weight changes of 0.3 μg could be estimated.

A mullite furnace tube was used to surround the specimen. This tube was sealed directly to the all-Pyrex glass vacuum system. After introducing the specimen into the reaction system and closing off, the system was evacuated for 16 hr at a pressure of 10^{-6} mm Hg or less. To avoid evaporation of metal at 1000°C and higher, the specimen and reaction tube were heated rapidly to the reaction temperature. After thermal equilibrium was established, purified oxygen was added to 0.1 atm pressure.

For the same surface treatment the reproducibility of the oxidation experiments was about 10-20%.

The furnace temperature was maintained constant to ±1.5°C by the use of a calibrated high-sensitivity recorder-controller and a calibrated Pt-Pt 10% Rh thermocouple.

Samples.—The 304 stainless steel analyzed 17.7 Cr, 8.34 Ni, 1.11 Mn, 0.02 P, 0.16 N, 0.11 C, and balance iron. Strips of 5 mil sheet were abraded through 4/0 polishing paper under purified kerosene. They were carefully cleaned before using (7). Depending on the amount of reaction, four specimen sizes and weights were used. The largest was 11.25 cm^2 in area and weighed 0.6831g while the smallest was 1.36 cm^2 in area and weighed 0.0820g.

Results

The results are presented in weight gain *vs.* time graphs. The weight gain is in micrograms per square centimeter and the time is in minutes. Although the oxide film is a mixture of oxides (8), we can estimate the thickness of the oxide by assuming the oxide to be Cr_2O_3 and by assuming a surface roughness ratio of unity. A factor of 60 is calculated to relate the weight gain to thickness in angstroms. An oxygen pressure of 0.1 atm is used for all of the experiments.

Both annealed and unannealed specimens were used. The annealed specimens were prepared by heating in a high vacuum system at a pressure of 9×10^{-6} mm Hg at 843°C for 2 hr and quenching. This treatment precipitates carbides and nitrides which could occur during normal oxidation at this temperature.

Oxidation at 500° and 600°C—unannealed specimens.—Figures 1 and 2 show the time courses of the experiments at 500° and 600°C. The oxide thicknesses and colors are given in Table I. No spalling of the oxide occurred on cooling the oxidized alloy to room temperature. After 6 hr of oxidation at 500°C, about 2.3 μg/cm^2 of oxide were formed. Since the room temperature oxide was not removed, the total oxide must include an additional 0.3-0.5 μg/cm^2. The reaction rate after 6 hr of reaction was of the order of 0.1 μg/cm^2 of oxide per hour at 500°C.

A plot of the weight gain squared against time shows a straight line between 2 and 6 hr of reaction time. A value of 1.67×10^{-16} $(g/cm^2)^2$/sec is calculated. No evidence was found for a transition in the kinetics of the reaction. We conclude that the reaction of 304 stainless steel with oxygen at 500°C is a slow reaction.

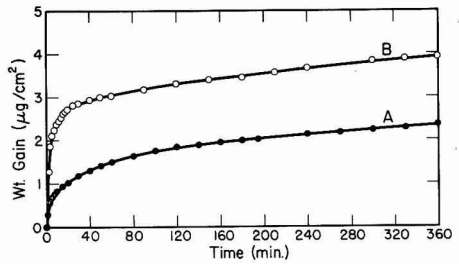

Fig. 1. Effect of temperature on oxidation of unannealed 304 stainless steel, abraded through 4/0, 7.6 cm of Hg of O_2; curve A, 500°C; curve B, 600°C.

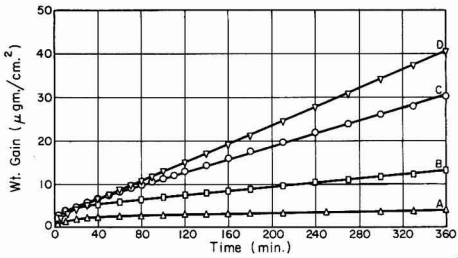

Fig. 2. Effect of temperature on oxidation of annealed stainless 304, abraded through 4/0, 7.6 cm of Hg of O_2; curve A, 700°C; curve B, 800°C; curve C, 850°C; curve D, 900°C.

Electron microscope observations on the edges of the specimens showed no evidence for oxide whiskers or platelets.

Oxidation at 700° and 1150°C.—Figures 2 and 3 show the time courses for the oxidation experiments over the temperature range of 700°-1100°C. Oxide thicknesses and colors are shown in Table I. None of the oxide films or scales spalled away from the metal on cooling to room temperature.

In this study we are particularly interested in transitions in the rate of oxidation and "breakaway" type of oxidation reactions. For this purpose we use

Table I. Thickness and color of oxide films on 304 stainless steels

Temp, °C	Unannealed Thickness,* μg/cm^2	Color	Annealed Thickness,* μg/cm^2	Color
500	2.33	Straw		
600	3.91	Purple		
700	8.01	Blue	3.95	Blue
750	12.33	Straw-pink		
800	24.6	Blue-green	13.1	Light purple
850	39.3	Gray	30.2	Gray-green
900	46.6	Gray	40.5	Gray-pink
950	90.0	Gray	56.8	Gray
1000			136.0	Gray
1050			254.0	Gray
1100			490.0	Gray
1150			905.0‡	Gray

* 6-hr experiments.
‡ 7-hr experiment.

the parabolic rate law to interpret the rate data. This law states that the weight gain, W, depends on the time, t, by the equation $W^2 = At + C$. Here A is the parabolic rate law constant and C is a constant. The parabolic rate law based on the principles of formation and diffusion of ions or lattice defects has been the most successful rate law for explaining oxidation. Parabolic rate law plots are used to test for changes in the mechanism of reaction. Figures 4-8 show parabolic rate law plots of the 800°, 850°, 950°, 1050°, and 1150°C experiments. The first evidence for a transition in the rate of oxidation was found in the 800°C parabolic plot shown in Fig. 4. After the initial period of reaction, a good fit was obtained with the parabolic rate law for the thickness range of 5-9 $\mu g/cm^2$. An increase in slope was observed in the parabolic rate law plot above this thickness. A value of 5.83×10^{-15} $(g/cm^2)^2/sec$ was calculated for the pretransition thickness range parabolic rate law constant.

Deviations from the parabolic rate law are also observed in the 850°C plot as shown in Fig. 5. This deviation occurs after 70 min of reaction or at an oxide thickness of 9 $\mu g/cm^2$. A similar transition

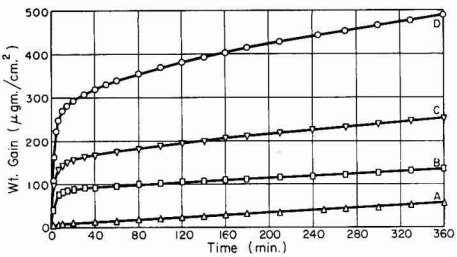

Fig. 3. Effect of temperature on oxidation of annealed stainless 304, abraded through 4/0, 7.6 cm of Hg of O_2; curve A, 950°C; curve B, 1000°C; curve C, 1050°C; curve D, 1100°C.

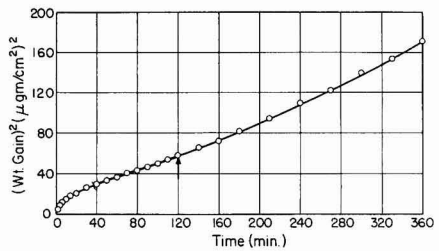

Fig. 4. Oxidation of stainless steel, 800°C, 7.6 cm of Hg of O_2; parabolic plot, abraded through 4/0; A = 5.83×10^{-15} $(g/cm^2)^2/sec$.

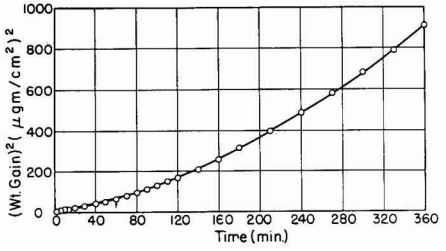

Fig. 5. Oxidation of stainless steel, 850°C, 7.6 cm of Hg of O_2; parabolic plot, abraded through 4/0; A = 1.79×10^{-14} $(g/cm^2)^2/sec$.

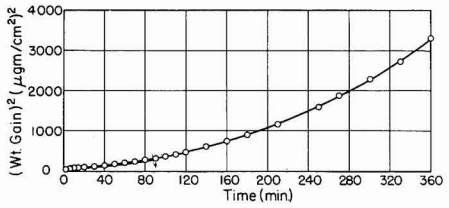

Fig. 6. Oxidation of stainless steel, 950°C, 7.6 cm of Hg of O_2; parabolic plot, abraded through 4/0; A = 2.78×10^{-13} $(g/cm^2)^2/sec$.

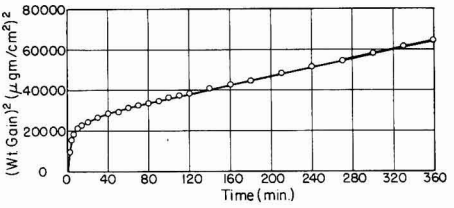

Fig. 7. Oxidation of stainless steel, 1050°C, 7.6 cm of Hg of O_2; parabolic plot, abraded through 4/0; A = 1.72×10^{-12} $(g/cm^2)^2/sec$.

thickness is found for the 900°C experiment. We conclude a transition occurs in the kinetics of the reaction for an oxide thickness of about 9 $\mu g/cm^2$. This transition thickness is the lowest we have observed for any metal or alloy. For the oxidation of chromium the first transition occurred at a thickness of 80 $\mu g/cm^2$.

Above 900°C it is not possible to observe the pretransition period of oxidation. The parabolic rate law plot of the 950°C experiment in Fig. 6 shows a continuously increasing slope. The initial value for the rate law constant is given in Fig. 6 and Table II. We interpret the changing value for the parabolic rate law constant as due to a change in oxide composition. The parabolic rate law of oxidation does not apply for the oxide composition range of 9-90 $\mu g/cm^2$. Instead the rate of oxidation follows the linear rate law.

Figure 7 shows a parabolic rate law plot for the 1050°C experiment. A straight line is found after the first hour of reaction.

A second transition is found to occur in the 1150°C parabolic rate law plot shown in Fig. 8. The rate law is observed to hold for the intermediate section of the plot. After 330 min of oxidation the rate law con-

Table II. Summary of parabolic rate law constants

Temp, °C	A. Unannealed $(g/cm^2)^2/sec$ Pretransition	Posttransition	B. Annealed $(g/cm^2)^2/sec$ Pretransition	Posttransition
500	1.67×10^{-16}			
600	3.33×10^{-16}			
700	1.08×10^{-15}		3.61×10^{-16}	
750	2.64×10^{-15}	8.34×10^{-15}		
800	9.16×10^{-15}	3.92×10^{-14}	5.83×10^{-15}	8.89×10^{-15}
850	1.11×10^{-14}	1.055×10^{-13}	1.79×10^{-14}	6.34×10^{-14}
900	2.36×10^{-14}	1.583×10^{-13}	2.38×10^{-14}	1.33×10^{-13}
950	1.193×10^{-13}	5.69×10^{-13}	7.22×10^{-14}	2.78×10^{-13}
1000			5.0×10^{-13}	5.91×10^{-13}
1050				1.728×10^{-12}
1100				6.11×10^{-12}
1150				1.67×10^{-11}

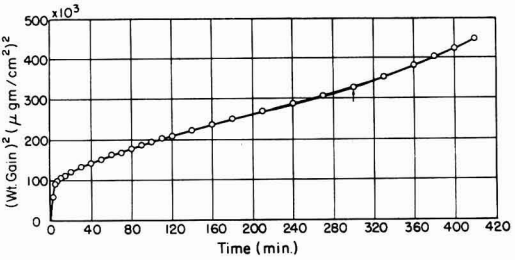

Fig. 8. Oxidation of stainless steel, 1150°C, 7.6 cm of Hg of O_2; parabolic plot, abraded through 4/0; A = 1.67 x 10^{-11} $(g/cm^2)^2$/sec.

stants increase. This increase is probably due to a vapor pressure effect which is discussed in a later section.

Temperature dependence.—To interpret the temperature dependence of the parabolic rate law constants A we use the simple form of the Arrhenius expression

$$A = Be^{-\Delta H/RT}$$

Here ΔH is the heat of activation of the rate-controlling mechanism, B is a constant, and R is the gas constant. ΔH is determined from the slope of a log A *vs.* $1/T$ plot. More elaborate equations may be used if the entropy terms are evaluated (9).

Table II shows a summary of the parabolic rate law constants for the annealed and unannealed samples. Pre- and posttransition values are given where possible. Figure 9 shows a log A *vs.* $1/T$ plot of the data.

Three straight lines are observed in Fig. 9. Curve DE gives the constants for the pretransition region. A value of 33,200 cal/mole for ΔH is calculated. The posttransition values are given by the line ABC. Line BC has about the same value for ΔH as line DE.

Point B shows a major change in the mechanism of oxidation. A heat of activation of 88,000 cal/mole is calculated.

We interpret the change in rate between line DE and line BC as due to a crystal structure transformation in the oxide system. Electron diffraction studies on a similar alloy by Hickman and Gulbransen (8) shows a crystal structure transformation occurring for this temperature range of oxidation.

Vapor pressure effect.—Figure 9 shows a drastic change occurs in the mechanism of oxidation at point B. We suggest that this change is due to the vapor pressure of the metals in the 304 stainless steel. We explained a similar change in the rate oxidation of chromium (1) at 900°C as due to the vapor pressure of chromium. At some temperature for all metals the rate of evaporation of metal into and through the oxide film acts to aid normal ion formation and transfer processes. Since all sides of the oxide crystals may be exposed in part to the metal vapor, a short circuit of the normal diffusion process is possible. However, if the oxide film is impervious to metal vapor, the metal transfer process may be limited. This occurs for oxide films on aluminum-iron alloys (4). Much smaller effects were observed for oxide films on simple chromium-iron alloys (4).

To test for the vapor pressure effect on 304 stainless steel we compare the rate of evaporation of metal from a clean surface of a 21.9 Cr-Fe alloy with the rate of oxidation calculated on the basis of chromium reacting. Due to the possibility of side reactions, such as decarburization, effecting the vapor pressure measurements, special alloys must be used. We have studied recently the vapor pressure of a clean 21.9 Cr-Fe alloy (4) both in the oxide-free condition and in the presence of an oxide film. Although this alloy differs in composition from the 8 Ni-18 Cr-74 Fe alloy, we feel that the two alloys do not differ appreciably in their vapor pressure curves since chromium is the metal vaporizing in each alloy.

Figure 10 shows a comparison of the rate of evaporation from an oxide-free surface of the 21.9 Cr-Fe alloy with the rate of oxidation of the 304 stainless steel. Below 1000°C the rate of oxidation is higher than the rate of evaporation. The two rates become equal at 1000°C, and above 1000°C the rate of oxidation is less than the rate of evaporation.

Since the oxide film is thick, the transition is not sharp. The effect of oxide films on the vapor pressure would act to lower curve A slightly.

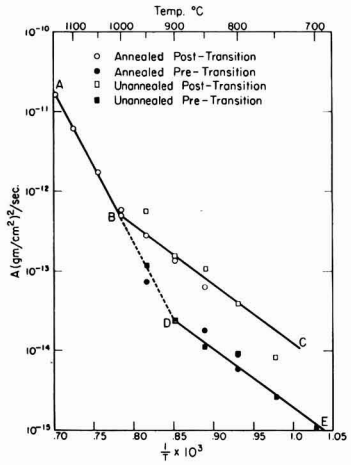

Fig. 9. Oxidation of 304 stainless steel. Log A *vs.* $1/T$. Curves A,B,C, posttransition; curves D,E, pretransition. ΔH_{AB} = 88,000 cal/mole.

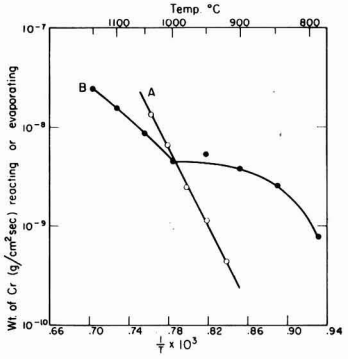

Fig. 10. Comparison rate of evaporation from clean 21.9 Cr-Fe alloy (curve A) with rate of oxidation of 304 stainless steel (curve B), log rate *vs.* $1/T$.

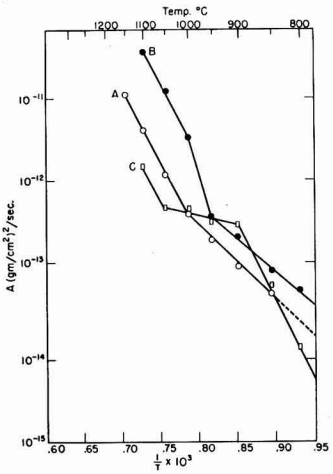

Fig. 11. Oxidation of stainless steel (A), chromium (B), Kanthal A_1 (C). Log *A* vs. 1/*T*.

Comparison with Kanthal Alloy.—Figure 11 shows a comparison of the parabolic rate law constants for Kanthal A_1 and chromium with the posttransition values for 304 stainless steel. Kanthal A_1 shows a transition in the rate of oxidation at 1050°C, 304 stainless steel at 1000°C, and chromium at 950°C. We have related all of these transitions to vapor pressure effects.

Since the aluminum oxide film is nearly impervious to the metal atoms the transition temperature is higher for Kanthal A_1. The effect of the Al_2O_3 film is shown by the nearly constant values for the parabolic rate law constants between 900° and 1050°C.

Aluminum has another favorable influence on the oxidation process. Aluminum in combination with iron and chromium forms oxides which are closely matched to the metal lattice. Thus, γ-Al_2O_3 and $FeAl_2O_4$ are both spinels which match closely the iron-iron spacings in the metal lattice.

Discussion

The effect of aluminum and nickel in chromium iron alloys can be considered from the electron configuration point of view. Aluminum can contribute one 3p electron to the unfilled 3d bands of iron and chromium with the result that aluminum is strongly bonded in the alloy. This is confirmed experimentally by the lowered chemical potential of iron and chromium in the alloy (4). Since nickel has a fraction of a 3d level unfilled, the bonding between nickel and iron and chromium is not as strong as when aluminum is added. Nickel is not expected to lower the chemical activity of iron and chromium to the same extent as aluminum.

Nickel forms a less stable oxide than aluminum. Therefore, solid phase reactions can occur in the oxide (10) which can lower the protective character of the oxide film. Although the initial rates of oxidation of stainless steel are low it would be expected that the oxide composition changes with time. Nickel oxide is also much more readily attacked by chlorides or acid vapors than aluminum oxide.

We conclude that both nickel and aluminum are good alloying elements to add in the chromium-iron series of alloys from a protection and corrosion point of view. The low permeability of the aluminum oxide film to iron and chromium atoms gives an alloy of high heat resistance. Nickel, on the other hand, gives an austenitic alloy of high strength with moderate oxidation resistance.

Manuscript received Oct. 27, 1961; revised manuscript received Feb. 26, 1962. This paper was prepared for delivery before the Los Angeles Meeting, May 6-10, 1962.

Any discussion of this paper will appear in a Discussion Section to be published in the June 1963 JOURNAL.

REFERENCES

1. E. A. Gulbransen and K. F. Andrew, *This Journal*, **104**, 334 (1957).
2. E. A. Gulbransen and K. F. Andrew, *ibid.*, **106**, 294 (1959).
3. E. A. Gulbransen and K. F. Andrew, Westinghouse Research Laboratories Scientific Paper 6-94602-1-P14, Nov. 20, 1957.
4. E. A. Gulbransen and K. F. Andrew, Westinghouse Research Laboratories Scientific Paper 6-94602-1-P20, June, 1958.
5. E. A. Gulbransen, *Trans. Electrochem. Soc.*, **81**, 187 (1942).
6. E. A. Gulbransen, "Advances in Catalysis," Vol. V, pp. 119-175, Academic Press, Inc., New York (1953).
7. E. A. Gulbransen and K. F. Andrew, *This Journal*, **99**, 402 (1952).
8. J. W. Hickman and E. A. Gulbransen, *Trans. Electrochem. Soc.*, **91**, 605 (1947).
9. E. A. Gulbransen, *Anals. N. Y. Acad. Sciences*, **58**, 830 (1954).
10. E. A. Gulbransen and W. R. McMillan, *Industrial and Engineering Chem.*, **45**, 1734 (1953).

Growth of Halide Layers on Copper Single Crystals

A. Goswami

National Chemical Laboratory, Poona, India

ABSTRACT

Structures and orientations of cuprous halides formed on copper (111), (110), and (100) faces by reaction with halogen vapors at room temperature have been studied and the crystal growth process discussed.

Previous electron diffraction studies (1-3) on the growth of oxide or sulfide films on copper single crystals in air or sulfur vapor at various temperatures showed that these films were crystalline and had two-degree orientation with respect to substrate if the substrate temperature was high enough, but were amorphous when formed at room temperature. During the initial stage of their growth, the films consisted of cuprous compounds alone. If the growth continued for a sufficiently long time and the temperature was favorable, the top layers consisted entirely of cupric compounds either with two-degree orientation or in polycrystalline state with or without a preferred orientation. Similar reactions, however, at room temperature with halogen vapors or by anodic treatment in halide solutions, produced, on the other hand, crystalline cuprous halides even when the time of reactions was sufficiently prolonged (4-6). Since there has been little work on the growth of cuprous halide films or on their epitaxial relationship to the substrate a study has been made on single crystals of copper and the results compared with those obtained by anodic treatments.

Experimental

Samples of copper with (111), (110), and (100) faces were prepared by cutting pieces from a single crystal rod, grinding, surfacing with different grades of emery, etching in nitric acid, and finally electropolishing in phosphoric acid in a manner already described in previous papers (1, 7). The diffraction patterns (not shown) from these faces revealed that they were extremely smooth and nearly parallel to (111), (110), and (100) planes of the copper lattice. The samples were then exposed to vapors of iodine or bromine for a few seconds and immediately transferred to an electron diffraction camera (cold cathode type, 60 kv) and examined by the reflection method, in more than one azimuth. The crystals were again treated in halogen vapor and re-examined. Similar studies were also made on polycrystalline copper (spec. pure) disks.

For comparison, these crystals after etching and reelectropolishing were treated anodically (4-6) in KI or KBr solution in the presence of H_2SO_4 for a few seconds to half a minute and the surface layers examined by the diffraction technique in a similar way.

Results

Halide layers formed on copper crystals by progressive reactions with halogen vapors showed various interference colors, *viz.*, brownish orange, pink, golden yellow, etc., depending on the thickness of the layers; they finally became pale yellow accompanied by considerable roughening of the surface.

The diffraction patterns from the halide films generally consisted of spots and faint rings passing through these spots. With the rotation of the copper crystals around an axis normal to the electron beam direction, the spot patterns changed, thus indicating that the halide crystals grew epitaxially on the substrates. In other words, they developed two-degree orientations such that certain planes and axial directions of the halide crystals were parallel, respectively, to the substrate face and to an important direction lying in that face. The ring patterns were due to the formation of polycrystalline material. Arc patterns, which did not change even with the rotation of copper crystals, showed the presence of one-degree orientated halide crystallites which had a common axis parallel to one another or had a common plane, but otherwise were randomly disposed in space. Clarity or sharpness of patterns depended to a large extent on the crystal size. Hence with increase in crystal size the clarity was better. It was also noticed that sometimes with progressive reaction the spot pattern changed and ultimately became confused by the appearance of many new spots, no doubt due to the formation of new crsytals with different orientations.

Measurements of d_{hkl} values from rings as well as spots and also of their relative intensities agree with those of γ-forms of halides alone.

On Cu(111) face.—Cuprous iodide formed on this face yielded diffraction patterns (Fig. 1 and 2) consisting of spots and faint rings, when the electron beam was grazing along the <110> and <112> axes of the crystal, respectively. The appearance of 111

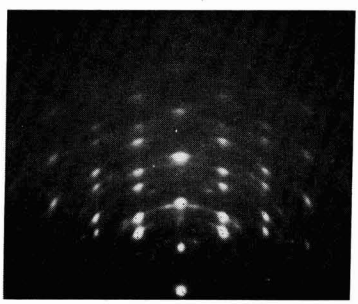

Fig. 1. 2-d {111} orientation of CuI; beam along <110>

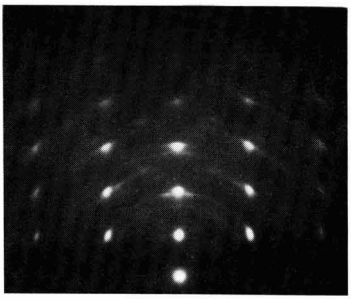

Fig. 2. 2-d {111} orientation of CuI; beam along <211>

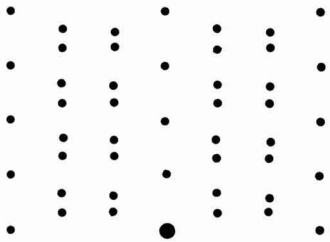

Fig. 3. Theoretical pattern for parallel and antiparallel {111} orientation of CuI; beam along <110> direction.

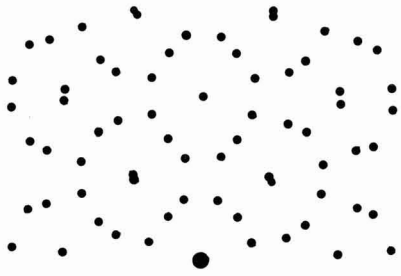

Fig. 4. Theoretical pattern for {115} orientation of CuI; beam along <110> direction.

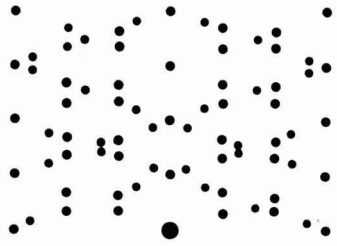

Fig. 5. Fig. 3 and 4 together

reflection and its higher orders in the plane of incidence for all azimuthal rotation of the crystal with respect to the beam, together with the fact that the spot patterns changed with the rotation of the crystal but repeated themselves after every rotation of 60°, clearly showed that the halide crystals grew epitaxially with a {111} orientation. The disposition of spots was such that <112> of cuprous iodide was parallel to <110> of Cu(111). Normally electron diffraction patterns from two-degree {111} oriented crystals would be symmetrical with the beam along <112> axis, and asymmetrical along <110>. The symmetrical nature of the diffraction patterns (Fig. 1 and 2) in both of the azimuths suggested that the deposit crystals consisted of parallel and antiparallel {111} orientations such that the electron beam was grazing along $[1\bar{1}0]$ and $[\bar{1}10]$ directions of the crystals, giving rise to symmetrical patterns. Figure 3 shows the patterns expected from such orientations.

A detailed consideration of the position of spots (Fig. 1), however, shows that a number of reflections (spots), *viz.*, 111 appearing approximately at 40°, 200 at 15°, 220 at 75°, 311 at 10° and 40°, and 422 at 52° from the plane of incidence, cannot be accounted for from Fig. 3. If, on the other hand, the halide crystals developed a two-degree {115} orientation, the positions of the spots are well explained, and also 115 spots would coincide with 333 reflection (spots) in the plane of incidence with the electron beam along <110> of the crystals (Fig. 4). Thus all these spots are well accounted for by the formation of crystals having both {111} and {115} orientations (Fig. 5).

It would seem unlikely, as pointed out before (8), that crystals would grow with an odd plane such as {115} parallel to a simple face such as (111). This orientation, however, could result from a single or multiple twinning process (8-10). Thus if an (111) orientated crystal twinned on its $(11\bar{1})$ plane, it would bring the $(\bar{1}\bar{1}5)$ plane of twinned crystals parallel to the initial (111) plane. In a similar way other orientation would result by multi-twinning process. This also explains the simultaneous presence of {111} and {115} orientated crystals. The faint spots at 1/3 or 2/3 of unit distance along a <111> direction are due to double diffraction as observed in many other cases (1, 10, 11).

Generally {111} oriented halide crystals had their <112> direction parallel to <110> of Cu(111), but sometimes they were azimuthally rotated by 30°, *i.e.*, the crystals grew with parallel orientations such that CuI <110>//Cu <110>.

Cuprous bromide also grew epitaxially in the same way as iodide, but the rate of reaction was much more rapid. The reaction with moist bromine vapor was similar to that for iodine or bromine.

On Cu(110) face.—On a Cu(110) face, dry iodine and bromine vapors formed halides which again developed a two-degree {111} orientation, but with their <110> axes parallel to <100> of Cu(110). Diffraction patterns were similar to Fig. 1 and 2.

In the presence of moist bromine vapor, however, halide crystals developed two-degree mixed {100} + {211} orientations such that $[0\bar{1}1]$ and $[01\bar{1}]$ of each were parallel to $[1\bar{1}0]$ of copper (similar to Fig. 6).

On Cu(100) face.—On a Cu(100) face, surface layers formed by reacting with iodine vapor yielded patterns consisting of spots and rings which became more distinct with increased time of reaction. The centered $\sqrt{2}$ type of rectangular patterns (Fig. 6) with 200 and higher orders of reflection in the plane of incidence, obtained when the electron beam was along the cube axis of the copper crystal, showed that the halide crystals grew epitaxially with {100}

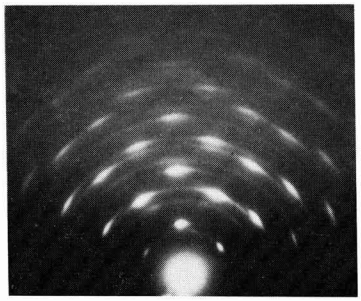

Fig. 6. 2-d {100} orientation of CuI; beam along <110> direction

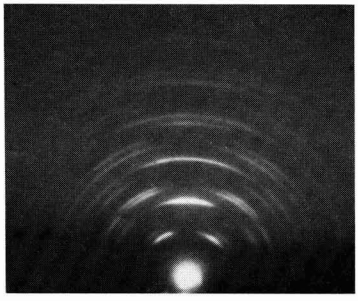

Fig. 7. 1-d {110} orientation of CuI

orientation, but with their axes azimuthally rotated by 45° with respect to the substrate crystal. The slight arcing of spots indicated that the crystals deviated from their mean position by a few degrees. There are indications that crystals had also developed a {111} twinned structure. Exposure to both dry and moist bromine vapors produced similar crystal orientations.

On polycrystalline copper.—The reaction products on polycrystalline copper were polycrystalline in nature, but they sometimes exhibited a strong one-degree {110} orientation (Fig. 7) depending on the time of reaction. The formation of polycrystalline films, even on single crystals, was facilitated with longer time of reaction, and ultimately they developed again a one-degree {110} orientation.

The texture of these crystals was also studied by the electron microscope. The technique used was to expose copper grids (≃400 mesh) to iodine vapor (very low concentration) for 10-16 hr after which time most of these grids were covered with iodide crystals. The growth was heavy and often all the holes in the grids were filled. Under a strong electron beam, the crystals melted quickly, and hence it was often difficult to photograph them in their original shape. The crystals appeared to be flaky, although sometimes needles were also observed (Fig. 8 and 9). By breaking the crystals in a Mickel microshaker it was possible to obtain good micrographs (Fig. 10).

Anodic treatment.—Copper samples treated anodically in bromide or iodide solution also formed cuprous halide crystals with similar orientations, although sometimes the halide crystals were mixed with Cu_2O crystals as reported earlier (5).

The crystal orientations obtained on different faces of copper together with the percentage lattice misfit are shown in Table I.

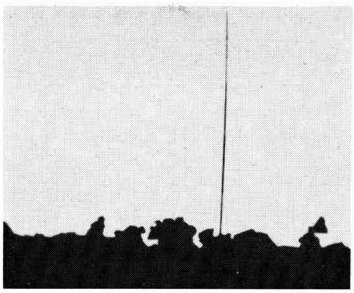

Fig. 8. Needles and flaky nature of CuI. Magnification 3500X

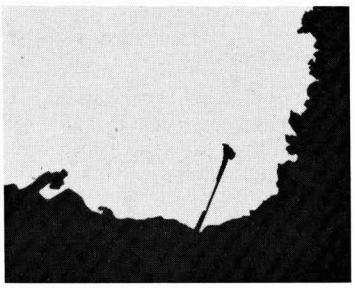

Fig. 9. Needles and flaky nature of CuI. Magnification 3500X

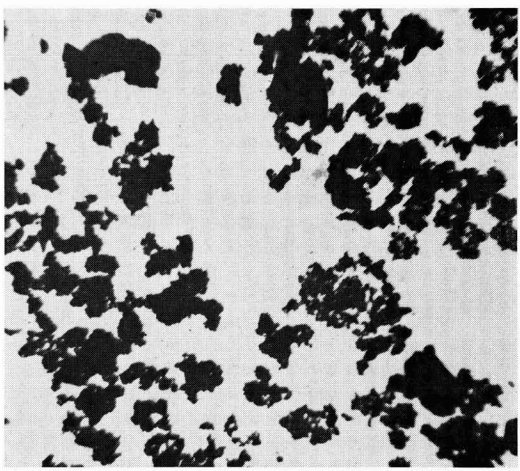

Fig. 10. Flakes of CuI. Magnification 7600X

Discussion

The halide layers formed were always cuprous in type, and no trace of cupric halide was observed. The intensities of all reflections, spot or otherwise, were consistent with the zinc blende type of structures (T^2_d).

It is, however, known that cuprous iodide and bromide exhibit polymorphism (12). The normal γ-forms (cubic $a_o = 6.051$Å and 5.6905Å, respectively, for CuI and CuBr) change to β varieties (h.c.p. $a_o = 4.31$Å, $c_o = 7.09$Å, $c_o/a_o = 1.646$ for CuI at 369°C, and 4.06Å, 6.66Å, 1.625 for CuBr at 430°C) and finally to α modifications ($a_o = 6.15$Å f.c.c. at 407°C for CuI and 4.56Å b.c.c. at 480°C for CuBr). In the present experiments only γ phases were de-

Table I. Orientations of halide films on copper single crystals

Copper substrate Plane	Axis	Orientations of cuprous halides Type	Plane	Axis	% Misfits on copper CuI	CuBr
(111)	<110>	1	(111)	<211>	+3	+9
		2	(111)	<110>	+68 (effective-16)	+57 (effective-21)
(110)	<100>	1	(111)	<110>	+19	+11
(110)	<110>	2	(115)	<110>		
		3	(100)	<100>	+19	+11
(100)	100		(100)	<110>	+19	+11
(111), (110), (100) and Polycrystalline copper			1-d	{110}*		

* 1-d = one-degree orientation.

tected in the top surface layers, although their formation lower down could not be ruled out.

It is thus seen that at room temperature the halides formed on single crystals of copper were crystalline even in very thin layers, whereas cuprous oxide and sulfide were not in that state (1-3). This difference appears to be related to the high mobility of halides which facilitates the epitaxial growth even at room temperature compared to oxide or sulfide (m.p. of CuI, CuBr, Cu_2O, and Cu_2S are 605°, 500°, 1232°, and 1100°C, respectively), since mobility at a particular temperature below the melting point is greater, the lower the melting point (13).

Epitaxially grown halides often developed more than one azimuthal orientation on the same face of a copper crystal (Table I), and hence the tolerable lattice mismatch varied. It is seen that the lattice misfit, which may be defined by $100(b-a)/a$, where a and b are the corresponding lattice spacings in the substrate and deposit, respectively, could be as high as +68% without affecting the epitaxial growth. It has often been suggested in the literature that a good fit is an *a priori* condition for epitaxial growth of crystals. Our work and also that of other (14) clearly shows that crystals can grow epitaxially on the substrate even when there is a considerable misfit and even in cases where the distribution of atoms in the contact planes is very dissimilar, *viz.*, in the development of two-degree {103} and {203} orientations of Cd or {205} and {101} of Zn on Cu(110) and (100) faces (4) and {100}, {203}, etc., of Zn on (100) of NaCl (15). It may only be said that the lower the lattice misfit, the greater is the probability that the deposit will grow thicker while remaining epitaxial. It may be pointed out here that when the lattice misfit is more than 50%, the effective mismatch is much less since the spacing between 2 or 3 atoms of one is often nearly equal to that of 3 and 4 of the other. Thus a misfit of +68% of CuI on Cu(111) is nearly equal to −16% (effective) (Table I).

The change of crystals from a two-degree orientation type to polycrystalline but random, and finally to a one-degree orientated type showed that the orientation of the surface layers was gradually changing with the reaction time. This appears to be related to the migration of copper ions from inside in an outward direction to react with halogen ions (atomic radius of $Cu^{1+} = 0.96$Å, $Br^{1-} = 1.96$Å), as in the case of the growth of Cu_2O and CuO layers (1). An alternate suggestion that the halides grow by the diffusion of halogen ions inward to the copper surface may not be ruled out completely, although their ionic sizes are unfavorable. Preferential grain boundary diffusion may however facilitate a process of this kind.

Acknowledgment

The author is thankful to Dr. M. K. Gharpurey for taking the electron micrographs.

Manuscript received June 19, 1961; revised manuscript received March 26, 1962. This is Communication No. 456 from the National Chemical Laboratory, Poona, India.

Any discussion of this paper will appear in a Discussion Section to be published in the June 1963 JOURNAL.

REFERENCES

1. A. Goswami and Y. N. Trehan, *Trans. Faraday Soc.*, **52**, 358 (1956); **54**, 1703 (1958).
2. K. Leu, Ph.D. Thesis, London University (1951).
3. Y. N. Trehan and A. Goswami, *Trans. Faraday Soc.*, **55**, 2162 (1959).
4. A. Goswami, Ph.D. Thesis, London University (1950).
5. A. Goswami, *Proc. Phys. Soc.*, **69B**, 583 (1956).
6. I. H. Usmani, *Phil. Mag.*, **32**, 89 (1941).
7. D. M. Evans, *et al.*, *Proc. Roy. Soc.*, **205A**, 17 (1951).
8. A. Goswami, *J. sci. & ind. Res.*, **13B**, 677 (1954); **15B**, 322 (1956).
9. Y. N. Trehan and A. Goswami, *Proc. Nat. Inst. Sci. (Ind)*, **25A**, 210 (1959).
10. A. Goswami, *Trans. Faraday Soc.*, **54**, 821 (1958).
11. A. Goswami, *J. Sci. indust. Res.*, **17B**, 133 (1958).
12. A.S.T.M. Card No. 6-0246, 0685, 0623, 0292, 0700, 0310.
13. D. M. Evans and H. Wilman, *Acta Cryst.*, **5**, 731 (1954).
14. D. W. Pashley, *Phil. Mag. Suppl.*, **5**, 173 (1956).
15. D. M. Evans, Ph.D. Thesis, London University (1950).

Manganese-Activated Cadmium Pyrophosphate Phosphors

R. C. Ropp

Chemical and Metallurgical Division, Sylvania Electric Products Inc., Towanda, Pennsylvania

ABSTRACT

The effects of preparation on absorption and excitation properties have demonstrated that $Cd_2P_2O_7$:Mn is a host-sensitized phosphor whose efficiency to 2537Å becomes appreciable only when a step involving refiring in a reducing atmosphere is employed. The experimental data allow an insight into the nature of the luminescent center in $Cd_2P_2O_7$:Mn.

The combination of manganese with cadmium phosphates to form luminescent systems is by no means new, and many authors have reported on such phosphors. $Cd_2P_2O_7$:Mn was described by Williams (1) as an efficient cathode-ray excitable phosphor. Fonda (2) described tribasic cadmium orthophosphate phosphors activated by manganese. Other investigators have described various modifications of the cadmium phosphate phosphors including fluorophosphate doubly activated by Pb and Mn (3, 4). Smith and Power (5), as well as Zelinskii *et al.* (6), described tribasic cadmium and zinc orthophosphates. The references to cadmium chlorophosphate phosphors are too numerous to mention. However, none of these authors recognized the effect of reduction on excitation properties, particularly for $Cd_2P_2O_7$:Mn.

The present work will describe a phenomenon whereby reduction of the matrix produces host-sensitization in $Cd_2P_2O_7$:Mn. A model will be postulated to show the nature of the luminescent center and the absorption properties as a function of preparation.

Method of Preparation and Measurement

The phosphors were easily prepared according to the following reactions:

1. $2CdNH_4PO_4 \cdot H_2O + 0.04\ MnNH_4PO_4 \cdot H_2O \xrightarrow{\Delta} Cd_2(P_2O_7)_{1.02}:Mn_{0.04} + 2.04NH_3 + 3.06\ H_2O$
2. $2CdNH_4PO_4 \cdot H_2O + CdO_2 + 0.04\ MnNH_4PO_4 \cdot H_2O \xrightarrow{\Delta} Cd_3(PO_4)_{2.04}:Mn_{0.04} + 2.04\ NH_3 + 3.06\ H_2O + 0.49\ O_2$

One could prepare $Cd_2P_2O_7$:Mn and $Cd_3(PO_4)_2$:Mn and refire with a volatile chloride to form cadmium chloroapatite:

3. $3Cd_3(PO_4)_2:Mn + CdCl_2 \xrightarrow{\Delta} 2\ Cd_5Cl(PO_4)_3:Mn$
4. $3Cd_2P_2O_7:Mn + xCdCl_2 \xrightarrow{\Delta} 2Cd_{3+0.5x}\ Cl(PO_4)_3:Mn + (X-1)Cl_2$

The use of HCl gas as a firing atmosphere enabled a further clarification of the gross reactions:

5. $Cd_3(PO_4)_2:Mn + 2HCl \xrightarrow{\Delta} Cd_2P_2O_7:Mn + CdCl_2 + H_2O$
6. $Cd_2P_2O_7:Mn + HCl \xrightarrow{\Delta}$ no change
7. $3CdNH_4PO_4 \cdot H_2O + 2CdO_2 + HCl \xrightarrow{\Delta} Cd_5Cl(PO_4)_3 + 3NH_3 + O_2 + 5H_2O$

Thus, $Cd_2P_2O_7$ was the stable structure once the matrix was formed in the absence of halogen. The apatite was stable otherwise.

Considerable effort was made to obtain $CdNH_4PO_4 \cdot H_2O$ and not $Cd_5H_2(PO_4)_4(H_2O)_4$ (7). The former gave a nearly stoichiometric $Cd_2P_2O_7$, whereas the latter gave $Cd_3(PO_4)_2 \cdot Cd_2P_2O_7$, a product containing 1.25 Cd atoms per 1.00 P atom. The similarity in x-ray diffraction patterns may lead to mistaken identity, particularly for mixtures containing small amounts of $Cd_5H_2(PO_4)_4(H_2O)_4$.

Manganese may be added to the phosphor mix in several forms, but was best added as $MnNH_4PO_4 \cdot H_2O$. CdO_2 (8) was preferred because of the ease in obtaining a purified material of high reactivity which gave a product of specific composition (CdO) when heated.

Measurements followed those described in a previous paper (9).

Experimental Results

Phosphors efficient to 2537Å irradiation were produced by prefiring in air to form the matrix and refiring in a reducing atmosphere. These results are shown in Table I. Note that refiring in a reducing atmosphere markedly improved the plaque response, but that refiring in air or N_2 did not. Thus, the effect could not be attributed to refiring alone, but to the combination. Prefiring in N_2-H_2 (40%) gave a black inert mass. The effect of firing atmosphere was pronounced, particularly for the pyrophosphate. If $Cd_2P_2O_7$:Mn was refired in HCl, bright phosphors were obtained, but in the case of $Cd_3(PO_4)_2$:Mn, HCl converted it to $Cd_2P_2O_7$:Mn according to reaction 5.

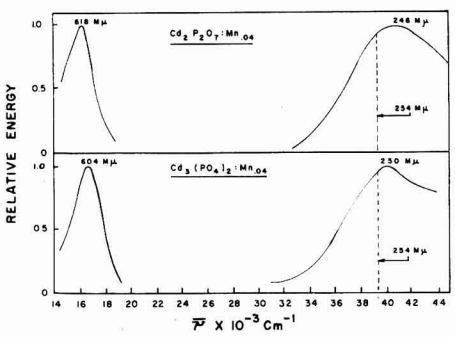

Fig. 1. Spectral properties of some cadmium phosphate phosphors

Table I. Effect of refiring

Nominal phosphor composition	Atmosphere: Prefiring	Atmosphere: Refiring	X-ray structure	Lum. color (2537Å excit.)	% Red plaque (vs. Cd borate std.)
$Cd_3(PO_4)_{2.10}:Mn_{0.04}$	Air	—	$Cd_3(PO_4)_2$	Dull pink	10
	N_2	—	$Cd_3(PO_4)_2$	Dull pink	19
	Air	Air	$Cd_3(PO_4)_2$	Dull pink	18
	HCl	—	Apatite	Bright orange	83
	Air	N_2	$Cd_3(PO_4)_2$	Dull pink	15
	Air	HCl	$Cd_2P_2O_7$	Bright red	67
	Air	N_2-H_2 (40%)	$Cd_3(PO_4)_2$	Dull pink	35
$Cd_2(P_2O_7)_{1.02}:Mn_{0.04}$	Air	—	$Cd_2P_2O_7$	Dull pink	15
	N_2	—	$Cd_2P_2O_7$	Dull pink	9
	HCl	—	Apatite	Orange	70
	Air	Air	$Cd_2P_2O_7$	Dull pink	20
	Air	HCl	$Cd_2P_2O_7$	Bright red	52
	Air	N_2	$Cd_2P_2O_7$	Dull pink	22
	Air	N_2-H_2 (40%)	$Cd_2P_2O_7$	Bright red	51

The emission properties of these phosphors were identical to those presented by previous authors (1, 4) for cathode-ray excitation (see Fig. 1). It was in the excitation and absorption spectra that differences were observed. Since $Cd_2P_2O_7$:Mn was by far the more efficient, the present discussion will be limited to this phosphor.

Effect of firing atmosphere.—Measurement of the excitation bands as a function of preparation is given in Fig. 2 for the $Cd_2P_2O_7$:Mn phosphors shown in Table I. (The discontinuity in the curves is the result of increasing the instrument gain at 34.0 x 10^3 cm^{-1} before proceeding to the lower energy absorption peaks.) When prefired under oxidizing or neutral conditions (air or N_2), the excitation band peaked at 2370Å and was relatively narrow, whereas on refiring under reducing conditions (N_2-20% H_2), the peak wavelength shifted to 2460Å and the 2537Å response increased markedly. The effect was not due to refiring alone since the phosphor refired in N_2 only did not change in its excitation spectrum. All spectra, and particularly the reduced phosphor spectrum, showed evidence of low level excitation spectra composed of several narrow bands in the near-ultraviolet and visible regions in addition to the broad excitation band in the higher energy region. The former have been termed edge-absorption bands (10), due to Mn^{+2}.

Figure 3 shows the spectral properties of $Ca_2P_2O_7$:Mn and $Sr_2P_2O_7$:Mn. Although these phosphors were previously said to be excited only by cathode rays (11), further reduction produced some excitation bands in the near-ultraviolet. $Zn_2P_2O_7$, $Mg_2P_2O_7$, and $Ba_2P_2O_7$, by contrast, were not found to form ultraviolet excitable phosphors even when the matrix was refired repeatedly in a reducing atmosphere. The excitation bands in $Ca_2P_2O_7$:Mn and $Sr_2P_2O_7$:Mn phosphors are due directly to energy absorption in the Mn^{+2} activator center and may be compared to the Mn^{+2} absorption bands in known phosphors such as Zn_2SiO_4:Mn^{+2} (10).

Effect of manganese.—Variation of manganese changed the relative response to 2537Å radiation, but did not shift the emission peak wavelength of $Cd_2P_2O_7$:Mn from 6180Å.

The relative plaque brightness as a function of Mn content and firing is given in Fig. 4. Note the large change in response on reduction of the preformed matrix. The plaque response to 2537Å irradiation increases to 8 mole % Mn, remains essentially constant to 20 mole % Mn and decreases beyond that

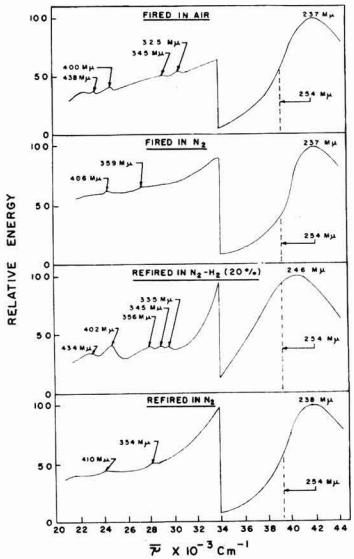

Fig. 2. Effect of firing atmosphere on excitation spectra of $Cd_2P_2O_7$:$Mn_{.04}$ phosphor.

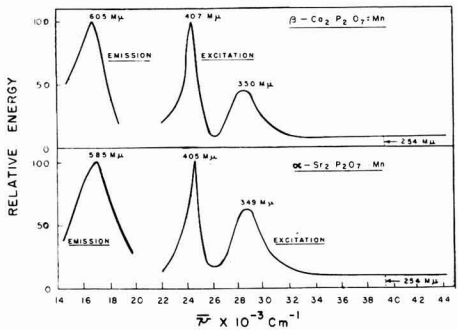

Fig. 3. Spectral properties of manganese-activated alkaline-earth pyrophosphates.

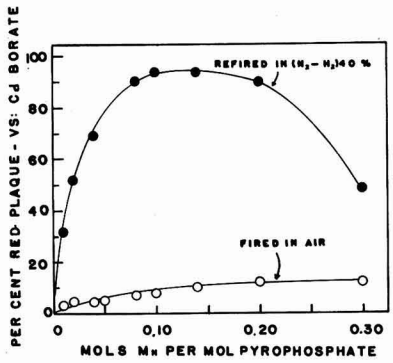

Fig. 4. Effect of manganese concentration on efficiency of $Cd_2P_2O_7$:Mn phosphor.

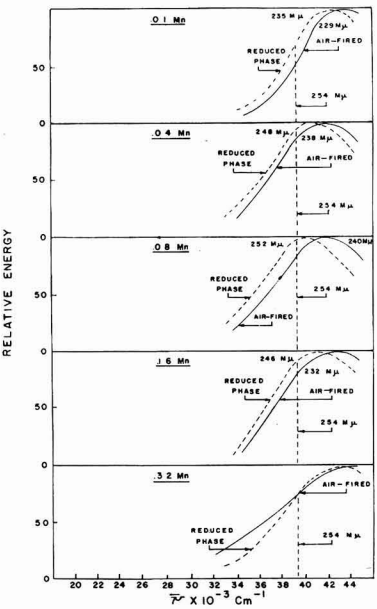

Fig. 5. Excitation spectra as a function of preparation conditions

concentration. It was further instructive to determine the effect of preparation atmosphere as a function of manganese on excitation spectra (see Fig. 5). In all cases, the excitation peaks are shifted toward lower energy by the reduction step and, in addition, these peaks shift with Mn content. However, when a concentration of 0.32 mole Mn is reached, a decided decrease in brightness was noted as reflected in the change in excitation spectra. The shift of peak wave number due to reduction was approximately constant irrespective of Mn content.

In order to establish that Mn was the primary activator, an analysis was made of the components and phosphor (see Table II). No other elements were present.

Reversibility.—The effect of reduction on response to 2537Å was reversible, and a phosphor which was efficiently excited lost brightness when reheated in air. This effect was a function of Mn content. One could heat and reheat the phosphor $Cd_2P_2O_7$:Mn alternately in an oxidizing or reducing atmosphere and change the response to 2537Å radiation providing the sintering point was not reached with consequent degradation of the structure.

Table II. Spectrographic analysis of components

	Impurities in ppm (Spec. Qual.)									
	Mn	Ca	Mg	Cu	Fe	Ni	Sn	Sr	Al	Si
$Cd_2P_2O_7$:Mn	29,600	500	—	0.5	5	5	50	50	—	—*
$CdNH_4PO_4 \cdot H_2O$	0.5	500	50	0.5	5	—	—	—	5	5
$Cd_2P_2O_7$	0.5	500	50	0.5	5	—	—	—	5	50*

* Fired in a silica crucible.

Unactivated $Cd_2P_2O_7$.—If $Cd_2P_2O_7$ was formed from $CdNH_4PO_4 \cdot H_2O$ by prefiring at 1800°F in air and then subjected to refiring in a 40% H_2-60% N_2 atmosphere, a phosphor was produced as shown in Fig. 6. Although the brightness was low under 2537Å excitation, the phosphor responded to the higher energy wavelengths. Chemical analysis of the Mn present in this phosphor gave a value of <0.0001% or 1 ppm. Note that the absorption band is similar to the excitation band.

The matrix, $Cd_2P_2O_7$, exclusive of Mn^{+2}, possessed a high-energy excitation band. This is the fundamental absorption band for the matrix. The incorporation of Mn^{+2} into $Cd_2P_2O_7$ to form $Cd_2P_2O_7$:Mn did not change the fundamental absorption band, as shown in Fig. 7. The absorption or excitation band shifted with reduction, when Mn was present, to a greater

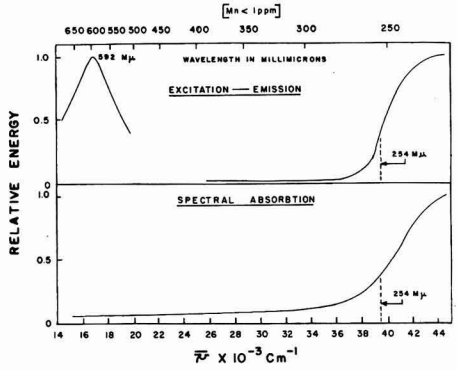

Fig. 6. Spectral properties of unactivated $Cd_2P_2O_7$

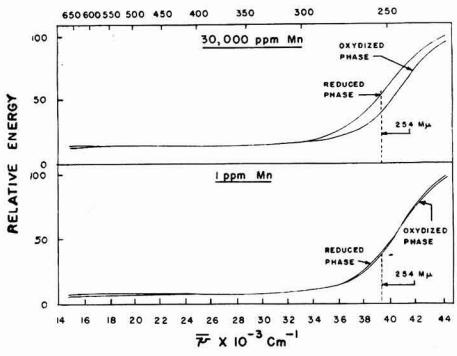

Fig. 7. Spectral absorption of $Cd_2P_2O_7$:Mn phosphor

extent than in its absence. The position of the excitation band also changed as a function of the Mn content and the shift was accentuated by reduction of the matrix (see Fig. 5). Reduction of the matrix increased the 2537Å absorption markedly in the phosphor containing 30,000 ppm Mn, but little in that containing 1 ppm Mn. In contrast, the matrices, $Ca_2P_2O_7$ and $Sr_2P_2O_7$, did not possess the broad excitation band (Fig. 3) at the higher energies (~2250Å), and therefore incorporation of Mn^{+2} did not produce 2537Å excitable phosphors.

Mn^{+2} as a luminescent center.—The spectroscopic functions of Mn^{+2} are well known. The ground state is $^6S_{5/2}$ and the four excited states are $^4G_{5/2}$, $^4D_{5/2}$, $^4P_{5/2}$, $^4F_{5/2}$, in order of ascending energy, for the free ion. In the presence of a crystal field, a d^5 ion such as Mn^{+2} has the symmetry $^6A_{1g}$ in a weak octahedral field. The configuration d^5 is exceptional in that no spin-allowed transitions are to be expected, since the ^6S ground state is not split significantly by the field (12), whereas the excited states are split, depending on the strength of the field. Weak absorptions are expected corresponding to the sextet-quartet transitions. It is generally accepted that yellow to red emission is indicative of Mn^{+2} in an octahedral site, whereas green emission is associated with Mn^{+2} in a tetrahedral site. However, in the absence of specific structure data for $Cd_2P_2O_7$, such an assumption would be illusory since the determination of the effect of crystalline field on the luminescent processes of Mn^{+2} presupposes a knowledge of site symmetry.

A long decay is characteristic of Mn^{+2} emission and probably arises from the spectroscopically forbidden transition, $^4G \rightarrow {}^6S$. Since $Cd_2P_2O_7$:Mn also possesses a long decay, it is logical to assume that the energy transition is identical since the emission is typical of Mn^{+2} as an activator. Coupled with the marked similarity in diffraction pattern between $Mn_2P_2O_7$ and $Cd_2P_2O_7$ (of which there is but one structure each), the data indicate that the luminescent center is composed of Mn^{+2} in a cationic site.

Discussion

The specific effect of reduction is difficult to assess since there are several end-results which could be attributed to reduction. Before discussing these, it would be well to summarize the observations made:

1. The matrix $Cd_2P_2O_7$, exclusive of Mn^{+2}, possessed a high-energy, stimulable excitation band. This is the fundamental absorption band for the matrix. The incorporation of Mn^{+2} into $Cd_2P_2O_7$ to form $Cd_2P_2O_7$:Mn did not change the fundamental absorption band, although a shift was observed with Mn content.

2. The equivalence between the absorption-excitation band of $Cd_2P_2O_7$ and the high-energy excitation band of $Cd_2P_2O_7$:Mn leads to the conclusion that $Cd_2P_2O_7$:Mn is a host-sensitized phosphor in which matrix absorption of radiant energy precedes fluorescence.

3. $Ca_2P_2O_7$:Mn and $Sr_2P_2O_7$:Mn are not host-sensitized. The excitation peaks are due to transitions in the Mn^{+2} activator.

4. Reduction of the matrix following formation shifts the excitation peak wave number to lower energy. Absorption bands due to Mn^{+2} are also observed.

5. The shift in peak wave number due to reduction is obtained only in the presence of manganese and is constant at each Mn^{+2} content.

6. The position of the excitation band is dependent both on Mn^{+2} content and reduction.

The logical conclusion to be drawn is that reduction simply increases the manganous ion concentration which causes a shift of the host lattice absorption edge. This explanation was first demonstrated for willemite by Kroeger (10). The data in Fig. 4 and Fig. 5 and observations 5 and 6 are thus explained. A relevant extension of this conclusion would include the role of the matrix, particularly since the host-lattice absorption edge is involved and since the experimental data indicate that host sensitization takes place. It is unlikely that the broad absorption band can be attributed to the manganese center alone.

If the effect were due entirely to the presence and number of Mn^{+2} activator centers, then one would expect the broad absorption band to be due to (*a*) the manganese center, or (*b*) the manganese center as affected by the lattice, that is, a manganese-lattice interaction. However, the broad absorption band cannot be due to transitions in the Mn^{+2} atom itself because of the edge absorption bands observed in the same spectra (Fig. 2), which are comparable to those of Mn^{+2} in $Ca_2P_2O_7$:Mn and $Sr_2P_2O_7$:Mn. Therefore, the possibility remained that the effect could be caused by an increase in the number of Mn^{+2} centers as well as an increase in the host-lattice coupling. This would give rise to a band whose width would increase or decrease with temperature.

One would then expect in the case of the comparable $Ca_2P_2O_7$:Mn and $Sr_2P_2O_7$:Mn phosphors that reduction should cause the appearance of a broad high-energy excitable band denoting that the effect of reduction was to increase the lattice-coupling of the Mn^{+2} center with its lattice surrounding. Although the position of this broad absorption peak would not be expected to be exactly at the same energy in $Ca_2P_2O_7$ or $Sr_2P_2O_7$, it should be close if the broad absorption band did arise only from the Mn^{+2} center, and not from the matrix, as in $Cd_2P_2O_7$:Mn.

Since it has been demonstrated that reduction does not result in broad absorption bands in these other phosphors, but only narrow bands directly attributable to Mn^{+2}, one can conclude that absorption is a function of both Mn content and reduction, but only in the presence of cadmium. Thus, it is probable that absorption by the matrix is involved rather than absorption in the manganese centers alone, and that host-sensitization occurs (observations 1 and 2).

One is then left with the conclusion that reduction affects both the matrix and the activator, Mn^{+2}. The effect cannot be chemical in nature since only changes in optical spectra are observed and no chemical changes were noted in the materials so treated, as determined by x-ray and infrared analysis.

Since reduction has an effect on the lattice as determined by absorption measurements, it is, perhaps, more logical to assume that the effect is electronic in

Table III. Spectroscopic levels for various ions

Atomic species	No. of Electrons	Transition	State Ground	State Excited
Mn III	23	$3d^5 \leftrightarrow 3d^4 3d^*$	$^6S_{5/2}$	$\leftrightarrow {}^4G_{5/2}$
Cd III	46	$4d^{10} \leftrightarrow 4d^9 4d^*$	$^1S_0$	$\leftrightarrow {}^3D_1$
Cd II	47	$4d^{10} \leftrightarrow 4d^{10} 5p^*$	$^2S_{1/2}$	$\leftrightarrow {}^2P_{3/2}$
Sb IV	48	$4d^{10}5s^2 \leftrightarrow 4d^{10}5s5p^*$	$^1S_0$	$\leftrightarrow {}^3P_1$
Sn III	48	$4d^{10}5s^2 \leftrightarrow 4d^{10}5s5p^*$	$^1S_0$	$\leftrightarrow {}^3P_1$
Pb III	80	$5d^{10}6s^2 \leftrightarrow 5d^{10}6s6p^*$	$^1S_0$	$\leftrightarrow {}^3P_1$
Tl II	80	$5d^{10}6s^2 \leftrightarrow 5d^{10}6s6p^*$	$^1S_0$	$\leftrightarrow {}^3P_1$

* Excited state.

nature. Since host-sensitization requires transport of energy by other than movement of charge, a study of energy transport processes within the crystal is applicable.

The theory of impurity-sensitized luminescence as developed by Dexter (13), and independently by Botden (14), is applicable to the present case. Impurity-sensitized luminescence refers to the luminescence mechanism whereby energy is absorbed in one type of center (the sensitizer) and emission occurs in a different type of center (the activator). The mechanisms involved in the transport and transfer of excitation energy from the absorbing to the emitting center are of particular concern.

For the $Cd_2P_2O_7$:Mn system, it is interesting to compare the electronic spectroscopic transitions which may be involved. These data are given in Table III, taken from ref. (15).

The last four species in Table III represent mercury-like ions which are known sensitizers as shown by Williams (16) and Seitz (17). In regard to the Cd III species, note that the transition to the excited state is a spin forbidden transition much like that of the activator center (Mn III). The electronic $d^{10}s$ configuration of the cadmium II species is similar to that of known sensitizers and involves a spectroscopically allowed transition. Thus, the effect of reduction could be assigned to the localization of an electron in the vicinity of a Cd^{+2} atom to form the spectroscopic species, Cd II:

$$Cd^{+2} + e^- \rightarrow (Cd)^+$$

This equation is meant to imply that an electronic defect exists which utilizes the modified energy levels of the ion. Thus, the presence of Cd^+ could lead to sensitization as proposed in Table IV. The resonance-exchange mechanism is applicable for the Cd^+ (II) species, but exchange would not be expected to occur between Cd^{+2} sites, since it is recognized that the strength of an electric quadrupole (qq) transition is weaker by a factor of 10^{-7} than that of an electric dipole (dd) transition (12). Thus, for the propagation of energy in both the oxidized and reduced phosphors, the following mechanism is possible as shown in Table IV. (The double-headed arrows denote the resonance exchange mechanism.)

Theoretically, one would expect, for Cd^{+2}, a very weak interaction only at nearest-neighbor sites between cadmium and manganese atoms, and the corresponding luminescent efficiency should be very low as is observed experimentally. In the reduced form, Cd^+(II), the transitions are allowed (S → P), and therefore the response to excitation should be much higher.

The formation of such a species is not entirely without basis since it is well known that x-ray irradiation of alkali halide crystals containing Ca^{++}, Sr^{++}, or Ba^{++} distributed in the cationic sites will form so-called Z centers, which, according to Seitz (18), involve electrons trapped by the alkaline-earth ions at the cationic sites. The spectral characteristics of these centers are comparable to the free Ca^+, Sr^+, or Ba^+ ions. Furthermore, Lushchik and Lushchik (19) have studied the absorption excitation and emission spectra of various homologous ions in alkali halides which included Cd^+.

The shift in absorption peak due to reduction is attributed to formation of the Cd^+(II) species, and the dependence of peak absorption energy on manganese content is attributed to formation of Cd^+(II)-Mn^{+2} pairs. It is unfortunate that specific structure data are not available so that a more quantitative estimate could be obtained of the luminescent center.

It is apparent that reduction has an effect on the energy gap of $Cd_2P_2O_7$, and a possible explanation would be the injection of carriers in the valence band with consequent effects on resistivities as well as excitation energies. Perhaps photoconductive or Hall-coefficient measurements might clarify this matter.

Acknowledgment

The author is indebted to Dr. C. W. W. Hoffman for x-ray measurements, to H. D. Layman and J. E. Webster for some of the preparations, and to Dr. J. S. Smith for valuable discussions.

Manuscript received May 26, 1961; final revised manuscript received March 16, 1962. This paper was prepared for delivery before the Chicago Meeting, May 1-5, 1960.

Any discussion of this paper will appear in a Discussion Section to be published in the June 1963 JOURNAL.

REFERENCES

1. F. E. Williams, U.S.Pat. 2,463,449 (1949).
2. G. R. Fonda, U.S. Pat. 2,605,227 (1952).
3. R. W. Wollentin, U.S. Pat. 2,865,863 (1958).
4. N. A. Gorbacheva, *Zhur. Eksptl. Teoret. Fiz.*, **21**, 305 (1951).

Table IV. Mechanism of energy transfer in $Cd_2P_2O_7$:Mn phosphor

Oxidized form

(a) $E_1 + Cd^{+2} \rightarrow (Cd^{+2})^* \xleftarrow[(10^{-7})]{(qq)}$

$Mn^{+2} \rightarrow (Mn^{+2})^* \rightarrow Mn^{+2} + E_2$

Reduced form

(b) $E_1 + Cd^+ \rightarrow (Cd^+)^* \xleftarrow[(10^4)]{(dd)}$ $(Cd^+)^* \xrightarrow{(dq)}$

5. A. L. Smith and A. D. Power, *This Journal*, **101**, 244 (1954).
6. V. V. Zelenskii, F. M. Pekerman, T. V. Timofeeva, and B. I. Vainberg, *Zhur. Eksptl. Teoret. Fiz.*, **20**, 395 (1950).
7. R. C. Ropp and R. W. Mooney, *J. Am. Chem. Soc.*, **82**, 4848 (1960).
8. C. W. W. Hoffman and R. C. Ropp, *ibid.*, **81**, 3830 (1959).
9. R. C. Ropp and R. W. Mooney, *This Journal*, **107**, 15 (1960).
10. F. A. Kroeger, "Some Aspects of the Luminescence of Solids," Elsevier Publishing Co., New York (1948).
11. E. Nakano and K. Takagi, *Nippon Kagaku Zasshi*, **78**, 1146 (1957).
12. L. E. Orgel, *J. Chem. Phys.*, **23**, 1004 (1955).
13. D. L. Dexter, *ibid.*, **21**, 836 (1953).
14. T. P. J. Botden, *Philips Research Repts.*, **7**, 197 (1952).
15. Circular 467, "Atomic Energy Levels," National Bureau of Stds., U.S. Dept. Commerce, U.S. Gov't Printing Office, Washington, D. C. (1958).
16. F. E. Williams, *J. Chem. Phys.*, **19**, 457 (1952).
17. F. Seitz, *ibid.*, **6**, 150 (1938).
18. F. Seitz, *Phys. Rev.*, **83**, 134 (1951).
19. N. E. Lushchik and Ch. B. Lushchik, *Optika i Spektroskopiya*, **8**, 839 (1960).

The Interface between Germanium and a Purified Neutral Electrolyte

W. H. Brattain and P. J. Boddy

Bell Telephone Laboratories, Murray Hill, New Jersey

ABSTRACT

Measurement of the differential capacity of the interface between germanium (100) and M/10 K_2SO_4, phosphate buffered to pH 7.4, yields data indicating that only the capacity of the semiconductor space charge region is observed. Analysis of the data yields the simple relationship for distribution of potential

$$\psi_s - \frac{kT}{e} \ln \lambda = V_E + K$$

where K is a constant for a given condition at the interface. Surface recombination velocity is found to be close to zero. This, coupled with the absence of capacity additional to the space charge region, indicates the absence of fast surface states under these conditions. Measurement of the surface conductivity of germanium as a function of surface potential does not agree with theory but is reproducible.

Measurements of the electrical properties of germanium surfaces in gaseous ambients have shown a marked dependence of these properties on the immediate history of the sample and the nature of the ambient. It is inferred that the variations are due either to trace impurities deposited on the surface during etching (1) or other cleaning and handling procedures, interaction with the ambient (2), or to physical defects in the surface (*e.g.*, emerging dislocations, steps, etc.) developed in different ways by different chemical environments. The variation in the observations precludes the interpretation that the properties are entirely those of the surface of a single crystal of germanium *per se*.

The object of the present work was to seek relationships between the chemical and electrical properties of such surfaces.

Recent investigations of the semiconductor solution interface have yielded detailed information on the electrical properties of both zinc oxide (3) and silicon (4). To the present time, with the exception of the work of Bohnenkamp and Engell (5), the potentially fruitful area of the germanium-electrolyte interface has been little studied from this point of view, although the basic electrochemistry of germanium is fairly well understood (6).

This paper describes some initial experiments on the electrical properties of germanium surfaces in contact with aqueous solutions. It has been found that in a properly purified solution of K_2SO_4 a germanium surface can be obtained free of fast surface states, *i.e.*, having no additional capacity over that of the space charge layer and no measurable decay of added carriers over and above body recombination.

Experimental

General.—The experiments were conducted in a Pyrex glass cell (shown schematically in Fig. 1) consisting of two compartments separated by a salt bridge containing a porous plug. The larger compartment contained the germanium electrode, which was connected to ground, and two large area plati-

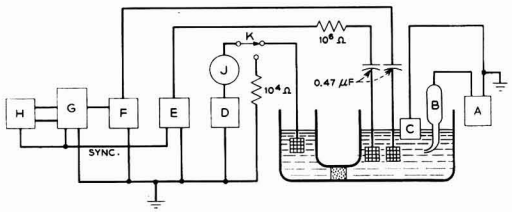

Fig. 1. Experimental arrangement: A, high impedance millivoltmeter; B, calomel electrode; C, germanium electrode; D, high impedance current source; E, pulsed voltage source; F, preamplifier; G, oscilloscope; H, exponential generator; J, ammeter; K, switch.

num gauze electrodes connected to external circuits through 0.47 μfd capacitors. A calomel electrode was connected through a second salt bridge and the germanium electrode potential measured on a high impedance (2 x 10^9 ohm) millivoltmeter. Stirring was achieved either by rotating the germanium electrode, or by means of a magnetically operated, Teflon enclosed stirring bar in the solution. The other compartment contained a third large area platinum gauze electrode connected directly through a high-impedance current source to ground. The atmosphere above the solution was purified nitrogen or helium. Provision was made for illuminating the germanium electrodes through windows set into the bottom and side of the cell, but unless otherwise stated the experiments were carried out in the dark. The temperature throughout was close to 25°C.

Electrodes.—Germanium electrodes were of two types. The simpler ones were either square (1-2.5 cm on a side) or circular (1 cm diameter) in cross section and 1-2 cm thick. Electrical contact was made either by rhodium plating one face and holding the electrode by vacuum onto a stainless steel chuck or by attaching a platinum wire with a solder containing indium. In the latter case the platinum wire was pulled through a glass tube until the back of the electrode was firmly against the end of the tube, which was then filled with paraffin wax which had been boiled for several days in 1M H_2SO_4, 1M KOH, and finally several changes of distilled water. The electrodes were not masked. To ensure a constant superficial area exposed to the solution for a given electrode in different experiments the following procedure was used. The adjustable electrode holder was lowered into the solution until contact was made, and by visual inspection the lower surface of the electrode was aligned with the solution surface. The electrode was then lowered an arbitrary 0.19 cm further into the solution.

The second type of electrode was more complex and requires special description. It takes the form

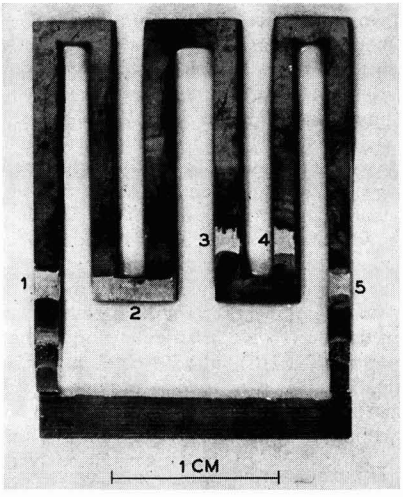

Fig. 2a. Germanium bridge. The scale is in centimeters

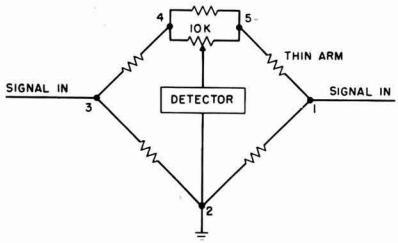

Fig. 2b. Electrical schematic of germanium bridge

of a bridge cut from a slice of single crystal germanium and is illustrated in Fig. 2a and shown schematically in Fig. 2b. The bridge had five contacts, the active arm being between 1 and 5. The other arms, which were much thicker, were not etched, their surfaces being left in a lapped or sandblasted condition making them insensitive to ambient changes. Contact to the bridge was by means of soldered platinum wires. During an experiment the thin portion of arm 1-5 was completely immersed, contacts 1 and 5, however, being kept out of the solution. The major advantage of the bridge is that it is internally temperature compensated provided there are no temperature differences in the bridge itself.

The arms were designed so that if either d-c or a-c power was applied between 1 and 3 a detector would read null between 2 and some point (x) between 4 and 5. This point was determined by adjustment of a calibrated 10,000 ohm Helipot connected between 4 and 5.

The condition for balance is

$$R_{12}R_{23}^{-1} = R_{1x}R_{x3}^{-1} = \beta \qquad [1]$$

where R_{12} is the resistance between contacts 1 and 2, etc. The added surface conductivity, $\overline{\Delta G}$, in the thin arm as defined by Brattain and Garrett (14) is

$$\overline{\Delta G} = (1 + \beta)wt(X_m - X)R_{45}(2e\mu_p\rho\mathcal{L}n_i(w + t)R_{15})^{-1} \qquad [2]$$

where X_m is the fractional helipot reading for minimum conductivity, X is the fractional reading at a point where $\overline{\Delta G}$ is to be evaluated, μ_p is hole mobility, ρ specific resistance, e electronic charge, $\mathcal{L}$ the Debye length, n_i the concentration of holes and electrons in intrinsic germanium, w and t the width and thickness of the thin part of arm 15. Due correction was made for those parts of 15 out of the solution. Appropriate measurements gave two independent estimates of the values of the resistances of each of the five arms, exclusive of contact resistance, which could also be evaluated. Since the dimensions of the arms were known, the specific resistance and its uniformity throughout the bridge could be determined. Once the bridge had been measured, any changes in the dimensions of arm 15 due to etching could be simply determined from the change in balance point at the conductivity minimum.

In the experiments contact 2 was at ground and so placed that R_{12} was equal to $R_{23} + R_{34} + R_{45}$, so that

the midpoint of arm 15 had equal resistance to ground either way around the bridge. When capacity measurements were made on this arm, contacts 1 and 5 were grounded to eliminate the potential drop to ground through the other arms.

Materials and purification.—The solutions were M/10 K_2SO_4 buffered to appropriate *p*H values. All solutions were gettered by stirring with finely crushed germanium for several hours before use. This was produced *in situ* by rapidly stirring a solution containing a few small pieces of high-purity germanium with a magnetically operated, Teflon enclosed stirring bar. Over the course of several hours collisions between the pieces produced a dense cloud of fine particles. In some cases the solutions were also pre-electrolyzed at a germanium cathode for up to 72 hr, but the data were identical in solutions which had been simply gettered. Generally, the germanium powder was left in the solution throughout the experiment. The solutions were made up either with de-ionized water or de-ionized water that had been distilled from permanganate solution. In both cases the data were identical, from which it may be concluded that the gettering process effectively removes any trace impurities originally present in the electrolyte or the D.I. water active with respect to a germanium surface. Analytical grade K_2SO_4 was used. In some experiments not described here, K_2SO_4 was recrystallized three times from distilled water and the buffer omitted. The data were exactly similar in both sets of experiments.

Nitrogen was passed over hot copper gauze. Helium was passed through anhydrite, Hopcalite, soda-lime, active copper on kieselguhr at 200°C (8), charcoal at −196°K and through a fitted disk into distilled water, the gas train being all glass. Identical results were obtained with either gas. The electrodes which were all oriented to the (100) face were etched in CP4 and rinsed in distilled water (or gettered D.I. water) before each experiment. In a few cases they were etched in M/10 potassium ferricyanide solution after the CP4. Anodic currents of 100-200 $\mu a/cm^2$ (n-type electrodes illuminated) were applied for around 5 min before data were taken. Ferricyanide appeared to produce a surface similar to that obtained after anodic etching whereas the CP4 surface (before anodic etching) was more variable with respect to the initial value of the surface potential and the behavior of the capacity.

Measurements.—The capacity of the germanium electrode solution interface was measured by means of a current pulse technique. Short duration square current pulses (up to a maximum value of 100 μa and of 1 μsec to 50 μsec duration, but most frequently 5 μsec) were applied from a pulsed constant voltage source, through a 10^6 ohm resistance and 0.47 μfd capacity in series, to one of the platinum electrodes in the larger compartment. The change of potential between the bulk of the germanium electrode and the solution was detected at the other platinum electrode in this compartment, amplified, and presented on an oscilloscope.

The form of the response, which was independent of the sign of the current pulse, is shown in Fig. 3.

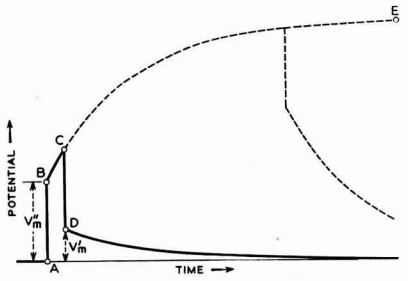

Fig. 3. Response of the interface to a short duration square current pulse.

When the pulse was turned on there was an initial potential change V''_M(A to B) which was generally vertical at the highest trace speed of our oscilloscope (0.1 μsec cm^{-1}). The potential increased with time from B to C where the pulse was turned off resulting in an instantaneous decrease (C to D) equal to V''_M. The residual potential V'_M at D decayed to the original potential in an exponential manner. In a typical experiment V'_M, V''_M and the time constant (τ) for decay of V'_M were measured, although in some cases only V'_M was measured. Care was taken to keep the differential pulse sufficiently small that the response was less than 25 mv. During an experiment the differential pulse was applied repetitively through the interface about 20 times per second, and the voltage response was continuously displayed.

The photovoltaic response of the electrodes was measured with a 40 cps square wave tungsten filament light source, the potential with respect to a platinum electrode in the solution being presented on an oscilloscope. The major point of interest here was to determine, as a function of doping, the electrode potential at which the "fast" response changed sign.

Both the interfacial capacity and the photovoltaic response were measured as a function of electrode potential, the bias being applied through the platinum electrode in the smaller compartment by means of a direct current source (D in Fig. 1). Two methods of varying the electrode potential were used. The first (method I) was simply to set a certain current through the electrode, wait for the electrode potential (V_E) to come to a steady value and then measure it and the quantities V''_M, V'_M and τ. Alternatively (method IIa) by manipulation of switch S the desired current could be set through the 10K ohm auxiliary resistor and then switched into the system for a brief period of time (approximately 1 sec) during which instantaneous values of V_E and V'_M were measured. The currents were such as to make the germanium anodic and were sufficiently small not to upset significantly the hole electron equilibrium in the electrodes. In an extension of the second method (method IIb) an additional current source, in parallel with D, was used to provide a continuous current (germanium anodic) superimposed on which was the manually pulsed current from D which could now be of either sign, but not sufficiently great in the negative sense to reverse the sign of the net current.

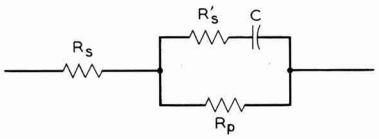

Fig. 4. Equivalent circuit of the interface

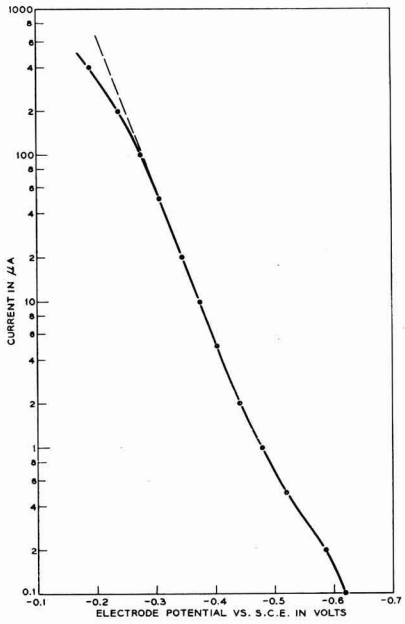

Fig. 5. Tafel curve for 1.1 cm² germanium electrode in $\frac{M}{10}$ K_2SO_4, phosphate buffered to pH 7.4.

Experimental Results

The response shown in Fig. 3 does not uniquely determine an equivalent circuit. It does, however, suggest a simple combination of resistance and capacity such as shown in Fig. 4, which is basically similar to a previously proposed model (5) with the addition of R'_s. Assuming any model, one can, from pulse data, calculate a differential resistance. If the method and analysis are valid, this differential resistance should agree with the differential resistance determined from the current-voltage curve taken at zero frequency. The d-c data are shown in Fig. 5, and in Fig. 6 is shown the comparison of differential resistance determined graphically from Fig. 5 and from the pulse data in Table I. The agreement is excellent except at the more negative potentials. This deviation is due to the fact that in order to measure the differential resistance correctly here by the pulse method the low-frequency response of our measuring system should be good down to 0.2 sec or better, whereas it actually falls off at about 0.05 sec. The agreement is independent of the equivalent circuit chosen provided only that the circuit is consistent with the response shown in Fig. 3 and that it has a continuous resistive path from one terminal to the other.

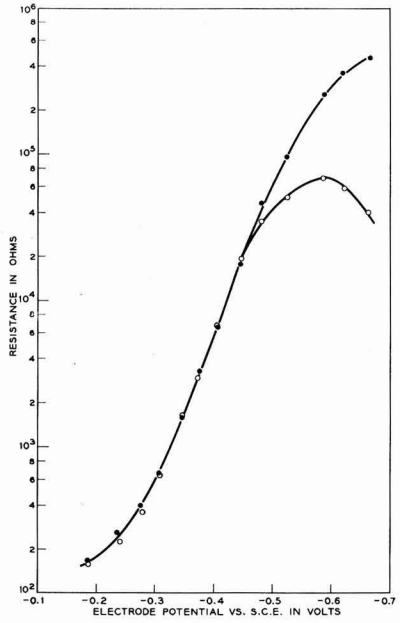

Fig. 6. Differential resistance *vs.* electrode potential, derived from Fig. 5 (•) and from pulse data (○).

It has been found in this case and in previous work (7) that at moderate current densities in the anodic direction the Tafel relation between d-c current and voltage is obeyed, subject to correction for a constant series resistance R_s (due to the germanium,

Table I. Analysis of a 25.5 ohm-cm p-type germanium electrode in terms of the equivalent circuit of Fig. 4

I, ma	V_E volts *vs.* S.C.E.	V''_M, mv	V'_M, mv	τ, μsec	R'_s/R_p	R_s, ohms	R_p, ohms	$R_p + R_s$, ohms	$\Delta V_E/\Delta I$, ohms	C 10^{-8}, farads	R^*_s, ohms	R^*_p, ohms	C^* 10^{-8}, farads
0.400	—0.189	12.5	1.18	15	1.27	103	81	161	167	11.5	125	36	42
0.200	—0.238	12.5	2.8	18	0.446	65	146	226	285	8.3	125	100	18
0.100	—0.277	13.7	4.8	22	0.27	76	281	361	440	6.5	137	224	10.4
0.050	—0.307	15.0	7.1	35	0.14	80	570	650	670	5.4	150	500	7.1
0.020	—0.345	17.3	10.7	69	0.063	98	1,560	1,640	1,600	4.2	173	1,570	4.6
0.010	—0.375	18.2	12.7	107	0.037	104	2,820	2,900	3,600	3.65	182	2,720	3.9
0.005	—0.403	17.7	14.1	231	0.015	99	6,580	6,660	6,700	3.45	177	6,520	3.5
0.002	—0.444	16.8	15.0	660		98	19,000	19,000	18,000	3.3	168	18,800	3.3
0.001	—0.480	16.8	13.6	1,360		98	37,000	37,000	46,000	3.7	168	37,000	3.7
0.0005	—0.521	15.0	10.2	2,700		80	55,000	55,000	97,000	4.9	150	55,000	4.9
0.0002	—0.586	11.4	5.0	7,200		44	72,000	72,000	260,000	10.0	114	72,000	10.0
0.0001	—0.619	9.8	3.45	8,500		28	59,000	59,000	360,000	14.5	98	59,000	14.5
0	—0.665	8.0	1.78	11,500		10	41,000	41,000	440,000	20.0	80	41,000	20.0

electrolyte, and leads) and provided the data are taken under conditions where the electron or hole concentration does not depart essentially from the equilibrium value. The departure of the current voltage curve in this region (as shown in Fig. 5) serves to determine R_s. This series resistance is found to be about one-half of the resistance necessary to explain the initial rise in V''_M in Fig. 3. This is the reason for including the resistance R'_s in Fig. 4. It should be emphasized that over most of the range of interest R_s and R'_s are small compared with R_p, and the exact values used from R_s equal to zero to R'_s equal to zero (their sum being known from V''_M) have very little effect on the calculated values of C and R_p. Assuming the circuit in Fig. 4, the following relations may be obtained

$$V''_M = i[R_s + R'_s(1 + R_s/R_p)^{-1}] \quad [3]$$

$$V'_M = C^{-1} i\, t(1 + R'_s/R_p)^{-2} \quad [4]$$

and

$$\tau = R_p(1 + R'_s/R_p)^{-1} i\, t(V'_M)^{-1} \quad [5]$$

whence

$$R'_s/R_p = t(V''_M - R_s i)(V'_M \tau)^{-1} \quad [6]$$

where i is the magnitude of the current pulse, t is the pulse duration, and τ is the decay constant for the voltage after the pulse is turned off. In these equations it has been assumed that t/τ is very small so that $\exp(-t/\tau)$ is equal to $(1 - t/\tau)$. For cases where this is not so, the appropriate correction has been made.

Typical data taken on a p-type electrode are shown in Table I. The magnitude of the current pulse was 0.1 ma and its duration was 5 μsec. R_s was taken as 80 ohms from Fig. 5. The starred values R_s*, R_p*, and C_p* are the results one would obtain if one assumed R'_s to be equal to zero, assuming V''_M and not Fig. 5 gives the correct value for R_s. The correct circuit is between these limits with the one for $R_s = 80$ ohms being the more likely. It is to be noted that for V_E more anodic than -0.300v the capacity values are considerably different in the two cases. In methods IIa and IIb, where we did not have time to take all the data shown in this table, we could not correct V'_M for t/τ being too large, and we could only calculate C on the basis of $R'_s = 0$. These two errors for very anodic potentials tend to compensate each other. For less anodic potentials it matters little which equivalent circuit one chooses.

Charge may be distributed over three distinct regions of the interface, the space charge layer in the germanium and its associated surface states ($C_{SC} + C_{SS}$), the Helmholtz region encompassing the geometrical interface, and the space charge (Gouy layer) in the solution. At the electrolyte concentrations used in this work the Gouy layer was essentially nonexistent, and all excess charge on the solution side of the interface can be considered to be in the Helmholtz layer. Typical values for the capacity of the Helmholtz layer (C_H) at a metal electrode (ca. 20 μfd/cm^2) are two to three orders of magnitude greater than calculated values for the minimum space charge capacitance in the semiconductor, so that since these capacities are in series the observed capacity at the interface is $(C_{SC} + C_{SS})C_H (C_{SC} + C_{SS} + C_H)^{-1}$ and since $C_H > 100\, C_{SC}$ the observed capacity should be C_{SC} to within about 1% in the absence of fast surface states. R'_s and R_p are the resistances to the flow of capacitative or faradaic current, respectively, from the bulk of the electrode to the bulk of the solution.

Figure 7 shows a typical curve of capacity *vs.* steady-state electrode potential at *p*H 7.4 measured on a simple electrode. An investigation of these curves as a function of *p*H indicated that over the range *p*H 5-12 they were similar in shape, but displaced along the electrode potential axis by an amount depending on the change in *p*H. Beyond *p*H 5 and 12, the curves changed shape and the minimum value increased by about a factor of 2. These data will be dealt with in detail at a later date. All the data contained in this paper were obtained at *p*H 7.4.

Figure 7 is in general agreement with Bohnenkamp and Engell (5) that a considerable part of the potential change occurs across the space charge region. Their data were taken at *p*H 0 and 14 and the minimum capacities were about a factor of 2 larger than we find at *p*H 7.4, but in agreement with our values at extremes of *p*H. It is of particular interest that our minimum capacity agrees closely with the theoretical value if the experimentally measured roughness factor of 1.3 is assumed (9).

Similar data taken instantaneously on the application of a current through the interface, method IIa as described previously, are shown in Fig. 8. Further data taken by method IIb are also shown in Fig. 8.

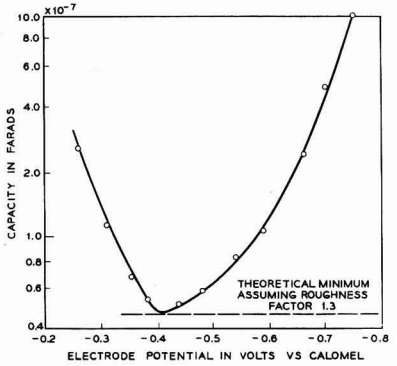

Fig. 7. Capacity *vs.* electrode potential (method I) for a 42.2 ohm-cm n-type germanium electrode.

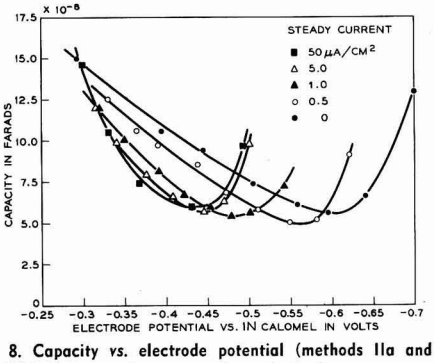

Fig. 8. Capacity *vs.* electrode potential (methods IIa and IIb) for a 25.5 ohm-cm p-type germanium electrode.

Additional experiments were conducted with the bridge electrodes. The capacity of the interface was measured exactly as for the simple electrodes, and good agreement was found for similarly doped material. The apparent variation in conductivity of the thin arm of the bridge was measured (Eq. [2]) as a function of electrode potential varied by method IIa.

The decay of photoconductivity in the thin arm was determined in two ways. The decay was compared directly with the signal from an exponential generator while the electrode potential was changed by method I. Method II does not allow sufficient time to adjust the exponential generator to an accurate reading so the procedure adopted in this case was to measure the increase in conductivity due to the 40 cps square light pulse, directed onto the thin arm only, the duration of which was long compared with the photoconductivity lifetime. Once the conductivity increase (observed as a square voltage response on the oscilloscope) was calibrated against the photoconductivity lifetime at one point (conveniently zero current density across the interface), the latter could be derived from the former by simple proportionality, the longer the lifetime the larger the photoconductive response. The results by either method yield the same result, namely, that over the accessible range of electrode potential the lifetime was essentially constant and equal to the body lifetime of the electrode material, *e.g.*, for the p-type bridge 640 ±40 μsec.

Discussion

Dewald (6) has discussed the distribution of potential and charge at the semiconductor-aqueous solution interface and has pointed out that when the solution is sufficiently concentrated the Gouy layer is suppressed, and in the absence of a considerable number of surface states near the semiconductor Fermi level or changes in surface dipole almost all of any potential change at the interface occurs across the space charge region in the semiconductor. Hence, in the absence of these effects, or of concentration polarization in the solution, changes in electrode potential should correspond to changes in the germanium surface potential.

It is anticipated that the observed capacity is due to the space charge layer plus surface states sufficiently fast to respond to the differential current pulse (3). If the assumption is made that the measured capacity is solely that of the space charge layer, then the surface potential (ψ_s) may be deduced by comparing the experimental capacity values (divided by the roughness factor) with the theoretical curve calculated from (10)

$$C_{sc} = dQ_{sc}/d\psi_s = A(dF/dY)dY/d\psi_s \qquad [7]$$

where Q_{sc} is the charge in the space charge layer, A is the electrode-solution interfacial area, and

$$F = \pm[\lambda(e^{-Y} - 1) + \lambda^{-1}(e^{Y} - 1) + (\lambda - \lambda^{-1})Y]^{1/2} \qquad [8]$$

where $\lambda = p/n_i$, p is hole concentration, and $Y = e\psi_s/kT$, ψ_s being the electrostatic potential (in volts) across the space charge region. The assumption is made in the above form of F that the carrier density does not depart appreciably from equilibrium under the conditions of our experiments.

Theory indicates that for the same steady-state conditions in identical solutions, the surface potential will vary with the doping of the electrode by an amount kT/e ln λ compared with intrinsic (6, 11). If the capacity we observe is that of the space charge layer and there are no potential changes in the system except across the space charge layer, then for all electrodes the plots of $\psi_s - kT/e$ ln λ *vs.* electrode potential should coincide and should be straight lines with a slope of unity. The data for variously doped electrodes is shown in Fig. 9. It is seen that only the first requirement is satisfied. There are two possible explanations for this behavior. Either the capacity values and, hence, the values of ψ_s are incorrect due to the existence of a sufficient number of fast surface states within the experimental range of $\psi_s - kT/e$ ln λ or there is a potential change in some other region of the interface.

In taking the above data it was observed that the behavior of the electrode potential, particularly at low current densities, was dependent on the immediately previous condition of the electrode, *i.e.*, was a particular current density established from a higher or lower value, the data in Fig. 9 being the final steady-state values. An analysis of the data taken by method IIa, in which the long time effects are disregarded, is shown in Fig. 10. In this case, over a range of potential, the electrodes behave in an ideal fashion and obey the simple relation

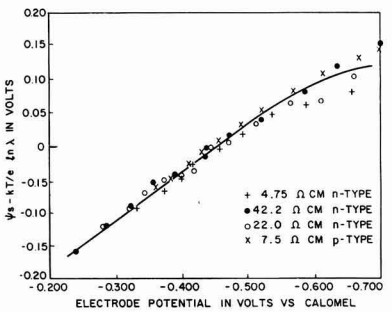

Fig. 9. ($\psi_s - \frac{kT}{e}$ ln λ) *vs.* **electrode potential (method I) for various electrodes.**

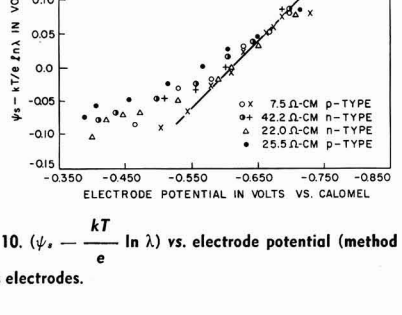

Fig. 10. ($\psi_s - \frac{kT}{e}$ ln λ) *vs.* **electrode potential (method IIa) for various electrodes.**

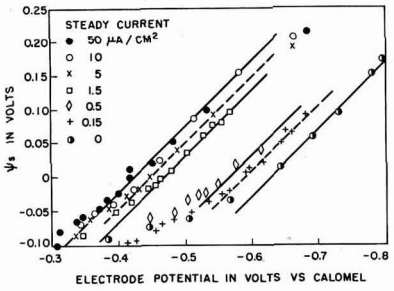

Fig. 11. ψ_s vs. electrode potential (method IIb) for a 22 ohm-cm n-type germanium electrode.

$$\psi_s = \frac{kT}{e} \ln \lambda = V_H + \text{constant} \qquad [9]$$

which has been predicted (6, 11). In Fig. 10 the points at the most negative potentials represent zero net current, while less negative potentials represent increasingly anodic polarization. Data taken by method IIb throw light on the reason for the departure from Eq. [9] at higher anodic current densities. It can be clearly observed from Fig. 11 that the constant in Eq. [9] varies with current density up to about 10 μa/cm^2, but at a sufficiently slow rate that for not too large changes in current it remains essentially constant during the time that the electrode potential and V'_M, *i.e.*, capacity, are read. The disposition of these lines is independent of the stirring rate, indicating that the potential shift is not due to concentration polarization in the solution. Concentration polarization may, however, be observed in unbuffered solutions of the same pH as shown in Fig. 12, where the capacity-electrode potential curves exhibit a similar shift over the range of current density from zero to approximately 10 μa/cm^2 and then, unlike the situation in Fig. 8, undergo a further shift at higher current densities.

The only remaining region where the potential shift may occur in buffered solutions is the Helmholtz layer. The potential may change appreciably in this region due either to a change in the adsorbed dipoles or to a change in the occupation of slow surface states. (The surface states must necessarily be slow since they do not respond to the capacity measure-

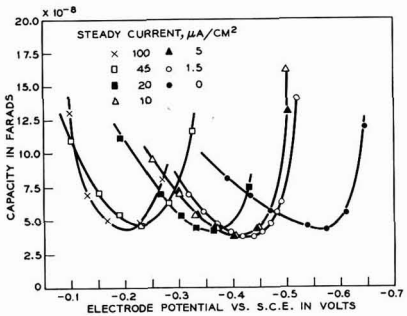

Fig. 12. Capacity vs. electrode potential (method IIa) for a 25.5 ohm-cm p-type germanium electrode in unbuffered $\frac{M}{10}$ K_2SO_4.

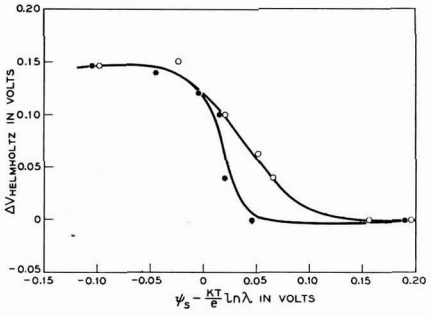

Fig. 13. $(\psi_s - \frac{kT}{e} \ln \lambda)$ vs. $\Delta V_{\text{Helmholtz}}$ for a 25.5 ohm-cm p-type electrode (○) and a 42.2 ohm-cm n-type electrode (●).

ments.) The present data are not sufficient to distinguish between these two possibilities. Figure 13 shows an analysis of some data taken by method I at low current densities. The surface potentials have been computed from the capacity and hence, knowing the surface potential, it is possible to deduce how changes in the electrode potential due to small anodic current are distributed between the space charge and Helmholtz layers. The space charge potential is known absolutely, while only changes in Helmholtz potential from the zero current value are obtained. The curves for n- and p-type electrodes show a sharp step in the Helmholtz potential over a fairly narrow range of surface potential. The value of $(\psi_s - kT/e \ln \lambda)$ at which this potential change occurs is approximately the same for both n- and p-type electrodes which would be expected for a surface state localized in energy. Unfortunately, equal values of $(\psi_s - kT/e \ln \lambda)$ represent also equal current densities across the interface, and the results do not clearly distinguish between a purely electrical effect dependent on surface potential and a chemical effect dependent on current density. Slow surface states, however, are usually considered to be associated with thick oxide films and disappear when such films are reduced in thickness (12). Under the conditions of our experiments, thick films are unlikely to be present (13). For this reason, it would seem more likely that we are observing a change in surface dipole due to adsorbed molecules or ions oriented at the surface. The structure of the adsorbed layer could be strongly affected by anodic current since this actually removes the surface atoms of the electrode. The various lines in Fig. 11 might then represent a steady state attained between the formation of an oriented adsorbed layer, probably of water molecules, and its disruption by anodic etching.

The constancy of the decay lifetime for excess carriers deduced from the bridge electrode and its close correspondence with the body lifetime indicates the absence of surface recombination centers over the investigated range of surface potential (approximately 0.2v on each side of the center of the gap).

Additional information is provided by fast photovoltaic response. In the absence of fast surface states,

this quantity should change sign at flat band (10), *i.e.*, $\psi_s = 0$. Experimentally, the range is $+0.03$ to -0.02v for the variously doped electrodes.

It may be concluded on the above evidence of the distribution of charge and potential and kinetic recombination effects that a germanium surface which has been recently anodically etched in nearly neutral solution is free from measurable densities of fast surface states. It should be emphasized here that this conclusion only applies to the case of the purified electrolyte. A similar conclusion with regard to the absence of fast states has recently been reached in the case of the zinc oxide electrode (3).

An attempt was made to calculate ψ_s from the bridge conductivity data. Here two questions arise. First, do the values of ψ_s calculated from the capacity changes in the thin arm of the bridge agree with results for the simple electrodes. These results are compared in Fig. 14. The agreement is reasonably good, considering that in the case of the bridge there is necessarily a distribution of potential along the thin arm and both the potential V_E and the capacity are some kind of average over this arm. The second question, how do the values of ψ_s calculated from conductivity agree with the capacity data, is illustrated in Fig. 15. Over a range of potential the agreement is fairly good, but at higher anodic potentials the two methods do not agree. The lack of success encountered in this attempt may be ascribed to two potential sources of error. There is a possibility of conduction through the solution by virtue of the fact that a potential difference must be applied across the electrode to measure the conductivity. In most cases this potential was quite small, about 10 mv between the ends of an arm 2 cm long, and the frequency of the applied signal kept low (17 cps) to reduce capacitative coupling through the solution. It is felt, however, that the major discrepancy arises from another source which is the fact that, due to the geometry of the bridge, at any interfacial current there will be a distribution of potential along the thin arm because of current flow along its length. Calculations indicate that at our maximum overvoltage of about 0.450v there is a potential difference between the ends and center of the thin arm of some 0.045v, becoming rapidly less at lower current densities. In this event there will be a fairly complicated averaging of surface conductivity along the length of the arm which could give deviations in the direction observed.

Although the conductivity experiment does not exhibit ideal behavior, the observed conductivities are a constant function of potential. This may be inferred from Fig. 16, where the bridge balance reading, being proportional to conductivity (see Eq. [2]), is plotted as a function of the electrode potential. These experiments were carried out over an extended period of time in solutions of *p*H 7.4, and include a correction for the reduction in thickness of the active arm each time it is etched, deduced from the balance reading for minimum conductivity. Insofar as capacity measurements carried out at the same time indicate a constant relationship between V_E and $(\psi_s - kT/e \ln \lambda)$, the V_E axis could be replaced by suitably normalized values of $(\psi_s - kT/e$

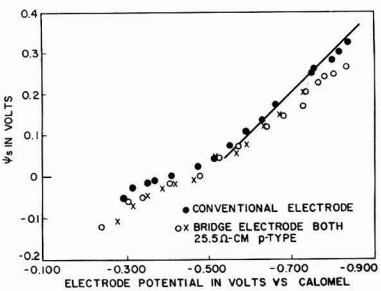

Fig. 14. ψ_s *vs.* electrode potential (method IIa) for a simple electrode (●), and a bridge (o,x) both 25.5 ohm-cm p-type.

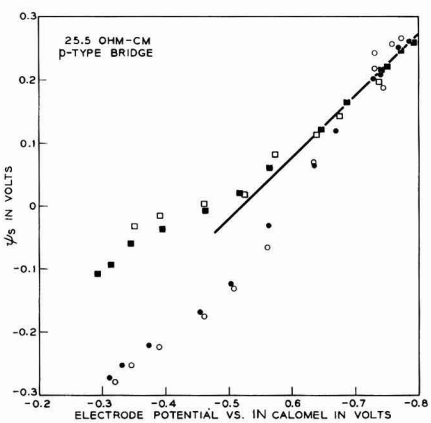

Fig. 15. ψ_s calculated from capacity (□,■) and from conductivity change (○,●) *vs.* electrode potential (method IIa) for a 25.5 ohm-cm p-type bridge.

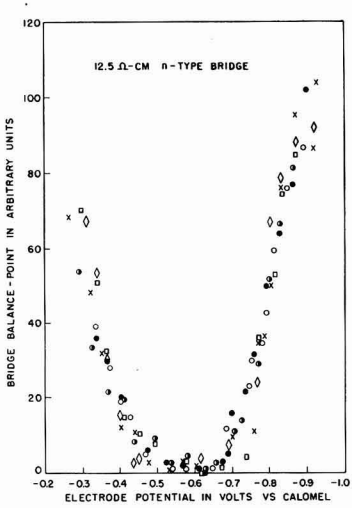

Fig. 16. Balance point (arbitrary units) of 12.5 ohm-cm n-type bridge *vs.* electrode potential (method IIa). The various symbols represent experiments carried out at different times. The thickness of the active arm is different in each case due to etching.

$\ln \lambda$), and conductivity measurements could be used to deduce this quantity from Fig. 16.

Conclusion

The capacity of the interface between a germanium single crystal electrode and an aqueous solution of K_2SO_4 buffered to *p*H 7.4 when measured by a high-frequency pulse method is explicable solely in terms of the space charge capacity in the electrode and reveals no fast surface states (less than ca. $10^{9.5}$ cm^{-2}) within $\pm 8\ kT/e$ measured from mid-gap. The conclusion of no fast surface states is supported by the absence of significant surface recombination phenomena. The distribution of potential across the interface in response to anodic bias is expressed by

$$\psi_s - \frac{kT}{e} \ln \lambda = V_B + K$$

where the quantity K is arbitrary and depends on steady-state current density up to 10 $\mu a\ cm^{-2}$, but otherwise at a given *p*H and for a given reference electrode is a constant.

Surface conductivity data yield incorrect values of the surface potential except at small polarizing currents, but are quite reproducible and could be used to predict surface potential if properly calibrated in terms of the capacity. It is the authors' conviction that values of surface potential deduced from the capacity are most likely the correct ones.

In other words, it is possible under these conditions to obtain an almost "perfect" germanium surface, *i.e.*, no fast states.

Acknowledgments

The authors are indebted to J. F. Dewald, U. B. Thomas, Jr., and D. R. Turner for helpful discussion, and to W. J. Sundburg for technical assistance.

Manuscript received Jan. 5, 1962; revised manuscript received March 19, 1962. This paper was prepared for delivery before the Detroit Meeting, Oct. 1-5, 1961.

Any discussion of this paper will appear in a Discussion Section to be published in the June 1963 JOURNAL.

REFERENCES

1. E. Harnick and Y. Margoninski, *J. Phys. Chem. Solids*, **8**, 96 (1959).
2. W. H. Brattain and J. Bardeen, *Bell System Tech. J.*, **32**, 1 (1953).
3. J. F. Dewald, *ibid.*, **39**, 615 (1960).
4. H. U. Harten, *Z. Naturforsch.*, **16a**, 459 (1961).
5. K. Bohnenkamp and H. J. Engell, *Z. Elektrochem.*, **61**, 1184 (1957).
6. J. F. Dewald in "Semiconductors," N. B. Hannay, Editor, Reinhold Publishing Co., New York (1959).
7. W. H. Brattain and C. G. B. Garrett, *Bell System Tech. J.*, **34**, 129 (1955).
8. F. R. Meyer and G. Ronge, *Z. angew. Chem.*, **52**, 637 (1939).
9. J. T. Law, *J. Phys. Chem.*, **59**, 543 (1955).
10. C. G. B. Garrett and W. H. Brattain, *Phys. Rev.*, **99**, 376 (1955).
11. W. H. Brattain in "The Surface Chemistry of Metals and Semiconductors," H. C. Gatos, Editor, John Wiley & Sons, Inc., New York (1960).
12. M. Lasser, C. Wysocki and B. Bernstein in " Semiconductor Surface Physics," R. H. Kingston, Editor, University of Pennsylvania Press (1957).
13. D. R. Turner, *This Journal*, **103**, 252 (1956).
14. W. H. Brattain and C. G. B. Garrett, *Bell System Tech. J.*, **35**, 1019 (1956).

Investigation of Some Uncommon Surface Treatments on Germanium

W. A. Albers, Jr.* and A. M. Rickel

Research Laboratories Division, The Bendix Corporation, Southfield (Detroit), Michigan

ABSTRACT

Several surface treatments have been applied to germanium and characterized with respect to the surface energy level configuration and the sensitivity to variations in ambient atmosphere. The characterization was accomplished by making simultaneous measurements of the a-c field-effect conductivity change and the surface recombination velocity, both as functions of surface potential. Experimental results suggest certain relationships between etched germanium surface properties and those properties resulting from a subsequent surface treatment, which may be exploited to yield a surface condition that is relatively passive to ambient atmosphere variations.

Attempts to stabilize and/or passivate semiconductor surfaces for the purpose of improving manufactured semiconductor device uniformity and reliability often involve a sequence of several distinct operations. It is well known that each step of such a sequence can contribute to the ultimate electrical properties of the resultant surface. It is not generally understood, however, just how these steps contribute, in a quantitative sense, to the resultant surface properties. The purpose of this paper is to report some preliminary studies of the effect of two successive surface operations on the electrical properties of the semiconductor surface. The two steps chosen for investigation are (i) an etching operation and (ii) a surface treatment applied to the etched surface. The surface treatments investigated are "uncommon" in the sense that they have not been reported extensively in the literature.

* Present address: General Motors Research Laboratories, Warren, Michigan.

The results of the measurements to be reported suggest a method of characterization of a given surface condition that affords a first-order approach to the "engineering" of surfaces into devices. The experimental data also yield some information about the interaction of the two operations on the surface that suggests possible approaches for obtaining relatively high degrees of surface passivation. Both of these aspects of the experimental results are discussed in some detail.

Experimental Approach

Rectangular sample with their large-area surfaces oriented in either the (100) or the (111) crystallographic planes were cut from 35 ohm-cm n-type single crystals of germanium. The rectangles were subsequently lapped to a thickness of 10.5 to 11.5 mils and then etched to a final thickness of 5.0 ± 0.1 mils in either CP4A or a 1:1:1 ratio of H_2O_2, HF, and H_2O.[1] A specific sample was then subjected to one of several surface treatments, the nature of which will be detailed later. Finally leads were attached,[2] and the sample was placed in the experimental apparatus.

The method employed for the characterization of a given surface treatment was to observe, simultaneously, the large-signal a-c field effect and the surface recombination velocity (s.r.v.) as a function of surface potential in various ambient atmospheres. The data were then analyzed in the manner employed by Many *et al.* (1) to obtain surface trap densities and energies. In addition, the sensitivity of the electrical properties of the experimental sample to changes in the ambient atmosphere was also monitored. The surface treatment data were then compared to similar data obtained on the etched, untreated surfaces previously described, which were employed as controls.

The apparatus for mounting the samples in order to accommodate the simultaneous measurement of the field-effect conductivity and the s.r.v. is drawn schematically in Fig. 1. The experimental technique is similar to those employed by Wang and Wallis (2), Bath and Cutler (3), and Rzhanov *et al.* (4), with some modification. The above authors all performed simultaneous measurements of the field-effect conductivity and the conductivity change on illumination. The photoconductivity was then related to the s.r.v. through suitable theoretical expresssions [see, for example, ref. (3)]. These workers used, for the most part, nonpenetrating illumination and, in some cases, field-effect electrodes were coupled to only one of the two large area surfaces of their experimental samples. The apparatus in Fig. 1 employs a germanium filter D which is thick compared to the sample thickness. The radiation that reaches the sample C is thus penetrating. If the filter is sufficiently thicker than the sample, the generated carrier density due to illumination is nearly constant throughout the volume of the illuminated portion of the sample. The germanium filter also serves as one of the two field-effect electrodes, the other being an ordinary brass plate A. The experimental specimen is sandwiched between these two electrodes and insulated from them by the mica spacers B. The germanium filter thus serves both as a field-effect probe and as a means of obtaining a low-level,[3] uniform generation of carriers in the specimen.

The circuitry for the field-effect observations was patterned after that of Low (5). A 200-v peak, 70 cps, alternating voltage was applied to the field effect probes, and the resulting change of sample conductivity *vs.* induced surface charge was displayed on an oscilloscope. An ordinary tungsten filament projector lamp was used as a source of illumination. The light was chopped at a rate of 120 cps so that, upon illumination, the photoconductivity pulse appeared superimposed on the ordinary field-effect curve. Since the chopping rate was out of sync with the field-effect voltage, the photoconductivity pulse ran back and forth on the field-effect pattern on the oscilloscope. By employing a high persistency phosphor, a double field-effect trace is obtained, the vertical separation being proportional to the photoconductivity voltage.[4] The necessity of calibrating the intensity of illumination is eliminated by obtaining a value of the s.r.v. by the photoconductivity decay method at the equilibrium surface potential (the value of the surface potential for zero induced surface charge). This value of the s.r.v. serves to calibrate the photoconductivity voltages obtained with the field effect.

The type of data that results from the methods of observation described above is presented in Fig. 2 and 3 for some typical surface treatments[5] (the surface treatments will be referred to only by abbreviated names in the text; the physical and chemical details are presented in an Appendix). In Fig. 2 is plotted the charge in "fast" surface states, Q_{ss}, as a

[1] The CP4A etch consists of a 5:3:3 ratio of nitric, hydrofluoric, and glacial acetic acids. The chemicals employed were all reagent grade or better, the HNO_3 was 70% by weight, the HF 48% by weight, and the H_2O_2 (unstabilized) 30% by weight. The H_2O was distilled and deionized.

[2] In order to avoid contaminating the previously prepared surface, the samples were made much longer than the active surface region under investigation; the attachment of leads was thus accomplished at a distance somewhat removed from the surface area of interest.

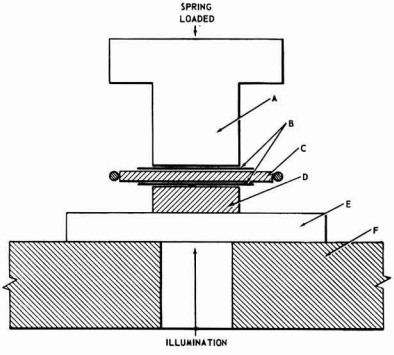

Fig. 1. Detail of sample mounting for field effect and photoconductivity measurements: A, brass field effect electrode; B, mica spacers; C, germanium sample; D, germanium filter and field effect electrode; E, quartz microscope slide mount for germanium filter; F, wall of enclosing box.

[3] The low generation level is a necessary condition for the applicability of the expressions relating s.r.v. and photoconductance (3).

[4] Photographs of oscilloscope traces like those discussed have been published by Rzhanov (4).

[5] For the purposes of this paper, a "surface treatment" is defined as an operation on the surface which does not involve the removal of germanium material, as opposed to an "etch," which does involve the removal of material.

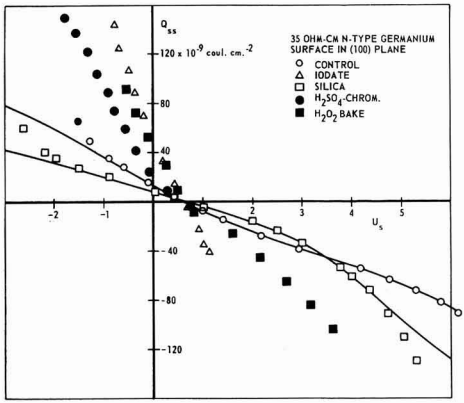

Fig. 2. Charge in fast surface states, Q_{ss}, as a function of surface potential, u_s, in units of kT/q for several surface treatments on an H_2O_2:HF:H_2O etched surface. Solid curves represent best theoretical fit for the control surface and the silica treatment.

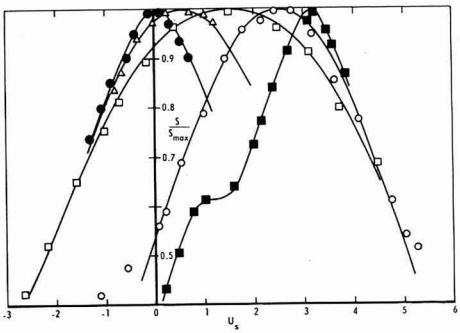

Fig. 3. Normalized surface recombination velocity, s/s_{max}, as a function of surface potential, u_s, in units of kT/q for the same samples as Fig. 2. Solid curves represent the best theoretical fit to the experimental points.

function of surface potential, u_s, in units of kT/q.[6] The corresponding curves of the normalized s.r.v., s/s_{max} *vs.* u_s are plotted in Fig. 3. The points represent data obtained experimentally while the solid curves are the theoretical curves which are the best fit with the experimental points. The result is that the densities and energies of the fast surface states can be deduced, thus partially characterizing each surface treatment.

The data of Fig. 2 and 3 were all obtained in a dry O_2 ambient atmosphere, after sufficient time was allowed for the sample surface to come to equilibrium with this atmosphere. The reason for choosing a reference atmosphere is due to the fact that the fast surface state configuration changes with varying ambient atmosphere. This effect is illustrated in Fig. 4. The data presented here are the result of varying the ambient atmosphere about a typical H_2O_2:HF:H_2O-etched surface.

It will be noted that there is an appreciable variation in some of the recombination trap parameters.

[6] The quantity u_s is defined as

$$u_s = \frac{q\phi_s}{kT}$$

where ϕ_s is the surface potential. The symbols employed for all other quantities throughout this paper follow those of ref. (1).

	u_o	$\frac{E_t - E_i}{kT}$	$\frac{C_p}{C_n}$	$N_t \times 10^{-11}$	S_{max}
○	1.8	5.5	36.5	2.3	320
△	1.0	4.3	7.4	0.7	370
■	2.0	5.0	54.4	..	370

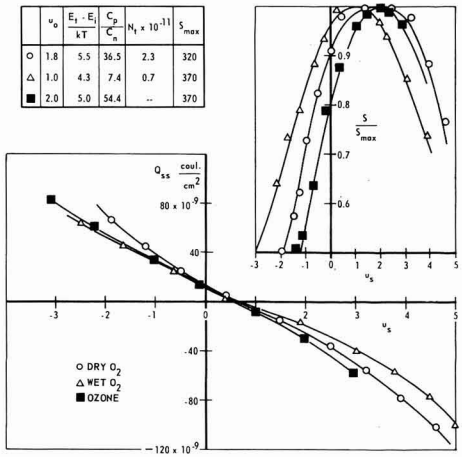

Fig. 4. Effect of varying ambient atmosphere on the surface state parameters. H_2O_2:HF:H_2O etched surface in a (100) plane of 35 ohm-cm n-type germanium.

The values of c_p/c_n, the ratio of hole-to-electron capture probabilities (which is proportional to $l\,n\,(u_o)$, u_o being the value of u_s about which the s.r.v. curves are symmetrical), and the state density, N_t, appear to vary considerably. On the other hand, the energy of the state (as measured from the center of the energy gap E_t) and the maximum value of the s.r.v., do not exhibit such drastic changes. This behavior is typical of most of the surfaces that we have investigated. It was found that a dry oxygen atmosphere yielded the most reproducible results, and thus, this atmosphere was chosen for the standard.

It follows that the variation of the surface properties with ambient atmosphere changes should be an essential part of characterizing any surface condition. We chose to do this by noting the value of the equilibrium surface potential in the field effect for two ambients, namely dry O_2 and wet O_2.[7] The difference in surface potential, Δu_s, and the mid-point of the range of Δu_s were thus obtained for these two ambients, the values of which are indicative of the sensitivity of the surface to ambient atmosphere changes. These data, along with data concerning surface state densities and energies are taken as a characterization of a given surface treatment. The data obtained on a total of 43 samples are summarized in the following section.

Results and Discussion

Some representative results, on (100) surfaces, are summarized in Table I. All of the data were obtained in a dry oxygen atmosphere at 295°K. Similar data were obtained on (111) surfaces, and, within experimental error, the data were substantially the same as those presented in Table I for the (100) surface. Although a total of 43 samples were investi-

[7] Dry O_2, in our case, was obtained by passing ordinary low dewpoint compressed cylinder oxygen through a Drierite column. Wet O_2 was obtained by bubbling dry O_2 through distilled, deionized water and filtering through Pyrex wool. The sample conductivity would stabilize, typically, about 3 min after admission of wet O_2. Although there was a slow, long term drift evident for several hours in either ambient atmosphere the measurements were performed in a time interval sufficiently small that this drift was insignificant.

Table I. Summary of experimentally determined surface energy level parameters and sensitivity to ambient atmosphere variations for several surface treatments

Dry O_2 atmosphere — Surfaces in (100) plane — $T = 295°K$

(a) H_2O_2:HF:H_2O etch

Surface treatment	Recombination levels								Trapping levels								Δu_s
	U_s	$\frac{C_{p1}}{C_{n1}}$	$\frac{E_{t1}-E_i}{KT}$	$N_{t1}\times 10^{-11}$	S_{max}	$C_{p1}\times 10^8$	$C_{n1}\times 10^8$	U_s	$\frac{C_{p2}}{C_{n2}}$	$\frac{E_{t2}-E_i}{kT}$	$N_{t2}\times 10^{-11}$	S_{max}	$C_{p2}\times 10^8$	$C_{n2}\times 10^8$	$\frac{E_t'-E_i}{KT}$	$N_t'\times 10^{-11}$	$\frac{E_t''-E_i}{KT}$	$N_t''\times 10^{-11}$	$\frac{E_t'''-E_i}{kT}$	$N_t'''\times 10^{-11}$	
Control	2.50	148	4.8	4.4	290	2.43	0.016	—	—	—	—	—	—	—	−1.0	3.0	—	—	<−5.0	>N_{t1}	(1.8) 5.5
Iodate	0.55	3.0	2.8	>10	420	~0.21	~0.07	—	—	—	—	—	—	—	—	—	—	—	—	—	(−0.4) 2.1
H_2O_2-bake	3.20	600	3.3	3.5	260	1.82	0.003	0.50	2.7	~1.0	6.0	104	0.030	0.011	—	—	—	—	—	—	(1.6) 4.5
Thermal oxide	4.00	~3000	~4.0	~10	210	~1.0	~10^{-4}	~1.0	~7.5	~1.5	~3.0	120	~1.0	~0.1	~−1.0	~3.0	—	—	—	—	(3.1) 1.8
Silica	1.50	20	5.0	6.0	315	2.07	0.103	—	—	—	—	—	—	—	−1.0	3.5	>7.0	>N_{t1}	<−6.0	>N_{t1}	(2.0) 5.0
H_2SO_4-chromate	0.05	1.1	1.0	>10	450	~0.59	~0.54	—	—	—	—	—	—	—	−1.5	~15	—	—	—	—	(−0.15) 2.0

(b) CP4A etch

Control	2.30	100	4.5	4.0	146	1.01	0.01	—	—	—	—	—	—	—	−1.1	2.5	>7.0	>N_{t1}	<−6.0	>N_{t1}	(2.2) 5.0
Iodate	0.50	2.7	3.3	>10	200	~0.25	~0.09	—	—	—	—	—	—	—	—	—	—	—	—	—	(−0.3) 2.0
H_2O_2-bake	3.00	400	3.2	5.0	130	0.53	0.001	0.6	3.3	~1.0	3.0	50	0.32	0.002	—	—	—	—	—	—	(1.8) 4.0
Thermal oxide	2.40	122	4.7	4.1	115	0.93	0.01	—	—	—	—	—	—	—	−1.5	1.3	>7.0	>N_{t1}	—	—	(1.8) 3.2
Bromine	3.00	400	6.2	~10	100	~1.34	~0.003	—	—	—	—	—	—	—	−1.3	2.2	>7.0	>N_{t1}	—	—	(1.0) 3.6

gated, the data for each surface condition in Table I represent results typical of, at most, three samples per surface treatment. In several cases, only two samples per surface treatment were prepared. Consequently, the results may be interpreted only in terms of trends, since the statistical sample sizes for each surface treatment were too small to establish any degree of confidence.

The data in Table I are organized into three primary groups. The first of these includes the parameters associated with energy levels which are active in recombination. The second group lists parameters of energy levels which are not active in recombination, referred to as trapping levels. The third group of data constitutes a measure of the sensitivity of a given surface condition to a variation of the ambient atmosphere. This appears in the column headed "Δu_s" in Table I. The quantity Δu_s, the total swing in surface potential, in units of kT/q, in going from a dry O_2 to a wet O_2 atmosphere, is listed along with the value of u_s at the midpoint of this swing. The midpoint values are the quantities in parentheses.

The data for each set of levels are broken up into several columns according to the following parameters: the value of the surface potential u_s, about which the s.r.v. curves are symmetrical, the ratio of the capture cross sections for holes and electrons c_p/c_n, the energy of the level $E_t - E_i$ in units of kT, the density of the level N_t, the maximum surface recombination velocity s_{max}, the capture cross section for holes c_p, and the capture cross section for electrons c_n. The subscript numerals refer to two separate recombination levels while the superscript primes represent different trapping levels. In many cases, only estimates of some of these parameters are available due to the fact that the applied electric field could not induce sufficiently large swings in surface potential. Where such estimates were made are evident in Table I as represented by appropriate symbols.

The main results suggested by the data are the following:

(*A*) The only significant difference between the two etched surfaces (controls in Table I) appears in the values of s_{max} and c_p. The energy and density of the recombination levels are comparable.

(*B*) The surface energy levels can be grouped as follows: (*a*) a recombination level between about 3.0 and 6.0 units of kT above the center of the gap; (*b*) a recombination level between about 1.0 and 1.5 units of kT above the gap center; (*c*) a trapping level about 1.0 to 1.5 units of kT below the center; (*d*) a trapping level at an energy somewhat greater than 7.0 units of kT above the gap center; (*e*) a trapping level at an energy somewhat greater than 6.0 units of kT below the gap center.

These are all consistent with the levels reported by several authors in the literature (2, 6-9).

(*C*) The iodate and H_2O_2-bake surface treatments yielded remarkably similar results on either of the etched surfaces.

In analogy, one could expect that thermal oxidation should also be similar for the two etched surfaces. Although the H_2O_2:HF:H_2O surface was successfully oxidized thermally, similar oxidation on a CP4A surface was not achieved. This is evident from the data of Table I, but additional support of this observation appeared in the form of oxide films on the samples. The thermal oxidation treatment on CP4A surfaces did not exhibit any interference colors or patterns characteristic of thick oxide layers. The thermally oxidized H_2O_2:HF:H_2O surface, however, exhibited uniform interference colors that suggested oxide film thicknesses of the order of 1000Å.

(*D*) It will be noted in Table I that, with the exception of the H_2SO_4-chromate treatment, a surface treatment on either control surface generally preserves the energy of the first recombination level. It appears to be characteristic of treatments that are known to be oxidizing (H_2O_2-bake and thermal oxidation), that a second recombination level is introduced. The H_2SO_4-chromate surface, however, does not preserve the first recombination level, but rather introduces a second recombination level in the $1.0 < (E_t - E_i/kT) < 1.5$ range. It is to be noted further that at least an order of magnitude reduction in the electron capture cross section for the first recombination level is associated with a heavily oxidized surface.

(*E*) The Δu_s column of Table I indicates that three of the surface treatments investigated (iodate, thermal oxidation, and H_2SO_4-chromate) are relatively

insensitive to ambient atmosphere variations, suggesting that such surface treatments could possibly be employed to passivate partially a semiconductor device surface. This aspect of the data will be developed more fully in a following section.

(*F*) Although not explicitly mentioned previously, weight loss measurements were taken for all of the surface treatments listed in Table I. The iodate, H_2SO_4-chromate, and bromine treatments exhibited weight losses after processing; the other treatments did not suffer a loss of weight within experimental error. The iodate and H_2SO_4-chromate weight losses were relatively small, *e.g.*, of the order of 2-4%. The weight loss for the bromine treatment, however, was of the order of 50-75%. We conclude that each of these treatments actually etches to some degree. The bromine treatment is definitely an etch and is thus improperly placed in the category of a surface treatment. The significant point to make is that it is just these surface treatments that alter most drastically the characteristics of the control surface. Those surface treatments which do not exhibit any evidence of etching seem to preserve the characteristics of the control surfaces to some extent.

(*G*) The most widely fluctuating trap parameter for recombination levels is the capture cross section for electrons, c_n. The capture cross section for holes, c_p, varies only approximately an order of magnitude in the range of surface conditions investigated. The value of c_n, however, experiences variations over a range of three orders of magnitude. Of particular interest is the reduction of c_n consistently observed for those surface treatments which are known to oxidize heavily (H_2O_2-bake and thermal oxidation).

The data as a whole clearly indicate the existence of at least two recombination levels and three trapping levels which are always present. Whether or not these levels can be observed experimentally depends on (i) the total range of u_s covered, (ii) the relative densities of the levels, and (iii) the capture cross sections for holes and electrons for each level. Evidently, the capture cross sections are relatively small for the trapping levels, rendering them inactive as recombination centers.

Result (*D*) above suggests a possible explanation of the origin of the two different recombination centers. It can be assumed that the levels in the range $3.0 < (E_t - E_i)/kT < 6.0$ are associated with a Ge-O bond of some form, while the levels in the $1.0 < (E_t - E_i)/kT < 1.5$ are associated with lack of stoichiometry and other imperfections in the Ge-to-GeO_x transition region. If it is further assumed that the heavy oxidation mechanism is one that requires the transfer of Ge atoms from the germanium-oxide interface to the outer surface of the oxide, then the origin of the two recombination levels could be as follows: the thin, equilibrium layer of oxide which results from etches gives rise to a relatively uniform and nearly perfect transition from germanium to the oxide. Thus, the first type of recombination level dominates. On heavy oxidation, however, the Ge atoms that are transferred to the outer surface of the oxide leave the transition region disturbed and farther removed from perfection. Thus, the second type of recombination level becomes more prominent, but not at the expense of the first type. The decrease in the capture cross sections for electrons that accompanies heavy oxidation may possibly be explained through an interaction between the two types of levels.

Employing the same assumptions of the previous paragraph, one could then explain the results observed for the H_2SO_4-chromate treatment as the domination of the second type of level while the first type is rendered insignificant. This would be possible if the H_2SO_4-chromate treatment is really etching moderately, yielding a resulting germanium-to-oxide transition region which is grossly disordered. Evidence that this explanation is reasonable comes from visual observation of the H_2SO_4-chromate treated surface. The resulting surface appears slightly textured, as compared to the original H_2O_2:HF:H_2O control surface, suggestive of a large number of nucleation sites for a surface layer decidedly different from the control surface.

Now, an extension of the arguments presented for the oxide surface layer can be employed to discuss some aspects of surface passivation. It will be noted that the smaller values of Δu_s (corresponding to surfaces relatively insensitive to ambient atmosphere variations) are correlated with large surface state densities. This is expected, since large quantities of trapped charge in surface states offer a more effective shield from the influence of a variation of surface charge. Let it be further noted that the thermal oxidation on an H_2O_2:HF:H_2O surface affords the smallest value of Δu_s. Based on our assumptions regarding the origin of the recombination states, it might then be possible to reduce the value of Δu_s by another large factor by thermally oxidizing one of the other surface treatments rather than the unstable control surfaces. What we really wish to emphasize is that the data suggest a very significant relationship between the etched surface characteristics and those characteristics which result from a subsequent surface treatment. It is concluded that a fruitful approach to the problem of passivating a semiconductor surface can be found in studying, in more detail, just what these relations are and how they can be exploited.

Application to Devices

The data of Table I can be employed to anticipate the effect of the listed surface treatments as applied to a semiconductor device. Most semiconductor rectifiers and transistors require that both the surface conductivity and the surface recombination velocity simultaneously assume their lowest practical values. It is further desirable that neither of these quantities vary with varying ambient atmosphere (passivated surface) and with time (stabilized surface). Information about all but the time variations is implicit in Table I.

Consider the plot of the change in conductivity $\Delta\sigma$ *vs.* surface potential, u_s, in units of kT/q in Fig. 5. A similar plot for any resistivity and type can be reproduced from the calculations of Kingston and Neustadter (10). Now this curve is independent of the surface treatment since it depends only on the

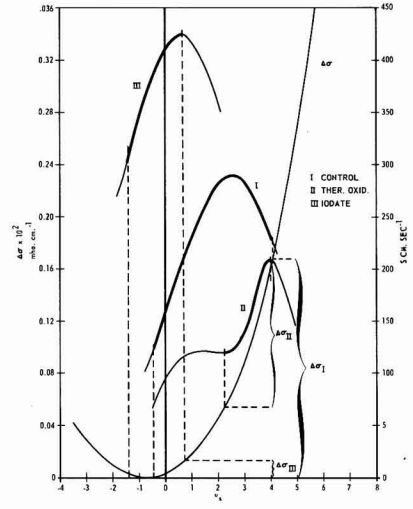

Fig. 5. Surface recombination velocity, s, and change in conductivity, $\Delta\sigma$, as functions of the surface potential, u_s, in units of kT/q for determining the range of s and $\Delta\sigma$ corresponding to a variation of the ambient atmosphere from dry to wet oxygen.

bulk potential and the surface potential regardless of how the value of surface potential is achieved. However, the surface recombination velocity as a function of surface potential does vary considerably with surface treatment (see Fig. 3). Thus, in order to establish both the value of the conductivity and the surface recombination velocity (s.r.v.) simultaneously for a given value of surface potential, it is necessary to superimpose the s.r.v. *vs.* u_s curve for each surface treatment. This has been done in Fig. 5 for three representative surface treatments (control, iodate, thermal oxidation) on an H_2O_2:HF:H_2O etched surface. The s.r.v. *vs.* u_s curves can be constructed from the data of Table I by putting the appropriate values of the listed surface recombination level parameters into the theoretical expression for the surface recombination velocity (2).

It is then possible, by employing the Δu_s column of Table I, to evaluate the ranges of conductivity and s.r.v. to be expected with a variation of ambient atmosphere from dry to wet oxygen as defined previously. Consider the s.r.v. curve I of Fig. 5, along with the $\Delta\sigma$ *vs.* u_s curve, appropriate for an H_2O_2:HF:H_2O etched surface on 35 ohm-cm n-type germanium. The Δu_s for this surface condition is 5.5 units of kT/q while the midpoint of this range is 1.8. Bracketing this range on the horizontal scale, it is found that the corresponding changes in the s.r.v. (portion of the curve that is heavy line) and the conductivity are from 125 through the maximum of 290 and back to 230 and $\Delta\sigma = 0.16$, respectively. Similar consideration of the iodate and thermal oxidation treatments yields corresponding ranges of s and $\Delta\sigma$, as indicated in Fig. 5. The significance of characterizing a surface treatment by including the Δu_s data is now apparent. It will be noted that, although the Δu_s of the thermal oxidation treatment is slightly smaller than the same quantity for the iodate treatment, the changes in both $\Delta\sigma$ and s.r.v., percentagewise, are smaller for the latter treatment. The reason for this result is that the midpoint of the Δu_s range is near the conductivity minimum (−0.4) for the iodate case, where the conductivity is varying relatively slowly as a function of u_s. The thermal oxidation case, however, exhibits a midpoint of Δu_s (3.1) which is on the portion of the conductivity *vs* u_s curve which is rapidly varying. The importance of stating not only the range of u_s but also the midpoint (or some such arbitrary reference) is thus evident.

It is conceivable, then, that extensive tabulation of data after the manner of Table I for the wide range of resistivities encountered in device technology could afford a device engineer a first-order approach to the engineering of surfaces into devices. Employing such tabulations, it should be possible to delineate the range of values of important parameters to be expected from a given surface treatment after a fashion similar to that discussed in connection with Fig. 5.[8]

There remains at least one major obstacle to device surface engineering. This has to do with the question of how the existence of a junction at the surface affects the important parameters associated with a given surface treatment. It is well known that many etches and/or surface treatments can be employed to delineate junctions in semiconductors. This, by definition, is evidence that a specific operation on a surface will yield characteristics in the vicinity of the junction that could be significantly different from the characteristics on the surface of homogeneous material. Thus, work such as that described above must be complemented with studies on materials containing junctions that come out to the surface.

Summary

An attempt has been made to define a method of characterizing a semiconductor surface condition which would be conducive to an engineering approach to the surface problem. This method consists of listing not only the surface parameters associated with surface traps, but including also the range and location, in values of surface potential, that are introduced by a specific surface condition. The methods discussed in this paper are not intended to be all-inclusive or final, but rather suggest an approach which could possibly allow for the eventual engineering of surfaces into semiconductor devices.

Features of the experimental data of particular interest are (*a*) the relatively constant capture cross sections for holes for the variety of surface conditions investigated, (*b*) the wide variation of capture cross sections for electrons, (*c*) the appearance of a second recombination level which is apparently associated with heavy oxidation, and (*d*) the reduction in sensitivity of the surface conductivity to variations of ambient atmosphere due to a relatively large concentration of charge in fast surface states which effectively "shield" the semiconductor from the influences of the atmosphere.

[8] It must be recalled that the approach considered in connection with Fig. 5 tacitly assumes that, in the range Δu_s, the surface parameters of Table I do not change. The fact that they do change is demonstrated in Fig. 4. The assumption has been made that the s.r.v. curves are not significantly different for a dry and a wet oxygen atmosphere. The ranges of s and $\Delta\sigma$ obtained are thus accurate only within the limits implied by such an assumption.

Acknowledgments

It is a pleasure to acknowledge the assistance of Mr. R. F. Voigts in the design and construction of the experimental apparatus and the procurement of experimental data.

Manuscript received Dec. 18, 1961; revised manuscript received March 9, 1962. This paper was presented in part before the Detroit Meeting, Oct. 1-5, 1961.

Any discussion of this paper will appear in a Discussion Section to be published in the June 1963 JOURNAL.

REFERENCES

1. A. Many, E. Harnik, and Y. Margoninski, "Semiconductor Surface Physics," R. H. Kingston, Editor, p. 85, University of Pennsylvania Press, Philadelphia (1957).
2. S. Wang, and G. Wallis, *Phys. Rev.*, **105**, 1459 (1957); *This Journal*, **106**, 231 (1959).
3. H. M. Bath and M. Cutler, *J. Phys. Chem. Solids*, **5**, 171 (1958).
4. A. V. Rzhanov, *Fizika Tverdogo Tela*, **2**, 2431 (1960). English Translation: *Soviet Physics-Solid-State*, **2**, 2166 (1960).
5. G. G. E. Low, *Proc. Phys. Soc. London*, **B68**, 10 (1955).
6. E. Harnik and Y. Margoninski, *J. Phys. Chem. Solids*, **8**, 96 (1959).
7. Y. Margoninski, *J. Chem. Phys.*, **32**, 1791 (1960).
8. Y. Margoninski and H. E. Farnsworth, *Phys. Rev.*, **123**, 135 (1961).
9. W. L. Brown, W. H. Brattain, C. G. B. Garrett, and H. C. Montgomery, "Semiconductor Surface Physics," R. H. Kingston, Editor, p. 111, University of Pennsylvania Press, Philadelphia (1957).
10. R. H. Kingston and S. F. Neustadter, *J. Appl. Phys.*, **26**, 718 (1955).

APPENDIX

Descriptions of Surface Treatments

H_2O_2 *bake.*—The sample is placed in contact with glass, flooded with a small amount of stabilized 30% H_2O_2, and baked in room atmosphere for 1 hr at 100°C.

Thermal oxidation.—The sample is placed in a flow of approximately 1 c.f.h. of dry oxygen for 72 hr at 500° ±10°C. (The sample is stored in methanol between the preparatory etch and the thermal oxidation surface treatment.)

Iodate.—The sample is treated for 1 hr at room temperature in an agitated solution containing HF, H_2SO_4, M/5 KIO_3, and H_2O in the proportions 4:1:1:2. The sample is rinsed in the sequence: H_2O, acetone, and H_2O, and is then stabilized by baking for several hours in room atmosphere at approximately 150°C.

Bromine.—The sample is placed in 4.0M KOH without agitation, warmed to 55°-60°C, held there for 20 min, and cooled to 35°C. The sample is then flooded free of KOH with a solution containing Br_2 and 4.00M KBr in the proportions 3:250, and is allowed to stand in this solution without agitation for 15 min. The KOH-bromine solution sequence outlined above is repeated as often as necessary, always flooding away one solution with the other, until visual inspection shows a uniform attack at the end of the 15-min exposure to the bromine solution. When this condition is satisfied, the sample is left in the bromine solution for 6 hr, without agitation, and is then rinsed in H_2O.

Silica.—The sample is placed in agitated HF for 1½ hr, and then silicic acid powder is added to the agitated solution until a 20% excess has been reached in 5 min according to the reaction

$$SiO_2 + 4HF \rightarrow SiF_4 + 2H_2O$$

The agitated solution is allowed to cool for ½ hr and then is flooded away with H_2O.

H_2SO_4-*chromate.*—The sample is warmed in agitated, M/20 $Na_2Cr_2O_7 \cdot 2H_2O$ solution in H_2SO_4 to 140°-145°C and is held at this temperature for 1 hr. The solution is then cooled to 35°C, and the sample is removed and rinsed in H_2O.

Descriptions of Chemicals Used

Bromine, analytical reagent.
Oxygen, "Airco" U.S.P.
Hydrofluoric acid, 49% electronic grade.
Silicic acid powder, 78% SiO_2, reagent grade.
Sulfuric acid, 97%, electronic grade.
Potassium hydroxide, reagent grade.
Potassium bromide, reagent grade.
Potassium iodate, analytical reagent.
Sodium dichromate, dihydrate, reagent grade.
Hydrogen peroxide, 30%, stabilized, electronic grade.
Acetone, electronic grade.
Methanol, absolute, electronic grade.
Water, distilled and deionized, used for all rinsing and preparation of solutions.

Selection of Germanium Transistor Parameters by Control of Moisture at Low Levels within the Device Encapsulation

Robert J. Gnaedinger, Jr., Steward S. Flaschen, Marie A. Hall, and Edward J. Richez

Semiconductor Products Division, Motorola Inc., Phoenix, Arizona

ABSTRACT

Experiments have been carried out which indicate that moisture in air at levels below 1% relative humidity (200 ppm H_2O) has a strong influence on the surface recombination velocity of germanium and on the parameters of transistor devices derived from it. By controlling the moisture partial pressure at any of various given levels within hermetically sealed transistors, it has been found possible to preselect different ranges of several, stabilized, device parameters, such as h_{fe}, I_{CO}, and I_{EO} without changing the device fabrication procedure. A method for controlling the moisture partial pressure using pairs of inorganic compounds is presented together with data obtained from its application to large-scale manufacture. In addition to showing the practical value of these controlled moisture materials, these results emphasize the need for a more precise knowledge of the moisture level present in the "dry" gaseous ambients commonly used in studies of semiconductor surface properties.

It is well-known that the chemical composition of the gas phase adjacent to a semiconductor surface plays an important role in determining the electrical properties of that surface (1-3). Water vapor is perhaps the most striking example of this fact. High relative humidities produce severe and erratic current leakage paths across the surface of silicon and germanium crystals; changes in the humidity at moderate levels produce pronounced changes in the surface conductivity and surface recombination velocity. In the manufacture of semiconductor devices it was this high sensitivity to changes in the moisture level which caused the introduction of hermetic sealing of devices. Yet, although this hermetic sealing generally removed the erratic behaviors associated with gross moisture, there remained day-to-day, seasonal, and aging variations in the parameters of production devices. In order to reduce these variations, it was found necessary to insert moisture adsorbing materials into the hermetically sealed device encapsulations. This technique yielded a more reproducible product, but it frequently accomplished this at the expense of large shifts in the levels of some of the device parameters.

It is the purpose of this paper to present the results of new experimental studies of the effects of moisture on the parameters of germanium transistors. These results indicate that the presence of moisture vapor at very low levels continues to exert a strong influence on semiconductor surface properties, a conclusion suggested by previous work (4-7), but not experimentally verified. In addition, these results show that the rather disruptive role commonly associated with moisture in the manufacture of semiconductor devices can be converted into a constructive one by selection and control of the moisture level. Lastly, these results emphasize the necessity of being able to make a quantitative, rather than qualitative, statement of the dryness level in the adjacent gaseous ambient in experimental studies of semiconductor surfaces and semiconductor devices.

Experimental Method

The experimental method consisted of establishing, in principle, a constant moisture partial pressure within an hermetically sealed semiconductor device. This controlled moisture pressure was achieved through the utilization of the thermodynamic equilibrium that exists between two chemical phases in different, but adjacent, degrees of hydration. This is illustrated by Eq. [1] where the

$$2CaSO_4 \cdot \tfrac{1}{2}H_2O(\text{Solid}) \rightleftarrows 2CaSO_4(\text{Solid}) + H_2O(\text{Vapor Phase}) \quad [1]$$

half-hydrate of calcium sulfate is shown in equilibrium with anhydrous calcium sulfate and water vapor. The equilibrium constant for this reaction is the water partial pressure (Eq. [2]). As long as specific, crystalline

$$K_{eq} = p_{H_2O} \quad [2]$$

phases of both solids are present in a closed system, and as long as sufficient time for equilibration has been allowed at a given temperature, the moisture partial pressure in the adjacent gas phase will remain constant, independent of the total amount of moisture enclosed in the system.

The equilibrium pressure of water will be temperature dependent, varying in accordance with an Arrhenius expression, as long as no phase changes occur in the two solids. In Eq. [3] $\Delta H°$ is the standard heat of reaction. ($\Delta H°$ can be

$$K_{eq} = A \exp -\Delta H°/RT \quad [3]$$

expected to have some temperature dependence. In addition, the water partial pressure will show a small dependence on total pressure if an inert gas is present in the system; this dependence is deter-

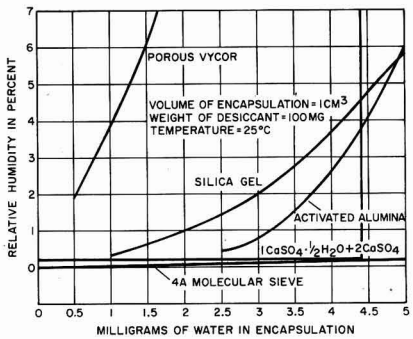

Fig. 1. Comparison of reactive and adsorptive moisture getters. Relative humidity *vs.* total encapsulated moisture.

mined by the volume change occurring in the reaction.)[1]

This type of behavior is distinctly different from the commonly used, adsorptive desiccants, *e.g.*, silica gel, activated alumina, etc., where the moisture partial pressure is strongly dependent on the total amount of moisture that is enclosed in the system. In Fig. 1[2] there is shown a comparison of the reactive type of moisture getter *vs.* the adsorptive types. This figure has been constructed for the following hypothetical situation. Consider that in a 1 cm^3 volume is 100 mg of getter. One then asks: What is the relative humidity in that volume at equilibrium at 25°C for various amounts of encapsulated water within that volume? The answer for the adsorptive getters is that there is a wide variation in the relative humidity with the amount of encapsulated moisture. In the example shown here, the molecular sieve shows variation, but at a very low level of relative humidity in comparison with the porous vycor, silica gel, and activated alumina. These curves show behaviors characteristic of true surface adsorption.[3] In contrast, the mixture of anhydrous and hemihydrated calcium sulfate shows a constant relative humidity up to the point where the anhydrous phase completely disappears. After this has occurred, the addition of further moisture causes an abrupt increase in the relative humidity.

If other chemical species are used in place of the calcium sulfate, different but similarly controlled moisture partial pressures can be achieved. In Table I are shown several systems of inorganic compounds together with calculated values of their equilibrium moisture partial pressures. All of the values shown have been computed from thermodynamic data in the literature (11), using the relation[4] given by Eq. [4]. Some have been qualitatively

$$\Delta F^\circ = -RT \ln K_{eq} \qquad [4]$$

[1] For further discussion of the subject of heterogenous equilibrium, see, for example, the treatise on the phase rule by Ricci (8).

[2] The data for this figure were obtained from Corning Glass (9) and Linde Company (10) and from thermodynamic data tabulated by the NBS (11). It was necessary to extrapolate the data to show the low relative humidity behavior of the adsorptive getters. The curves shown should be considered purely qualitative.

[3] See, for example, the treatise on surface films by Harkins (12).

[4] No value is listed for ΔF° of formation of $Ba(OH)_2$. Since it was observed that the ΔS° for the reaction $Ca(OH)_2 \rightleftarrows CaO + H_2O$, was identical to that for the $Mg(OH)_2$ reaction, this same value was assumed for $Ba(OH)_2$ in order to calculate the ΔF°. Note also that fugacity = pressure at these low pressures (13).

Table I. Equilibrium moisture partial pressures above several inorganic compound systems as calculated from thermodynamic data

System	Partial pressure at 25°C in mm of Hg
$BaO:Ba(OH)_2$	2×10^{-15} (approx)
$CaO:Ca(OH)_2$	5×10^{-9}
$MgO:Mg(OH)_2$	5×10^{-4}
$B_2O_3:HBO_2$	3×10^{-2}*
$CaSO_4:CaSO_4 \cdot \frac{1}{2}H_2O$	3×10^{-2}**
$HBO_2:H_3BO_3$	1×10^{-1}
$CaSO_4 \cdot \frac{1}{2}H_2O:CaSO_4 \cdot 2H_2O$	5†
Liquid water	23.76

* Calculated for a glassy B_2O_3 phase.
** Calculated for the β-hemihydrate and the β-anhydrous phases.
† Calculated for the β-hemihydrate phase.

checked by the Knudsen Method of measuring the rate of effusion through a pin hole.[5]

The materials listed above have been found experimentally to satisfy the criteria of chemical and electrical inertness with respect to germanium device surfaces, as shall be seen subsequently, apparently exerting influence on the devices primarily through their control of the moisture partial pressure.

Experimental Results

The following results were obtained by encapsulating, within hermetically sealed transistors, the specified "controlled ambient" materials in amounts sufficient to maintain the required, two solid phase system. The germanium pnp power transistors were processed normally through electrolytic etch in basic solution, rinse, and dry. The specified materials were then added and the encapsulation sealed immediately in room air. The materials were added with no attempt to prevent their contacting the germanium surface.

The high-frequency, germanium pnp transistors were processed normally through electrolytic etch, rinse, dry, and vacuum bake. The controlled ambient materials were then added and the encapsulation sealed immediately. In this case physical contact between the materials and the germanium was prevented for mechanical reasons.

Figure 2 shows the effect of different moisture controlling materials on the power gain of germanium power transistors. Each chart is a histogram showing the distribution of devices in the various power gain ranges for the given controlled ambient mixture. (The power gain range to the right of 41 db contains devices with P.G. $\geqq$ 41 db.) The ordered dependence of power gain on the calculated moisture partial pressure (Table I) at these very low levels is strikingly apparent. Increasing the moisture pressure increases the power gain.

Parameter measurements were made following a 96 hr thermal treatment at 125°C and a subsequent recovery at room temperature for a minimum time of 12 hr.

[5] Our measured values on reagent grade hemihydrate of calcium sulfate were approximately 0.06 mm of Hg at 25°C. Several phase modifications of anhydrous and hemihydrated calcium sulfate are reported in the literature. The value shown in Table I was calculated for the β-phase of each.

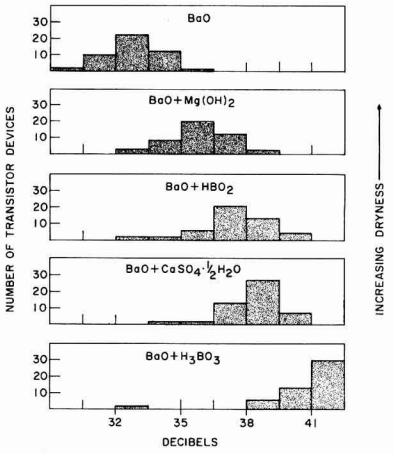

Fig. 2. Effect of moisture level on power gain of germanium pnp power transistors.

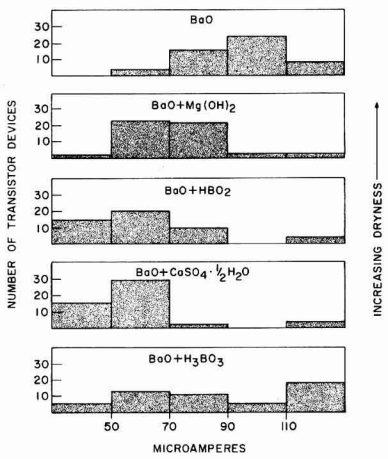

Fig. 3. Effect of moisture level on low voltage saturation current of germanium pnp power transistors.

The designed function of the BaO in these mixtures is to dehydrate a portion of the hydrated phase in order to establish the two phase equilibrium. The BaO becomes completely converted to $Ba(OH)_2$ by this process and does not apparently affect the equilibrium in any other manner. That this is, in fact, the real function of the BaO is borne out by the behavior of the data; in addition, it was verified experimentally by varying the ratio of BaO to $CaSO_4 \cdot \frac{1}{2}H_2O$ and by using mixtures of $CaSO_4 \cdot \frac{1}{2}H_2O$ and $CaSO_4$ without BaO, both of which produced results that were statistically indistinguishable from the $BaO + CaSO_4 \cdot \frac{1}{2}H_2O$ results shown in Fig. 2.

Each of the histograms in Fig. 2 was prepared from 50 devices which were randomly selected from one week's production run. Statistical analysis of the data used for Fig. 2 indicates that the difference between the mean of each mixture and that of the BaO lies in the interval shown in Table II, with 95% confidence. From this it can be seen that by reducing the moisture level from a calculated 50 ppm ($BaO + CaSO_4 \cdot \frac{1}{2}H_2O$) in air to an extremely dry condition (BaO), the power gain can be lowered by about 6 db. [It might be noted that "vacuum bake-out" plus molecular sieve getter gives power gains that are similar to the $BaO + Mg(OH)_2$ system.]

Table II. Comparison of mean power gains of pnp germanium power transistors for different controlled ambient materials

Mixture	No. of devices	Mean P.G. after thermal treatment	P.G.—P.G. (BaO) ± 95% confidence limits
BaO	240	32.9	—
$BaO + Mg(OH)_2$	46	35.8	2.9 ± 0.8
$BaO + HBO_2$	45	37.6	4.7 ± 0.8
$BaO + CaSO_4 \cdot \frac{1}{2}H_2O$	49	38.5	5.6 ± 0.7
$BaO + H_3BO_3$	48	42.6	9.7 ± 1.1

BaO represents 5 day, 48 devices per day. Remainder represent single days. Comparison is with 5 day BaO average, this being the control group. A histogram for one of these BaO groups is given in Fig. 2.

These represent good devices in the sense that both emitter and collector diodes showed reasonable reverse breakdown voltages and collector to emitter punch-through voltages were reasonably high.

The behavior of the common emitter current gain was measured and was as expected from the power gain measurements, *i.e.*, P.G. (db) $\propto \log h_{fe}$ for the same emitter current.

Figure 3 shows histograms of the low voltage saturation current for the same devices used in Fig. 2. (The cell to the right of 110 μa contains devices with $I_{CBO} \geqq 110$ μa.) The temperature of measurement was $26° \pm 1°C$. As can be seen, there is again an ordered dependence of I_{CBO} on the calculated moisture pressure. Increasing the moisture level decreases the I_{CBO} of these devices, except for the orthoboric acid group which shows a bimodal distribution. After further recovery at room temperature, this distribution becomes unimodal, like the other groups, with a strong peak in the cell with the lowest current. Since the power gain in this group recovers more rapidly from the 125°C heating than does the I_{CBO}, it appears that in this case those chemical processes, which affect the surface recombination velocity, stabilize within 12 hr; on the other hand, there appears to be an additional factor affecting the I_{CBO}, which factor requires a longer time for recovery than does the surface recombination velocity.

Figure 4 shows that the effect of ambient moisture control persists up to 100°C. Here each histogram includes 100 devices. The low voltage saturation currents of devices containing the metaboric acid mixtures are clearly well below those of the dryer devices which were given a "vacuum bake-out" and which contain molecular sieve.

Other device parameters were also followed in these experiments. The low voltage I_{EBO} showed a behavior that was very similar to that of I_{CBO}. The breakdown voltages of the collector junctions were approximately the same for all of the "controlled ambient" materials except for the boric acid groups which caused breakdown at lower voltages.[6] The emitter breakdown voltages behaved in a manner similar to those for the collectors.

[6] The orthoboric acid appeared to lower the breakdown voltage slightly. The metaboric acid lowered it by an average of about 20v. Thus, it appears that the boric acids may be acting in some capacity in addition to providing moisture.

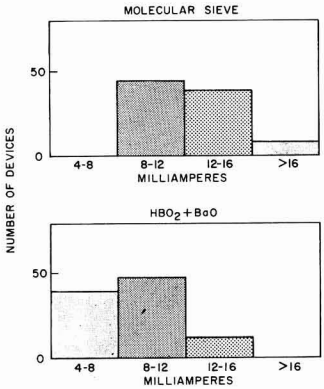

Fig. 4. Effect of controlled ambient material on low voltage saturation current of germanium pnp power transistors at 100°C.

Cold tests showed no diode looping associated with condensed water, a result consistent with the low relative humidities within these devices. Strenuous shake tests produced no changes in most parameters and only slight changes (within specifications) in others.

The effects of 1000 hr of 125°C shelf aging on the power gain and the low voltage I_{CBO} are presented in Tables III and IV.[7] These data indicate that accelerated aging at 125°C of these devices containing controlled ambient materials produces changes that are comparable to current production practice.

[7] The device groups in Tables III and IV are not the same as those in Table I. The small differences in the means for the same controlled ambient material can be ascribed to differences in group sizes and to variations in production runs.

Table III. Thermal aging of pnp germanium power transistors at 125°C for 1000 hr, effect on power gain

Mixture	No. of devices	Mean P.G. after thermal treatment	Mean P.G. after 1000 hr at 125°C	Change in mean with 95% confidence limits
BaO	19	32.4	33.0	0.6 ± 0.2
Molecular sieve	239	35.2	34.9	−0.3 ± 0.1
BaO: $Mg(OH)_2$	20	36.1	35.1	−1.0 ± 0.3
BaO: HBO_2	237	38.8	37.2	−1.6 ± 0.1
*BaO: $CaSO_4 \cdot \frac{1}{2}H_2O$	113	39.5	38.2	−1.3 ± 0.2

* This group received 1300 hr at 125°C.

Table IV. Thermal aging of pnp germanium power transistors at 125°C for 1000 hr, effect on low voltage I_{CBO}

Mixture	No. of devices	Median** after thermal treatment, μa	Median** after 1000 hr at 125°C, μa	Per cent change in median with 95% confidence limits
BaO	19	75.9	80.8	6.4 (2.8-10.0)
Molecular sieve	239	68.7	81.0	18.1 (16.5-19.8)
BaO: $Mg(OH)_2$	20	58.1	68.0	17.1 (4.5-31.1)
BaO: HBO_2	237	50.3	71.6	40.5 (37.6-43.5)
*BaO: $CaSO_4 \cdot \frac{1}{2}H_2O$	113	62.1	57.9	−4.0 (−7.4-−0.5)

* This group received 1300 hr at 125°C.
** Median computed from the formula:
Median = $10^{\overline{\log I}}$, where $\overline{\log I}$ is the mean value of log I_{CBO}.

Comparisons were made of the rate of stabilization of h_{fe}, after canning, at room temperature *vs.* that at 125°C, all measurements being made at room temperature. In the case of BaO, greater than 95% of the total drop in h_{fe} after 1000 hr at 125°C had occurred within the first day. On the other hand, the room temperature stabilization showed a continuously dropping h_{fe} out to 1000 hr, with a constantly decreasing rate. At 1000 hr the h_{fe} level was still considerably higher than in the devices that were heated at 125°C. It is not clear from these data whether or not the h_{fe} level during 25°C stabilization is asymptotically approaching the level rapidly attained at 125°C (although this is the best surmise). Likewise it is not clear that the stabilization process at 25°C is kinetically controlled by the oxidation of the germanium surface, or by the dehydration of the surface oxide, or by the desorption of moisture from the device interior, or by the uptake of water by the BaO.

The effect of power aging ($T_j = 90$°C and $V_{CE} = 40$v) is shown in Table V. Tabulated there are the power gains of eight devices of each group: BaO, molecular sieve, and BaO + $CaSO_4 \cdot \frac{1}{2}H_2O$. Measurements were made after 125°C thermal treatment at 500 hr and at 1000 hr. There appears to be little difference in power aging behavior with these different controlled ambient materials and the molecular sieve. Statistical analysis corroborates this observation for the above groups and also for BaO + HBO_2 and BaO + $Mg(OH)_2$, on both power gain and low voltage I_{CBO} parameters.

Table V. Power aging of pnp germanium power transistors with $T_j = 90$°C and $V_{CE} = 40$v, effect on power gain

Initial	500 hr	1000 hr
Eight devices containing BaO		
32.3	32.0	32.1
33.2	33.0	32.7
32.5	32.7	32.7
33.0	33.2	33.2
34.9	34.9	35.2
34.0	34.3	34.5
34.6	34.7	35.0
34.5	34.7	35.0
Eight devices containing molecular sieve		
41.7	38.0	38.4
36.4	36.5	36.3
36.8	35.8	35.5
37.8	37.6	37.8
40.2	40.4	40.9
39.4	40.3	40.7
41.4	41.5	41.8
40.4	40.6	40.8
Eight devices containing BaO + $CaSO_4 \cdot \frac{1}{2}H_2O$		
39.4	39.4	39.5
38.2	38.3	38.2
34.0	34.0	34.2
35.2	35.3	35.3
39.0	39.1	39.4
40.1	40.7	41.0
39.2	39.1	39.6
38.2	38.6	36.4

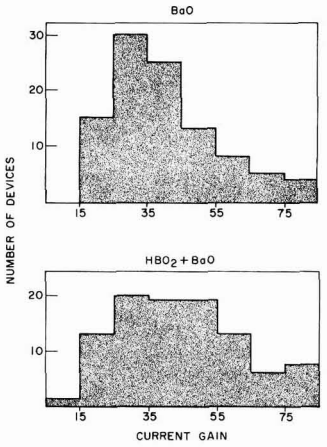

Fig. 5. Effect of moisture level on current gain of germanium pnp high-frequency transistors.

Controlled ambient materials were applied to another device, a high-frequency pnp germanium transistor. Figure 5 shows the effect of moisture control on the current gain of this diffused junction device. These histograms were each prepared from 100 devices, representing 20 random samples from the production on each of five days. The enhancement of gain achieved by controlling the moisture at a finite level over that obtained in the very dry condition is most evident in the high gain portion of the distributions. Parameters were measured on these devices after a thermal treatment of 144 hr at 125°C. The histogram was prepared from these data. The median β's in these two groups were: BaO, 35.9; BaO + HBO_2, 39.6. The median value of β has been calculated on the basis of a log normal distribution.

Figure 6 shows the effect of 125°C shelf aging on β. The initial aging pattern is distinctly better with metaboric acid than with the very dry system containing BaO. At longer times the two curves appear to age downward at about the same rate with the controlled moisture system maintaining its enhanced current gain relative to the very dry system.

Discussion

The data presented above indicate that certain parameters of germanium transistors depend very sensitively and reproducibly on moisture partial pressures at levels from about 80 ppm to below 1 ppm in air. The parameters thus affected are those which are strongly influenced by surface recombination velocity (or surface generation rate). The simplest interpretation to be made of these observations is that even at these very low partial pressures, sufficient water is adsorbed onto the germanium (or germanium oxide) surface to affect the surface properties appreciably. According to the work of Law (14), monolayer adsorption of water onto a germanium surface does not become complete until a relative humidity of about 10% is reached (this relative humidity in air at 1 atm pressure at 25°C corresponds to about 2000 ppm of H_2O). Consequently, the present results suggest that water plays perhaps its dominant role in affecting surface recombination velocity in the region below one monolayer, a conclusion that is consistent with the work of Law and Meigs (4).

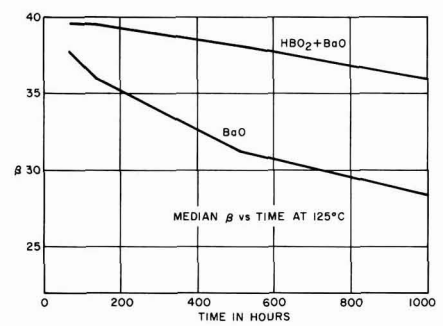

Fig. 6. Effect of ambient moisture control on elevated temperature shelf aging of β. High-frequency germanium transistors.

The detailed mechanism of how adsorbed water achieves this effect is not clear. However, since water is known to induce n-type channels (15) on p-type germanium, it has been postulated that adsorbed water molecules behave like slow, hole-trapping states. This same postulate has been used to explain observations of the effect of Brattain-Bardeen ambient cycling on the surface recombination velocity of germanium (16).[8] On the other hand, more recent work by Margoninski and Farnsworth (18), and others, has suggested that adsorbed water modifies the fast state energies and densities as well as slow state densities. (It should be borne in mind, however, that these latter studies used very moist ambients, resulting in multiple layers of adsorbed water in a region where the adsorption isotherm is rising very rapidly with increasing relative humidity. Thus, not only are films of water present, with attendant effects associated with ion drift and other electrolytic phenomena, but also the film thickness is in questionable control; severe complications in reproducibility and interpretation of measurements are present. It might be hoped that ambient cycling between a truly dry ambient and one that produces less than monolayer adsorption would give results that can be reproduced.) No structure has yet been proposed for either the slow or fast states, although it has been suggested that they are associated somehow with the formation of hydroxy groups in the surface oxide (1, 7) during a slow hydration reaction. [At higher moisture partial pressures, Hutson (19) ascribes the effect of water on surface potential to a dielectric polarization of the multilayer water film about unspecified surface donor ions; the first monolayer was specifically excluded from his analysis.]

However, the slow hole-trapping state model can be used to give a qualitative explanation of the results presented here. Figure 7 consists of a conventional energy band diagram for an n-type semiconductor as it terminates at a surface. Adsorbed water molecules are shown symbolically as $H_2O \oplus$ after

[8] Brattain and Bardeen (1), Stevenson and Keyes (16), and Many, Harnik, and Margoninski (17) consider the theory of surface recombination velocity.

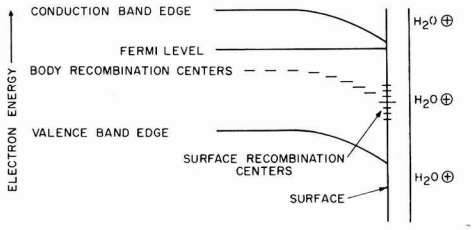

Fig. 7. Simple model of the effect on the surface recombination velocity of water adsorbed on an n-type semiconductor.

electronic equilibration with the crystal, in accordance with the slow state model. If it is assumed that the water molecules are neutral when first adsorbed, they must then give up electrons to the semiconductor during the equilibration process. These electrons may be trapped predominantly in fast surface states, if the latter are sufficiently numerous, resulting in a negligible effect on the surface conductivity and the surface potential. This was the result found in the original field-effect transistor experiments (20). However, if the fast surface states are relatively few in number, the electrostatic field associated with the ionized slow states will penetrate into the semiconductor, resulting in a strong effect on the surface conductivity and the surface potential, as shown in the Fig. 7.

This simplified model is sufficient to explain the present data as can be seen as follows: Although the electron population in the surface traps is increased by moisture, the electric field in the surface space charge region opposes the diffusion of holes toward the surface. This latter accounts for the reduction of injected carrier loss and the consequent increase in alpha with higher moisture levels. At the same time the higher electron population in the fast surface traps reduces the likelihood of thermal generation of holes at the surface since vacant electron traps are necessary. This accounts for the reduction of the surface generated component of the low voltage, reverse diode current with increasing moisture.

In order to obtain estimates of the surface recombination velocity at the different moisture levels, $h_{fe} - I_E$ plots were fitted to the Webster equation (21), which relates h_{fe} to doping, geometry, and surface recombination velocity. Figure 8 shows typical $h_{fe} - I_E$ plots for power transistors from several groups of controlled ambient encapsulants. The dominating influence of surface recombination velocity at low I_E is clear. The power gain distributions previously presented corresponded to $I_E = 0.5$ amp, where the effects of surface recombination velocity are being partially masked by strongly reduced emitter injection efficiencies due to conductivity modulation in the base.

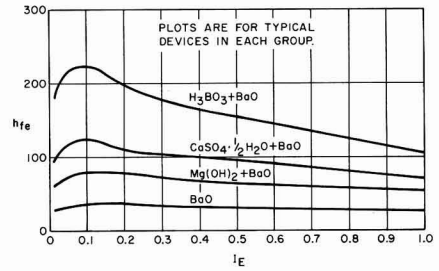

Fig. 8. h_{fe} vs. I_E for germanium pnp power transistors encapsulated with different controlled ambient mixtures.

Table VI. Surface recombination velocities for different controlled ambient mixtures as approximated using Webster's formula for germanium pnp alloy transistors

Moisture control mixture	Surface recombination velocity (approx), cm/sec
BaO	4000
$Mg(OH)_2 + BaO$	2000
$HBO_2 + BaO$	1000
$CaSO_4 \cdot \frac{1}{2}H_2O + BaO$	1000
$H_3BO_3 + BaO$	500

Only very approximate fits to Webster's equation were made. The results are shown in Table VI. Qualitatively, they suggest that in going down from a relative humidity of approximately 0.4% (H_3BO_3 system) to very low moisture levels, one can change the surface recombination velocity by a factor of about ten.

It should be noted that the effect of adsorbed moisture (as slow states) on device parameters will depend on the distribution of fast states and other slow states already present at the surface; the effects will also depend on the conductivity type of the body region. This is clearly demonstrated in the experiments of Buck and McKim (22) on silicon.

Experiments have also been carried out with silicon devices containing controlled ambient materials. The parameters of some of these devices have been affected in a similar pronounced manner; the behavior pattern seems to be consistent with that found with germanium devices, as described above.

Conclusion

1. These experiments have indicated that moisture vapor in air within the sealed, device encapsulations has a pronounced effect on the surface recombination velocity of germanium transistors at extremely low relative humidities, relative humidities as low as 10^{-3}% (0.2 ppm).

2. These experiments indicate the necessity of carrying out studies of semiconductor surface properties with a quantitative knowledge of the moisture level present in the gaseous ambient adjacent to the surface.

3. These experiments suggest that the use of ambient control materials for the stabilization of moisture partial pressures can be an asset in semiconductor device production. These materials allow the selection and control of certain device parameter levels over wide ranges without the requirement of modifying the body construction of the device.

Acknowledgment

This study was initiated with the active and willing assistance of David A. Kallander, Camille M. Lutfy, and Dale R. Lowe. It has proceeded only because of the complete cooperation we have received from individuals in the production and quality control

departments of Motorola's Semiconductor Products Division, in particular, Valmore E. Turcotte, John R. Welty, and Leo E. Dwork. It prospered under the protective wing of our statistical guardian angel, Dr. Irwin Miller of Arizona State University. And lastly, it is our pleasure to acknowledge manuscript suggestions by Dr. Trevor E. Law, Dr. Raymond M. Warner, Jr., and the reviewers of this paper.

Manuscript received Nov. 1, 1961; revised manuscript received Feb. 23, 1962. This paper was prepared for delivery before the Indianapolis Meeting, April 30-May 3, 1961.

Any discussion of this paper will appear in a Discussion Section to be published in the June 1963 JOURNAL.

REFERENCES

1. W. H. Brattain and John Bardeen, *Bell System Tech. J.*, **32**, 1 (1953).
2. R. H. Kingston, *J. Appl. Phys.*, **27**, 101 (1956).
3. N. B. Hannay, Editor, "Semiconductors," Chap. 16, "Semiconductor Surfaces," by J. T. Law, Reinhold Publishing Corp., New York (1959).
4. J. T. Law and P. S. Meigs, *J. Appl. Phys.*, **26**, 1265 (1955).
5. A. J. Wahl and J. J. Kleimack, *Proc. Inst. Radio Engrs.*, **44**, 494 (1956).
6. J. J. A. Ploos van Amstel, *Philips Tech. Rev.*, **22**, 181 (1961).
7. J. T. Wallmark and R. R. Johnson, *RCA Rev.*, **18**, 512 (1957).
8. J. E. Ricci, "The Phase Rule," p. 140, D. Van Nostrand Co., Inc., New York (1951).
9. "Vycor Brand Porous Glass, Code 7930—A Unique Drying Agent," T. H. Elmer and M. E. Nordberg, Research and Development Laboratory, Corning Glass Works.
10. "General Information on Linde Molecular Sieves," Linde Company.
11. "Selected Values of Chemical Thermodynamic Properties," Circular of the National Bureau of Standards 500, issued Feb. 1, 1952.
12. W. D. Harkins, "The Physical Chemistry of Surface Films," Chap. 3, Reinhold Publishing Corp., New York (1952).
13. G. N. Lewis and W. Randall, "Thermodynamics," Chap. 17 and 24. McGraw-Hill Book Co., Inc., New York (1923).
14. J. T. Law, *J. Phys. Chem.*, **59**, 67 (1955).
15. W. L. Brown, *Phys. Rev.*, **91**, 518 (1953).
16. D. T. Stevenson and R. J. Keyes, *Physica*, **20**, 1041 (1954).
17. R. H. Kingston, Editor, "Semiconductor Surface Physics," p. 85, "Surface Recombination Processes," A. Many, E. Harnik, and Y. Margoninski, University of Pennsylvania Press, Philadelphia (1957).
18. Y. Margoninski and H. E. Farnsworth, *Phys. Rev.*, **123**, 135 (1961).
19. A. R. Hutson, *ibid.*, **102**, 381 (1956).
20. W. Shockley, "Electrons and Holes in Semiconductors," Section 2.1b, D. Van Nostrand Co., Inc., Princeton (1950).
21. W. M. Webster, *Proc. Inst. Radio Engrs.*, **42**, 914 (1954).
22. T. M. Buck and F. S. McKim, *This Journal*, **105**, 709 (1958).

The Role of Selenium Vapor Pressure in the Formation of Silver Doped Manganese Selenide

W. D. Johnston

Research Laboratories, Westinghouse Electric Corporation, Pittsburgh, Pennsylvania

ABSTRACT

The effect of selenium vapor pressure on MnSe containing small additions of Ag_2Se has been studied by both weighing and electrical measurements. Three distinct regions have been noted. At low selenium pressures selenium is taken up by the mixture to form the mixed valence compound $Ag_xMn_{(1-x)}Se\oplus_x$. The value of $\oplus$, the hole concentrations, increases as a function of the selenium pressure until all Ag_2Se is used up and the sample becomes a single phase. At this equivalence point the pressure then increases rapidly with little change in composition. Finally, the pressure becomes sufficiently high that manganese vacancies are produced. These regions are described in terms of mass action expressions which link the vapor pressure with vacancies and electrical charge carrier concentrations.

The substitution of monovalent lithium for divalent manganese in MnSe has been shown to be possible up to 11 atomic %, *i.e.*, $Li_{0.11}Mn_{0.89}Se$ (1). Throughout this composition range the rock salt symmetry of MnSe is maintained. The products of such substitutions have been found to be electrical conductors with the conductivity increasing with lithium content. An electrically balanced formula for the composition $Li_xMn_{(1-x)}$ Se may be given as $Li^+_xMn^{+3}_xMn^{+2}_{(1-2x)}Se^=$ or alternatively $Li^+_x\oplus_xMn^{+2}_{(1-x)}Se^=$. The formulas are written for convenience in ionic form. In the latter formula $\oplus$ refers to holes and emphasizes that the holes are not localized on any particular manganese at normal temperatures (2).

A survey was made to determine what other doping additives could be used in order to induce p-type semiconductivity in MnSe. To this end Na, Cu, Ag, Au, Tl, and Cu were substituted for Mn. Selenium was replaced by As, P, and Si. The only successful doping agents proved to be Na and Ag as indicated by room temperature electrical measurements. The silver seemed to be soluble to only about 2 atomic % on the basis of a discontinuity in the thermoelectric power *vs.* resistivity curve as shown in Fig. 1. In this preliminary survey the reactants were fired iso-

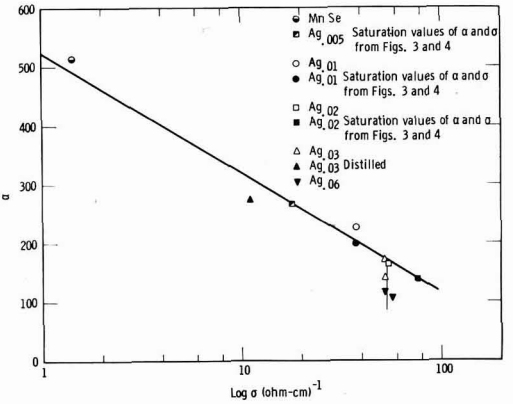

Fig. 1. α vs. log σ for $Ag_xMn_{(1-x)}Se$

thermally at 800°C in small sealed Vycor tubes. Additional qualitative experiments with silver substituted MnSe showed that the doping level decreased as selenium was removed by volatilization at elevated temperatures. The study described in this paper was undertaken in order to understand this relationship more fully. In brief the experiment performed was designed to give the stoichiometry or charge carrier concentration at various pressures of selenium vapor.

Experimental

The stoichiometry of the MnSe used in this work was critical to the success of the experiments. MnSe was prepared from −60 mesh vacuum distilled manganese and −60 mesh 99.99% selenium supplied by the American Smelting and Refining Company. The reactants, including a 10% excess of selenium, were either placed in a graphite crucible and sealed in Vycor or alternatively they were sealed in a Vycor tube which had been carbon coated by the pyrolysis of acetone. The material was heated up slowly to avoid any sudden evolution of heat to a final temperature of 700° and held for 24 hr. The product was crushed to 160 mesh and reheated for another 24 hr at which point the excess selenium was distilled off at 800°C. The recrushing was necessary to react all the manganese, and the 800° distillation quantitatively removed the excess selenium.

Products of the type $x/2$ Ag_2Se + $(1-x)$ MnSe were prepared from a mixture of a −100 mesh powder composed of weighed amounts of the stock MnSe and silver and selenium powders. The powders were pressed at 15,000 lb in a 3/8 in. diameter carbide die. The pellet was sealed in a graphite crucible and Vycor tube which had been previously outgassed. The mixture was heated isothermally at 800°C for 20 hr, then one end of the tube was placed at room temperature and volatile material, if any (none was ever observed), was allowed to distill to the room temperature end. The pellets obtained in this manner were clearly composed of two phases consisting of a small amount of shiny material distributed in the black pellet.

For the vapor pressure studies a 6g pellet of $x/2Ag_2Se$ + $(1-x)$ MnSe as prepared above was weighed and placed in a graphite boat which was sealed in a 12 in. long 19 mm diameter Vycor tube. In one end of the tube was a ½ in. long chamber which contained selenium. The pellet was held at the other end. The tube was placed in a two zone furnace such that the pellet was maintained at 800°, and the temperature of the selenium reservoir was at some lower temperature which could be chosen at will. The selenium reservoir temperature was arranged to be the coldest temperature of the tube, and thus the selenium vapor pressure was controlled by this temperature. In this manner the reaction

$$\frac{x}{4}\,Se_2 \text{ vapor} + x/2Ag_2Se + (1-x)\ MnSe \rightleftarrows Ag_xMn_{(1-x)}Se$$

may be studied. By quenching the sample tube at the end of the experiment and weighing the pellet, the uptake of selenium may be determined. Since selenium requires two electrons to be donated from the lattice to form the selenide ion ($Se^=$), creating two holes, the weight uptake of selenium may be expressed in terms of the hole concentration of the MnSe phase. It should also be noted that for each selenium added from the vapor two silvers are also added to the MnSe lattice and thus are equal to the hole content. It was found that equilibrium was achieved in less than 16 hr at all selenium pressures since an additional 16 hr or more did not result in a substantial additional weight change (generally less than ½ mg). Data were taken at random temperatures of the selenium reservoir which results in both adding and removing selenium from the sample in a random manner.

The first run however was an exception to this and was always at 600° reservoir temperature since, as will be seen later, the selenium pressure generated at 600° generally is sufficient to drive the formation reaction to completion. This first experiment thus acts as a check on the stoichiometry of the starting material. Apparently manganese and silver are not lost in any measurable amount from the pellets, nor does handling result in any appreciable weight loss since, on removal of the selenium added during a series of experiments by distilling this selenium to a room temperature reservoir, the starting weight is reproduced to within ± 1 mg.

As mentioned previously, repeat measurements are reproducible in pellet weight to ~ ½ mg. The weight changes recorded in this work range from 2-3 mg obtained at the lowest selenium additions to 30 mg at the highest selenium additions. The effect of this error is clearly visible in the wide scatter of the data at the low pressure-low selenium addition region of Fig. 2.

One must inquire as to the uptake of selenium vapor by MnSe and Ag_2Se individually in order to evaluate properly the uptake of the mixture. The MnSe case has been studied in detail, and the results are shown in Fig. 2. The change in weight of Ag_2Se maintained at 800° has been examined after equilibration with both a 600° selenium reservoir and a room temperature reservoir. In the case of the distillation to room temperature a weight loss

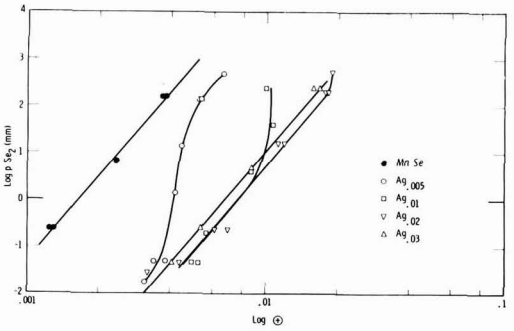

Fig. 2. Log p Se_2 vs. log $\oplus$ for $Ag_xMn_{(1-x)}Se$

of 0.24% was observed. In the case of the 600° Se reservoir experiment the sample gained a total ~ 1.1% by weight of selenium and was a liquid at 800°[mp reported (3) 897°] which liberated selenium on cooling. This weight change is negligible when one considers that only small amounts of Ag_2Se are used in the experiments combined with MnSe.

The selenium vapor pressure used is that reported by Brooks (4). It is taken as being purely dimeric Se_2. This approximation is not strictly correct since at 800°C and a pressure of Se_2 of 1 atm the pressure of the hexamer, Se_6, would be 0.02 atm (5). However, the relative pressure of the hexamer decreases rapidly with decreasing pressure of the dimer, and therefore, the 2% contribution is the worst possible case. The use of a lower sample temperature than 800°C would rapidly lead to an increased hexamer content, so 800° must be considered a minimum operating temperature to avoid this additional complication in the calculations.

After each experiment electrical measurements were made. Resistivities were measured by the standard four terminal technique and the thermoelectric power was measured as described elsewhere (6).

Samples of $Ag_xMn_{1-x}Se$ where $x = 0.01$, 0.02, 0.03, and 0.06 were made for the preliminary studies by firing all reactants in small isothermal sealed tubes at 800°C. In this way the samples would decompose until their equilibrium vapor pressures were reached. The samples where $x = 0.03$ and 0.06 were examined by x-ray and metallography. The x-ray patterns of both samples showed NaCl cubic MnSe and weak lines of β-Ag_2Se. By metallography the small amounts of a second phase appears in the grain boundaries and may have been liquid at one time.

Results

The results of the vapor pressure experiments are summarized in Fig. 2. This figure gives the appearance of a group of titration curves which in fact it is. The figure gives a plot of log vapor pressure *vs.* log of the electron hole concentration as determined by the weight of the sample pellet, assuming each selenium added permits the formation of two holes. The data can be described in terms of three distinct regions. There is the doping region in which selenium vapor is taken up while a corresponding amount of Ag_2Se is reacted. This continues until the total amount of Ag_2Se present has been reacted. At the conclusion of this region $Ag_xMn_{(1-x)}Se$ is completely formed. The next region is the equivalence point region or the controlled valence region. Finally, there is the vacancy region. The figure shows that in the doping region the curves coincide within the rather large experimental error. This region is shown on the graph as a straight line with slope = 6. As the equivalence point for each sample is reached, the curve rapidly becomes vertical. It would be expected that the vertical region would occur exactly where there is selenium uptake equal to Ag_2Se added. Any departure from this is assumed to reflect experimental error. In the sample $Ag_{0.005}Mn_{0.995}Se$, the only one where measurements could be made substantially beyond the equivalence point, the curve again assumes a slope similar to that of the doping region. Further, this region is approaching the data for MnSe containing no silver additions which also has a slope =6. This additional uptake beyond the silver equivalence point represents the creation of manganese vacancies in the lattice.

From Fig. 2 it is clear why the phase boundary suggested in Fig. 1 comes about. The data plotted in Fig. 2 are terminated at nearly 1 atm of Se_2. This occurs near the equivalence point for $Ag_{0.02}Mn_{0.98}Se$. Insufficient Se has been added for the formation of $Ag_{0.03}Mn_{0.97}Se$. In fact, this composition is impossible at a sample temperature of 800° under any circumstances. If the Se_2 reservoir temperature were increased to 800°C (the sample temperature), Fig. 2 indicates that the selenium uptake would only be sufficient for the formation of $Ag_{0.027}Mn_{0.973}Se$. The selenium pressure would be 3.5 atm at these conditions on the basis of an extrapolation of the data of Brooks (4).

The electrical conductivity data corresponding to the sample compositions in Fig. 2 are plotted in Fig. 3. The correspondence between Fig. 2 and Fig. 3 is quite apparent. The doping region is again of slope 6. The equivalence points for $x = 0.005$, 0.01, and 0.02 are at conductivities 19, 37, and 76 ohm^{-1} cm^{-1}. Thus the conductivities at the equivalence point es-

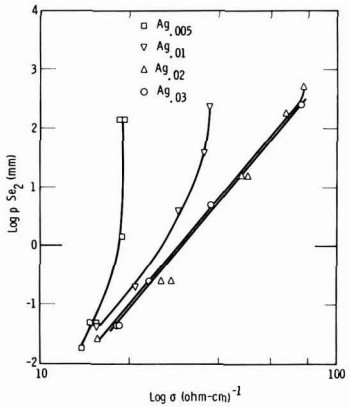

Fig. 3. Log p Se_2 vs. log σ for $Ag_xMn_{(1-x)}Se$

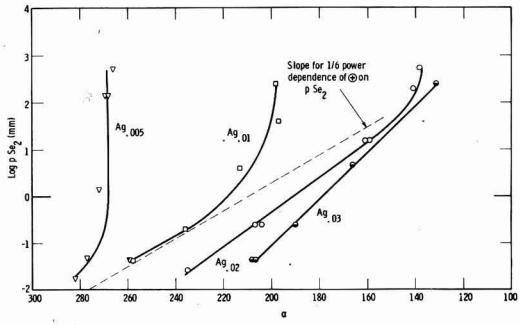

Fig. 4. Thermoelectric power of $Ag_xMn_{(1-x)}Se$ as a function of log p Se_2.

sentially double with each doubling of x, as would be expected. The data on this graph are actually probably more accurate than that of Fig. 2 since the data in Fig. 2 involves a very large weighing error at low selenium additions.

Thermoelectric power data corresponding to the compositions of Fig. 2 and Fig. 3 are plotted in Fig. 4. At the equivalence point the thermoelectric power, α, changes from +137 to +197 to +268 μv/°C for $x = 0.02$, 0.01, and 0.005. Theoretically a decrease of ~60 μv/°C for each doubling of $\oplus$ would be expected since $\alpha \sim -k/e \ln \oplus + C$ so there is agreement at this point (6). In the doping region however, the curves might be expected to coincide on the basis of Fig. 2 and 3. Actually at a given selenium pressure the higher the value of Ag in this region the lower value of α. This is due to the presence of the second phase of n-type Ag_2Se in the product which will give rise to internal circulating currents between the p- and n-phases. [Ag_2Se normally (7) has the electrical properties $\alpha = -150$ μv/°C and $\sigma = 10^3$ ohm^{-1} cm^{-1}.] As indicated earlier in Fig. 1, this has a large effect on α, but little effect on σ. In Fig. 4 a slope corresponding to that of Fig. 2 and 3 is indicated by a dotted line showing that where the silver content is low there is good agreement with this slope but, as the silver content increases, the deviation becomes marked showing the effect of increased amounts of the Ag_2Se second phase.

No data for MnSe are given in Fig. 3 and 4 in spite of the fact that considerable nonstoichiometry was indicated in Fig. 2. It was found that all MnSe samples had nearly constant values of α and σ of ~ +500 μv/°C and 1 ohm^{-1} cm^{-1}, respectively. Actually, values of α as low as ~ +280 and values of σ are high as ~15 would be expected from the figures, and further the values would be expected to vary systematically with composition. Evidently the vacancy structure of MnSe is not stable at room temperature, and the vacancies are eliminated rapidly on quenching with the probable formation of $MnSe_2$. This experience indicates the risk associated with inferring high-temperature data from room temperature electrical measurements as is frequently done. Such inferences from weight data are much more sound since weight data are not structure sensitive and processes involving changes in weight are much slower than just an atomic or electronic rearrangement. This comparison also bears out the hypothesis that has been held for some time that doped semiconductors are thermally much more stable than those relying only on nonstoichiometry for the control of charge carriers.

Discussion

A number of cases involving the relationship between the electrical conductivity and the vapor pressure of a gaseous component have been reported in the literature. These are generally cases of simple nonstoichiometry. The approach is usually through the use of mass action. The groundwork was laid in 1930 by Wagner and Schottky (8). It has been pursued experimentally by Wagner (9), Hauffe (10), and others. A graphical method of approximating these interactions has been introduced by the Phillips workers, notably Kroger and Vink (11). A similar approach using semiconductor terminology has recently been discussed by Brebrick (12). A simple mass action approach will be used in the discussion to follow.

The simplest case to be treated is that of nonstoichiometric MnSe. The chemical equation may be written

$$MnSe + \frac{x}{2} Se_2 \rightarrow MnSe_{1+x} \boxed{Mn^{\circ}}_x \oplus_{2x}$$

where $\boxed{Mn^{\circ}}$ is assumed to be a neutral (or doubly ionized) manganese vacancy, and $\oplus$ is a hole. With respect to the manganese lattice, the manganese vacancy as written has a net charge of −2 and is therefore a potential trap for holes. The mass action expression for this equation may be written

$$K_1 = \frac{\boxed{Mn^{\circ}}^2 \oplus^4}{p\,Se_2}$$

but since $2 \cdot \boxed{Mn^{\circ}} = \oplus$

$$K_1 = \frac{\oplus^6}{4\,p\,Se_2}$$

Thus it can be seen that the slope of the log p Se_2 *vs.* log $\oplus$ plot should have a slope of 6 as is indeed observed. The agreement indicates that the manganese vacancies are not trapping electron at the temperature of the experiments, in accord with the starting equation.

This same approach may be used beyond the equivalence point in the silver doped samples

$$Ag_xMn_{(1-x)}Se \oplus_x + \frac{y}{2} Se_2 \rightarrow Ag_xMn_{(1-x)}Se_{1+y} \boxed{Mn^{\circ}}_y \oplus_{x+2y}$$

Here the expression for the equilibrium constant turns out to be the same as before, but now $\oplus = Ag + 2\boxed{Mn^{\circ}}$

so

$$K_1 = \frac{(\oplus - Ag)^2 \oplus^4}{4\,p\,Se_2}$$

This is clearly not a simple exponential. A series of curves were calculated using K_1 derived from the MnSe data and the silver concentrations of the experiments and are shown in Fig. 5. The derived

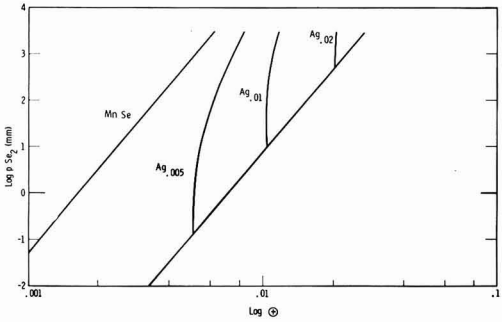

Fig. 5. Derived log p Se_2 vs. log $\oplus$ calculated using log $K_1 = -16.1$.

curves give the very slow change in composition with changing selenium pressure near equivalence points and then a less steep approach to the MnSe curve. The MnSe and $Ag_xMn_{(1-x)}Se$ curves will become indistinguishable when $\oplus >> Ag$. At that point the $Ag_xMn_{(1-x)}Se$ curve will have a slope of 6. Thus both the equivalence region and the vacancy region are described by one equation.

The region in which doping occurs has not been successfully evaluated in these terms. The over-all formation reaction may be written

$$\frac{x}{2}\,Ag_2Se + \frac{x}{4}\,Se_2 + 1 - x\,MnSe \rightarrow Ag_x \oplus_x Mn_{(1-x)}\,Se$$

If Ag_2Se is assumed to be at a fixed activity, a slope of 8 would be derived for the plot of Fig. 2. The observed slope is 6, however. The lack of agreement is believed to be due to the changing activity of Ag_2Se with selenium pressure that has been demonstrated earlier and which has also been described in the work of Wagner (13), Miyatani (14), and Rahlfs (15).

The presence of a phase containing selenium vacancies as a result of the silver addition, *i.e.*, $Ag_xMn_{(1-x)}Se_{1-x/2}\boxed{Se}_{x/2}$, instead of a two phase mixture of $x/2$ $Ag_2Se + (1-x)MnSe$ can be ruled out since it would lead to a variation in vapor pressure with the silver content at the start of the selenium addition which is far beyond the experimental error involved. Instead the data are completely independent of the silver content in this region. Moreover insolubility of Ag_2Se in MnSe has been demonstrated, at least at room temperature, by visual observation and thermoelectric power measurements. Therefore, in terms of the ternary phase diagram, the process of selenium addition can be described in terms of cutting across the tie lines of the Ag_2Se-MnSe binary field.

Finally one might consider the behavior of $Li_xMn_{(1-x)}Se$ within this framework. A rather serious attack of Vycor by lithium precludes any accurate experimental work since a continuous undoping will arise from this attack. Electrical data indicate, however, that at least in the case of $Li_{0.03}Mn_{0.97}Se$ the material probably is completely within the controlled valence range throughout the range of selenium pressures used in this work. It is also reasonable to suppose that when $x = 0.11$ in $Li_xMn_{(1-x)}Se$, which is the previously reported phase boundary composition (1), the selenium equilibrium vapor pressure has increased to the vicinity of 1 atm. This in itself would require a large extension of the range of controlled valence by the mechanism of lowering the doping curve for $Li_xMn_{(1-x)}Se$ away from the vacancy curve which is common to both systems.

Acknowledgments

The author wishes to thank Drs. R. L. Longini, A. J. Panson, Y. L. Sandler, and J. Weissbart for many useful discussions and critical review of this manuscript. Technical assistance was rendered by Mr. D. E. Sestrich. This work was done in connection with U. S. Navy Bushipe Contract No. NOBS-78365 WGO No. WG 79150 CE.

Manuscript received Dec. 8, 1961; revised manuscript received March 2, 1962.

Any discussion of this paper will appear in a Discussion Section to be published in the June 1963 JOURNAL.

REFERENCES

1. W. D. Johnston and R. R. Heikes, *J. Am. Chem. Soc.*, **80**, 5904 (1958).
2. R. R. Heikes, R. McGuire, and R. J. Happel, *Phys. Rev.*, **121**, 703 (1961).
3. M. Hansen, "Constitution of Binary Alloys," McGraw-Hill Book Co., New York (1958).
4. L. S. Brooks, *J. Am. Chem. Soc.*, **74**, 227 (1952).
5. D. R. Stull and G. C. Sinke, "Thermodynamic Properties of the Elements," American Chemical Society, Washington (1956).
6. R. R. Heikes and R. W. Ure, "Thermoelectricity," Interscience Publishers, New York (1961).
7. J. B. Conn and R. C. Taylor, *This Journal*, **107**, 977 (1960).
8. C. Wagner and W. Schottky, *Z. Physik, Chem.*, **B11**, 163 (1930).
9. C. Wagner, *ibid.*, **B22**, 181 (1933); H. H. Baumback and C. Wagner, *ibid.*, **B22**, 199 (1933); H. H. Baumback and C. Wagner, *ibid.*, **B24**, 59, (1934); C. Wagner and E. Koch, *ibid.*, **B32**, 439 (1936).
10. K. Hauffe and A. L. Vierk, *ibid.*, **196**, 160 (1950); K. Hauffe and J. Block, *ibid.*, **196**, 438 (1951); K. Hauffe and H. Greenwald, *ibid.*, **198**, 248 (1951.)
11. F. A. Kroger and H. J. Vink, *J. Phys. Chem. Solids*, **5**, 208 (1958); F. A. Kroger and H. J. Vink, "Solid State Physics," Academic Press Inc., New York (1956); J. Bloem, *Philips Research Rept*, **11**, 273 (1956). F. A. Kroger, H. J. Vink, and J. van der Boomgaard, *Z. Physik, Chem.*, **203**, 1 (1954).
12. R. F. Brebrick, *J. Phys. Chem. Solids*, **4**, 190 (1958).
13. C. Wagner, *J. Chem. Phys.*, **21**, 1819 (1953).
14. S. Miyatani, *J. Phys. Soc., Japan*, **13**, 317 and 341 (1958).
15. P. Rahlfs, *Z. Physik. Chem.*, **B31**, 157 (1936).

Electrical Conductivity of Nonstoichiometric α-Nb_2O_5

E. H. Greener and W. M. Hirthe

College of Engineering, Marquette University, Milwaukee, Wisconsin

ABSTRACT

The electrical conductivity of reduced α-Nb_2O_5 was measured after prior reduction in 10^{-6} atm of air from 350°-1150°K for both single crystals and sintered specimens. The conductivity of single crystals was found to be exponentially dependent on temperature with an activation energy of 0.9 ev in the range from 1150°-650°K and 0.2 ev in the range from 650°-350°K. The electrical conductivity of sintered specimens was also found to be exponentially dependent on temperature, but only a single activation energy was obtained over the entire temperature range. This activation energy was dependent on defect concentration and varied from 1.0 ev for the smallest degree of reduction to almost zero at the highest degree of reduction where the behavior was essentially that of a degenerate semiconductor. An explanation based on overlapping orbitals of trapped electrons is offered to explain both the dependence of activation energy on defect concentration and the absence of a low-temperature activation energy in sintered material. Finally, two mechanisms are discussed to explain the observed conductivity of reduced α-Nb_2O_5. Comparison of conductivity data and thermoluminescence data tends to favor a model in which two trapped electrons are excited from an oxygen vacancy to the "d" band of the niobium cations.

A discussion of the past work on the electrical properties of Nb_2O_5 has been presented in an earlier paper (1). In this work α-Nb_2O_5 has been shown to be a metal-excess n-type semiconductor. The defect producing this structure is most probably an oxygen ion vacancy which has trapped two electrons. A possible energy band model for the defect oxide semiconductor appears in Fig. 1.

In near-stoichiometric α-Nb_2O_5, between 600°-900°C, the conduction band carrier concentration[1] $[\ominus]$ has been shown to obey a law of the form

$$[\ominus] = \sqrt{K_{o_1}K_{o_2}}\, P_{O_2}^{-1/4} \exp -(W_D + E_1)/2kT \quad [1]$$

where K_{o_1} and K_{o_2} are, respectively, the temperature independent terms of the equilibrium constants for the creation of the defect (Eq. [2]) and the excitation of the first electron from the oxygen vacancy trap (Eq. [3]). W_D is the energy required to create the defect, and E_1 is the energy necessary to excite the first electron from the defect into the conduction band. Experimentally, the quantity $-(W_D + E_1)/2$ was found to be 1.65 ev (Fig. 2).

These reactions may be summarized as

$$O_i^{2-} \rightleftharpoons \frac{1}{2} O_2 + O_v^{x} \qquad -W_D \quad [2]$$

$$O_v^{x} \rightleftharpoons O_v^{\cdot} + \ominus \qquad -E_1 \quad [3]$$

[1] The temperature dependence of conduction band carrier mobility in near-stoichiometric α-Nb_2O_5 is assumed to be negligible when compared to the change in conduction band carrier concentration over the temperature range 600°-900°C. A discussion of this is included in the earlier paper (1).

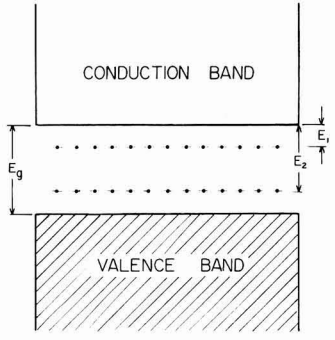

Fig. 1. Band model for a metal-excess oxide semiconductor with an oxygen ion vacancy trapping two electrons.

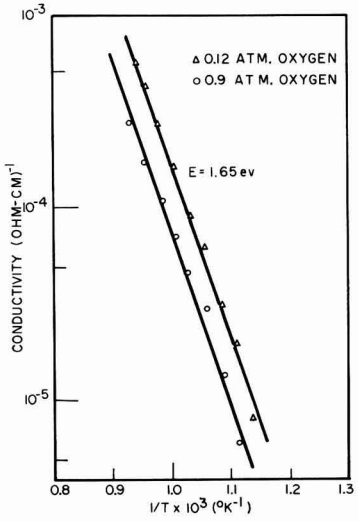

Fig. 2. Logarithm of the conductivity of sintered near-stoichiometric α-Nb_2O_5 as a function of $1/T$ for two oxygen pressures. The value of 1.65 ev calculated from the slopes of these curves represents $(W_D + E_1)/2$.

where O_i^{2-} is an oxygen ion in a normal lattice position, O_v^x is an oxygen vacancy which has trapped two electrons in its field, $O_v^{\cdot}$ is an oxygen vacancy from which an electron has been excited, and $\ominus$ is an electron in the conduction band.

It is further possible to write an analogous expression for the excitation of the second electron

$$O_v^{\cdot} \rightleftharpoons O_v^{\cdot\cdot} + \ominus \qquad -E_2 \quad [4]$$

where $O_v^{\cdot\cdot}$ is an oxygen ion vacancy from which both electrons have been excited, and E_2 is the energy necessary to excite the second electron from the vacancy trap into the conduction band.[2]

Thus, the conductivity of near-stoichiometric α-Nb_2O_5 is seen to depend on both temperature and oxygen partial pressure.

In the case of materials of near-stoichiometric composition, Eq. [2], [3], and [4] control the change in conduction band carrier concentration with temperature and pressure. Consequently, E_1 and E_2 cannot be separated from W_D. On the other hand, if the concentration of defects were increased so that the change in conduction band carrier concentration would be controlled by Eq. [3] and [4] it should be possible to determine E_1 and E_2 experimentally.

Experimental Details

Small single crystals of α-Nb_2O_5 approximately 2 mm in diameter were kindly furnished by Linde Air Products Company. Flat surfaces were ground and polished with 420 grit carborundum on the crystals for electrical contact. No chemical analysis of the Linde crystals or knowledge of their perfection was available. Since the dimensions of the Linde crystals were very irregular the data for these specimens are reported as conductance rather than as conductivity.

High-purity Nb_2O_5 powder furnished by the Fansteel Metallurgical Corporation was a mixture of α and β modifications. It was cold-pressed without a binder at a pressure of 40,000 psi and sintered at temperatures between 1300° and 1350°C for 2 hr. After this treatment, the Nb_2O_5 existed entirely as the α modification. The apparent densities of the sintered compacts were measured pycnometrically and were found to be within 80-90% of the theoretical density of 4.55 g/cm³ reported by Holtzberg *et al.* (2). Rectangular parallelepipeds approximately ½ x ¼ x 0.05 in. were cut from the sintered compacts and used for conductivity specimens, the surfaces being polished with 420 grit carborundum.

The equipment for measurement of resistance as a function of temperature in the range 300°-1000°K and oxygen partial pressure has been described previously (1, 3). Two types of apparatus were used: the first system consisted of a furnace in a vacuum bell jar, and in the second, a Vycor tube connected to a vacuum system separated the specimen from the furnace. The single crystals were investigated in the bell jar whereas the sintered specimens were investigated in the Vycor tube. Because of the size limitations, the two-probe technique was used for single crystals whereas four-probe techniques were used for sintered specimens. Compositional changes were measured by weight loss, the entire weight change being attributed to the loss of oxygen.

[2] Another possible explanation for the occurrence of a second activation energy is mentioned at the end of the paper.

Experimental Results and Discussion

In an attempt to freeze in a constant defect concentration the reduction was carried out directly in the vacuum apparatus. Specimens were held at 10^{-6} atm O_2 for from 1 to 8 hr at temperatures from 700° to 900°C. The specimens were cooled quickly (5°-10°C/min for the sintered specimens, faster for the single crystals) *in vacuo*, and resistance readings were taken on cooling. It is felt that in the case of the data reported in this paper this treatment was successful in maintaining the defect concentration produced by the high-temperature reduction. Slower cooling or holding at the higher temperatures produced discontinuities in the log σ *vs.* $1/T$ curve due to further reduction. No such discontinuities were found in the data reported in this investigation.

A typical run on a single crystal of Nb_2O_5 in a vacuum of 10^{-6} atm of air in the temperature range from 300° to 1000°K is given in Fig. 3. Essentially the same log σ *vs.* $1/T$ curve was obtained for six different specimens initially reduced at 800°-850°C for from 2 to 4 hr. The observed data can be rationalized with the normal semiconductor equation

$$\sigma = \sigma_0 \exp(-E_D/2kT) \qquad [5]$$

where E_D is the energy of the donor level, k is Boltzmann's constant, and T is the absolute temperature. The activation energy calculated from the high-temperature slope is about 0.9 ev (E_2) and from the low-temperature slope about 0.2 ev (E_1). The break in the log σ *vs.* $1/T$ curve occurs at $1/T$ x 10^3 equal

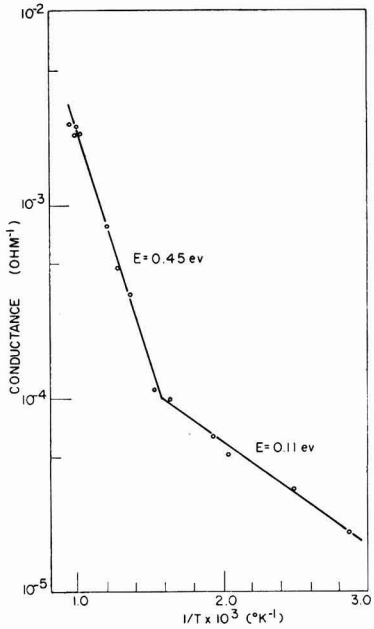

Fig. 3. Logarithm of the conductance of single crystal α-Nb_2O_5 as a function of $1/T$ after reduction at 800°C for 4 hr in a vacuum of 10^{-6} atm of air. The values of 0.45 ev and 0.11 ev calculated from the slopes of the curve represent $E_2/2$ and $E_1/2$, respectively.

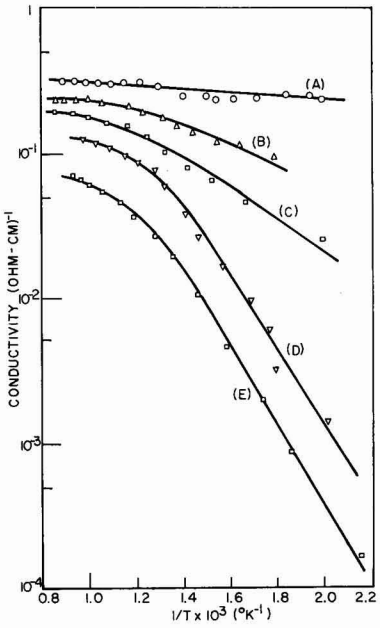

Fig. 4. Logarithm of the conductivity of sintered α-Nb_2O_5 in 10^{-6} atm of air as a function of $1/T$ for the following reduction treatments in a vacuum of 10^{-6} atm of air: (A) 8 hr at 875°C; (B) 8 hr at 860°C; (C) ½ hr at 860°C; (D) 8 hr at 750°C; (E) ½ hr at 800°C.

to 1.5 or 650°K which corresponds to a thermal energy of about 0.06 ev. The change in slope of the curve is due to the exhaustion of electrons trapped at E_1 because the thermal energy at 650°K is within $4kT$ of E_1.

Typical curves of log σ *vs.* $1/T$ for reduced sintered specimens shown in Fig. 4 can be characterized by two distinct regions. In the low-temperature region the conductivity changes exponentially with temperature and can be represented by a straight line, the slope of which will yield the activation energy from the donor level according to Eq. [5]. In the high-temperature region the conductivity is essentially independent of temperature and can be explained on the basis of an exhaustion process in which the thermal energy is large enough to excite all trapped electrons from available donor centers, but is too small for any intrinsic excitation to occur. The thermal energy for exhaustion is compared with the energy level of the donor state in Table I for all curves in Fig. 4 and can be seen to be within approximately $4kT$ of the donor level E_2. For the smallest degree of reduction attempted, the observed activation energy is (according to Eq. [5]) 1.0 ev. This is in good agreement with 0.9 ev obtained from the high-temperature slope of the single crystal curve.[3] As the degree of reduction and consequently the concentration of defect levels and trapped electrons increases, the conductivity also increases. In addition, there is a decrease in the activation energy due to the fact that the electrons trapped in donor levels can no longer be considered as isolated defects because their orbitals begin to overlap. As treated by Pearson and Bardeen (4), increasing the concentration of donor levels to the point where overlapping occurs moves the Fermi level up toward the conduction band. This will lower the activation energy necessary for electronic excitation and the beginning of the exhaustion region will occur at successively lower temperatures as is seen in Fig. 4.

[3] Since good agreement was obtained between the high-temperature activation energies of the single crystal (two-probe method) and sintered specimens (four-probe method), contact resistance was not deemed to be a problem in the case of the single crystal studies. Certainly if any problem were to exist it would have appeared in the high-temperature range of measurement where specimen resistance is lower than in the low-temperature range. Since the high-temperature activation energies agreed, it is reasonable to assume that contact resistance is not a problem in the low-temperature range of measurement.

Table I. Comparison of thermal energy for exhaustion with energy level of the donor state

Curve	Thermal energy for exhaustion from Fig. 4	Activation energy from Fig. 4
A	Degenerate	
B	0.08	0.15
C	0.09	0.23
D	0.09	0.45
E	0.10	0.50

This may be the reason why only a single activation energy is obtained with sintered materials over the same temperature range where two activation energies are found in single crystals. For obvious reasons, the kinetics of reduction of the sintered materials can be considered to be faster than that for single crystals. Consequently, even at the smallest degree of reduction in sintered specimens, the concentration of oxygen vacancies and trapped electrons would be higher than for single crystals receiving the identical reduction treatment. The electrons trapped at E_1 will be more loosely bound than those traped at E_2 (Eq. [3] and [4]) and can be thought of as having a larger orbit. Therefore a concentration of defects sufficient to cause overlapping of the E_1 levels may be insufficient to cause overlapping of the E_2 levels. In this case the E_1 level would shift toward the conduction band in a manner analogous to the shifting of the E_2 level in Fig. 4. Since from the single crystal data the E_1 level is about 0.2 ev, the smallest reduction attained in this investigation may provide a sufficient number of defects to shift the E_1 level within $4kT$ (at room temperature $4kT = 0.1$ ev) of the conduction band. If this occurs, the first level would be exhausted at all temperatures utilized in this research, and the conductivity of sintered specimens would change only through excitation of electrons from the second level into the conduction band.

At the highest degree of reduction (curve A, Fig. 4) the conductivity is essentially independent of temperature over the entire temperature range investigated, and thus the material in this region may be classified as a degenerate semiconductor, *i.e.*, both E_1 and E_2 levels are exhausted. Since in a degenerate semiconductor the Fermi level may be considered to be in the conduction band, the exponential term for the dependence of the conductivity may be replaced by unity, and the conductivity σ may be expressed as

$$\sigma = \sigma_o Nev \qquad [6]$$

where N is the number of carriers in the conduction band, e is the electronic charge, and v is the electronic mobility. Thus, if it is possible to estimate the number of carriers and measure the conductivity, a calculation of the electron mobility could be made. From x-ray data of Holtzberg and co-workers (2), it is possible to estimate the total number of molecules in Nb_2O_5/cc as 1.2×10^{20}. This means that there would be 6×10^{20} normally occupied oxygen anion lattice sites. From measurement of weight changes, however, it was found that the compositional change from insulator to degenerate semiconductor amounted to the change Nb_2O_5-$Nb_2O_{4.95}$, with the composition $Nb_2O_{4.95}$ corresponding to about 1% vacancies per cubic centimeter. Since an oxygen vacancy can trap two electrons, N can be approximated as 1.2×10^{19}/cc. From Fig. 4 the conductivity for the degenerate case can be approximated as 10^{-1} ohm-cm. Therefore, the electron mobility is of the order of 10^{-1} cm^2/volt-sec. This value of mobility is close to that found by Breckenridge and Hosler (5) for the case of heavily reduced TiO_2 and was related by them to a conduction process in the narrow "d" band of Ti ions. Thus, by analogy to the TiO_2 case, it would be possible for the narrow "d" band of the Nb cation to act as the conduction band.

Conclusion

On the basis of the conductivity studies presented, two alternative mechanisms may be offered.

1. Excess electrons produced as a result of reduction are locally trapped at Nb^{4+} ions. Since an oxygen vacancy may be considered to have a virtual charge of +2, these Nb^{4+} ions would be found near a vacancy. Conduction might take place via excitation of an electron from an Nb^{4+} ion into the conduction band (high-temperature activation energy) or by "hopping" of an electron from an Nb^{4+} site to an Nb^{5+} site (low-temperature activation energy). The activation energies are summarized in Table IIa. Mitoff (6) has recently treated the case for hopping in NiO. He reports an activation energy of about 0.2 ev over the same low-temperature range used in this investigation. A standard diffusion analysis can treat this problem quite adequately; *i.e.*, the conductivity σ may be expressed as

$$\sigma = nev = nev_o \exp(-E/kT) \qquad [7]$$

where n is the number of carriers trapped in defect levels, e is the electronic charge, and the term $v_o \exp(-E/kT)$ expresses the temperature dependence of the mobility.

2. Excitation of two electrons from an oxygen vacancy trap into the "d" band of the Nb^{5+} ions according to Eq. [3] and [4]. The observed activation energies substituted into the standard semiconductor equation (Eq. [5]) yield the energies necessary to excite these electrons from a vacancy trap into the conduction band, Table IIb. Recent thermoluminescence studies by Greener, Fehr, and Angino (7) tend to substantiate this model. In this investigation specimens of powdered near-stoichiometric α-Nb_2O_5 were subjected to Co^{60} and u.v. irradiation after which they exhibited two thermoluminescence peaks. The activation energies calculated from these peaks closely correspond to those calculated from single crystal conductance data based on activation to a band from two discrete levels (Tables IIb and IIc). This suggests that the trapping mechanisms in both experiments were the same.

Table II. Summary of activation energies

	(a) Mechanism 1 (Activation energies from Fig. 3)	(b) Mechanism 2 (Activation energies from Fig. 3)	(c) Thermoluminescence
E_1	0.1	0.2	0.4
E_2	0.9	0.9	0.9

Further, two activation energies were obtained in powdered material. In the case of thermoluminescence experiments one may expect an extremely small concentration of electrons trapped at vacancies. For example, irradiation produces no color change, while reduction does. Thus no overlapping of electrons trapped at E_1 occurs, and a second activation energy is seen which is in good agreement with the single crystal conductance data. The hopping mechanism discussed earlier (mechanism 1) could not give rise to a thermoluminescence peak. It is also of interest to note that a Bohr He model for the traps predicts that the energy to excite the second electron from the vacancy is about four times the energy to excite the first. Such a relationship is evident in Table II.

Although at present the model which best explains all experimental data seems to be the excitation of two trapped electrons into the "d" band of the niobium cations, the final decision as to which mechanism occurs must depend on an experiment which can differentiate between the temperature dependence of carrier concentration and carrier mobility. In the case of excitation into a band it is the carrier concentration which is exponentially dependent on temperature whereas in the case of a hopping process the mobility is exponentially dependent on temperature. Clearly in order to distinguish between the two possible mechanisms, Hall Effect data would be most valuable.

Acknowledgment

The authors wish to acknowledge the Office of Naval Research for their support of the portion of this work done at Northwestern University.

Manuscript received Dec. 18, 1961; revised manuscript received March 1, 1962. This paper was prepared for delivery before the Indianapolis Meeting, April 30-May 3, 1961.

Any discussion of this paper will appear in a Discussion Section to be published in the June 1963 JOURNAL.

REFERENCES

1. E. Greener, D. Whitmore, and M. Fine, *J. Chem. Phys.*, **34**, 1017 (1961).
2. F. Holtzberg, A. Reisman, M. Berry, and M. Berkenblit, *J. Am. Chem. Soc.*, **79**, 2039 (1957).
3. E. Greener, Ph.D. Thesis, Northwestern University (1960).
4. G. Pearson and J. Bardeen, *Phys. Rev.*, **75**, 86 (1949).
5. R. Breckenridge and W. Hosler, *ibid.*, **91**, 793 (1953).
6. S. Mitoff, *J. Chem. Phys.*, **35**, 882 (1961).
7. E. Greener, G. Fehr, and E. Angino, *J. Am. Ceram. Soc.*, **45**, 93 (1962).

Cross Sections and Ohmic Resistance of Diffusion Pipes in Silicon

A. Goetzberger and C. Stephens

Shockley Transistor, Unit of Clevite Transistor, Palo Alto, California

ABSTRACT

Diffusion pipes were deliberately produced by contamination with phosphorus as described previously by Goetzberger and their cross sections measured as a function of depth from the surface by removing thin layers of silicon by anodic oxidation. The results are in qualitative agreement with theory as derived from a simple diffusion model. In particular some pipes were found having diameters that increase with depth, and others were found having decreasing diameters. "Submerged pipes" were also detected experimentally for the first time. Deviations from the predicted theoretical behavior were relatively unimportant and seem to be caused by enhanced diffusion close to the surface by the finite size of the n-type source and by the influence of background doping. The proposed theoretical model was further confirmed by measurement of the ohmic resistance of pipes which was in agreement with predictions based on spreading resistance from the concentration end of the pipe.

This paper reports new investigations on diffusion pipes in silicon. In an earlier paper (1) it had been shown that pipe-like regions of high donor concentration through diffused p-layers in silicon can originate from localized sources of n-type impurity on the surface.

It had further been shown that this n-type impurity was phosphorus in the majority of cases and that pipes are formed by diffusion from the localized sources. The results reported in (1) were recently confirmed by Flint (2) who was able to detect a high concentration of phosphorus in pipes with an electron probe x-ray analyzer. According to the diffusion theory given in (1), pipes should have different profiles dependent on diffusion conditions (Table I and Fig. 1). Of particular interest are the so-called "submerged" pipes (case IV). This type of pipe cannot be detected on the surface because it does not contain a junction intersecting the surface.

In this publication evidence that all the predicted shapes exist is reported. This evidence, obtained with a sectioning technique employing anodic oxidation, is discussed below.

The results of the profile measurements were checked by measuring the ohmic resistance of a number of pipes. Since pipes result from diffusion from the surface, the resistivity along a pipe increases from the surface according to a diffusion distribution. The most important contribution to the resistance, therefore, arises from the spreading resistance in the bulk material lying beyond the end of the pipe. The area of the conducting channel through the diffused layer can thus be estimated from resistivity measurements and is found in a later section to compare with optical measurements of the pipe shape.

Table I. Pipe shapes for different diffusion conditions

Case	Condition	Shape
I	$C_{o2} > C_{o1}$, $D_1t_1 > D_2t_2$	Ellipsoid
II	$C_{o2} > C_{o1}$, $D_1t_1 < D_2t_2$	Hyperbola of rotation
III	$C_{o2} > C_{o1}$, $D_1t_1 = D_2t_2$	Cylinder
IV	$C_{o2} < C_{o1}$, $D_1t_1 < D_2t_2$	Hyperbola of rotation (submerged pipe)

Definition of symbols: C_o is surface concentration; D, diffusion coefficient; t, diffusion time; subscript 1 refers to the plane diffusion; subscript 2 refers to the spherical pipe diffusion.

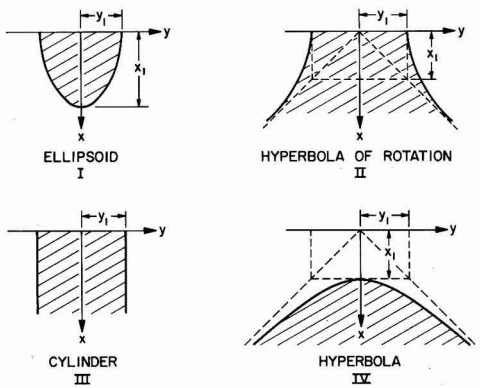

Fig. 1. Four different pipe shapes according to mathematical model.

Cross Section Measurements

Experimental procedure.—Diode preparation and observation of pipe diameter at the surface were identical to the procedures described in (1). Pipes were introduced into boron diffused p^+n planar diodes by exposure to P_2O_5 aerosol before boron predeposit and were optically observed by light emission from microplasmas at the surface.

Afterwards the thickness of the silicon slices containing diodes with pipes was reduced in small in-

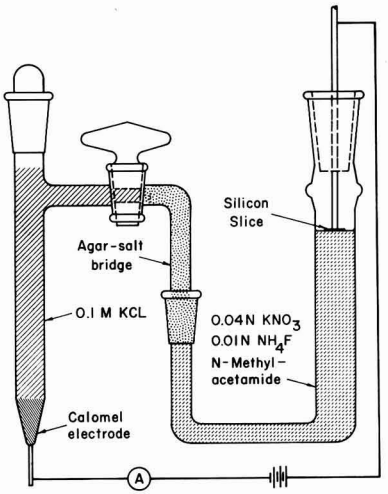

Fig. 2. Anodic oxidation apparatus

crements by anodic oxidation, and the variation of the pipe shapes studied. The technique of anodic oxidation of silicon has been described by Schmidt (3), and Tannenbaum (4). The procedure followed in this investigation had been worked out by McDonald and Collins (5). One anodization step in the apparatus shown in Fig. 2 removes approximately 0.05μ. After each anodization the oxide was removed in HF, and after every five oxidation steps the thickness of the removed layer and the diameter of the pipe were measured. Thickness was determined by weighing with a microbalance with an accuracy of $\pm$ 4 μg, corresponding to a depth accuracy of 0.016μ for a slice of 1 cm^2 area. This accuracy, however, is only applicable for slices of uniform doping over the whole surface because it has been observed during this investigation that the etching rate is different for n- and p-type and for different resistivities. Therefore the depth measurements represent only an average over the whole slice and may not apply accurately to the pipes themselves. The error is thought to be less than 10%.

The dimensions of the pipes were determined by taking photomicrographs of the diodes under reverse bias, utilizing avalanche radiation to delineate the intersection of the pipes with the surface. Some of the pipes deviated from a circular geometry. In these cases the diameter was always measured in the same direction.

An alternative to the avalanche method is the chemical staining technique (6). The avalanche method was chosen because of its greater reproducibility.

Results.—When phosphorus was introduced as an aerosol before boron predeposition, in general a greater percentage of pipes were found to have diameters which decreased with depth corresponding to the ellipsoidal type. The remainder of the pipes showed a widening with increasing depth; this type of pipes is believed to be due to unintentional contamination during or before the oxidation step with

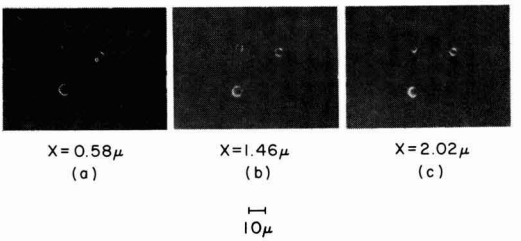

Fig. 3. Group of pipes showing constriction. Light emission photographs are taken at increasing depths. X is depth of cross section.

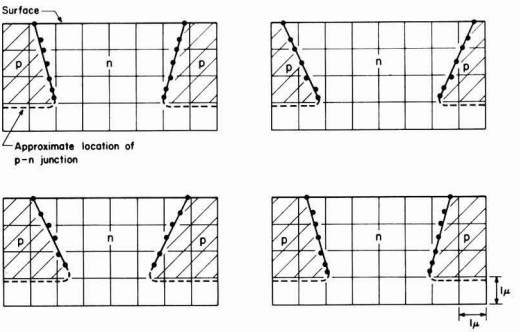

Fig. 4. Cross sections for four different pipes showing constriction

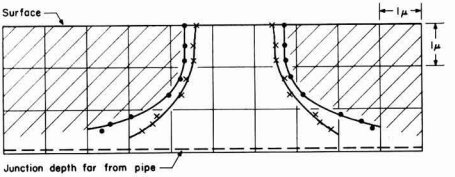

Fig. 5. Cross section of a pipe showing widening of diameter with depth.

consequently larger values of Dt for the phosphorus than for the boron.

Figure 3 a-c shows light emission from the same group of pipes as it appeared at different depths. The cross sections of two of these pipes and of some others found in the same sample are given in Fig. 4.

Figure 5 shows the cross section of a pipe with increasing diameter, the two outlines corresponding to two perpendicular directions across the pipe which was not exactly circular.

In Fig. 6 the detection of a submerged pipe during sectioning is shown. In Fig. 6a a small light spot can be seen to the left of a well-developed pipe. At greater depths this light spot developed into a ring of light characteristic for a pipe. It can be assumed that the light emission that emerges before the pipe itself is sectioned is caused by avalanche breakdown at the top of the n-region where the impurity gradient is increased.

In Fig. 7a the cross section of this pipe is given. The two traces again apply to two perpendicular directions. Figure 7b shows a similar structure found in another diode.

Discussion.—The observed pipe cross sections are in qualitative agreement with the theory given in

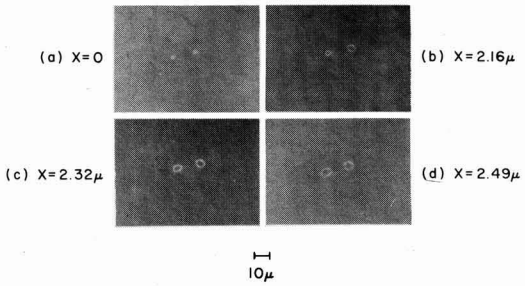

Fig. 6. Light emission photographs showing detection of a submerged pipe. X is depth of cross section.

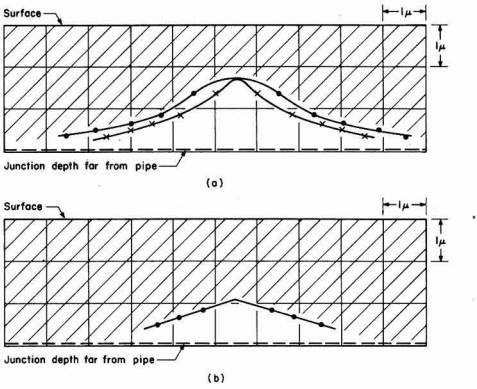

Fig. 7. Cross sections of two submerged pipes

(1). The following deviations from the expected behavior can be noticed: (*A*) Pipes which show a decrease in diameter in depth (Fig. 4) are wider at the surface than the expected ellipsoid. (*B*) Pipes showing an increase in diameter with increasing depth, including the submerged types, do not follow a hyperbolic outline exactly, but show more curvature at the bottom end.

Effect (*A*) might be caused by enhanced diffusion close to the surface as has been reported by different observers (4, 5, 7). Little is known about diffusion along surfaces, but in general it is assumed to be much faster than bulk diffusion. Because the observed effect can be explained adequately by a small modification of the bulk diffusion coefficient, it is believed to be due to enhanced bulk diffusion and probably not to surface diffusion.

Effect (*B*) can be accounted for by (i) finite extension of the source initially over the surface and (ii) influence of the doping of the crystal from which the slice was prepared; this constant concentration term was not taken into consideration in the simple mathematical model.

For several pipes an evaluation of phosphorus content was carried out using the known data of the plane diffusion and a diffusion time for the pipes corresponding to the time elapsed after introduction of phosphorus. The number of phosphorus atoms per pipe was estimated as between 10^8 and 10^9, in good agreement with earlier estimates (1) based on measurements of the growth rate of pipes.

Submerged pipes had an impurity content in the lower range, as anticipated.

It should be noted here that the lower limit for the phosphorus content which will make a pipe observable is determined by the surface concentration of the plane boron diffusion. If the surface concentration of the plane diffusion is lowered, then the number of impurity atoms required to form comparable types of pipes will be lowered by the same factor.

One of the results of the present investigation is a proof of existence of the submerged pipes (Fig. 7). This type is characterized by relatively small amounts of impurities which started diffusing a considerable time before diffusion of the p-type layer is frequently found in planar devices. The long high-temperature oxidation necessary to produce the initial oxide layer provides a chance for submerged pipes to be introduced. It appears to be very difficult to avoid contamination with phosphorus during this step. In the opinion of the authors this problem will have to be solved before large area planar devices become technically feasible in silicon.[1]

Pipe Resistance

Technique of measurement and results.—The main problem in measuring the resistance through a pipe is the small size of the pipe areas. James and Flint (8) attempted to measure the ohmic resistance by placing a fine probe in the center of a pipe. They obtained only a rough estimate of the resistance.

In this investigation a different contacting method was chosen. Contact to the pipe was made by means of a shallow diffused n^+-layer of a lateral extension smaller than the planar p-type junction containing the pipe (Fig. 8). Application of this technique is possible because, owing to the high doping level at the surface, the top part of the pipe does not contribute appreciably to its resistance. Before diffusion of the contacting emitter layer certain diodes containing pipes were photographed to obtain the pipe diameter. The n^+-layer was then produced by conventional oxide masking and photoresist techniques. Only those devices which contained a single pipe were selected for measurement. In order to be sure that no submerged pipes were also contacted by the n^+-layer, after the resistance had been measured the specimens were anodically sectioned and examined again for the presence of submerged pipes.

The arrangement for resistance measurement is shown in Fig. 8. Separate probes were used for

[1] For example, in device production submerged pipes can produce emitter-collector shorts in structures which, prior to the emitter diffusion, exhibit perfectly satisfactory collector base junctions.

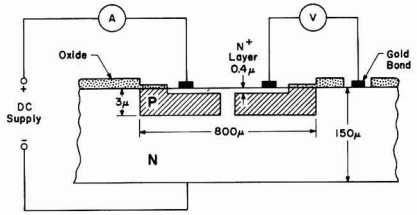

Fig. 8. Technique for measurement of ohmic resistance of pipe

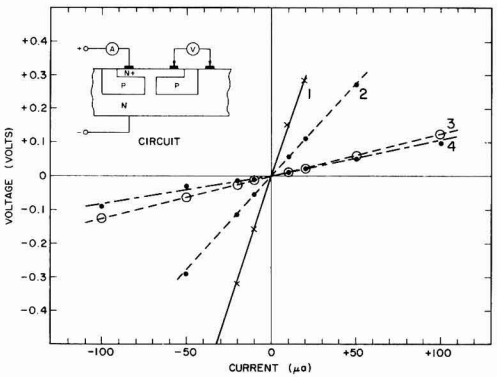

Fig. 9. V-I curves for four different pipes, which were used to determine ohmic resistance.

voltage and current readings so that the influence of contact resistances could be eliminated. All the resistances measured were ohmic in the range between −0.5 and +0.5v. At higher voltage the measurements were disturbed by injection effects within the npn structure. Voltage *vs.* current values for four different pipes are given in Fig. 9.

Discussion.—In Table II the results of the resistance measurement are presented. The first column gives the number of the pipe, the second the measured resistance. In the third column the observed diameters of the pipes at the surface are listed. These diameters had been measured before the contacting n^+-layer was diffused. For comparison the diameter of the pipe was calculated from the spreading resistance on the basis of two different models (9). The first model assumes that current spreads from a disk of negligible resistance of diameter d into the bulk silicon of resistivity ρ. Resistance in this case is given by

$$R = \frac{\rho}{2\,d}$$

In the second model resistance is thought to arise by spreading of current into the bulk from a hemisphere with negligible resistance, and diameter d

$$R = \frac{\rho}{\pi\,d}$$

(A rigorous treatment would require calculation of the spreading resistance of a hemispherical diffusion distribution whose top part is cut off by the junction.) For both cases d was calculated for $\rho = 3$ ohm-cm from the measured R values. These d-values are given in the third and fourth column of Table II.

The pipes in Table II can be separated into two groups. One group (No. 1 and 2) consists of pipes with a small diameter. For these we calculate a diameter which is too small with either model. The other group which consists of bigger pipes (No. 3 and 4) can best be approximated by the spherical model.

Table II. Results of pipe resistance measurements

No.	R measured, K ohms	d measured, μ	d_{calc}, disk model, μ	d_{calc}, spher. model, μ
1	11.0	5	1.35	0.87
2	5.5	6.2	2.7	1.75
3	1.2	8	12.5	8.0
4	1.1	10	13.6	8.7

In order to explain the disagreement for the first group, we have to assume that the diameters at the junction are smaller than at the surface. Indications for such a constriction of these pipes were indeed found when the sample containing the slice was sectioned anodically. Occurrence of surface contamination, however, prevented accurate measurements of pipe diameters close to the junction. We conclude, however, that in general the agreement with the model is satisfactorily within the limits set by experimental errors.

Conclusions

Pipes through diffused layers that were found in a preceding paper to be caused by diffusion of n-type impurity from localized specks of contamination were studied in detail in this investigation. Cross sections of pipes that were obtained by anodic oxidation were found to be in qualitative agreement with theory. Three types of pipes were found corresponding to the theoretically postulated type shapes: ellipsoid (I), hyperbola of rotation (II), and submerged hyperbola of rotation (IV). The existence of the latter type, which had only been postulated theoretically, was thus confirmed.

Deviations from the calculated shapes can be explained by enhanced diffusion close to the surface.

Measurement of the ohmic resistance of a number of pipes gave satisfactory agreement between optically and electrically determined pipe diameters.

Acknowledgments

The authors wish to thank W. Shockley for many helpful suggestions. They also are indebted to B. McDonald and R. Julien for the preparation of samples. This research was supported by Air Force Cambridge Laboratories under Contract AF 19(604)8060.

Manuscript received Jan. 15, 1962.

Any discussion of this paper will appear in a Discussion Section to be published in the June 1963 JOURNAL.

REFERENCES

1. A. Goetzberger, To be published in *Solid State Electronics;* also *IRE Trans. E. D.*, **8**, 429 (1961), and Interim Scientific Report No. 1, Contract AF 19(604) 8060.
2. P. S. Flint, Paper given at the Detroit Meeting, Electrochemical Society, October 1961.
3. P. F. Schmidt in "Semiconductors and Phosphorus," p. 570, Interscience Publishers, New York (1958).
4. E. Tannenbaum, *Solid State Electronics*, **2**, 123 (1961).
5. B. McDonald and F. C. Collins, *Bull. Am. Phys. Soc.*, **6**, 106 (1961).
6. C. S. Fuller and J. A. Ditzenberger, *J. Appl. Phys.*, **27**, 544 (1956).
7. A. Goetzberger and W. Shockley, *Bull. Am. Phys. Soc.*, **4**, 455 (1959).
8. B. D. James and P. S. Flint, Paper given at the Chicago Meeting, Electrochemical Society, April-May 1960.
9. W. Shockley, "Electrons and Holes in Semiconductors," p. 99, D. Van Nostrand Co., Inc., Princeton, N. J.

Hysteresis in the Large-Signal Field Effect in Semiconductor Surfaces

D. R. Frankl

General Telephone & Electronics Laboratories Inc., Bayside, New York

ABSTRACT

The finite generation and recombination rates of excess minority carriers can lead to large hysteresis effects even at frequencies $<<(2\pi\tau)^{-1}$ in large-signal field effect measurements. The hysteresis loop occurs on the inversion-layer side of the conductance *vs.* field curve and widens with increasing frequency and with increasing minority carrier lifetime in the sample. Experimental results on germanium and a simple theoretical treatment are presented.

Owing to the existence (usually) of a large concentration of slow surface states in semiconductors, any changes in sample properties induced by constant transverse electric fields tend to decay to zero. In other words, equilibrium field effects usually vanish. However, since at least in most germanium and silicon surfaces there is a large separation in the time constants of the slow and fast states, it is often possible to achieve a "quasi-equilibrium" condition, with the carriers in the bands and the fast states virtually in equilibrium, but with the carriers in the slow states virtually unaffected. The usual analysis (1) of field-induced conductance changes, to obtain information about the fast states, entails the implicit assumption that this condition exists.

The experimental requirement is that the time variations of the applied field be too rapid to be followed by the slow states, yet slow enough to be followed by all other processes affecting the carrier concentrations. These include drift and diffusion of free carriers, trapping in and release from fast states, and generation and recombination of minority carriers.

The latter processes are of principal concern in this paper. As is well known (2), under small-signal a-c conditions their finite rates lead to a relaxation in the field-effect mobility, centered at a frequency $f = (2\pi\tau)^{-1}$ (τ = sample lifetime), which for ordinary samples lies in the neighborhood of 10 kcps. Under large signal conditions, this effect can lead to appreciable departures from quasi-equilibrium even at much lower frequencies, and these give rise to hysteresis in the curve of conductance *vs.* applied field. The purpose of this paper is to illustrate this hysteresis effect, and to present a simple theoretical treatment to account for the order of magnitude of the observed deviations.

Theory

We consider, for definiteness, a p-type sample, and let P, N, and N_t be, respectively, the numbers per unit area of free holes, free electrons, and electrons trapped in fast surface states, all measured relative to some arbitrary reference level such as the flat-band condition. Also let P^0, N^0, and N_t^0 be the corresponding quasi-equilibrium values of these quantities. Then the induced surface charge density at any instant is

$$CV = -e(\Delta P - \Delta N - \Delta N_t) \qquad [1]$$

where C is the capacitance per unit area between field plate and sample, V the applied voltage, Δ denotes change from zero-voltage value. The excess surface conductance is, neglecting the surface mobility correction (3) which is usually small

$$\Delta\sigma = e(\mu_n\Delta N + \mu_p\Delta P)$$

$$= e[\mu_n\Delta N + \mu_p(\Delta N + \Delta N_t - CV/e)] \qquad [2]$$

where μ_n and μ_p are the electron and hole mobilities, respectively, Hence, the departure from the quasi-equilibrium conductance is

$$\delta\sigma = e[(\mu_n + \mu_p)\,\delta N + \mu_p\delta N_t] \qquad [3]$$

where $\delta N \equiv N - N^0$, etc.

It remains to compute δN and δN_t from the rate equations governing the approach to quasi-equilibrium. These are, in general, quite complicated (4), and an exact treatment was not attempted. Instead, we introduce the following simplifying assumptions:

1. The carriers in each band are separately in equilibrium among each other. This requires that the field period be $>>$ the time constant for redistribution, by diffusion, of localized excess carrier concentrations. From the diffusion equation, this time constant may be estimated to be $\leq B^2/D$ (D is the diffusion constant, $2B$ the sample thickness) which is, for germanium at room temperature, about 10^{-5} sec. Hence, the assumption should be reasonably valid for the low frequencies of interest here. Since the assumed distribution is essentially the same as the fundamental decay mode distribution (6) for small surface recombination velocity, this assumption permits us to write the rate equations in terms of the ordinary lifetime, as measured, for example, in photoconductive decay.

2. The transitions between the traps and at least one of the bands are so rapid (2) that the trapped carriers are always in equilibrium with this band. Then two limiting cases may be distinguished, depending on which band this is.

Case A, Traps in equilibrium with conduction band.—In this case, as the applied field is increasing electrons are generated and some of these fall into the traps. Hence

$$\frac{dN}{dt} = \frac{N^0 - N}{\tau} - \frac{dN_t}{dt} \qquad [4]$$

Note that this equation gives an underestimate for dN/dt since, in actuality, some fraction of the rate dN_t/dt comes from transitions to the valence band. This must be so because at least some of the surface states are the generation-recombination centers. In discussing this case, therefore, we are assuming that these centers comprise a negligible fraction of all the fast states. Since the latter are in equilibrium with the conduction band, we may take

$$\frac{dN_t}{dt} = \beta \frac{dN}{dt} \qquad [5]$$

where

$$\beta = \frac{dN_t}{dN} \cong \frac{dN_t^0}{dN^0} \qquad [6]$$

Then [4] becomes, in terms of the phase angle $\phi = \omega\tau$

$$\frac{d\,\delta N}{d\phi} + \frac{\delta N}{(1+\beta)\omega\tau} = -\frac{dN^0}{d\phi} \qquad [7]$$

The solution that vanishes at the accumulation-layer extreme of the voltage cycle (taken as $\phi = 0$) is

$$\delta N(\phi) = -\int_0^{\phi} d\phi' \frac{dN^0}{d\phi'} \exp\left[-\int_{\phi'}^{\phi} \frac{d\phi''}{(1+\beta)\omega\tau}\right] \qquad [8]$$

If ω is not too large, the exponential factor is very small except when $\phi' \cong \phi$, so that we may approximate [8] by

$$\delta N(\phi) \cong -\int_0^{\phi} d\phi' \frac{dN^0}{d\phi'} \exp\left[\frac{\phi' - \phi}{[1+\beta(\phi)]\omega\tau(\phi)}\right]$$

$$\cong -(1+\beta)\omega\tau \frac{dN^0}{d\phi}\left[1 - \exp\frac{-\phi}{(1+\beta)\omega\tau}\right]$$

$$\cong -(1+\beta)\omega\tau\, dN^0/d\phi \qquad [9]$$

This result states that N lags behind N^0 by the amount that the sum of $N^0 + N_t^0$ changes in one lifetime. Physically, the reason for this is that $N + N_t$ together form an equilibrium population that is generated at a rate proportional to the deficit in N only.

From [5] we have

$$\delta N_t = \beta\, \delta N \qquad [10]$$

and Eq. [9] and [10] provide the values to be inserted in [3]. The computation will be illustrated in the next section.

Case B, Traps in equilibrium with valence band.—In this case, the rapid communication with the majority-carrier band keeps δN_t always essentially equal to zero. The sole rate equation is then simply

$$\frac{dN}{dt} = \frac{N^0 - N}{\tau} \qquad [11]$$

giving, in the same approximation as was used in [9],

$$\delta N(\phi) = -\omega\tau(\phi) \frac{dN^0}{d\phi} \qquad [12]$$

Experimental Results and Discussion

The experimental method used in this work has been described in detail elsewhere (7). In brief, a small constant current is passed through the sample (a thin plate) and the voltage drop between two probes is displayed on the Y axis of an oscilloscope while the field voltage is displayed on the X axis. Thus, with suitable scale factors and with proper precautions to balance out spurious signals due to the displacement current, the oscillogram gives directly $\Delta\sigma$ *vs* V. With the addition of chopped light, τ can also be measured from the instantaneous photoconductance.

Typical dark curves for a p-type sample are shown in Fig. 1. The hysteresis occurs in the n-type surface conductivity branch of the curve and increases with increasing frequency. With n-type samples the hysteresis occurs in the other branch. And with either type of sample the width of the loop at a given frequency may vary widely depending on the surface treatment; with high-lifetime surfaces the loop is wide and *vice versa*.

The computation of the quantities entering Eq. [9], [10], and [12] is illustrated in Fig. 2, 3, and 4. Values of u_s are obtained by the usual analysis (1) of the lowest-frequency curve, and N^0 is then calculated as $N^0 = n_i L_D G(u_s, u_B)$, where n_i is the intrinsic concentration, L_D the Debye length, and G is the function tabulated by Kingston and Neustadter (8) and others (9); finally, $dN^0/d\phi$ is obtained by graphical differentiation. These quantities are shown in

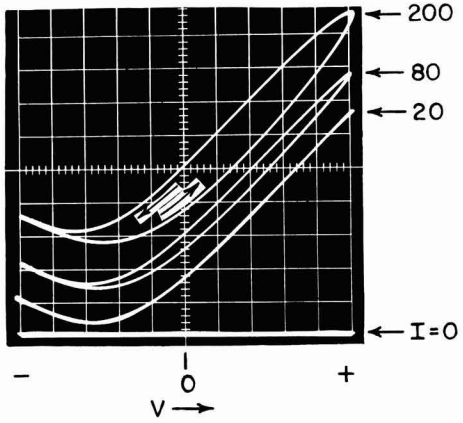

Fig. 1. Oscillograms of conductance *vs.* voltage on field plate at frequencies of 20, 80, and 200 cps for a p-type Ge sample. The field amplitude was about 10^5 v/cm. The line marked $I = 0$, obtained with no current through the sample, illustrates the cancellation of spurious signals.

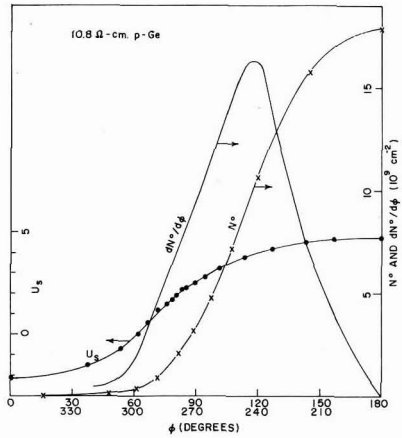

Fig. 2. Values of u_s, N^o, and $dN^o/d\phi$, as functions of the phase angle ϕ.

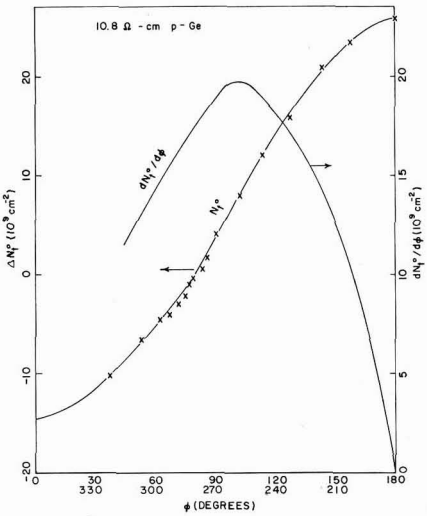

Fig. 3. Values of N_t^o and $dN_t^o/d\phi$ as functions of the phase angle ϕ.

Fig. 2. N_t^o and $dN_t^o/d\phi$, computed similarly, are shown in Fig. 3. Finally β, the ratio of the two derivatives, and τ, measured separately, are shown in Fig. 4.

The hysteresis data obtained on the same surface at higher frequencies are illustrated in Fig. 5. Here the total vertical separation $2|\delta\sigma|$ between the branches of the loop is plotted as function of the applied voltage. (Note that $V = -V_a \cos\phi$ as we have defined ϕ). Calculated curves for the two limiting cases discussed above are also shown. It is seen that the curve for Case A fits the data quite well at the right-hand end, but deviates markedly at the left. This deviation occurs because at these low values of u_s, the assumption of no communication between traps and valence band is untenable. At the extreme left-hand end of the loop, the curve for Case B gives an approximate fit to the data, but it is clear that over an appreciable range of surface potentials the true situation is intermediate between the two limiting cases. We shall not attempt to analyze this in detail.

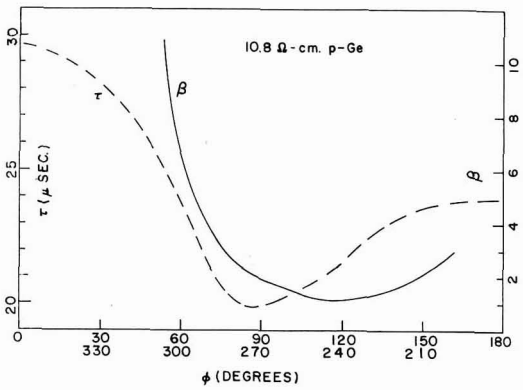

Fig. 4. Values of β and τ as functions of the phase angle ϕ

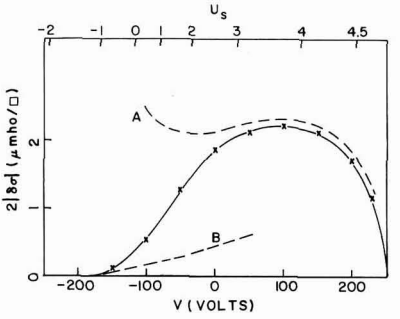

Fig. 5. Total vertical separation $2|\delta\sigma|$ between branches of hysteresis loop at 200 cps. Solid line is experimental; broken lines are theoretical for the two limiting cases discussed in the text.

The loop width at constant ϕ is found experimentally to be quite closely proportional to the frequency, as predicted by Eq. [9], [10], and [12], over the range from about 100 to 500 cps. However, below about 100 cps, the widths deviate from proportionality toward smaller values. The reason is the onset of another hysteresis mechanism, the exchange of charge with the slow surface states, which produces a loop that extends over the entire curve and widens with decreasing frequency. It is usually, although not always, possible to find a frequency at which the over-all hysteresis is negligible.

At frequencies above about 500 cps (in the present samples) still another effect was observed to set in: the mean of the two branches of the hysteresis loop sags below the equilibrium curve. This corresponds to the beginning of the field-effect mobility relaxation found by Montgomery (2). In samples with very high lifetime, this effect would set in at lower frequencies and might cause appreciable errors in field-effect measurements. This is particularly true when point-by-point methods (10) are used, since the hysteresis might easily be overlooked. It is one of the advantages of the oscilloscope method used here that any appreciable hysteresis present is clearly evident and serves as a warning that caution must be exercised in interpreting the results.

Acknowledgments

It is a pleasure to thank A. E. Feuersanger for assistance in the experiments and helpful discussions. Especial thanks are due also to H. C. Montgomery for pointing out some deficiencies in an earlier formulation of the theory.

Manuscript received Oct. 18, 1961; revised manuscript received Jan. 18, 1962. This paper was prepared for delivery before the Detroit Meeting, Oct. 1-5, 1961.

Any discussion of this paper will appear in a Discussion Section to be published in the June 1963 JOURNAL.

REFERENCES

1. H. C. Montgomery and W. L. Brown, *Phys. Rev.*, **103**, 865 (1956).
2. H. C. Montgomery, *ibid.*, **106**, 441 (1956).
3. J. R. Schrieffer, *ibid.*, **97**, 641 (1955); R. F. Greene, D. R. Frankl, and J. Zemel, *ibid.*, **118**, 967 (1960).
4. For treatments of the small-signal case, cf. C. G. B. Garrett, *ibid.*, **107**, 478 (1957) and F. Berz, *J. Electronics and Control*, **6**, 97 (1959).
5. A. Many and R. Bray, article in "Progress in Semiconductors," A. F. Gibson, Editor, **3**, 117, John Wiley & Sons, Inc., New York (1958).
6. W. Shockley, "Electrons and Holes in Semiconductors," p. 318 ff, D. Van Nostrand Co., Inc., New York (1950).
7. D. R. Frankl, *This Journal*, **109**, 238 (1962).
8. R. H. Kingston and S. F. Neustadter, *J. Appl. Phys.*, **26**, 718 (1955).
9. D. R. Frankl, *ibid.*, **31**, 1752 (1960); C. E. Young, *ibid.*, **32**, 329 (1961).
10. A. Many and D. Gerlich, *Phys. Rev.*, **107**, 404 (1957).

Thermodynamic Functions for the Tantalum-Hydrogen System

M. W. Mallett and B. G. Koehl

Battelle Memorial Institute, Columbus, Ohio

ABSTRACT

Equilibria in the tantalum-hydrogen system were determined in the range 300°-700°C, at hydrogen pressures of 10-1000 mm of Hg, and atomic fractions, N_H, 0.05-0.333. A single-phase solid solution of hydrogen in tantalum was produced throughout the experimental ranges. Obedience to Sieverts' law is approached at 500°C and higher for compositions below $N_H = 0.20$. The data were used to calculate the relative partial molar and total enthalpies, entropies, and free energies for formation of the solid solutions.

In order to evaluate properly the effects of interstitial elements on the mechanical properties of a metal, it is useful and, in some cases, necessary to know their kinetics of sorption by and diffusion in the metal. The literature is lacking in this type of information for the behavior of hydrogen and tantalum. At the temperatures of interest, above 300°C, the tantalum-hydrogen system shows a continuous solid solution up to compositions corresponding to $TaH_{0.5}$ and higher. It has been demonstrated (1, 2) that kinetic data for such a system are more readily rationalized when kinetic experiments are designed to produce a reaction product of constant composition. Therefore, it was necessary to know the equilibria of the tantalum-hydrogen system before starting the kinetic experiments. A number of earlier observations on the solubility of hydrogen in tantalum have been made (3). However, all of the data, with exception of those of Sieverts and Bergner and Sieverts and Brüning, appear to suffer from the impurity of the tantalum. The results show gross effects presumably of dissolved or surface oxide inhibiting reaction and quantitatively affecting the solution. Sieverts' equilibria were too limited for our purpose since they are largely for a pressure of 760 mm of Hg.

A recent paper (4) by Kofstad, Wallace, and Hyvönen gave good equilibrium data for a number of compositions of interest and for temperatures up to 400°C. Because our study was to cover temperatures up to 700°C, it was necessary to determine equilibria for the temperature range of 400°-700°C not covered by the literature. In addition, data were taken at 300°-400°C for comparison with the work of Kofstad *et al.*

Also, some thermodynamic functions readily obtainable from the equilibrium factors were calculated.

Material

The tantalum used in this work was obtained from the Wah Chang Corporation of Albany, Oregon. It had been electron-beam melted to an ingot, 3½ in. in diameter, and cold forged and swaged to a 7/16-in. diameter. Final fabrication was carried out at Battelle and consisted of cold swaging to rod, ¼ and ⅛ in. in diameter, and vacuum annealing for 1 hr at 1200°C. A length of the ⅛-in. rod was cold rolled to 0.0146-in. sheet for equilibrium experiments. The analysis of the tantalum before final fabrication is given in Table I.

Pure hydrogen was obtained from the thermal decomposition of uranium hydride prepared from dry tank hydrogen and degreased uranium chips.

Equilibrium Studies

Experimental procedure.—The method to obtain equilibrium data has been described (5). Briefly, the data were obtained as follows: A measured quantity of hydrogen was added to the calibrated reaction tube containing approximately 4g of sheet tantalum. At the desired temperature, the system was allowed to come to constant (equilibrium) pressure as measured on a mercury manometer. The equilibrium composition was calculated from the equilibrium

Table I. Analysis of tantalum

Element	PPM by weight
Al	<20
B	<1
C	42
Cd	<1
Cr	<20
Cu	<40
Fe	<100
Mg	<20
Mn	<20
Mo	<20
Nb	700
Ni	<20
Pb	<20
Si	<100
Sn	<20
Ti	<150
V	<20
W	<300
Zn	<20
H_2	<2*
O_2	<20*
N_2	3

Average BHN 80.1
* Vacuum-fusion analysis after final fabrication.

pressure, specimen weight, volume of gas addition, and gas capacity of the reaction system at the experimental room and furnace temperatures.

Results

The pressure-temperature-composition equilibria of the tantalum-hydrogen system were determined in the range 300°-700°C, 10-1000 mm Hg pressure, and atomic ratios, H/Ta, of about 0.05-0.50. These atomic ratios correspond to atomic fractions N_H for hydrogen of about 0.05-0.333. Equilibrium pressures were measured for at least three different temperatures for each composition. Figure 1 is a logarithmic plot of the equilibrium pressure against the H/Ta ratio. The plot shows that the isotherms are linear at temperatures of 500°C and higher; at lower temperatures, the isotherms show curvature which becomes increasingly marked with decrease in temperature. This curvature suggests a trend toward the formation of two phases at lower temperatures. However, since none of the isotherms shows an invariant pressure, no two-phase region was indicated in our experimental range. It seems that such a region would appear only at some temperature below 100°C.

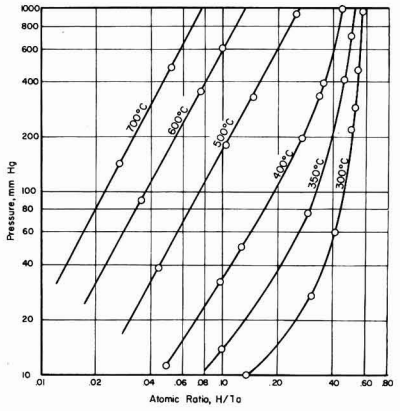

Fig. 1. Logarithmic plot of isotherms in the Ta-H system. Additional points at 300°C: 5.3 mm at H/Ta = 0.05, 7.4 mm at H/Ta = 0.10.

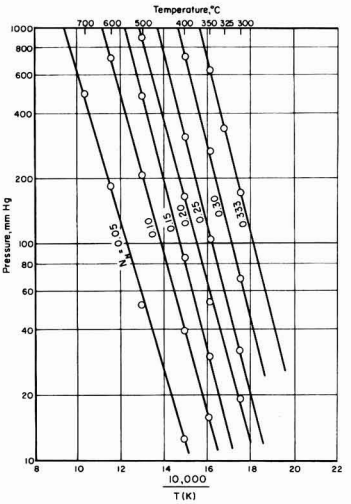

Fig. 2. Representative isopleths for the Ta-H system

After completion of this paper, a thesis by Veleckis (6) came to the authors' attention. He calculated the critical temperature to be −58.5°C at the H/Ta ratio of 0.205.

The equilibria were interpreted in terms of the conditions needed to form various products (solid solutions) having definite H/Ta and N_H ratios. This placed the data in the most convenient form for use in subsequent kinetic experiments. Several representative constant composition lines or isopleths are shown in Fig. 2. The equilibria for a given composition in these plots of logarithm of equilibrium pressure against reciprocal temperature can be expressed as

$$\log_{10} P_{mm} = -[A/T\ (K)] + B \qquad [1]$$

Values for the constants A and B determined by the method of least squares are given in Table II.

Since it may be desirable to relate thermodynamic and kinetic properties rather directly, the compositions are listed primarily according to round N_H values or atomic fractions of H.

Table II. Equations for equilibrium pressures

N_H*	Atom ratio, H/Ta	Constants in** $\log_{10} P_{mm} = -A/T + B$	
		A	B
0.05	0.0526	3480 ± 50	6.26 ± 0.06
0.10	0.1111	3620 ± 30	7.00 ± 0.05
0.15	0.1765	3860 ± 10	7.69 ± 0.02
0.20	0.2500	3740 ± 80	7.78 ± 0.13
0.25	0.3333	3800 ± 60	8.14 ± 0.09
0.30	0.4286	3960 ± 110	8.77 ± 0.17
0.333	0.5000	4020 ± 5	9.26 ± 0.01

* N_H = atomic fraction of H.
** ± values in this table are the probable errors for A and B.

Table III. Equilibrium pressure isotherms for Ta-H solid solutions

$\text{Log}\ \frac{\sqrt{P}}{N_H}$ mm

N_H	300°	304°*	325°	324°*	350°	349.5°*	400°	402°*	500°	600°	700°
0.05	1.391	1.305		1.420	1.635	1.579	1.842	1.819	2.177	2.435	2.640
0.10	1.343	1.305		1.420	1.596	1.579	1.811	1.819	2.163	2.427	
0.15	1.294	1.305		1.420	1.564	1.579	1.795	1.819	2.167		
0.20	1.327	1.307		1.423	1.590	1.581	1.812	1.822	2.171		
0.25	1.355	1.351		1.470	1.621	1.637	1.848	1.882			
0.30	1.450	1.487		1.613	1.728	1.757	1.964	(2.011)**			
0.333	1.599	1.649	1.746	1.777	1.880	(1.909)**	2.124	(2.158)**			

* Data from ref. (4). All temperatures in °C.
** Values extrapolated from low-temperature isotherms.

A comparison of the equilibrium pressure isotherms of the present study and those of Kofstad *et al.* is given in Table III. The agreement between the two sets of data is reasonable. A point worthy of note is that the pressures for the higher concentrations are consistently lower for the present study. This may indicate that our tantalum contained less interstitial contamination, particularly oxygen, than the metal of Kofstad. As will be seen later, the lower pressures also are reflected in lower relative partial molar free energy values at 350°C.

Also, it appears from the collective data that the Sieverts law is obeyed approximately for the N_H composition range 0.05-0.20. This is evidenced by the (relative) invariance of the value of $\log \sqrt{P}/N_H$ for different compositions at a given temperature. Large deviations from the Sieverts law are seen for higher compositions. That these deviations are related to entropy effects rather than enthalpy changes will be shown later. Deviations were also found by Kofstad at compositions lower than those of this study.

Thermodynamic Functions

When the dissolution of hydrogen in tantalum is expressed as

$$\tfrac{1}{2}\,H_2\,(\text{gas}) \rightleftharpoons H_i\,(\text{dissolved in Ta}) \qquad [2]$$

the relative partial molar free energy of hydrogen in a given Ta-H solution (i) is

$$\bar{F}_{H_i} - \tfrac{1}{2}F^\circ_{H_2} = RT \ln (P_{H_2})^{1/2} \qquad [3]$$

P_{H_2} is the pressure of hydrogen gas in equilibrium with the solution at temperature T and R is the gas constant.

The values for the relative partial molar enthalpies, $\bar{H}_H - H^\circ_{H_2}/2$, and entropies, $\bar{S}_H - S^\circ_{H_2}/2$, were calculated by the method of least squares from plots of $\log \sqrt{P}$ against reciprocal temperature. This treatment also yielded the probable errors for these values. The free energy values were then calculated according to

$$\Delta F = \Delta H - T\Delta S \qquad [4]$$

which applies to both the integral and partial molar quantities. The calculated relative partial molar thermodynamic functions for hydrogen in solution in tantalum are given in Table IV.

The relative partial molar enthalpy (the negative of the heat of dissociation) decreases systematically with increasing hydrogen content, if the value for

Table IV. Relative partial molar thermodynamic functions* for hydrogen in Ta-H solid solutions

N_H:	0.05	0.10	0.15	0.20	0.25	0.30	0.333
			This Study				
Temperature range, °C	400°-700°	350°-600°	300°-500°	300°-500°	300°-400°	300°-400°	300°-350°
$\bar{F}_H - \frac{F^\circ_{H_2}}{2}$ cal/g-atom	−3149	−2406	−1987	−1566	−1202	−673	−104
$\bar{S}_H - \frac{S^\circ_{H_2}}{2}$ eu/g-atom	−7.73 ± 0.14‡	−9.42 ± 0.10	−11.00 ± 0.04	−11.21 ± 0.29	−12.02 ± 0.21	−13.47 ± 0.40	−14.60 ± 0.03
$\bar{H}_H - \frac{H^\circ_{H_2}}{2}$ cal/g-atom	−7965 ± 115‡	−8275 ± 75	−8840 ± 25	−8550 ± 190	−8690 ± 130	−9065 ± 245	−9200 ± 15
			From ref. (4) for 350°C				
$\bar{F}_H - \frac{F^\circ_{H_2}}{2}$ cal/g-atom	−3310	−2510	−2010	−1600	−1210	−520	−1
$\bar{S}_H - \frac{S^\circ_{H_2}}{2}$ eu/g-atom	−9.9	−11.1	−12.1	−12.7	−13.6	−14.8	−14.9
$\bar{H}_H - \frac{H^\circ_{H_2}}{2}$ cal/g-atom	−9500	−9400	−9500	−9500	−9700	−9700	−9300

* The relative partial molar free energies, enthalpies, and entropies are for 1 g-atom of hydrogen.
† These free-energy values are for 350°C only.
‡ The ± values in this table are probable error.

N_H 0.15 is omitted. This indicates an increase in hydrogen binding in the Ta-H lattice over the N_H range 0.05-0.333. This agrees with the conclusions of Kofstad who reported an increase in partial heat of dissociation.

The relative partial molar entropy also decreases rapidly with increasing hydrogen contents. This may be caused by the decreasing availability of interstitial sites as more hydrogen is added to the metal. Thus, the enthalpy and entropy changes in the tantalum-hydrogen system make for opposite deviations in behavior from Sieverts' law. However, abnormal increases in pressure are observed with increasing hydrogen concentration indicating that the entropy effect is the stronger. This, of course, is a demonstration of a rise in relative partial molar free energy, $\overline{F} - F^{\circ}_{H_2}/2$, such as shown by calculated values for 350°C given in Table IV.

The relative partial molar enthalpies and entropies of the tantalum-hydrogen system show the same trends and are of the same general magnitude as those of the niobium-hydrogen system (7). However, for a given temperature and composition, the tantalum-hydrogen system shows the higher dissociation pressure of hydrogen, *i.e.*, the relative partial molar free energy for the dissolution reaction is higher.

An equation for calculating the partial molar free energy for tantalum in a given solution and the total free energy of formation of the solution was obtained by modification of the Duhem-Margules equation (8)

$$N_{Ta}\, d\,\overline{F}_{Ta} + N_H\, d\,\overline{F}_H = 0 \qquad [5]$$

where N is the mole or atom fraction. Since $N_{Ta} + N_H = 1$

$$N_{Ta}\, d \ln N_{Ta} + N_H\, d \ln N_H = 0 \qquad [6]$$

From Eq. [3]

$$d\,\overline{F}_H = RT\, d \ln P^{1/2}_{H_2} \qquad [7]$$

at constant temperature. Transposing one term of Eq. 5, dividing by N_{Ta}, and then substituting the equivalent of $d\,\overline{F}_H$ from Eq. [7]

$$d\,\overline{F}_{Ta} = -\frac{N_H}{N_{Ta}}\, d\,\overline{F}_H = -RT\,\frac{N_H}{N_{Ta}}\, d \ln P^{1/2}_{H_2} \qquad [8]$$

Also, from Eq. [6] by multiplying by RT and dividing by N_{Ta}

$$RT\, d \ln N_{Ta} + RT\,\frac{N_H}{N_{Ta}} \ln N_H = 0 \qquad [9]$$

Subtracting Eq. [9] from [8]

$$d\,\overline{F}_{Ta} = RT\, d \ln N_{Ta} - RT\,\frac{N_H}{N_{Ta}}\, d \ln \frac{P^{1/2}_{H_2}}{N_H} \qquad [10]$$

Integrating, we obtain

$$\overline{F}_{Ta_i} - F^{\circ}_{Ta} = RT\left[\ln N_{Ta_i} - \int_{N_H=0}^{N_{H_i}} \frac{N_H}{N_{Ta}}\, d \ln \frac{P^{1/2}_{H_2}}{N_H}\right] \qquad [11]$$

which is the equation for the relative partial molar free energy for tantalum in solution. The standard reference states at any temperature are 1 atm pressure for hydrogen and the pure hydrogen-free condition for tantalum.

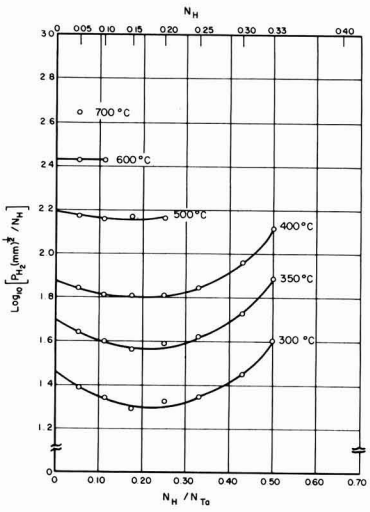

Fig. 3. Equilibrium isotherms for the tantalum-hydrogen system

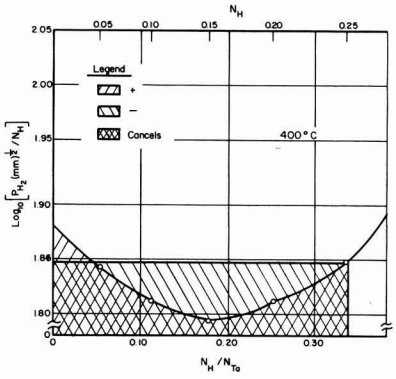

Fig. 4. Integration for $N_H = 0.25$ at 400°C

The negative integral in Eq. [11] is the natural logarithm of the activity coefficient of tantalum in a solution (i). To solve the equation it is necessary to integrate the last term graphically. To help visualize the areas to be integrated it is useful to consider the case of integration by parts where the negative integral becomes

$$-N_{H_i}/N_{Ta_i} \ln \frac{P^{1/2}_{H_2}}{N_{H_i}} + \int_{N_H=0}^{N_{H_i}} \ln \frac{P^{1/2}_{H_2}}{N_H}\, d\, N_{H_i}/N_{Ta_i}$$

Figure 3 shows several equilibrium isotherms plotted for integration. The 500° and 600°C curves approach the horizontal position which would indicate obedience to Sieverts' law. Figure 4 is a plot of a typical curve expanded for graphical integration. The negative and positive areas involved for the composition, $N_H = 0.25$ are indicated. The regions of overlap where the terms cancel each other are shown in cross-hatch. The computed relative partial

Table V. Relative partial molar free energies for tantalum in tantalum-hydrogen solutions

	$\bar{F}_{Ta_i} - F°_{Ta}$ (cal/mole of alloy)					
	Temperature, °C					
N_{Ta}	300°	350°	400°	500°	600°	700°
0.95	—54.0	—56.8	—62.8	—77.0	—87.4	—99.2
0.90	—105	—113	—128	—156	—179	
0.85	—159	—175	—198	—246		
0.80	—222	—257	—286	—341		
0.75	—329	—374	—408			
0.70	—527	—576	—640			
0.666	—754	—839	—935			

molar free energies for tantalum are listed in Table V.

The equation for the total free energy of formation for a given solution (i) is a combination of Eq. [3] and [6].

$$\Delta F_{f_i} = N_{H_i}\left(\bar{F}_{H_i} - \frac{1}{2}F°_{H_2}\right) + N_{Ta_i}(\bar{F}_{Ta_i} - F°_{Ta}) \quad [12]$$

Values for ΔF_{f_i} are given in Table VI. Equations of the same basic form as Eq. [11] and [12] were used by Katz and Gulbransen (7) for calculating the thermodynamic functions for the columbium-hydrogen system.

Both the relative partial molar free energy values (for tantalum) *vs.* temperature plots and the total free energy *vs.* temperature plots for each composition were linear. Therefore, the respective enthalpy and entropy functions and their probable errors could be calculated by a least squares treatment of the data for a given composition. It follows that both functions were invariant over the experimental temperature range. The relative partial molar enthalpies and entropies of tantalum in several hydrogen-in-tantalum solutions are given in Table VII. Corresponding total enthalpies and entropies for these solutions ranging in compositions from $N_H = 0.05$ to 0.333 are given in Table VIII.

Data of Kofstad *et al.* (4) are listed for comparison in Tables VI and VIII. Although their total enthalpies ranged from 96 to 307 cal/mole higher than those of our study their total free energies were higher by only 7 to 27 cal/mole.

The uncertainties in the values of $\bar{H}_{Ta_i} - H°_{Ta}$ and

Table VI. Total free energies of formation in the tantalum-hydrogen system

	ΔF_f (cal/mole of alloy)						
	Temperature, °C						
N_H	300°	350°	350°*	400°	500°	600°	700°
0.05	—228	—211	(—230)	—198	—173	—144	—116
0.10	—382	—343	(—370)	—308	—240	—166	
0.15	—516	—447	(—470)	—348	—260		
0.20	—603	—518	(—540)	—430	—250		
0.25	—697	—581	(—600)	—457			
0.30	—773	—605	(—620)	—448			
0.333	—780	—593	(—600)	—414			

* Data from ref. (4).

Table VII. Relative partial molar enthalpies* and entropies† of tantalum in tantalum-hydrogen solutions

N_{Ta}	$\bar{H}_{Ta_i} - H°_{Ta}$	Probable error	$\bar{S}_{Ta_i} - S°_{Ta}$	Probable error
0.95	14.8	±2.1	0.117	±0.003
0.90	42.9	±4.1	0.255	±0.006
0.85	100	±11	0.445	±0.017
0.80	115	±10	0.593	±0.015
0.75	127	±27	0.798	±0.043
0.70	119	±37	1.12	±0.06
0.666	286	±26	1.81	±0.04

* Cal/mole of alloy.
† Cal/deg-mole of alloy.

$\bar{S}_{Ta_i} - S°_{Ta}$ in the present study are from 9 to 30% and 2 to 5%, respectively. Since the investigations of similar systems have either omitted presenting uncertainties in values for these functions or even the values themselves, no comparison can be made. However, because of the indirect means of deriving these values the uncertainties appear quite reasonable. It is seen that the uncertainties in the values for relative partial molar energy functions for tantalum have an insignificant effect on the total energy functions. This is evidenced by the probable errors for ΔH_f and ΔS_f which are of the order of only 1%.

Acknowledgments

The authors wish to express their appreciation for the sponsorship of this research by Materials Central, Directorate of Advanced Systems Technology, Wright Air Development Division, Wright-Patterson Air Force Base, Ohio, and for permission to publish this paper. The work was performed under Contract No. AF-33(616)-7604. They also wish to thank Dr. John W. Droege of Battelle Memorial Institute for his helpful discussions.

Manuscript received Dec. 15, 1961; revised manuscript received March 7, 1962. This paper was prepared for delivery before the Los Angeles Meeting, May 6-10, 1962.

Any discussion of this paper will appear in a Discussion Section to be published in the June 1963 JOURNAL.

REFERENCES

1. W. M. Albrecht and M. W. Mallett, *This Journal*, **105**, 610 (1958).
2. W. M. Albrecht, W. D. Goode, Jr., and M. W. Mallett, *ibid.*, **106**, 981 (1959).

Table VIII. Total enthalpies* and entropies† of formation in the tantalum-hydrogen system

					Kofstad's data	
N_H	ΔH_f	Probable error	ΔS_f	Probable error	ΔH_f	ΔS_f
0.05	—384	±2	—0.275	±0.003	—480	—0.40
0.10	—789	±4	—0.713	±0.005	—940	—0.92
0.15	—1242	±10	—1.27	±0.01	—1410	—1.5
0.20	—1618	±8	—1.76	±0.01	—1860	—2.1
0.25	—2077	±20	—2.41	±0.03	—2370	—2.8
0.30	—2636	±27	—3.25	±0.04	—2860	—3.6
0.333	—2873	±17	—3.66	±0.03	—3180	—4.08

* Cal/mole of alloy.
† Cal/deg-mole of alloy.

3. G. L. Miller, "Tantalum and Niobium," pp. 445-447, Academic Press, Inc., New York, (1959).
4. P. Kofstad, W. E. Wallace, and L. J. Hyvönen, *J. Am. Chem. Soc.*, **81**, 5015 (1959).
5. W. M. Albrecht, M. W. Mallett, and W. D. Goode, Jr., *This Journal*, **105**, 216 (1958).
6. E. Veleckis, "Thermodynamic Properties of the System Nb-H, V-H, and Ta-H," AFOSR-1107.
7. O. M. Katz and E. A. Gulbransen, "Thermodynamic Functions for the Columbium-Hydrogen System," Scientific Paper 11-0807-11-P3, May 20, 1960, Westinghouse Research Lab. Presented at Columbium Metallurgy Symposium, Lake George, N. Y., June 6, 1960.
8. L. S. Darken and R. W. Gurry, "Physical Chemistry of Metals," p. 259, McGraw-Hill Book Co., Inc. (1953).

New Experiments on Thermoosmosis

Charles W. Carr and Karl Sollner

Department of Physiological Chemistry, University of Minnesota, and Laboratory of Physical Biology, National Institute of Arthritis and Metabolic Diseases, National Institutes of Health, Bethesda, Maryland

ABSTRACT

Thermoosmosis, the transport of liquid across a membrane which separates two solutions of identical composition but different temperature, was studied by means of a specially constructed apparatus. No thermoosmosis was observed with water or aqueous solutions of nonelectrolytes. With aqueous solutions of electrolytes thermoosmosis occurs across electrically charged membranes but not across uncharged membranes. While thermoosmotic effects are small their reproducibility is good. The rate of thermoosmosis is proportional to the temperature difference across the membrane. The direction of the thermoosmotic movement depends on the sign of charge of the membrane and the nature and concentration of the electrolyte in the solution. The results confirm those of Lippmann and Aubert (1907, 1912) and prove their tentative conclusion that thermoosmosis with electrolytic solutions is an electrochemical phenomenon and related to electroosmosis. The present results show in addition that the direction and rate of thermoosmosis depend in a strikingly similar manner on those factors which determine the direction and rate of anomalous osmosis, namely, the charge of the membrane and the nature and concentration of the electrolyte. This similarity is strongly suggestive evidence of a fundamental, close relationship between the two phenomena.

The study of the fundamental aspects of membrane phenomena has almost always been carried out in isothermal systems. Very little attention has been paid to the possible effects which might arise when the temperature of a liquid on one side of a membrane is different from that on the other. This is not surprising in view of the fact that the study of nonisothermal phenomena in liquid systems, such as the Ludwig-Soret effect (that is the uneven distribution of solute due to a thermal gradient in a solution) and thermopotentials in electrolytic systems, was for a long time a neglected field of research, not only because of the inherent complexity of nonisothermal systems in general, but also because they seemed to be somewhat outside the conventional scope of physical chemistry.

In the last two decades, however, novel and to a large extent successful attempts have been made to treat nonisothermal phenomena from a theoretical point of view (1, 2). Thus experimental information on nonisothermal membrane phenomena has assumed a renewed physicochemical interest. In addition nonisothermal phenomena deserve some interest because very few processes in nature occur under completely isothermal conditions. Temperature gradients of varying magnitude certainly exist across numerous types of living membranes and could conceivably influence the transfer of solvent and solutes across such membranes.

Thermoosmosis

Only a limited number of well-controlled experiments to determine the possible magnitude of nonisothermal membrane effects are reported in the literature. Lippmann (3) and Aubert (4) (in Lippmann's laboratory) were the first to describe the phenomena which occur when a membrane separates a cold from a hot solution. A transfer of liquid across the membrane, which they called "thermoosmosis," was observed in numerous instances with solutions of electrolytes; with nonelectrolytes the effect was doubtful or nonexistent. With some membranes (parchment paper and regenerated cellulose) an osmotic flow was observed from the side of the warmer to the side of the cooler liquid. With other membranes (pig's bladder, gelatin, and animal parchment) the osmotic flow was in the opposite direction. The phenomenon also seemed to be dependent on the presence of some foreign material that could be leached from the membrane. In addition, membranes which in use had become inactive could be restored to a state of activity by traces of suitable electrolytes, and similarly, certain membranes which were naturally inactive became active in the presence of some electrolytes. On the basis of their experiments, Lippmann and Aubert concluded that the thermoosmosis which they observed was linked closely to electroosmosis. This view was shared by Freundlich who, more specifically, surmised a funda-

mental similarity between thermoosmosis and anomalous osmosis (see below) (5).

The work of Ernst, and Ernst and Koczkás (6) on thermoosmosis was criticized by Ursprung (7) and need not be considered further here. Derjaguin and Sidorenkov (8) reported that appreciable quantities of water and other liquids are transported through sintered glass filters by thermoosmosis. Hutchison, Nixon, and Denbigh (9) have repeated and expanded these experiments and conclude that the results of the former investigators are due almost entirely, if not entirely, to the thermal expansion of the liquid. They agree with Lippmann and Aubert that there is no observable thermoosmosis of pure liquids across an inert barrier such as sintered glass or porous clay. Hutchison, Nixon, and Denbigh are of the opinion that those instances where thermoosmosis definitely occurs are most likely due to some electrokinetic mechanism; they also point out that probably not a single case of thermoosmosis has been found which can be explained on the basis of classical thermodynamics.

Riehl (10) in a paper on a rapid method of determining Ludwig-Soret coefficients by the use of a membrane separating a hot from a cold solution observed the transport of moderate quantities of liquid across membranes, but did not study this phenomenon further.

Winterkorn (11) finds a very close correlation between the mass movement of water in soils under a thermal gradient and the electrokinetic properties of these systems and believes that the thermal osmotic effects in soils may be an instance of thermoosmosis.

Haase (12) expressed the feeling of those familiar with the literature when he stated recently that only a few, and in part questionable, observations on thermoosmosis in liquid systems are extant (while analogous processes in gaseous systems were proven beyond doubt and are amenable to theoretical treatment). Haase has presented theoretical considerations concerning thermoosmosis with pure liquids and with solutions of nonelectrolytes and carried out experiments to test his conclusions; he did not consider thermoosmosis in systems with electrolytic solutions.

Thermoosmosis, a Problem in the Electrochemistry of Membranes

A review of the quoted and the other available literature indicates that thermoosmosis in systems free of electrolytes, if it occurs at all, is in all instances much less pronounced than in many systems with electrolytic solutions. The published data suggest that the essential mechanism of thermoosmosis in electrolytic systems is electrochemical in nature, most likely related in some manner to electroosmosis. Thus, it seemed promising to attack the problem of thermoosmosis from an electrochemical point of view and apply to it some of the current basic information on the electrochemistry of membranes as exemplified by the classical work on the electrochemistry of membranes by Loeb (13), by Michaelis (14), the fixed charge theory of electrochemical membrane behavior of Teorell (15) and Meyer and Sievers (16), and the work on "activated" membranes carried out in our laboratories (17-24).

The degree of the electrochemical activity of ionic membranes, for instance their electromotive action, their electroosmotic efficacy, or their ability to give rise to anomalous osmosis are more pronounced the greater the density of ionic groups at the walls of the pore system which constitutes the membrane (17-24). These ionic groups may be an inherent part of the matrix material from which the membranes are prepared or they may be introduced by intentional "activation" such as a chemical reaction, *e.g.*, oxidation which creates ionic groups, adsorption of ionic materials such as polyelectrolytes or proteins on formed membranes, and mixing of polyelectrolytes with the matrix material before the membranes are cast (17-24). It is evident that the methods of activating membranes should be very helpful in determining whether thermoosmosis is really an electrochemical effect. If this is the case, activated membranes with solutions of electrolytes should show greatly enhanced thermoosmotic effects as compared with nonactivated ones.

Experimental

An apparatus similar to that used by Aubert (4), was constructed for measuring thermoosmosis; it is shown in Fig. 1 and 2.

Essentially the apparatus consists of two very narrow circular chambers separated by a membrane, the two chambers being arranged for heating and cooling, respectively (see Fig. 1a and 1b.) Two round

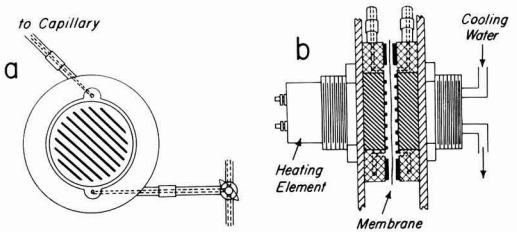

Fig. 1. Cell for the study of thermoosmosis across membranes (slightly schematic): (a) side view of a solution compartment; (b) cross-sectional view of main parts of thermoosmosis cell.

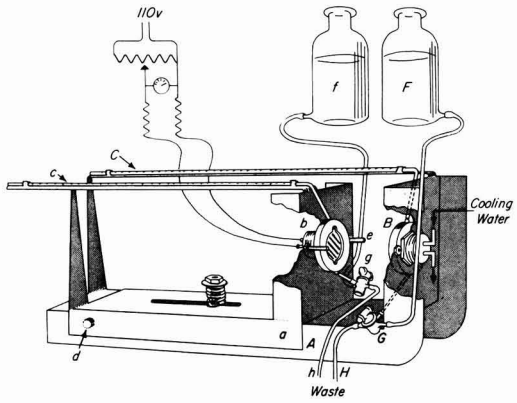

Fig. 2. Complete thermoosmosis apparatus with thermoosmosis cell and auxiliary equipment.

copper blocks of 50.7 mm diameter are set in hard rubber rings of 90 mm outer diameter. One of the blocks was heated by a 100-w (nominal at 110v) electric heater whose temperature was adjusted by a variable voltage control, routinely set at 60v (corresponding to about 30w) unless otherwise stated; the other copper block was cooled by water circulating through it, the temperature of which was maintained at 25°C. The surfaces of both copper blocks were painted with an inert and electrically insulating lacquer thus excluding corrosion and any possibility of an outside electrical connection between the solutions in the two compartments. Rubber gaskets 1 mm in thickness with an internal opening of 56 mm in diameter (and small cut outs for the inlet and outlet for the solution) were cemented to the hard rubber rings surrounding the copper blocks. To keep the membrane in an exactly defined, unchanging position, several narrow strips of the gasket material (about 1 mm in width) were cemented parallel, in opposite diagonal positions onto each of the copper blocks. When a membrane was clamped between these two parts, two cylindrical chambers were formed, each 55 mm in diameter and 1 mm in depth. The free membrane area, not blocked by the rubber strips, was about 20 cm^2. Each chamber was connected with a horizontal glass capillary. In the assembled apparatus (see below) the two capillaries were on the same level to prevent the development of any difference in hydrostatic pressure in the chambers while an experiment is in progress. A scale graduated in millimeters was attached under each capillary so that the rate of movement of the meniscus could be observed.

These essential parts of the thermoosmotic cell were mounted in the apparatus shown in Fig. 2 consisting of an L-shaped stand *A* and an L-shaped sledge *a* which can be moved back and forth along the longer limb of the stand *A*. The two assemblies (Fig. 1b) which form the thermoosmosis cell proper, *B* and *b*, connected to the measuring capillaries *C* and *c* (inner diameter about 0.9 mm) are mounted in the upright parts of *A* and *a* as shown in Fig. 2. To put the apparatus together for an experiment, it is first turned 90° into the vertical position with the sledge *a* raised and held by the catch bolt *d*. The membrane to be used is then placed over the lower copper block and rubber gasket, *B*, mounted on *A*; it should be large enough to cover all of the gasket. The assembly with the upper copper block, *b*, mounted on the sledge *a*, is then lowered onto the membrane. The two parts are then clamped tightly together with two large screws *e*. The apparatus is then returned to the horizontal position. Figure 2 shows in addition the arrangement for filling and flushing the two cell compartments by means of two solution reservoirs *F* and *f*, the three-way stopcocks *G* and *g*, and the attached waste lines *H* and *h*.

For an experiment the chambers were filled by gravity feed with the same solution from the two reservoirs. The positions of the menisci in the capillaries *C* and *c* are regulated by the three-way stopcocks, *G* and *g*. With both chambers at the same temperature, the apparatus is allowed to stand for 30 min, the position of the meniscus in each tube being observed every 5 min to ascertain that there are no leaks. When it has been established that the system is watertight, the heater for the one chamber is turned on, and the cooling water is circulated through the copper block of the other chamber. When the assembly has warmed up, a steady state is reached in which the rate of movement of the menisci in the two capillaries becomes constant; this usually requires 15-30 min after the start of the experiment. Thereafter readings of the positions of the menisci are taken every 10 or 15 min for about 1 hr, confirming thereby that the observed rate of water movement is constant at least during this period.[1] This rate is take as a measure of the magnitude of the thermoosmosis.[2]

The solutions must be carefully degassed by boiling (and replacement of the water lost by equally carefully degassed water); 15-20 min vigorous boiling were adequate. With not properly degassed solutions, gas bubbles form, particularly in the compartment of the hot solution and give rise to spurious volume readings.

The possibility of a disturbing thermometric effect must also be considered. As will be shown later, with distilled water in the apparatus no thermoosmosis is observed, *i.e.*, there is no continuous unidirectional movement of the meniscus. There is also no detectable fluctuation in the position of the meniscus after the steady state has been attained. Thus a significant contribution of the thermometric effect to the observed volume changes during the experimental period is ruled out.

All membranes used were of the porosity of conventional dialyzing membranes. They included membranes prepared from electrochemically rather inactive collodion of high purity which were used without further treatment; collodion membranes that had been made strongly electronegative by oxidation with NaOH (20);[3] and collodion membranes that had been made electropositive by the adsorption of protamine (23).[4] The preparation and properties of these types of membranes have been described previously (17-24).[5] In addition, some

[1] In the limited number of experiments which were carried out over 3-4 hr, a gradual but significant decrease in the rate of liquid movement occurred, an effect reported already by Aubert (4).

[2] The described apparatus and the technique used are obviously not suitable to determine minor thermoosmotic effects which might occur during the warming up period. Our experimental procedure, like that of Aubert, is designed to study processes which extend over periods substantially longer than the warming up period. A thermoosmotic process which comes to a stop during the warming up period and is not of the magnitude of at least a sizable fraction of the total thermometric (thermal expansion) effect occurring during this period, would not be detected. Any negative result obtained by our experimental method should be considered in this light.

[3] Collodion in contact with alkaline solution is not hydrolyzed in a straightforward manner to cellulose and nitric acid; rather, it undergoes a gradual decomposition of a complicated nature. Nitrite is formed in large quantities and the nitrocellulose is gradually oxidized. The oxidation of collodion membranes by means of alkaline solutions tends to produce membranes of higher electrochemical activity than conventional oxidizing agents.

[4] Protamines are simple strongly basic proteins, ordinarily derived from salmon sperm, with molecular weights of about 4000 in the hydroxyl form. They are of somewhat varying composition, most probably consisting of 19 molecules of arginine, a dibasic amino acid with a pK of 12.5, and six or seven monobasic amino acids. The ionizable groups in the protamine molecule, which are not blocked by the formation of peptide linkages, are: one carboxyl group, one imino group, and 19 guanidino groups.

[5] It should be noted that the activation of the wide pored membranes of the dialyzing type by oxidation (to render them acidic) or the adsorption of protamine (to make them basic in character) does not change to an extent which is significant in the present connections either their water permeability or their osmotic behavior with solutions of nonelectrolytes, while electroosmosis or anomalous osmosis across them are increased manyfold.

experiments were carried out with cellophane and animal parchment.

A shortcoming of our thermoosmosis apparatus is the lack of provisions for the measurement of the temperature difference between the two sides of the membrane.[6] For the purpose at hand, however, this shortcoming is more apparent than real, since our aim here is the comparison of the behavior of different membranes and different solutions under otherwise constant, standardized conditions. The temperature difference across membranes must vary to some extent according to their different thicknesses and water contents. However, the difference in temperature can be assumed to be virtually the same across generically related membranes of the same thickness and water content. The nonactivated, the oxidized, and the protamine collodion matrix membranes with which the bulk of the experiments were carried out fall into this category.

In the experimental results presented later, a flow of liquid from the hot side to the cold side is arbitrarily assigned a positive sign, a flow in the opposite direction a negative sign. This convention was chosen to avoid confusion in the discussion, when the flow of liquid in thermoosmosis will be compared to the flow of liquid in anomalous osmosis. The results obtained from the rates of movement of the menisci in the capillaries are expressed in $mm^3/100\ cm^2$ of membrane area per minute. It is estimated that the reproducibility of a given measurement is about $\pm$ 1 $mm^3/100\ cm^2$-min.

Results and Discussions

Our initial survey experiments were concerned with the influence of the nature of the membrane, and of the nature and the concentration of various solutes. A summary of representative data is given in Table I. The results were clear cut: In systems with pure water, thoroughly freed of all solutes, thermoosmosis does not occur to an extent detectable with our equipment, that is less than 0.3 $mm^3/100\ cm^2$-min. The same holds true with solutions of sucrose in agreement with the observation of Aubert who did not observe any thermoosmosis with solutions of various nonelectrolytes. With solutions of electrolytes, however, thermoosmosis may occur depending on the electrical charge of the membrane. The effect is not measurable in our system with cellophane membranes or membranes prepared from pure collodion, which are known to be rather inactive electrochemically, having only a few stray fixed ionic wall groups in their pores (18-20). "Activated" or inherently active membranes such as oxidized collodion membranes or protamine collodion matrix membranes or membranes of animal parchment are thermoosmotically active, corresponding to the fact that they are electrically charged, carrying numerous fixed ionic groups in their pore structure.

The direction of the thermoosmotic flow in the majority of simple systems is from the hot to the cold compartment–"positive" in our terminology.

It may be useful to add here that the thermoosmotic effect, as stated already by Aubert, becomes larger with an increase of the temperature difference between the solutions in the hot and cold compartment. It would require a special, rather elaborate arrangement to determine accurately the magnitude of the driving force, that is the temperature drop across the membrane itself.[6] We confined ourselves to the simple expedient of correlating the extent of thermoosmosis to the voltage applied to the heating element of the hot side of our apparatus. While water of 25°C flowed at a constant rate through the copper block of the cold side, a stepwise increased voltage, 30, 40, 50, 60, and 65v, was applied to the heater. The corresponding rates of thermoosmosis with an oxidized collodion membrane and 0.01*M* K_2SO_4 solution were: 1.3, 2.2, 6.3, 10.8, and 11.4 $mm^3/100\ cm^2$-min. When these values are plotted against the square of the voltage applied to the heater, they are found to lie on a straight line within the limits of the accuracy of the data and to be proportional to the square of the voltage, that is proportional to the quantity of heat which flowed across the thermoosmosis cell. The temperature drop across the membrane proper must be assumed to be proportional to the flux of heat across the cell. Therefore it can be concluded that the rate of thermoosmosis is proportional to the driving force, the temperature difference between the two membrane-solution interfaces, a not unexpected result.

The results of Table I, and of other experiments omitted here, fully confirm those of Aubert. There is excellent agreement with respect to the most important points, namely, the influence of the nature of the solute, the direction of the thermoosmosis as dependent on the nature of the membrane, and the order of magnitude of the observed effects. Our observation that the electrochemical "activation" of membranes increases thermoosmosis many-fold

[6] In the narrow solution compartments of our apparatus, which are indicated by other considerations, stirring of the liquid is due only to natural convection, and therefore rather ineffective. In addition, adjacent to the membrane, there are unstirred (Nernst) layers of solution which are of the same order of magnitude in thickness as the membrane itself. Thus, a large fraction of the temperature difference between the two bulk solutions is not operative across the membrane. In further work it will be advisable to use membranes of greater thickness, 1 mm or more, than that of the membranes used here (30-50μ), combined with effective mechanical stirring.

Table I. Thermoosmosis with different solutions across various membranes†

Membrane	Solution	Rate of thermoosmosis in $mm^3/100\ cm^2$-min*
Nonoxidized collodion	H_2O	0.0
	0.02*M* K_2SO_4	0.0
Oxidized collodion	H_2O	0.0
	0.02*M* KCl	+6.4
	0.02*M* K_2SO_4	+18.0
	Sucrose	0.0
Protamine-collodion	H_2O	0.0
	0.02*M* KCl	+5.4
	0.02*M* $MgCl_2$	+13.2
Cellophane	H_2O	0.0
	0.02*M* K_2SO_4	0.0
Animal parchment	0.02*M* NaOH	−11.3

† The voltage applied to the heater was 60v in all instances.
* A positive sign represents flow of solution from the hot side to the cold side, a negative sign the reverse.

strongly supports the hypothesis of Lippmann and Aubert that thermoosmosis is of an electrochemical nature and probably closely linked to electroosmosis.

As stated before, Freundlich had surmised that thermoosmosis might be closely related to anomalous osmosis (5). In the course of our experiments two regularities of importance in this connection have been noted consistently. First, thermoosmosis across acidic membranes, such as oxidized collodion membranes, is always stronger with uni-bivalent electrolytes such as K_2SO_4 than uni-univalent salts; with basic, electropositive membranes, such as protamine collodion matrix membranes, the effect is stronger if the electrolyte has a bivalent cation. Second, without exception the thermoosmotic effect was strongest with solutions in a medium concentration range (with most systems about 0.01-0.03*M*) and considerably smaller at lower and higher concentrations. These regularities are also very characteristic for the phenomenon that is known in the literature as "anomalous osmosis." Thus, it seems indicated to compare the influence of concentration on the transport effects arising in thermoosmosis and in anomalous osmosis.

The term anomalous osmosis is commonly used to denote those osmotic phenomena arising with solutions of electrolytes which seem to be contrary to the common experience that the flow of liquid across a membrane which separates a solution from pure solvent (or a more dilute solution) occurs ordinarily toward the side of the more concentrated solution, and at a rate roughly proportional to the concentration difference. In the very common instance of "anomalous positive osmosis" the rate of movement of liquid toward the side of the solution depends on the concentration of the solution used, the rates of flow in a medium range of concentrations being much higher than with more concentrated or more dilute solution. In the relatively rare instances of "anomalous negative osmosis" a flow of liquid occurs toward the side of the pure solvent (or the more dilute solution).

Investigators in this field agree unanimously that anomalous osmosis through porous membranes is an electrochemical phenomenon (25). Its magnitude is closely correlated with the product of the electrokinetic charge of the membrane and the dynamic membrane potential which results from the diffusion of electrolyte across the membrane as stressed particularly by Bartell (26, 27) and Loeb (13). The details of the mechanism of anomalous osmosis across porous membranes are still controversial and the subject of continuing investigation (25, 28-31). One of us proposed some time ago that anomalous osmosis arises from the interaction of pores which yield different potentials (for instance, due to their different width), when the electrolytic solute diffuses across the membrane (25, 28). Local electric circuits arise, superficially similar to the local circuits assumed generally in corrosion. One set of pores acts as the source of the driving electromotive force, another set of pores plays the role of an electroosmotic diaphragm through which the current is driven passively, thereby producing electroosmosis according to the electrokinetic charge of the pores. Schlögl, in a most ingenious manner, has developed the idea that anomalous osmosis arises in the individual pores, without interaction of different pores (29). According to Schlögl, the potential which arises at each pore due to the diffusion of the electrolyte across it, acts as a moving force on the pore water according to the electrokinetic charge of the latter. Whichever of these and similar concepts may ultimately be proven correct, the electrochemical character of anomalous osmosis seems beyond doubt.

Most experiments on anomalous osmosis have been performed with systems in which a membrane separates pure water from a solution of an electrolyte, and the pressure rise in an osmometric capillary is read after an arbitrarily chosen time (20 min in the experiments presented below). The observed effect consists of two components, the true anomalous osmosis and the normal osmotic effect as it arises also with nonelectrolytes. To avoid this uncertainty and to determine the magnitude of true anomalous osmosis Grim and Sollner had recourse to the easily demonstrated fact that anomalous osmosis does not occur with electroneutral membranes (22). Accordingly, with membranes which can be charged and discharged reversibly (without significant changes in geometrical structure), such as many proteinized membranes, the osmotic effects caused by an electrolyte can be measured both when only normal osmosis arises (with the membrane in the electroneutral state) and when normal as well as anomalous osmosis occurs (with the membrane in a charged state). The difference between these two effects is considered as the true anomalous osmosis. Using this procedure Grim and Sollner have measured the true anomalous osmotic effects arising in systems in which the concentration ratio of the two solutions separated by the membrane was 2:1. Such systems are, of course, more similar to those used in the thermoosmosis studies, where the membrane separates solutions of equal concentration, than to the conventional solution-water system.

Figure 3 presents data on the extent of thermoosmosis across an oxidized, electronegative, collodion membrane with K_2SO_4 as electrolyte (heater set at 60v), and two sets of data on anomalous positive osmosis with the same electrolyte; the one set was obtained with an oxidized collodion membrane by the pressure rise method (18), the other one by the volume method with an oxyhemoglobin collodion matrix membrane in the negative state (at *p*H 10.0) (22).

Figure 4 gives analogous data on thermoosmosis with $MgCl_2$ across an electropositive protamine collodion matrix membrane (heater set at 60v), and data on anomalous positive osmosis by the pressure rise method across a similar protamine collodion membrane,[7] and by the volume method across the same oxyhemoglobin membrane referred to in Fig.

[7] The data shown in Fig. 4 for the pressure rise methods were actually obtained by Abrams and Sollner (23) with $CaCl_2$ as the electrolyte. The work of Loeb (13) and experience in our own laboratories show that there is no reason to believe that the curve would be any different in its form if $MgCl_2$ had been used instead of $CaCl_2$.

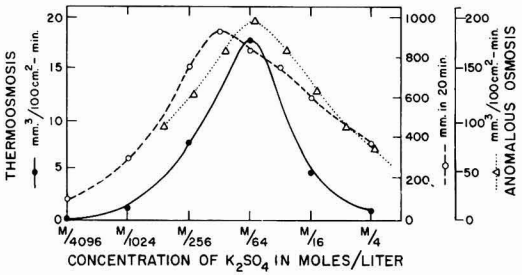

Fig. 3. Comparison of thermoosmosis and anomalous osmosis across negatively charged, acidic membranes; ——●—— thermoosmosis; — — ○ — — anomalous osmosis by the pressure rise method; . . . . △ . . . . anomalous osmosis by the volume transport method.

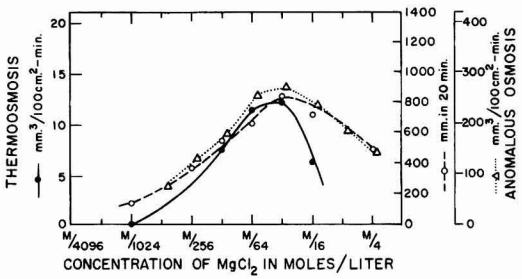

Fig. 4. Comparison of thermoosmosis and anomalous osmosis across positively charged, basic membranes; ——●—— thermoosmosis; — — ○ — — anomalous osmosis by the pressure rise method; . . . . △ . . . . anomalous osmosis by the volume transport method.

3, but now in the positively charged state (at *p*H 4.0) (22).

Figures 3 and 4 show the great similarity of the concentration dependence of thermoosmosis and of anomalous positive osmosis; the maximum effects of thermoosmosis and of anomalous osmosis occur in the same concentration range, with a fairly sharp decline both at higher and lower concentrations. In view of this correlation the next, obvious step was to test whether or not thermoosmosis occurs in the opposite direction (from the cold to the hot compartment) in systems the analogues of which are known to give anomalous negative osmosis.

Anomalous negative osmosis has been shown to arise in systems which satisfy these requirements: (i) the electrolyte must be such that its faster diffusing ion has the same sign as the charge of the membrane, and (ii) the porosity and charge density of the membrane and the concentration of the electrolyte must be adjusted so that the membrane potential is in the direction which gives the more dilute solution the same charge as that of the membrane (28).

In those instances where anomalous negative osmosis has been observed, the concentration of electrolyte necessary to produce maximal effects is considerably higher than that to produce maximal anomalous positive osmosis with the same membranes (and different electrolytes). For example, with positive membranes, acids, particularly di- and tri-basic acids, are especially effective in the concentration range of 0.5-1.0*M*; similarly, with negative membranes LiCl and strong bases will produce anomalous negative osmosis in this concentration range.

We have carried out a limited number of test experiments on thermoosmosis, simulating the above-described conditions which produce anomalous negative osmosis. In all instances the movement of liquid was from the cold to the hot compartment, that is the direction opposite to that in the experiments shown in Fig. 3 and 4. For example, with a protamine collodion matrix membrane, 0.5*M* H_3PO_4, and the same temperature gradient as used before, the rate of flow was −7.4 mm³/100 cm²-min. Similarly, with 0.02*M* NaOH[8] and oxidized collodion membranes, the rate of flow was −8.4 mm³/100 cm²-min.

These results confirm our anticipation based on the previous results which showed a strong correlation of thermoosmosis and anomalous positive osmosis. That the correlation of thermoosmosis and anomalous negative osmosis in appropriate systems is equally strong lends further strength to the hypothesis that mechanisms of thermoosmosis and anomalous osmosis are intimately related. However, we are not prepared at this time to propose a detailed mechanism for thermoosmosis. Before this can be done, it will be necessary to have measurements of the thermopotentials which arise under the conditions of the experiments. If one considers that the rate of anomalous osmosis in 2:1 concentration systems is at least 10 times larger than that of thermoosmosis under our experimental conditions (compare Fig. 3 and 4), and that the membrane potentials which arise in the former systems are of the order of 10 mv, it can be seen that the thermopotential required to produce the observed thermoosmosis may be only of the magnitude of 1 mv or less. Further, one should try to correlate the thermoosmotic mass movement with the Ludwig-Soret distribution of electrolytes across membranes. With such further information available, it will be of considerable interest to discuss possible mechanisms of thermoosmosis in the light of current theories of anomalous osmosis.

[8] This is not the optimum concentration for NaOH, but higher concentrations could not be used because the membranes are rapidly destroyed when such solutions are heated.

Acknowledgment

The authors wish to express their gratitude to the National Foundation for Infantile Paralysis under whose auspices this study was started in 1945, and to the Josiah Macy, Jr. Foundation which during the year 1946 supported the bulk of the experimental work presented in this paper.

Manuscript received Aug. 16, 1961; revised manuscript received Feb. 1, 1962. This paper was presented before the Colloid Division of the American Chemical Society at the Chicago Fall Meeting, 1946.

Any discussion of this paper will appear in a Discussion Section to be published in the June 1963 JOURNAL.

REFERENCES

1. S. R. DeGroot, "L'Effet Soret, Diffusion thermique dans les phases condensées," N. V. Noord-Hollandsche Uitgevers Maatschappij, Amsterdam (1945).

2. K. G. Denbigh, "The Thermodynamics of the Steady State," Methuen and Co. Ltd., London (1951).
3. G. Lippmann, *Compt. rend.*, **145**, 104 (1907).
4. M. Aubert, *Ann. chim. phys.*, [8], **26**, 145, 551 (1912).
5. H. Freundich, "Kapillarchemie," 2nd ed., p. 371, Akademische Verlagsgesellschaft, Leipzig (1922); 3rd ed., Vol. 1, *ibid.*, 386 (1930).
6. E. Ernst, *Nature*, **141**, 80 (1938); E. Ernst and J. Koczkás, *Z. Physik.*, **109**, 625 (1938); E. Ernst, *Kolloid Z.*, **87**, 276 (1939).
7. A. Ursprung, *Protoplasma*, **33**, 200 (1939).
8. B. Derjaguin and G. Sidorenkov, *Compt. rend. (Doklady) Acad. Sci. USSR.*, **32**, 622 (1941).
9. H. P. Hutchinson, I. S. Nixon, and K. G. Denbigh, *Discussions Faraday Soc.*, **3**, 86 (1948).
10. N. Riehl, *Z. Elektrochem.*, **49**, 306 (1943).
11. H. F. Winterkorn, Proc. 27th Ann. Meeting Highway Research Board, 443 (1947).
12. R. Haase, *Z. phys. Chem., (N.F.)*, **21**, 244, 270 (1959).
13. J. Loeb, *J. Gen. Physiol.*, **1**, 717 (1918-19); **2**, 173, 255, 387, 563, 577, 659, 673 (1919-20); and many more papers in the succeeding volumes of the same journal.
14. L. Michaelis and collaborators, *Biochem. Z.*, **158**, 28 (1925); **161**, 47 (1925); **162**, 258 (1925); **164**, 23 (1925); **173**, 411 (1926); *J. Gen. Physiol.*, **10**, 575, 671, 685 (1926-27); L. Michaelis, *Bull. Natl. Research Council*, **69**, 119 (1929); *Kolloid Z.*, **62**, 2 (1933); etc.
15. T. Teorell, *Proc. Soc. Exptl. Biol. Med.*, **33**, 282 (1935); *Proc. Natl. Acad. Sci. U.S.*, **21**, 152 (1935); *Z. Elektrochem.*, **55**, 460 (1951); *Progr. Biophys. Biophys. Chem.*, **3**, 305 (1953); *Discussions Faraday Soc.*, **21**, 9 (1956).
16. K. H. Meyer and J.-F. Sievers, *Helv. Chim. Acta*, **19**, 649, 665, 987 (1936); K. H. Meyer, *Trans. Faraday Soc.*, **33**, 1073 (1937).
17. K. Sollner, *J. Phys. Chem.*, **49**, 47, 171, 265 (1945); *This Journal*, **97**, 139C (1950); *Ann. N. Y. Acad. Sci.*, **57**, 177 (1953); K. Sollner, S. Dray, E. Grim, and R. Neihof, "Ion Transport Across Membranes," H. T. Clarke and D. Nachmansohn, Editors, p. 144, Academic Press Inc., New York (1954); "Electrochemistry in Biology and Medicine," T. Shedlovsky, Editor, p. 65, John Wiley & Sons, Inc., New York (1955); K. Sollner, *ibid.*, p. 33.
18. K. Sollner and I. Abrams, *J. Gen. Physiol.*, **24**, 1 (1940).
19. K. Sollner, I. Abrams, and C. W. Carr, *ibid.*, **24**, 467 (1941); **25**, 411 (1942); K. Sollner and J. Anderman, *ibid.*, **27**, 433 (1943); K. Sollner and C. W. Carr, *ibid.*, **28**, 1 (1944); H. P. Gregor and K. Sollner, *J. Phys. Chem.*, **50**, 53 (1946); etc.
20. K. Sollner, I. Abrams, and C. W. Carr, *J. Gen. Physiol.*, **25**, 7 (1941).
21. K. Sollner and R. Neihof, *Arch. Biochem. Biophys.*, **33**, 166 (1951); R. Neihof, *J. Phys. Chem.*, **58**, 916 (1954).
22. E. Grim and K. Sollner, *J. Gen. Physiol.*, **40**, 887 (1957).
23. I. Abrams and K. Sollner, *J. Gen. Physiol.*, **26**, 369 (1943); C. W. Carr, H. P. Gregor, and K. Sollner, *ibid.*, **28**, 179 (1945); H. P. Gregor and K. Sollner, *J. Phys. Chem.*, **50**, 88 (1946); M. Lewis and K. Sollner, *This Journal*, **106**, 347 (1959); etc.
24. M. H. Gottlieb, R. Neihof, and K. Sollner, *J. Phys. Chem.*, **61**, 154 (1957).
25. K. Sollner, *Z. Elektrochem.*, **36**, 36 (1930).
26. F. E. Bartell and C. D. Hocker, *J. Am. Chem. Soc.*, **38**, 1029, 1036 (1916); F. E. Bartell and O. E. Madison, *J. Phys. Chem.*, **24**, 444, 593 (1920).
27. F. E. Bartell, Colloid Symposium Monograph, **1**, 120 (1923).
28. K. Sollner, *Z. Elektrochem.*, **36**, 234 (1930); A. Grollman and K. Sollner, *Trans. Electrochem. Soc.*, **61**, 477, 487 (1932); K. Sollner and A. Grollman, *Z. Elektrochem.*, **38**, 274 (1932).
29. R. Schlögl, *Z. phys. Chem. (N.F.)*, **3**, 73 (1955).
30. Y. Kobatake, *J. Chem. Phys.*, **28**, 146, 442 (1958); *Progr. Theoret. Phys. (Kyoto)*, Supplement No. *10*, 226 (1959).
31. O. Kedem and A. Katchalsky. *J. Gen. Physiol.*, **45**, 143 (1961); A. Katchalsky, "Membrane Transport and Metabolism," A. Kleinzeller and A. Kotyk, Editors, pp. 69-86, Academic Press, New York and London (1961).

Anodic Oxidation of Methanol on Platinum

I. Adsorption of Methanol, Oxygen, and Hydrogen on Platinum in Acidic Solution

M. W. Breiter and S. Gilman

Research Laboratory, General Electric Company, Schenectady, New York

ABSTRACT

The coverage of bright platinum electrodes with methanol, oxygen, and hydrogen was determined as a function of potential and bulk concentration of methanol in perchloric acid. Two different techniques which lead to the same results for the coverage with the respective species are described. The methanol coverage was obtained for equilibrium conditions at open circuit and under the conditions of a quasistationary current-potential curve. The methanol coverage is potential independent between +0.1 and +0.6v and decreases rapidly with potential above +0.6v during the anodic sweep of the current-potential curve. The oxygen coverage differs only slightly in 1*N* $HClO_4$ and 1*N* $HClO_4$ + 1M CH_3OH. Hydrogen adsorption is decreased by 75% if the saturation coverage of methanol is present on the surface.

The mechanism of the anodic oxidation of lower alcohols on solid electrodes, particularly platinum, is of great importance in connection with fuel cell technology. An intensive study of one particular system, acid methanol, was carried out since it was felt that the results would advance the understanding of similar systems. Results on the mechanism of the anodic methanol oxidation will be reported in a series of papers. The first paper deals with the adsorptive properties of platinum with respect to

methanol, oxygen, and hydrogen in 1N $HClO_4$, containing different amounts of methanol.

Current-potential curves and analytic determination of the reaction products in different solutions have been mainly used to come to conclusions on the reaction mechanism (1-7). It is assumed in the existing theories of the oxidation mechanism that adsorption of methanol plays an important role. However, little is known about the adsorption of methanol in the so-called double layer region, about a possible simultaneous adsorption of hydrogen and methanol in the hydrogen region, and of methanol and oxygen in the oxygen region. A detailed description of the three well-known potential regions can be found in a paper (8) on the adsorption of amyl alcohol at platinum in which similar problems were discussed.

Pavela (3) was the first to establish direct experimental evidence for the adsorption of methanol on platinized platinum. He kept the electrode at open circuit in solutions of water and methanol for 15 min and then briefly immersed it in distilled water. The electrode was then immersed in 1*N* NaOH and an anodic charging curve measured. An arrest is observed which Pavela attributes to the quantitative oxidation of methanol to formic acid. The adsorbed amount is computed from the transition time of the arrest and the current. Pavela found a saturation coverage for methanol concentrations $C_M > 0.5M$. The experimental adsorption isotherm is in fairly good agreement with Langmuir's isotherm.

Pavela's procedure is based on two conditions: (*A*) Methanol is desorbed only to a negligible amount during the rinsing while only an adherent liquid layer of methanol is removed. (*B*) All the adsorbed methanol is oxidized before the anodic formation of a chemisorbed oxygen layer starts. As the fulfillment of the conditions was not verified, Pavela's results may include a considerable error. Therefore other techniques were developed and used to obtain the equilibrium coverage with methanol at open circuit and the coverage under the conditions of a potentiostatic current-potential curve. A comparison of the methanol coverage under the two conditions shows that equilibrium coverage is attained in the double layer region during the anodic sweep of current-potential curves. The oxygen coverage was measured as a function of potential in the base electrolyte solution and in solutions containing methanol. The information on methanol adsorption and oxygen coverage under different conditions has not been available in the literature. The results of this paper will be used to discuss the potentiostatic current-potential curve in a second paper of the series.

Experimental

Two techniques were used for the determination of the coverage with methanol, hydrogen, and oxygen. The first method is the potentiostatic application of voltage pulses to the electrode by means of a Wenking potentiostat. The second method consists in the chronopotentiometric (galvanostatic) application of current pulses. The form of the pulses was chosen such as to meet the experimental requirements for the determination of the adsorbed amount of one of the three species.

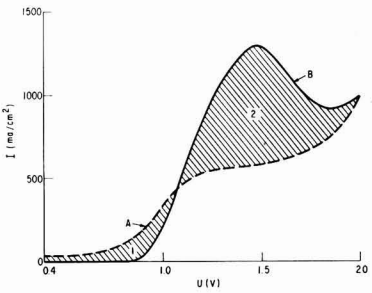

Fig. 1. Potentiostatic i-U-curves with v = 800 v/sec in 1*N* $HClO_4$ + 1M CH_3OH (curve B) and in 1*N* $HClO_4$ (curve A) starting from the open-circuit potential.

Potentiostatic technique.—A single triangular potential sweep of very short duration was applied to study methanol adsorption. The anodic sweep started at a desired potential and extended to 2.0v. It could also be started when the electrode potential changed linearly and periodically as under the conditions of a potentiostatic current-potential curve. The current was registered as a function of potential (or time) by means of an oscilloscope during the fast potential sweep. The nonstationary anodic current-potential curves (i-U-curves) were measured in the electrolyte (1*N* $HClO_4$) and in 1*N* $HClO_4$ with different amounts of methanol. Curve B in Fig. 1 was obtained in 1*N* $HClO_4$ + 1M CH_3OH and curve A in 1*N* $HClO_4$. The sweep started at the open-circuit potential of the platinum electrode in the respective solutions. All the potentials in this paper are referred to a hydrogen electrode in the same solution. The voltage speed of the sweep was 800 v/sec. The methanol was Spectro-quality Reagent (Matheson Coleman & Bell), the perchloric acid Analytical Reagent (Mallinckrodt), the water was double distilled with a specific resistivity of 8.10^6 ohm-cm at 25°C. Methanol concentrations up to 1M were used. The solutions were intensively stirred with argon before the measurements. The measurements were made in a Pyrex glass vessel with three compartments. The vessel was thermostated at 30°C. The prehistory of the electrode influences the i-U-curves markedly and is always given. The electrode pretreatment for the curves in Fig. 1 is described in the next section on the equilibrium coverage with methanol.

Shaded area 2 minus shaded area 1 (see Fig. 1) yields the charge, Q_M(coul/cm²) required for the removal of the adsorbed methanol by anodic oxidation, or

$$Q_M = \int_o^t i_B dt - \int_o^t i_A dt \qquad [1]$$

The applicability of the potentiostatic technique is based on four conditions: (*A*) The number of coul/cm² which are used for the anodic formation of an oxygen layer and for oxygen evolution during the sweep is the same in the electrolyte and in the solution containing methanol. (*B*) The same number of electrons per molecule is involved in the oxidation, independent of the adsorbed amount of meth-

anol. (*C*) The nonfaradaic currents which change the charge of the double layer are the same in the electrolyte and in the solution containing methanol. (*D*) The anodic sweep is sufficiently rapid that oxidation of methanol which diffuses to the electrode during the sweep is negligible.

The precision of the determination of $\ominus_M$ by the potentiostatic method is estimated at ± 0.1. The i-U-curves (see Fig. 1) coincide at high potentials. This shows that the electrode surface is oxidized to the same extent in the electrolyte and in the solution with methanol. Condition (*A*) is approximately fulfilled. This conclusion is supported by the result that the oxygen coverage of the electrode under the conditions of a potentiostatic current-potential curve is nearly the same at any potential independent of the methanol concentration as described in the section on the oxygen coverage. The coincidence of the i-U-curves is evidence that all the adsorbed methanol is removed during the anodic sweep. The i-U-curves have the same shape independent of the adsorbed amount of methanol. This suggests the fulfillment of condition (*B*). It was estimated that condition (*C*) might introduce an error of up to 7%. The nonfaradaic currents are relatively large due to the high voltage speed. They will differ to some extent as the double layer capacity is likely to be smaller during the sweep in the solution with methanol than in the electrolyte solution. Simultaneous adsorption of amyl alcohol and oxygen on platinum resulted in a lowering of the double layer capacity in the oxygen region (8). The same effect can be expected for methanol. To verify the fulfillment of condition (*D*), i-U-curves were measured at different voltage speed in 1*N* $HClO_4$ + 1M CH_3OH. Figure 2 represents the result. Q_M is plotted *vs.* log *v*. A limiting value for Q_M is obtained for $v > 200$ v/sec. Therefore the determination of Q_M was carried out with $v = 800$ v/sec. As condition (*D*) is fulfilled for 1M CH_3OH, it is valid for $C_M < 1M$ also.

The oxygen coverage at potentials in the oxygen region was obtained by interrupting the circuit at the desired potential and applying a potential of + 0.4v very rapidly. This was done with the Western Electric 275 C Relay. The oxygen layer is completely reduced at + 0.4v. The area under the current-time curve gives the amount Q_o in coul/cm² of adsorbed oxygen. The reduction occurs very fast

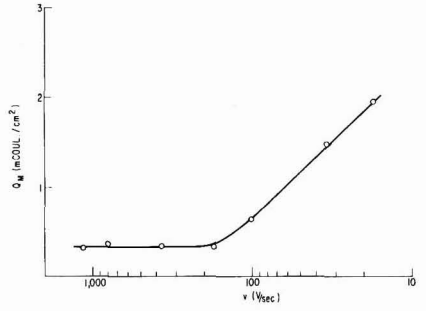

Fig. 2. Adsorbed amount Q_M of methanol in 1*N* $HClO_4$ + 1M CH_3OH as a function of the voltage speed *v* of the potentiostatic sweep.

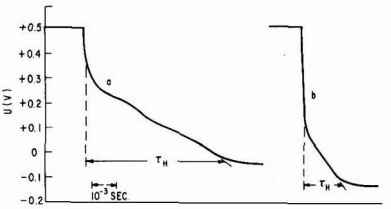

Fig. 3. Cathodic charging curves from 0.5v with 0.06 amp/cm² in 1*N* $HClO_4$ (curve a) and in 1*N* $HClO_4$ + 1M CH_3OH (curve b). The determination of the transition time τ_H for the hydrogen branch is shown.

(in about 5.10^{-3} sec). Therefore the influence of a simultaneous oxidation of methanol which diffuses to the surface is negligible.

Galvanostatic technique.—The second method consists in taking cathodic charging curves from different initial potentials. Q_o is determined as a function of potential in the oxygen region from the transition time of the oxygen branch of the charging curve and the current density (9). The length of the hydrogen branch yields the number Q_H of coul/cm² to fill the sites available for hydrogen adsorption. If the charging curve starts at a potential where methanol is adsorbed, the number N_M of hydrogen adsorption sites which are occupied by adsorbed methanol can be computed from the decrease in Q_H. Curve a in Fig. 3 is a charging curve with 0.06 amp/cm² from + 0.5v in 1*N* $HClO_4$, curve b from + 0.5v in 1*N* $HClO_4$ + 1M CH_3OH. Both curves were taken during the anodic sweep of potentiostatic current-potential curves with $v = 30$ mv/sec by switching from the potentiostatic to the galvanostatic circuit when the potential reached + 0.5v. Curve b shows a marked decrease in the length of the hydrogen branch. If ${}_sQ_H$ designates the number of coul/cm² for the cathodic formation of a completely covered surface in the electrolyte and Q_H is the value in the presence of methanol, then for potentials $U \geqq + 0.3v$

$$N_M = ({}_sQ_H - Q_H) \cdot L/\mathbf{F} \qquad [2]$$

F is the faraday and *L* is Avogadro's number. It was found from charging curves starting between + 0.8 and + 1.5v that ${}_sQ_H$ was approximately the same (0.34 mcoul/cm²) in all solutions. The above concept was used by Oikawa and Mukaibo (10) to study the adsorption of acetic acid on platinum, and by Franklin and Sothern (11) for the adsorption of nitrides on platinum. These authors took the quantity

$$\theta' = \frac{{}_sQ_H - Q_H}{{}_sQ_H} \qquad [3]$$

as a measure for the coverage with organic substance. This implies the validity of the relation

$$\theta = \frac{Q_M}{{}_sQ_M} = \theta' \qquad [4]$$

for the whole range of θ' values. The validity of relation [4] has already been questioned by one of the authors (8). The objection is based on the possibility that hydrogen atoms could be adsorbed on

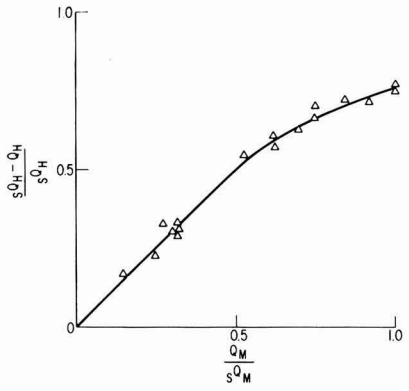

Fig. 4. Apparent coverage $\frac{{}_sQ_H - Q_H}{{}_sQ_H}$, as determined from the decrease of the hydrogen arrest of the cathodic charging curve, as a function of the coverage $\frac{Q_M}{{}_sQ_M}$, determined with the anodic potential sweep.

sites which are not accessible to methanol adsorption for geometric reasons. θ and θ' were determined for various concentrations of methanol in 1*N* $HClO_4$ under the conditions of a quasi-stationary potential sweep. The values reported for θ were obtained potentiostatically and those for θ' were obtained galvanostatically. Figure 4 gives the experimental results. Equation [4] is fulfilled for $\theta' \leqq 0.5$. Above $\theta' = 0.5$ the $\theta' - \theta$ curve bends and tends toward $\theta' = 0.75$ for $\theta = 1$. Only 75% of the sites which are accessible to the adsorption of hydrogen atoms are available for methanol adsorption. The calibration curve in Fig. 4 permits interconversion of θ and θ'. Since the galvanostatic method is simpler than the potentiostatic one, it was used in many cases. Adsorption isotherms of organic substances which were determined solely from the decrease of the amount of adsorbed hydrogen are in error for $\theta' > 0.5$. The latter statement holds for any method of determining Q_H. The fair agreement between θ and θ' for $\theta' < 0.5$ confirms the reliability of the potentiostatic and the galvanostatic method. The accuracy for θ' is estimated at $\pm$ 0.1. Precision for θ by the potentiostatic method is better than 0.03.

Results and Discussion

Adsorption Isotherm for Methanol

It is well known from reported polarization curves that methanol is oxidizable at relatively low potentials. Therefore the isotherm for equilibrium conditions can only be determined with certainty if the adsorption occurs at open circuit. The following pretreatment led to reproducible results. The electrode was polarized at 1.8v for 15 sec and at 1.55v for 30 sec while stirring with bubbled argon. Under these conditions the electrode surface is completely stripped of organic materials and is completely covered with an adsorbed oxygen layer. Desorbed organic materials are swept into the bulk solution and highly diluted. Then the stirring was interrupted and the potential held at 1.55v for 1½ additional minutes. The potential was then stepped instantaneously to + 0.4v and held there for 0.015 sec. This time is sufficient for the reduction of the chemisorbed oxygen layer. After 0.015 sec the circuit was opened. After a specified period at open circuit, Q_M was determined by the potentiostatic method. Two minutes were sufficient for establishment of adsorption equilibrium at all bulk concentrations of methanol. The described procedure was carried out in all solutions with the potentiostat and suitable circuits of Western Electric C275 Relays. The pretreatment described above not only provides a reproducible surface state for methanol adsorption, but largely excludes the possibility that oxidation products formed during the measurements or during the removal of the oxygen layer are adsorbed.

The potential shifts toward less positive values than +0.4v at open circuit in solutions with methanol. The potential which is reached after 2 min depends on the bulk concentration of methanol. Potential shifts of the described nature which start from a surface free of adsorbed oxygen and hydrogen were reported by Shlygin and co-workers (4, 5) as evidence for an electron-radical oxidation mechanism for CH_2O, HCOOH, CH_3OH, and other oxidizable substances. However, Vielstich (12) has stated that the measured open-circuit potentials are likely to be mixed potentials. Two interpretations for the potential shift, between which a distinction cannot yet be made, are more probable than Shlygin's interpretation. A small amount of hydrogen atoms is formed cathodically during the potential shift. The cathodic current is equal to an anodic current of methanol oxidation at the same electrode. As the rate of methanol oxidation becomes smaller with decreasing potential, a final open-circuit potential is approached. The amount of hydrogen formed in 2 min is still immeasurable. On the other hand the adsorbed methanol molecules may dissociate into radicals and hydrogen atoms to a small extent (1, 2). The adsorbed hydrogen atoms produce the potential shift. Traces of adsorbed hydrogen are detectable by anodic charging curves if the electrode rests for 20 min at open circuit in 1*N* $HClO_4$ + 1M CH_3OH.

Figure 5 represents isotherms of methanol adsorption at different times after opening the circuit (15

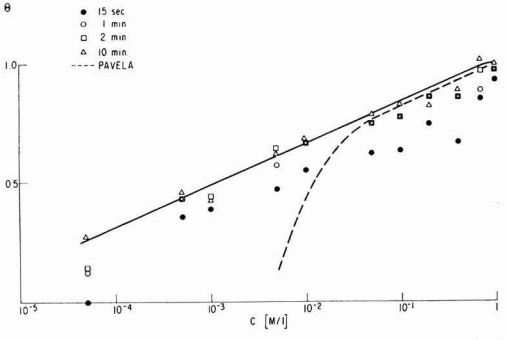

Fig. 5. Methanol coverage after different times at open circuit. The solid line represents the isotherm, the dashed line Pavela's results.

sec, 1 min, 2 min, and 10 min). Equilibrium coverage is practically achieved after 2 min. $\theta = Q_M/{}_sQ_M$ is plotted against log C_M. A semilogarithmic representation is chosen since a relatively large coverage is already found at small C_M-values. The saturation value ${}_sQ_M$ was reached for $C_M > 0.4M$ and is approximately equal to ${}_sQ_H$. It was 0.3 mcoul/cm² for the measurements in Fig. 5. If 0.75 ${}_sQ_H$ is taken as representing the number of platinum atoms available for methanol adsorption and if six electrons are involved in the oxidation of the adsorbed methanol, one methanol molecule occupies 4.5 platinum atoms. If the oxidation goes only to formic acid (4 electrons) the number of occupied platinum atoms is three. Both numbers appear acceptable as the cross section of the methanol molecule is about 25Å² (13), and the distance between platinum atoms in the (111)-plane is about 3Å.

Pavela's tabulated Q_M-values for platinized platinum were used to compute an isotherm. This isotherm is plotted as a dashed line in Fig. 5 while our results correspond to the solid line. Agreement exists at high concentrations while Pavela's values are too low at low concentrations. Obviously conditions (*A*) and (*B*) of Pavela's procedure discussed in the introduction are not fulfilled.

The adsorption isotherm in Fig. 5 is linear in a large concentration range. Temkin's isotherm describes the results to a first approximation. Such behavior is characteristic of a heterogeneous surface. Although an indication of steps is given by the experimental points, the experimental precision does not allow a decision as to whether or not these steps are a real phenomenon. The attainment of saturation coverage does not appear as pronounced on the semilogarithmic plot as on a linear plot.

Methanol-Coverage under the Conditions of a Potentiostatic Current-Potential Curve

Potentiostatic current-potential curves of fuel oxidation have peaks (1, 2, 5, 7, 12, 14) characteristic of every fuel. The method devised by Will and Knorr (15) was used here. A periodic triangular voltage sweep from +0.1 to 1.5v was applied to the electrode by means of the electronic potentiostat. The voltage speed was 30 mv/sec. After a certain potential was reached the potentiostatic circuit was interrupted manually by means of a Western 275C Relay. A cathodic charging curve was taken immediately after the interruption. The coverage was determined in the way described in the previous section. The current-potential curves became independent of time in unstirred solutions after a few cycles had been impressed.

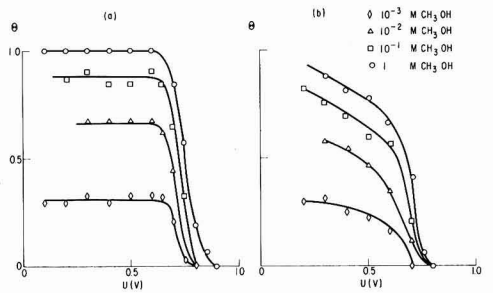

Fig. 6. Methanol adsorption at different potentials during the anodic sweep (Fig. 6a) and the cathodic sweep (Fig. 6b) of potentiostatic current potential curves in different solutions.

Figure 6a represents the coverage as a function of potential and of the bulk concentration of methanol during the anodic potential sweep, Fig. 6b during the cathodic sweep. The θ-values at +0.2 and +0.1v were determined by the potentiostatic method. The coverage is independent of potential between 0.1 and 0.6v at all concentrations during the anodic sweep. Then it decreases rapidly with potential. The θ-U-curves have a similarity with corresponding curves for the adsorption of organic substances on mercury (16) although the cause for desorption differs greatly. In this case it is due to the oxidation of methanol on platinum in the potential range of desorption. This effect will be discussed in the second paper. The methanol adsorption between 0.9 and 1.5v is very small and plotted as equal to zero in Fig. 6a and 6b where the abscissa is not extended beyond +1.0v. However, this statement may be slightly in error as the reproducibility of ${}_sQ_H$ is about ±10%.

A comparison between the θ values of Fig. 5 and the potential-independent values in Fig. 6a suggests that equilibrium is practically established under the conditions of a quasistationary potentiostatic current-potential curve. The rate of oxidation is not yet sufficient to lead to a decrease in coverage.

The coverage increases during the cathodic sweep at all concentrations and does not reach the constant value of the anodic sweep before 0.1v. The θ-U-curves show that the coverage is formed rapidly in the beginning while the attainment of a final value above 0.5 is slow. No adsorption takes place above 0.8v. The electrode remains covered with a chemisorbed oxygen layer between 1.0 and 1.5v during the cathodic sweep (see next section). Methanol adsorption starts after about 75% of the oxygen coverage is reduced.

So far it has been assumed that the coverage under the conditions of a potentiostatic current-potential curve is due to methanol adsorption. This need not necessarily be true as an oxidation peak is observed between 0.8 and 0.6v during the cathodic sweep (1, 2, 7, 12). It is conceivable that intermediates are formed then which are more strongly adsorbed than methanol and remain on the surface during the following part of the sweep. At the higher methanol concentrations the intermediates might produce as much as 50% of the measured θ-value (see Fig. 6b). However, a comparison of the potential-independent θ-value during the anodic sweep with the θ-value of the adsorption isotherm at the same concentration shows fair agreement between the two coverages. The agreement suggests that the coverage during the sweep is due mainly to methanol adsorption. The influence of intermediates is probably within the error of the θ-determination ($\leqq$10%). An accidental agreement is felt to be unlikely for all concentrations.

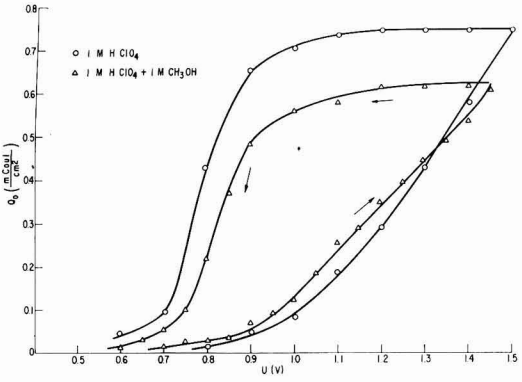

Fig. 7. Oxygen adsorption at different potentials during the anodic and cathodic sweep of potentiostatic current potential curves in 1N $HClO_4$ and in 1N $HClO_4$ + 1M CH_3OH.

Oxygen Coverage

It is well known that the anodic formation of a chemisorbed oxygen layer starts on platinum in acidic solutions at about +0.8v *vs.* a hydrogen electrode in the same solution. The coverage increases with potential. Approximately a monolayer is attained at +1.5v (9). The influence of the oxygen layer on the form of the potentiostatic current potential curves was already recognized and correctly interpreted in the early work on fuel oxidation (1, 2). However, a quantitative determination of the oxygen coverage under the conditions of a potentiostatic current-potential curve is not yet reported in literature. The oxygen coverage was determined by the potentiostatic method and the galvanostatic method at different potentials in the oxygen region during a potentiostatic current potential curve with 30 mv/sec in 1N $HClO_4$ and in 1N $HClO_4$ + 1M CH_3OH. The results obtained by the two methods agree fairly well.

The adsorbed amount Q_o obtained galvanostatically is plotted in Fig. 7 as a function of potential for the two solutions. A correction for the double layer charging during the oxygen branch of the cathodic charging curve was not made as the change of the double layer capacity with potential during the charging curve is not known. This leads to an error in the Q_o-values estimated to be less than 10%. The Q_o-U-curves are nearly the same in both solutions. This follows from the Q_o-U-curves during the anodic sweep. The potential of reversal differed by 50 mv in the two solutions. Therefore, the Q_o-U-curves are shifted against each other during the cathodic sweep. However, the same shape of the Q_o-U-curves is observed. There is an indication that the oxygen coverage is a bit larger at the same potential in 1N $HClO_4$ + 1M CH_3OH than in 1N $HClO_4$ up to +1.3v during the anodic sweep. Q_o increases more rapidly with potential above 1.3v in 1N $HClO_4$ than in 1N $HClO_4$ + 1M CH_3OH. The influence of methanol on the Q_o-U-curve is small. Therefore the Q_o-U-curve in 1N $HClO_4$ can be taken as a good approximation for the Q_o-U-curve in the presence of methanol up to $C_M = 1M$.

Manuscript received Dec. 6, 1961; revised manuscript received March 12, 1962. This paper was prepared for delivery before the Los Angeles Meeting, May 6-10, 1962.

Any discussion of this paper will appear in a Discussion Section to be published in the June 1963 JOURNAL.

REFERENCES

1. E. Müller and A. R. Miro, *Z. Elektrochem.*, **27**, 54 (1921).
2. S. Tanaka, *ibid.*, **35**, 38 (1929).
3. T. O. Pavela, *Ann. Acad. Sci.* Fennicae, Series A, II. Chemica, **59** (1954).
4. G. A. Martinyuk and A. I. Shlygin, *Zhur. fir Khim.*, **164**, 32 (1958).
5. A. I. Shlygin and G. A. Bogdanovsky, *Proc.* 4th Conference on Electrochemistry, Moscow 1956, pp. 282-286, Academy of Sciences, Moscow (1959).
6. See Extended Abstracts of Papers Presented at the Sessions of the Battery Division and at Joint Symposia on Fuel Cells with the Corrosion, Industrial, Electrolytic, and Theoretical Divisions of The Electrochemical Society, October 1961, Abstract No. 109, p. 138, No. 113, p. 149, No. 116, p. 159, No. 17, p. 38, No. 8, p. 42, No. 19, p. 45.
7. L. R. Griffith, R. P. Buck, *et al.* Proceedings 15th Annual Power Sources Conference, p. 16.
8. M. Breiter, *This Journal*, **109**, 425 (1962).
9. See M. Becker and M. Breiter, *Z. Elektrochem.*, **60**, 1080 (1956).
10. M. Oikawa and T. Mukaibo, *J. Electrochem. Soc. Japan*, **20**, 568 (1952).
11. T. C. Franklin and R. D. Sothern, *J. Phys. Chem.*, **58**, 951 (1954).
12. W. Vielstich, Paper presented at the Joint Symposia on Fuel Cells of The Electrochemical Society, May 1961.
13. W. D. Harkins, *Chem. Rev.*, **29**, 385 (1941).
14. Ye. M. Skobets and N. N. Atamenko, Kiev. Forestry Institute, Report VII, Zavodskaja Lab. Vol. 15, pp. 1291-1299.
15. F. C. Will and C. A. Knorr, *Z. Elektrochem.*, **64**, 258 (1960).
16. See M. Breiter and P. Delahay, *J. Am. Chem. Soc.*, **81**, 2938 (1959).

Studies on Alternating Current Electrolysis

IV. Mathematical Treatment of Reversible Electron Transfer with Alternating Voltage Control and Distorted Current

A. Edward Remick and R. A. Marcus[1]

Departments of Chemistry, Wayne State University, Detroit, Michigan and Polytechnic Institute of Brooklyn, Brooklyn, New York, respectively

ABSTRACT

A mathematical treatment is developed which yields equations relating faradaic current, voltage, and time when an alternating voltage is applied to an electrolytic cell composed of a plane and auxiliary electrodes immersed in a solution containing initially supporting electrolyte and only reversibly oxidizable or reducible species. Both oxidant and reductant are taken to be soluble, and specific adsorption is assumed to be absent. The voltage across that branch of the equivalent circuit through which only faradaic current flows is assumed to be periodic with fixed amplitude and with or without an additional direct applied voltage component; the resultant current is distorted. Diffusion controlled kinetics is postulated, and it is assumed that equilibrium is essentially established at the electrode surface. The equations developed show that a "steady state" (*i.e.*, a periodic state) is quickly attained, yield diagnostic tests of use in establishing the reversible mechanism, make it possible to determine the standard potential, and finally yield for the periodic state a relation between faradaic current and time. These results are then generalized so as to include systems in which the reversible electrochemical step is followed by a sufficiently slow secondary reaction step. One diagnostic result of interest in the latter connection is that the mean faradaic current vanishes in the periodic state, regardless of the amplitude or of the shape of the applied periodic potential, when the follow-up reaction occurs to a negligible extent.

The problem of developing a mathematical description of the chemical effects of alternating current on reversible redox systems has been attacked with varying degrees of success by several investigators (1-12) subject to the following restrictions: (*a*) undistorted voltage and current waves, and/or (*b*) both components of the redox system must either be present in the solution initially or present at the electrode's surface as the result of superimposed direct current. Berzins and Delahay (8) assumed what in the classification of Delahay, Senda, and Weis (17) may be called alternating voltage (A.V.) control [*i.e.*, controlled sinusoidal potential difference across that branch of the equivalent circuit for one electrode through which only faradaic (*f*) current is flowing]. They derived an equation for the instantaneous value of the (distorted) faradaic current as a function of time. This equation contained transient terms and a "steady-state" (or, better, a "periodic-state") term. Plane electrodes were involved.

Recently Matsuda and Delahay (13) extended the A.V. control problem to derive an equation for the transient current produced by faradaic rectification after the periodic component had reached a steady state. Their equation was restricted to small values of the A.V. and to solutions initially containing both oxidant and reductant.

Koutecky (14), assuming A.V. control, derived an equation for the instantaneous value of the faradaic current as a function of time for the general case of a periodic voltage of optional wave shape and applied it to the special cases of sine waves, square waves, and triangular waves. His equations were largely, although not entirely, concerned with the conditions characteristic of polarography (*i.e.*, dropping electrode), but his work and an initial portion of the present work are related. We shall be concerned with stationary electrodes, with a treatment for (in some ways) slightly more general systems, with a detailed treatment of the statement of the periodic state, and with devising a method of determining the standard potential and other properties (*m* and *n* below) of a reversible electrochemical step in an otherwise irreversible process.

In the present paper we shall discuss a system undergoing A.V. electrolysis with or without superimposed direct applied voltage for the case employing voltage control when the initial concentration of either oxidant or reductant is zero. Clearly, large A.V. amplitudes may be necessary to bring concentrations at the electrode surface into the poised region where reasonable accuracy in potential-concentration relationships may be achieved.[2]

This case is of only limited practical interest for

[1] Alfred P. Sloan Fellow; N.S.F. Senior Post Doctoral Fellow at Institute of Mathematical Sciences, New York University (1960-61).

[2] A certain experimental difficulty which, it has been suggested [p. 313 of ref. (17)], could complicate interpretation of the more usual (low amplitude) A. V. control systems, is absent here because of the different method used to interpret the results.

potentiometrically reversible redox reactions but should be important in the study of oxidations or reductions involving "follow-up" mechanisms, *e.g.*

$$\text{Red} \rightleftharpoons \text{ne} + \text{Ox (fast)}$$

$$\text{Ox} \rightleftharpoons \text{products (slow)}$$

especially when the half-life period of the unstable (or highly reactive) intermediate substance is short compared to the polarographic drop time but long compared to the period of the A.V. in a usable frequency range.

General Assumptions

In the theoretical treatment along the lines indicated, the following restrictions and assumptions will be made.

(i) A plane electrode is used and conditions for the semi-infinite linear diffusion are achieved.

(ii) A. V. control is employed (A. V. alone or with a superimposed direct voltage component).

(iii) The only depolarizer initially present is the reductant. (This is an unessential restriction, as noted later, and is made only to emphasize the case that is of practical interest here.)

(iv) A supporting electrolyte eliminates migration of the depolarizer and also keeps the pH constant through buffer action. Convection is assumed absent.

(v) "Spontaneous depolarization" (15) occurs only by diffusion, *i.e.*, the depolarizer concentration at the electrode changes only by diffusion or electron transfer to the electrode and not by secondary chemical reaction or by convection.

(vi) Specific adsorption is absent.

(vii) Electrochemical equilibrium exists between the electrode and the concentrations of the electrochemically active species just outside the region effectively occupied by the electrical double layer.

(viii) In view of the transient nature of faradaic rectification, it will be ignored as a possible source of disturbance of over-all concentration after a steady state (*i.e.*, a periodic state) is achieved.

In principle, the above assumptions are all that are needed. In practice, however, it is desirable that the electrolytic resistance is rendered negligible by the high concentration of supporting electrolyte, and that the working electrodes of the electrolytic cell are a measuring electrode and an unpolarizable auxiliary electrode. A negligible resistance ensures an undistorted voltage wave across the faradaic branch, a very desirable restriction, as discussed later. It should also be noted that when a second faradaic process of the above type occurs, it can be treated as a parallel branch in the equivalent circuit.

Assumption (vii) that chemical equilibrium is achieved with alternating voltage does not imply that the charge transfer resistance (Grahame's θ) is zero, but it does mean that the θ is negligible in comparison with the mass transfer resistance (diffusion) for the experimental conditions, *i.e.*, that the frequency used is low enough to enable close approach to equilibrium in a small fraction of a cycle. The validity of this assumption in the case of a poised ferrocyanide-ferricyanide solution was demonstrated by Remick and McCormick (16) who showed that the introduction of the Nernst equation into Grahame's equations for the faradaic admittance (6) adequately predicted the experimentally observed relation of depolarizer concentration to polarization resistance and capacitance up to the highest frequency used, *viz.*, 5000 cps. Less reactive systems would be expected to behave reversibly only up to lower frequencies.

The assumption that electrochemical equilibrium exists between the electrode and species just outside the double layer implies that the salt concentration is high, so that the width of the double layer is appropriately small. Were this condition not fulfilled, one would have to include in the diffusion equation of the i^{th} electrochemically active species the usual migration term $(D_i e_i/RT)(\partial\phi/\partial x)C_i$, ϕ being the potential at point x, and D_i, e_i, and C_i being the diffusion coefficient, charge and concentration (at x) of species i.[3]

The system as a whole will also be undergoing a periodic buildup and disappearance of the electrical double layer at the electrode. The total current at any time is the sum of this nonfaradaic current and the faradaic current i_f calculated below. That is, as discussed by Grahame (6), the additional process of charging and discharging the double layer can be regarded as corresponding to a condenser (of capacity depending on instantaneous voltage) in parallel with the faradaic branch of the equivalent circuit. We consider first the behavior of the faradaic branch.

Boundary Value Problem

The reversible electrode reaction

$$\text{Red} \rightleftarrows m\ \text{Ox} + ne \qquad [1]$$

involves the soluble species Red and Ox whose charge types are not specified. In Eq. [1] m and n are rational numbers. The molar concentrations of these species, respectively, will be symbolized by C_R and C_{ox} and the bulk concentration of Red by C^o_R. C_R and C_{ox} are functions of the time, t, and the distance, x, from a plane parallel to the electrode surface but just outside the electrical double layer region. To express diffusion control, Fick's second law will be employed as usual, expressed in terms of concentration rather than activities:

$$\partial C_{ox}(x, t)/\partial t = D_{ox}[\partial^2 C_{ox}(x, t)/\partial x^2] \qquad [2]$$

$$\partial C_R(x, t)/\partial t = D_R[\partial^2 C_R(x, t)/\partial x^2] \qquad [3]$$

where D_R and D_{ox} are diffusion coefficients. Equations [2] and [3] will be solved subject to the initial and

[3] This assumption concerning the width of the double layer will often be satisfied even when the assumption would be inaccurate for systems for which a kinetic boundary condition is appropriate (*i.e.*, a boundary condition such as $-D\partial C/\partial x = kC_{ox} - k'C_R$ at the electrode surface). In this kinetic case, Bockris (26) believed that the "zeta potential" is largely suppressed at concentrations above ca. 1*N*. This conclusion, however, was not substantiated by Breiter, Kleinerman, and Delahay (27) whose calculations (based on a theoretical equation which was found to be in accord with experimental data obtained in the polarographic reduction of iodate ions) indicated that the zeta potential might well be ca. 0.05v even in 1M solution. Since electron transfer proceeds from positions immediately adjacent to the electrode, we see that for double layer effects to be negligible in the kinetic case, the double layer should be narrower than a few Angstroms. In the electrochemical equilibrium case (assumption vii), however, to satisfy our assumption, it merely suffices that diffusion be rapid across the double layer so that concentration ratios inside it are given by a local Nernst (*i.e.*, Boltzmann) relation. Accordingly, our assumption will often be valid when it is not valid to neglect double layer effects on rate constants for electron transfer to the electrode.

boundary conditions (and to the assumption of a bounded solution):

$$C_R(x, 0) = C^\circ_R \quad [4]$$

$$C_{ox}(x, 0) = 0 \quad [5]$$

$$D_{ox}\,\partial C_{ox}(x, t)/\partial x + m\,D_R\,\partial C_R(x, t)/\partial x = 0 \quad \text{at } x = 0 \quad [6]$$

plus a condition on $C_{ox}(0, t)$.

If one considers instead of [5] the alternative condition that $C_{ox}(x, 0)$ equals a nonzero quantity C°_{ox}, Eq. [7], [13], and [15] remain valid, if $C_{ox}(x, t)$ in [7] is replaced by $C_{ox}(x, t) - C^\circ_{ox}$, and f in [13] and [15] by $f - C^\circ_{ox}$. Equation [8] remains intact, but in Eq. [9] and [14] the second C_{ox} and f should be replaced by $C_{ox} - C^\circ_{ox}$ and $f - C^\circ_{ox}$, respectively.

In Appendix I, Eq. [2] to [6] are solved by[4] the Laplace transform method. The solution is given by

$$i_f = -nFA(D_{ox}/\pi)^{1/2}\frac{\partial}{\partial t}\int_0^t C_{ox}(0, t-\tau)\tau^{-1/2}\,d\tau \quad [7]$$

As the boundary condition at $x = 0$, we employ the Nernst relation between $C_{ox}(0, t)$ and $C_R(0, t)$ for $t > 0$:[5]

$$\tilde{E}_f p(\omega t) = E'_o + (RT/nF)\ln\{C_{ox}(0,t)^m/C_R(0,t)\} \quad [8]$$

where $\tilde{E}_f$ is the amplitude of the applied alternating voltage, $p(\omega t)$ is any continuous periodic function of ωt, of period 2π and of unit amplitude, and E'_o is a quantity defined later.

From Eq. [8] and Eq. [24] of Appendix I, it follows that for $t > 0$, $C_{ox}(0, t)$ in Eq. [7] satisfies the relation:

$$[C_{ox}(0,t)]^m = [C^\circ_R - (D_{ox}/D_R)^{1/2}\,C_{ox}(0,t)/m]\exp[(nF/RT)(\tilde{E}_f p(\omega t) - E'_o)] \quad [9]$$

The quantity E'_o is defined through the following argument: Since the electrolytic resistance is assumed negligible, the potential difference across the cell is the sum of the two half-cell potentials, $E_a + E_c$, where E_c is the half-cell potential across the auxiliary unpolarizable electrode. If E_d is the direct component of the applied potential, we thus have

$$E_a = E_d + \tilde{E}_f p(\omega t) - E_c \quad [10]$$

Writing E_a in terms of its standard potential E_o of the reversible step of the half-cell, we have

$$E_a = E_o + (RT/nF)\ln\{C_{ox}(0,t)^m/C_R(0,t)\} \quad [11]$$

From Eq. [10] and [11], Eq. [8] is obtained with E'_o given by

$$E'_o = E_o + E_c - E_d \quad [12]$$

Delahay, Senda, and Weis (17) have emphasized the desirability that, in specifying the type of control used, both the alternating and mean components of the current or voltage control should be designated. The argument of the preceding paragraph shows that we are here dealing with the case of A.V. control, with $\overline{E}_{cell} = E_d$ (when the mean value of $p(\omega t)$ is zero), *i.e.*, with $\overline{E}_a = \overline{E}_c - E_d$.

It sometimes happens that $\tilde{E}_f p(\omega t)$ is treated as a piecewise continuous function,[6] for example, when it is treated as a square wave applied potential. Strictly speaking, it is continuous, but is approximated by this discontinuous function. To adapt Eq. [13] to this case, one uses the fact that the derivative of a step function is a Dirac δ-function (19).[7]

Applications of Equations [7] and [9]

Silverman and Remick (18) observed oscillographically that a periodic state was achieved very rapidly using $\tilde{I}_{cell}$-control, [*i.e.*, A.C. control (17)], plane electrodes, and solutions initially containing only one component of a reversible redox system. We know of no comparable experimental demonstration involving A.V. control; however, Eq. [7] and [9] can be shown to predict the attainment of a periodic state. Moreover, this periodic state is a convenient one for application of the equations to experimental data. Accordingly, we first show how these equations lead to the periodic state.

For this purpose, it is very convenient to introduce a function $f(\omega\theta)$ which agrees with $C(0, \theta)$ for $\theta > 0$, but which is the periodic continuation of $C(0, \theta)$ for $\theta \leq 0$.

In Appendix II it is then shown that Eq. [7] can be rearranged to give

$$i_f = nFA(\omega D_{ox}/\pi)^{1/2}\left\{\int_0^\infty \frac{\partial}{\partial y}[f(\omega t - y)]y^{-1/2}\,dy - \tfrac{1}{2}\int_{\omega t}^\infty f(\omega t - y)y^{-3/2}\,dy\right\} \quad [13]$$

where $f(\omega t - y)$ satisfies Eq. [14] for all t. Equation [14] is obtained from Eq. [9] by replacing $C_{ox}(0, t)$ by $f(\omega t - y)$.

$$[f(\omega t - y)]^m = [C^\circ_R - (f(\omega t - y)/m)(D_{ox}/D_R)^{1/2}]\exp\{(nF/RT)[\tilde{E}_f p(\omega t - y) - E'_o]\} \quad [14]$$

In Appendix II, it is shown that $f(\omega t - y)$ is bounded by some quantity, M say, so the second integral in [13] tends to zero as ωt tends to infinity

[4] Equation [7] can also be obtained, after a somewhat involved series of substitutions, from the first half of Eq. [21] of ref. (14). However, the derivation given in Appendix I of this paper has certain advantages for our purposes and is referred to later.

[5] The apparent discontinuity between the limit which this $C_{ox}(0, t)$ approaches as $t \to 0$ and that which Eq. [5] approaches as $x \to 0$ causes no difficulty. It is indeed a standard type of discontinuity (22) in diffusion and heat conduction problems.

[6] It may be recalled that a piecewise continuous function is one which has in any finite interval at most a finite number of discontinuities.

[7] In the case of piecewise continuous $p(\omega t)$, one may utilize Eq. [22] and [9] as follows. Piecewise continuous $p(\omega t)$ implies piecewise continuity of the function $C_{ox}(0, t)$ defined by Eq. [9], and even (Appendix II) its finiteness for the $p(\omega t)$ of interest. Its Laplace transform $\overline{C}_{ox}(0, s)$ therefore exists and has "nice properties." Consider now the contour integral expression obtained for $C_{ox}(x, t)$ by applying the usual Inversion Theorem (23) to Eq. [22], where $\overline{C}_{ox}(0, s)$ has just been described. This expression has the desirable convergence behavior outlined in ref. (23) (uniform convergence in x and in t) and one may proceed to test as discussed in ref. (23) whether it and the corresponding contour integral for $u(0, t)$ (u is defined in Appendix II) satisfy the differential equations and boundary conditions. $\partial C_{ox}(x, t)/\partial x$ and thereby i_f may be obtained then by differentiating under the integral sign. Indeed, some of the proofs in Appendices II and III might well have been shortened through use of the contour integral.

Equations [13] and [15] do not apply at those times t for which $f(\omega t)$ is discontinuous since Eq. [24] of Appendix I (and hence Eq. [9]) does not.

since its majorant, $M\int_t^\infty y^{-3/2}\,dy$, behaves in this way. Hence, this integral is a transient term. The first integral in [13] is periodic in ωt, because $f(\omega t - y)$ is periodic in ωt (as shown in Appendix III), its derivative, therefore, being periodic also, and because its limits are not functions of t. This integral, therefore, describes the periodic state.

An equivalent form of Eq. [13], derived in Appendix II, is given by Eq. [15], the first integral being the periodic term and the second being the same transient term as in Eq. [13].

$$i_f = -\tfrac{1}{2}\, nFA\,(\omega D_{ox}/\pi)^{1/2}\{\int_0^\infty [f(\omega t) - f(\omega t - y)]\,y^{-3/2}\,dy + \int_{\omega t}^\infty f(\omega t - y)\,y^{-3/2}\,dy\} \quad [15]$$

Using these equations, it is shown, incidentally, in Appendix III that the mean value of the periodic state integral in Eq. [13] or [15] is zero, for arbitrary periodic functions $p(\omega t)$ and for arbitrarily large amplitudes. This theorem generalizes earlier discussions by other investigators for small amplitudes. It should have diagnostic value since it would obviously be false if the irreversible follow-up reaction occurred appreciably.

To examine a possible way for determining E'_os and other properties, it is convenient to convert the integral for the periodic state into a "reduced" form. That is, we proceed to deduce an "equation of corresponding states" for the faradaic current and for its dependence on applied potential.

We see from Eq. [14] that at any given temperature $f(\omega t - y)$ depends on nE'_o, m, C°_R and on the value of the function nE_f at the time $\omega t - y$ (taking $\sqrt{D_{ox}/D_R} \cong 1$). Therefore, we may write (for given T), $f(\omega t - y)$ as a function of C°_R, of nE'_o, of m, of the value of nE_f at time ωt, and of y.[8] Similar remarks apply to the y-derivative of $f(\omega t - y)$. Accordingly, the periodic state term in either [13] or [15] satisfies the formal relation:

$$i_f = nFA\,(\omega D_{ox}/\pi)^{1/2}\int_0^\infty h(y, nE'_o, m\,nE_f, C^\circ_R)\,dy \quad [16]$$

where the function h can be written in the two equivalent forms (forms which differ only by a quantity whose integral from 0 to ∞ vanishes):

$$\left.\begin{aligned} h &\equiv y^{-1/2}\,\partial f(\omega t - y)/\partial y \\ h &\equiv \frac{1}{2}\,y^{-3/2}\,[f(\omega t - y) - f(\omega t)] \end{aligned}\right\} \quad [17]$$

Equation [16] is a convenient one for our purposes, for we see from Eq. [13] that at a given temperature, C°_R and electrode area A, a plot of nE_f *vs.* $i_f/n\,(\omega D_{ox})^{1/2}$ depends only on nE'_o and m. Therefore, by adjusting the direct voltage E_d and (in multiples of some preassigned amplitude) $\tilde{E}_f$, the E_f *vs.* i_f plot could be made to conform to a standard shape, a shape which, for any preassigned nE'_o, $n\tilde{E}_f$, C°_R and T, depends only on m. From the value of E_d needed to attain this specified nE'_o, E_o could be calculated from Eq. [12], n could be determined from the $\tilde{E}_f$ needed to attain the standard shape, and m could be determined from the C°_R-dependence of the data. (For example, for $m = 1$ Eq. [14] shows that $f(\omega t - y)$ is directly proportional to C°_R, so h and hence i_f in [16] are directly proportional to C°_R, for any given E_f.) Again, Eq. [16] provides other diagnostic tests. A plot of $i_f/\omega^{1/2}$ *vs.* E_f should be independent of ω and of $\tilde{E}_f$.[9]

Instead of plotting E_f *vs.* i_f, i_f can be plotted *vs.* ωt, after first writing Eq. [16] for the periodic state in the appropriate reduced form. Since $E_f = \tilde{E}_f p(\omega t)$, the integrand in [16] can be written as a function of ωt and of $n\tilde{E}_f$ as well as of y, nE'_o, m, and C°_R. Once again, for any given C°_R, T and electrode area, the adjusting of E_d and, in multiples of some amplitude, of $\tilde{E}_f$, would lead to a standard shape which depends on m. The values of E_o and n could then be determined as before, and m could be determined from the C°_R dependence of the plot. Again, as before, diagnostic tests could be devised: The plot of $i_f/\omega^{1/2}$ *vs.* ωt should be independent of ω and, if $m = 1$, should be proportional to C°_R.

In actual fact, one measures total current rather than only the faradaic branch. The nonfaradaic component is independent of C°_R, so that a plot of i *vs.* E_f or *vs.* t would now be a linear function of C°_R when $m = 1$. On the other hand, no standard shape of a plot of i *vs.* E_f or t can be attained simply by adjusting E_d and $\tilde{E}_f$.[10]

Accordingly, in this situation, recognizing that under the assumptions listed earlier, the total current is the sum of the faradaic and nonfaradaic branches and that the nonfaradaic component is independent of C°_R, the value of i_f corresponding to any particular phase angle of E_f can be obtained by subtracting from the measured, instantaneous current the value of that current when $C^\circ_R = 0$. Examples where this type of subtraction has been made in potentiometric work may be found in ref. (25) and (16). If the condition mentioned earlier that the iR be negligible had not been imposed, no such subtraction process would be permissible for obtaining i_f, for the iR drop at any given t would cause the instantaneous potential drop across the electrode to depend on C°_R, contrary to assumption. Furthermore, since the cell is a nonlinear circuit element, the iR drop through the bulk of the solution would contain harmonics which would invalidate the assumption of a sinusoidal E_f.

Information about the characteristic behavior of the integral in Eq. [16], and hence about the faradaic current, can be deduced either from numerical integration or from investigation of the properties of known reversible systems. However, some prelimi-

[8] The value of E_f at $(\omega t - y)$ is determined if one knows for all t its value at ωt and if one knows y, i.e., $E_f(\omega t - y)$ is a function of the function $E_f(\omega t)$ and of y.

[9] To be sure, at small values of $\tilde{E}_f$, points on this plot corresponding to large values of i_f will not be attained. Note that although i_f and E_f depend on $\tilde{E}_f$, the plot does not.

[10] For, if nE'_o and $n\tilde{E}_f$ were each made to conform to their preassigned values by such adjustments, the nonfaradaic current *vs.* E_f plot would then differ from system to system: Any two systems normally differ in E_o and hence, for a preassigned nE'_o, in E_d (cf. Eq. [12]). But for a given E_d, a plot of nonfaradaic current *vs.* E_f would be a standard one only for a preassigned E_d and $\tilde{E}_f$.

nary insight into its behavior as far as the dependence of i_f on E_f in Eq. [16] can be obtained as follows. We shall consider, by way of a concrete example, the important case in which $m = 1$, $D_{ox} = D_R$, and $p(\omega t)$ is sin ωt. The integral for the periodic state in Eq. [16] becomes (using it in the form of Eq. [13], after introducing Eq. [14] and performing the differentiation:

$$i_f = -\frac{nFA\,C^o_R\,nF\,\tilde{E}_f}{(\pi/\omega D_{ox})^{1/2}\,RT}\int_o^\infty \frac{\exp\left[nF(\tilde{E}_f \sin(\omega t - y) - E'_o)/RT\right]\cos(\omega t - y)y^{-1/2}\,dy}{\{1 + (D_{ox}/D_R)^{1/2}\exp\left[nF(\tilde{E}_f \sin(\omega t - y) - E'_o)/RT\right]\}^2} \quad [18]$$

When $|nF\,E'_o/RT| >> 1$ and $\tilde{E}_f << |E'_o|$, the coefficient of $y^{-1/2}$ cos $(\omega t - y)$ in the integrand, is very small at all times, *i.e.*, for all $|E_f| \leq \tilde{E}_f$.[11] Accordingly, i_f is then small for all such E_f, a result expected on physical grounds. In the very special instance that $\tilde{E}_f$ is sufficiently small, the integral in Eq. [18] becomes[12]

$$\pi^{1/2}\cos\left(\omega t - \frac{\pi}{4}\right)\exp(-nFE'_o/RT)/[1 + (D_{ox}/D_R)^{1/2}\exp(-nFE'_o/RT)]^2 \quad [19]$$

When $\tilde{E}_f$ becomes comparable in magnitude with E'_o, however, the current will become large at the appropriate times and, because of the sensitivity of the exponential terms to $\tilde{E}_f$, this effect should presumably occur fairly suddenly as $\tilde{E}_f$ is increased. Indeed a plot of faradaic current *vs.* $\tilde{E}_f$ may ultimately provide a convenient way for the determination of E'_o.

Up to this point, we have restricted our attention to reversible systems. If in addition, the reversible electrochemical step [1] is followed by an irreversible decomposition of the product of [1] to yield an electrochemically inactive substance, Eq. [3] to [6] remain unchanged, as does Eq. [8]. Only Eq. [2] is modified, namely, through the addition of the reaction rate term. If the irreversible step is very slow, this additional term represents only a minor perturbation of Eq. [2]. Physical considerations indicate that the solution for i_f should depend continuously on the value of the reaction rate constant in this perturbation term. When this constant is sufficiently small, therefore, the results will approach those previously obtained. That is, our final equations are still applicable, provided the irreversible step is sufficiently slow. As mentioned earlier, it is this situation where the present equations are likely to be of the most interest.

[11] For $E'_o > 0$, the numerator is then very small and the denominator is about unity. For $E'_o < 0$, the denominator is very large compared with unity, so that the first factor in the integrand approximately equals $(D_R/D_{ox})\exp\{nF\,[E'_o - \tilde{E}_f \sin(\omega t - y)]/RT\}$ which is very small.

[12] Upon expanding cos $(\omega t - y)$ and recalling that

$$\int_o^\infty y^{-1/2}\cos y\,dy = \int_o^\infty y^{-1/2}\sin y\,dy = (\pi/2)^{1/2}$$

and noting that cos ωt + sin $\omega t = \sqrt{2}\cos(\omega t - \frac{\pi}{4})$, Eq. [19] is obtained.

Manuscript received May 29, 1961; revised manuscript received April 10, 1962.

Any discussion of this paper will appear in a Discussion Section to be published in the June 1963 JOURNAL.

REFERENCES

1. J. E. B. Randles, *Discussions Faraday Soc.*, **1**, 11 (1947).
2. B. Breyer and F. Gutman, *ibid.*, **1**, 19 (1947); B. Breyer, F. Gutman, and S. Hacobian, *Australian J. Sci. Research*, **A3**, 558, 567 (1950); **A4**, 595 (1951); B. Breyer and S. Hacobian, *ibid.*, **A4**, 604, 610 (1951); *Australian J. Chem.*, **7**, 225 (1954).
3. B. Ershler, *Zhur. Fiz. Khim.*, **22**, 683 (1948); K. Rozental and B. Ershler, *ibid.*, **22**, 1344 (1948).
4. H. Gerisher, *Z. physik. Chem.*, **198**, 286 (1951); *ibid.*, (*N.F.*) **1**, 278 (1954).
5. M. Fournier, *Compt. rend.*, **232**, 1673 (1951).
6. D. C. Grahame, *This Journal*, **99**, 370C (1952).
7. P. Delahay and T. J. Adams, *J. Am. Chem. Soc.*, **74**, 5740 (1952).
8. T. Berzins and P. Delahay, *Z. Elektrochem.*, **59**, 792 (1955).
9. I. Tachi and T. Kambara, *Bull. Chem. Soc. Japan*, **28**, 25 (1955).
10. M. Senda and I. Tachi, *ibid.*, **28**, 632 (1955).
11. T. Kambara, *Z. physik. Chem.* (*N.F.*), **5**, 52 (1955).
12. H. Matsuda, *Z. Elektrochem.*, **62**, 977 (1958).
13. H. Matsuda and P. Delahay, *J. Am. Chem. Soc.*, **82**, 1547 (1960).
14. J. Koutecky, *Collect. Czech. Chem. Communs*, **21**, 443 (1956).
15. M. Wien, *Ann. Physik. u. Chem.*, **58**, 37 (1896).
16. A. E. Remick and H. W. McCormick, *This Journal*, **102**, 534 (1955).
17. P. Delahay, M. Senda, and C. H. Weis, *J. Am. Chem. Soc.*, **83**, 312 (1961).
18. J. Silverman and A. E. Remick, *This Journal*, **97**, 335 (1950).
19. *cf* B. Friedman, "Principles and Techniques of Applied Mathematics," p. 440, John Wiley and Sons, Inc., New York (1956).
20. *cf* A. E. Taylor, "Advanced Calculus," p. 599, Ginn and Co., New York (1955).
21. Ref. (20), p. 529.
22. H. S. Carslaw and J. C. Jaeger, "Conduction of Heat in Solids," 2nd ed., pp. 304-5, 27 or 30, etc., Oxford University Press, London (1959).
23. Ref. (22), pp. 479-480.
24. Ref. (22), p. 301.
25. J. E. B. Randles, *Discussions Faraday Soc.*, **1**, 11 (1947).
26. J. O'M. Bockris, "Modern Aspects of Electrochemistry," p. 219, Academic Press Inc., New York (1954).
27. M. Breiter, M. Kleinerman, and P. Delahay, *J. Am. Chem. Soc.*, **80**, 5111 (1958).

APPENDIX I
Derivation of Eq. [7]

We let $u(x,t)$ denote the quantity

$$u(x,t) = C^o_R - C_R(x,t) \quad [20]$$

Seeking a bounded solution of Eq. [2] to [6], we introduce boundary conditions [4] and [5] into the Laplace transforms of Eq. [2] and [3], respectively, and obtain two differential equations in the domain $x > 0$ which can easily be solved to give equations for the transforms, $\bar{u}$ and $\bar{C}_{ox}$:

$$\bar{u}(x,s) = \bar{u}(0,s)\,\exp(-s^{1/2}x/D_R^{1/2}) \quad [21]$$

$$\bar{C}_{ox}(x,s) = \bar{C}_{ox}(0,s)\,\exp(-s^{1/2}x/D_{ox}^{1/2}) \quad [22]$$

where s is the Laplace variable.

Differentiation of these equations with respect to x followed by evaluation at $x = 0$ and combination with the transform of Eq. [6] yields

$$\bar{C}_{ox}(0,s) = \bar{u}(0,s)\, m (D_R/D_{ox})^{1/2} \qquad [23]$$

Taking the inverse transform of Eq. [23] gives

$$m\, u(0,t) = C_{ox}(0,t) (D_{ox}/D_R)^{1/2} \qquad [24]$$

except at points of discontinuity, using a uniqueness theorem (24).

The instantaneous anodic current, i_f, is related to the flux according to Eq. [25]

$$i_f = nFAD_{ox}[\partial C_{ox}(x,t)/\partial x]_{x=0} \qquad [25]$$

wherein we use the convention that an anodic current is negative, and where A denotes the electrode area. The term $[\partial C_{ox}(x,t)/\partial x]$, may be calculated from the preceding equations as follows. Differentiating Eq. [22] with respect to x and setting $x = 0$, one finds

$$[\partial \bar{C}_{ox}(x,s)/\partial x]_{x=0}$$

$$= -\bar{C}_{ox}(0,s)\,(s/D_{ox})^{1/2} = -s\bar{C}_{ox}(0,s)\,(D_{ox}s)^{-1/2}$$

$$= [-s/(\pi D_{ox})^{1/2}] \int_0^\infty e^{-st}\, C_{ox}(0,t)\, dt \int_0^\infty e^{-\tau t}\, t^{-1/2}\, dt \qquad [26a]$$

$$= [-s/(\pi D_{ox})^{1/2}] \int_0^\infty e^{-st} \left[\int_0^t C_{ox}(0,t-\tau)\,\tau^{-1/2}\, d\tau\right] dt \qquad [26b]$$

$$= -(\pi D_{ox})^{-1/2} \int_0^\infty e^{-st} \left[\frac{\partial}{\partial t}\int_0^t C_{ox}(0,t-\tau)\,\tau^{-1/2}\, d\tau\right] dt \qquad [26c]$$

where we have introduced into (a) the fact that $s^{-1/2}$ is simply the Laplace transform of $(\pi t)^{-1/2}$. In obtaining (b) we have employed the convolution theorem for Laplace transforms, and in obtaining (c) we have used the standard relation between the Laplace transform of a function (here of $\int_0^t C_{ox}(0,t-\tau)\tau^{-1/2}\, d\tau$) and of its derivative.

It is now immediately apparent from [26c] that

$$[\partial C_{ox}(x,t)/\partial x]_{x=0} = -(\pi D_{ox})^{-1/2} \frac{\partial}{\partial t}\int_0^t C_{ox}(0,t-\tau)\,\tau^{-1/2}\, d\tau \qquad [27]$$

Equation [7] of the text is then obtained from [25] and [27].

APPENDIX II

Derivation of Eq. [13] and [15] from [7]

We shall consider the behavior of Eq. [7] for times greater than 0, and we may therefore replace $C_{ox}(0,t-\tau)$ in that equation by the function $f(\omega t - \omega\tau)$, which satisfies Eq. [14] for all values of the argument of f, positive or negative. The time derivative in Eq. [7] can then be written as in Eq. [28], after first performing the differentiation and making use of the identity

$$\partial f(\omega t - \omega\tau)/\partial t = -\partial f(\omega t - \omega\tau)/d\tau$$

$$\frac{\partial}{\partial t}\int_0^t f(\omega t - \omega\tau)\,\tau^{-1/2}\, d\tau$$

$$= f(0)\, t^{-1/2} - \omega \int_0^t \left[\frac{\partial}{\partial(\omega\tau)} f(\omega t - \omega\tau)\right] \tau^{-1/2}\, d\tau \qquad [28]$$

where $f(0)$ is to be obtained from Eq. [14] by setting $\omega t - y$ equal to zero there.

Introducing into Eq. [28] a change of variable, $y = \omega\tau$, the right-hand side of the equation becomes:

$$f(0)\, t^{-1/2} - \omega^{1/2} \int_0^\infty \left[\frac{\partial}{\partial y} f(\omega t - y)\right] y^{-1/2}\, dy$$

$$+ \omega^{1/2} \int_{\omega t}^\infty \left[\frac{\partial}{\partial y} f(\omega t - y)\right] y^{-1/2}\, dy \qquad [29]$$

It is evident from Eq. [14] that $f(\omega t - y)$ is a bounded function[13] of $\omega t - y$, so that upon integrating the third term of [29] by parts we get in place of [29]

[13] For any value of $\omega t - y$, $f(\omega t - y)$ is the positive root of an algebraic equation, all of whose coefficients are finite. The roots of such equations always lie in a finite region of the complex plane.

$$-\omega^{1/2} \int_0^\infty \frac{\partial}{\partial y} f(\omega t - y)\, y^{-1/2}\, dy + \frac{\omega^{1/2}}{2}\int_{\omega t}^\infty f(\omega t - y)\, y^{-3/2}\, dy \qquad [30]$$

From Eq. [7], [28], and [30], Eq. [13] then follows.

The first integral in Eq. [13] can also be written in the alternative form

$$\lim_{\epsilon\to 0^+} \int_\epsilon^\infty \frac{\partial f}{\partial y}\,(\omega t - y)\, y^{-1/2}\, dy \qquad [31]$$

Upon integrating by parts, this term becomes

$$-\lim_{\epsilon\to 0^+}\left[f(\omega t - \epsilon)\,\epsilon^{-1/2} - \frac{1}{2}\int_\epsilon^\infty f(\omega t - y)\, y^{-3/2}\, dy\right]$$

$$= -\frac{1}{2}\lim_{\epsilon\to 0^+}\left[\int_\epsilon^\infty f(\omega t - \epsilon)\, y^{-3/2}\, dy - \int_\epsilon^\infty f(\omega t - y)\, y^{-3/2}\, dy\right] \qquad [32]$$

where we have introduced the identity

$$\epsilon^{-1/2} = \frac{1}{2}\int_\epsilon^\infty y^{-3/2}\, dy$$

Rewriting the integrals in [32] as:

$$[f(\omega t - \epsilon) - f(\omega t)] \int_\epsilon^\infty y^{-3/2}\, dy + \int_\epsilon^\infty [f(\omega t) - f(\omega t - y)]\, y^{-3/2}\, dy \qquad [33]$$

and proceeding to the limit $\epsilon = 0$, the first expression in [33] varies as (constant) (ϵ) $(\epsilon^{-1/2})$ using the conditions on f specified in footnote[14] and so vanishes. Introducing the second integral of [33] into [31], Eq. [15] is obtained.

APPENDIX III

Proof that the Mean Value of i_f Equals Zero in the Periodic State

In this section we consider the behavior at positive times, and it follows therefore that $t >> t_0$. Thus, we may replace C_{ox} by f.

It is first noted that physical arguments show that there can be only one positive solution of Eq. [14] for $f(\omega t - y)$, even when this equation has more than one solution (*i.e.*, when $m \neq 1$). All other solutions must either be negative or partly imaginary. We further note that since $p(\omega t) = p(\omega t + 2\pi)$, $f(\omega t - y)$ and $f(\omega t - y + 2\pi)$ satisfy the same Eq. [14]. Because of the uniqueness of the physically real $f(\omega t - y)$ just mentioned, it then follows that for our positive f's, $f(\omega t - y + 2\pi) = f(\omega t - y)$, *i.e.*, $f(\omega t - y)$ is also a periodic function of ωt with the same period as $p(\omega t)$.

We next observe that the mean value of the integral describing the periodic state is obtained by averaging it with respect to ωt over a period of 2π. Using Eq. [15], the integral which occurs in this average can be written in the equivalent form

$$-\frac{1}{4\pi}\int_\theta^{\theta+2\pi}\left[\lim_{\epsilon\to 0^+}\int_{y=\epsilon}^\infty [f(\omega t) - f(\omega t - y)]\, y^{-3/2}\, dy\right] d(\omega t) \qquad [34]$$

where θ is any large value of ωt. It can easily be shown[14] that the convergence of the y-integral as $\epsilon \to 0^+$ is uniform in ωt and, hence, lim and $\int$ can be interchanged, using a standard theorem [20]. Thus we obtain

$$-\frac{1}{4\pi}\lim_{\epsilon\to 0^+}\int_{\omega t=\theta}^{\theta+2\pi}\left[\int_{y=\epsilon}^\infty [f(\omega t) - f(\omega t - y)]\, y^{-3/2}\, dy\right] d(\omega t) \qquad [35]$$

[14] For ϵ small and y lying in the interval $(0,\epsilon)$, $|f(\omega t) - f(\omega t - y)| \cong \left|\frac{\partial}{\partial \omega t} f(\omega t)\right| \cdot y$, whence $\left|\int_0^\epsilon [f(\omega t) - f(\omega t - y)]\, y^{-3/2}\, dy\right| \leq N\int_0^\epsilon y^{-1/2}\, dy = 2N\epsilon^{1/2}$, where N, an upper bound to the derivative, is independent of ωt. Actually the differentiability of $f(\omega t)$ needn't have been used. The milder Hölder condition, $|f(\omega t) - f(\omega t - y)| \leq$ constant $\cdot\ y^\alpha$ but where $\alpha > \frac{1}{2}$, would have sufficed.

Because of the readily proven convergence of the y-integral with respect to the upper limit (∞), uniform in ωt, [35] may be written as

$$-\frac{1}{4\pi}\lim_{\epsilon\to 0^+}\lim_{L\to\infty}\int_{\omega t=\theta}^{\theta+2\pi}\left[\int_{y=\epsilon}^{L}[f(\omega t) - f(\omega t - y)]y^{-3/2}\,dy\right]d(\omega t) \quad [36]$$

The integrals $\int_\epsilon^L [f(\omega t) - f(\omega t - y)]y^{-3/2}\,dy$ and $y^{-3/2}\int_\theta^{\theta+2\pi}[f(\omega t) - f(\omega t - y)]d(\omega t)$ exist for any $\epsilon > 0$ and L, and the double integral also exists not only for continuous $f(\omega t)$ but also for piecewise continuous $f(\omega t)$. It then follows from a standard theorem [21] that the order of integration can be interchanged. We obtain

$$-\frac{1}{4\pi}\lim_{\epsilon\to 0^+}\lim_{L\to\infty}\int_{y=\epsilon}^{L} y^{-3/2}\left[\int_\theta^{\theta+2\pi}[f(\omega t) - f(\omega t - y)]d(\omega t)\right]dy \quad [37]$$

But, since $f(\omega t)$ was seen earlier to be a periodic function of ωt, it is true that

$$\int_\theta^{\theta+2\pi} f(\omega t)\,d(\omega t) = \int_\theta^{\theta+2\pi} f(\omega t - y)\,d(\omega t) \quad [39]$$

since it is easily shown that the value of a periodic function averaged over its period is independent of the initial value of the phase angle.

We see, therefore, that the ωt integral in Eq. [37] must vanish which proves the desired result.

This result of Appendix III can be proven under milder restrictions, such as piecewise continuity of $f(\omega t)$. As pointed out in the text, Eq. [15] for i_f is valid for piecewise continuous $f(\omega t)$, except at the isolated points of discontinuity of the latter. The derivation of Eq. [35] from [34] proceeds as before, when points ωt of discontinuity of f are excluded. The derivation of [37] from [35] and the use of [38] remain valid. Thus, if one defines i_f arbitrarily but finite at the isolated points of discontinuity of $f(\omega t)$, the mean value of i_f is zero in the periodic state for piecewise continuous functions $f(\omega t)$.

SYMBOLS

A, area of electrode's surface, cm^2.
C_{ox}, concentration of oxidant, mole l^{-1}.
C_R, concentration of reductant, mole l^{-1}.
C^o_R, concentration of reductant in bulk of solution, mole l^{-1}.
D_{ox}, diffusion coefficient of oxidant, cm^2 sec^{-1}.
D_R, diffusion coefficient of reductant, cm^2 sec^{-1}.
E_a, half-cell potential difference of measuring electrode, v.
E_c, half-cell potential difference of auxiliary, nonpolarizable electrode, v.
E_f, half-cell potential difference between electrode and the solution just outside of electrical double layer, in Ox-Red system under investigation, v.
E_d, direct component of applied cell potential, v.
$\tilde{E}_f$, amplitude of the periodic E_f wave, v. $E_f = E_f p(\omega t)$.
E_o, standard potential of the Ox-Red system, v.
E'_o, $E_o + E_c - E_a$.
$\bar{E}_{cell}$, mean cell potential, v.
f, function of, (a particular function).
f, (as a subscript) faradaic.
F, faraday (96514 abs.-coulombs g-equiv.$^{-1}$).
h, function of, (a particular function).
i_f, instantaneous faradaic current, amp.
m, number of oxidant molecules produced from oxidation of 1 mole of reductant.
n, number of electrons involved in oxidation of 1 mole of reductant.
R, gas constant (8.3166 x 10^7 erg deg^{-1} mole^{-1}).
t, time, sec.
T, absolute temperature.
u, $C^o_R - C_R$.
x, perpendicular distance from a plane which is parallel to the planar electrode of Ox-Red system, but which is just outside the electrical double layer region.
ω, angular frequency of alternating voltage, sec^{-1}.

Technical Notes

The Discharge Properties of α-PbO_2 in Dilute H_2SO_4 Electrolyte

Harry B. Mark, Jr.

Department of Chemistry, University of North Carolina, Chapel Hill, North Carolina

The discharge properties and discharge mechanism of β-PbO_2 in H_2SO_4 electrolyte have been studied in considerable detail (1-3). There is disagreement as to the mechanism (1-3), but the experimental characteristics of the discharge, such as reduction overpotentials, shape of the potential-time discharge curves, etc., are well known (1, 3). Although some of the electrochemical properties (electrodeposition conditions and self-discharge) of α-PbO_2 have been the subject of considerable study (4-8), there is little information in the literature concerning the properties of pure α-PbO_2 under an applied discharge current (3, 4, 9). Almost no work has been reported on the properties of pure α-PbO_2 in dilute H_2SO_4 electrolyte, although a previous paper (3) showed that the discharge properties of β-PbO_2 change considerably and in an unexpected way as the acid strength of the electrolyte decreases. The discharge capacities of lead storage batteries, which have positive plates containing a mixture of α-PbO_2 and β-PbO_2, have been studied (10), and there is a brief description of the discharge curve obtained in 4.4M H_2SO_4 for an anodized Pb electrode (6). Microphotographs of the cross section of this electrode and x-ray and electron diffraction patterns seemed to indicate that there is a layer of a mixture of the two modifications of PbO_2 between the lead metal and the β-PbO_2 film which was in contact with the electrolyte (4). The discharge of an electrode, which consists of a layer of α-PbO_2 between a layer of β-PbO_2 and a Pt support, in a 4.4M H_2SO_4 electrolyte has been reported (9).

In this investigation the discharge in dilute (0.1M) H_2SO_4 of α-PbO_2 and β-PbO_2 have been studied, as

also electrodes consisting of a layer of α-PbO_2 on top of a layer of β-PbO_2 and *vise versa*. The effect of variation of discharge current and theoretical discharge capacity were also studied. A comparison of the experimental results obtained by this study indicate that the discharge mechanism of the two forms in dilute H_2SO_4 are quite different. These property differences were not very apparent in the experimental results reported in the work which used a more concentrated acid electrolyte, which may mask the effects arising from the two different mechanisms or may result in yet a third discharge mechanism. Both forms might discharge by this third or combination mechanism in the concentrated acid electrolyte.

Experimental Procedure

Preparation of electrodes.—The PbO_2 was electrodeposited on Pt cylinders sealed in glass as described in previous work (3). The electrodes had an apparent surface area of 8 cm^2. The β-PbO_2 was deposited from a solution of 0.020M $Pb(NO_3)_2$ and 0.3M HNO_3 with a current density of 10 ma/electrode (1.25 ma/cm^2) at room temperature for 4 to 40 min. The α-PbO_2 was deposited from a solution of 1.5M NH_4OH and 6.5M $NH_4C_2H_3O_2$ saturated with $Pb(C_2H_3O_2)_2$ (3,5) with a current density of 10 ma/electrode for 3 to 40 min at room temperature.

Discharge apparatus.—The discharge cell used was described previously (3). A saturated calomel electrode (SCE), which was used as the reference electrode, made contact with the solution in the cell through an agar-agar KCl bridge. A stream of nitrogen was used to stir the electrolyte, and a cylindrical sheet of lead metal was used as the anode.

Currents for discharge were furnished by an electronic constant-current source (11). The electromotive force of the cell was applied to a high input impedence (about 10^{11} ohms) follower amplifier of gain of −1. The output of the follower amplifier was fed first to a voltage inversion amplifier (gain of −1) and then to a voltage divider to attenuate the signal. The signal was then recorded by a Sargent model SR recorder. The follower and inversion amplifiers were constructed from plug-in analog computer amplifiers using circuits designed by DeFord (12).

When the electrodes had come to open-circuit equilibrium, as shown by constancy of potential for 15 min, a current, either continuous or interrupted (3), was introduced into the circuit. Previous work (3) has shown that under the conditions used no corrections are necessary for iR drop, electrolyte concentration polarization, and self-discharge.

Results

Examples of the discharge curves for α- and β-PbO_2 in 0.10M H_2SO_4 saturated with $PbSO_4$ and with excess solid phase are shown in Fig. 1. Curve 1 is for α-PbO_2 when an interrupted discharge current of 3 ma/electrode was passed. The α-PbO_2 electrode does not reach a steady-state closed-circuit potential in the time allowed, and the electrode recovers, when the current is interrupted, to a lower equilibrium open-circuit potential than it had before discharge. Thus, reliable and reproducible overpotentials could not be obtained for α-PbO_2 electrodes (3). Curve 2 is a typical continuous discharge of α-PbO_2 (a current density of 5 ma/electrode was passed in this example). The electrode does not reach a steady-state closed-circuit potential even under prolonged continuous discharge. Toward the end of discharge the potential decreases more and more rapidly. The actual discharge capacity of this electrode was only 40 ma-min, although the theoretical capacity was 250 ma-min. The actual capacity of all α-PbO_2 electrodes tested in H_2SO_4 electrolyte was considerably less than the theoretical and was independent of the theoretical capacity. When an α-PbO_2 electrode had reached the state of discharge indicated by point e of curve 2, it was removed from the cell and placed in a solution of KI and $HC_2H_3O_2$. The formation of considerable I_3^- indicated that appreciable PbO_2 remained undischarged. The surface of an α-PbO_2 electrode, that was initially very smooth and shiny black, was observed at point e to be covered with a white and strongly adhering uniform film of $PbSO_4$ (4). If this film was removed by a solution of $NH_4C_2H_3O_2$ (6) and the electrode returned to the cell, the initial open-circuit potential was reattained and the electrode rejuvenated. Further discharges could then be made. The surface of the α-PbO_2 after removal of the $PbSO_4$ was black but no longer smooth and shiny. By washing the electrode with $NH_4C_2H_3O_2$ each time the potential broke down sharply and then continuing the discharge, 80-90% of the theoretical discharge capacity can be obtained. Much larger current densities could be passed through α-PbO_2 than could be passed through β-PbO_2 (3) without destruction of the electrode. No potential minimum was found on the second discharge of α-PbO_2 as was reported by other investigators (9) using a 4.4M H_2SO_4 electrolyte.

The above experiments suggest that the $PbSO_4$ film may be the only cause of the poor discharge

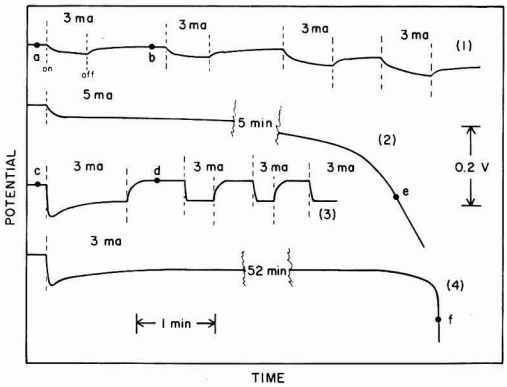

Fig. 1. Potential-time curves of α- and β-PbO_2 electrodes discharging under constant current. The electrolyte was 0.1M H_2SO_4 (sat. with $PbSO_4$): curve 1, α-PbO_2 under successive short constant current discharges of 3ma/electrode; curve 2, α-PbO_2 under continuous constant current discharge of 5 ma/electrode; curve 3, β-PbO_2 under successive short constant current discharges of 3 ma/electrode; curve 4, β-PbO_2 under continuous constant current discharge of 3 ma/electrode.

capacity of α-PbO_2. To check this, two discharges were made in 1.0M $HClO_4$ electrolyte which gave 93 and 94% of the theoretical capacity (based on 100% current efficiency on electrodeposition). The Pt electrodes were entirely bare at the end of discharge.

The curves for the interrupted discharge of β-PbO_2 (curve 3 of Fig. 1) were quite different from those of α-PbO_2 (curve 1) under similar conditions. The potential of the first discharge went through a pronounced minimum before reaching a steady-state closed-circuit potential and, on subsequent discharges, passed through very slight minima which were barely detectable. The β-PbO_2 electrode recovers to a more positive open-circuit equilibrium potential after the first discharge than it had initially, and recovers to this new emf after each subsequent discharge until the electrode breaks down (3). Discharge overpotentials for single β-PbO_2 electrodes are quite reproducible (3). On continuous discharge β-PbO_2 electrodes go through a potential minimum, reach a steady closed-circuit potential which remains constant for a long time, and finally the potential drops very rapidly, as shown by curve 4 of Fig. 1. Removal of the electrode at point f in the discharge shows that most of the PbO_2 (70-95%) has been reduced. Some I_3^- is formed on placing the electrode in acidic KI, but bare Pt is seen over much of the surface. For the particular electrode used as the example in curve 4, a test showed that about 75% of the PbO_2 had discharged electrolytically. All attempts to rejuvenate β-PbO_2 electrodes at this point by washing with $NH_4C_2H_3O_2$ were unsuccessful. Although there were some crystals of white $PbSO_4$ (before washing) widely scattered on the PbO_2 surface, there was no white film as observed for α-PbO_2.

Partially discharged α-PbO_2 electrodes which were allowed to recover to open-circuit equilibrium were washed with 40% $NH_4C_2H_3O_2$ solution to strip off the $PbSO_4$ on the surface and the wash solution analyzed for Pb^{++} by a dithizone method (13). This test indicated that practically all of the $PbSO_4$ produced on discharge of α-PbO_2 remained on the surface of the electrode, as shown in Table I. Blank tests showed that the correction for the reduction of PbO_2 by the 40% $NH_4C_2H_3O_2$ was negligible. A similar test on partially reduced β-PbO_2 electrodes showed that only part (16-50%) of the $PbSO_4$ produced on discharge remained on the surface after recovery, as shown in Table II.

Table I. Per cent $PbSO_4$ on the surface of α-PbO_2 electrodes at open-circuit equilibrium following discharge in an electrolyte of 0.1M H_2SO_4 saturated with $PbSO_4$

Discharge conditions			% $PbSO_4$ produced by discharge remaining on electrode surface
Current, ma/electrode	Time, min	$i - t$ ma-min	
1.5	10	15	105
3.0	5	15	98
3.0	4	12	96
4.0	4	16	96
5.0	3	15	95
5.0	2	10	90

Table II. Per cent $PbSO_4$ on the surface of β-PbO_2 electrodes at open-circuit equilibrium following discharge in an electrolyte of 0.1M H_2SO_4 saturated with $PbSO_4$

Discharge conditions			% $PbSO_4$ produced by discharge remaining on electrode surface
Current, ma/electrode	Time, min	$i - t$ ma-min	
2.0	21	42	16
1.0	35	35	37
1.5	40	60	19
2.3	15	34.5	50
1.2	15	18	42

The overpotentials obtained for interrupted discharges of α-PbO_2 were considerably less than those for β-PbO_2, and the rates of growth and decay of polarization were greater for β-PbO_2 than α-PbO_2, as shown by comparing curves 1 and 3 of Fig. 1. The initial open-circuit potential of α-PbO_2 was somewhat higher than that of β-PbO_2, in agreement with other work (6, 7). The larger overpotentials of β-PbO_2 may be a result of smaller true surface areas of β-PbO_2 electrodes which would increase the double layer capacity of the electrodes. However, the much rougher appearance of the β-PbO_2 surface indicates that it has the larger surface area.

Rüetschi and Cahan (6) studied the discharge of a film produced by anodizing Pb and Pb alloys (film consists of a layer of a mixture of the two modifications of PbO_2 between an external layer of pure β-PbO_2 and the metal). They found that the discharge curve went through an initial potential minimum before reaching a closed-circuit plateau. As the discharge continued, the potential went through a second minimum and came to a second, still lower, steady-state potential. The potential then dropped sharply as the film of PbO_2 was completely discharged. They suggested that the two potential plateaus represented the discharge of α- and β-PbO_2, respectively, and the difference between the plateaus represented the differences in the overpotential for the two modifications. Because the present investigation showed that the shapes of the discharge curves of the two pure modifications are quite different, these characteristics could be used in studies of the discharge properties of electrodes consisting of layers of the two modifications.

Electrodes were made consisting of a thin layer of α-PbO_2 (theoretical discharge capacities varying from 30 to 70 ma-min) on the Pt and a thin exterior layer of β-PbO_2 (capacities varying from 30 to 150 ma-min). The β:α ratios varied from 0.6 to 3. These electrodes were discharged by passing constant currents of 3-12 ma/electrode, and the discharge potentials were recorded. All the discharge curves had the characteristic shape of curve 2 of Fig. 2. In no case were two plateaus and two minima observed. Initially the discharge curves resembled that of pure, undischarged β-PbO_2 electrodes. As the capacity of the β-PbO_2 layer was nearing exhaustion, about point h of curve 2, the potential started to drift downward, and the electrode from there to the end of the discharge resembles that of an α-PbO_2 electrode which was partially discharged. If the current was interrupted at a point along the line

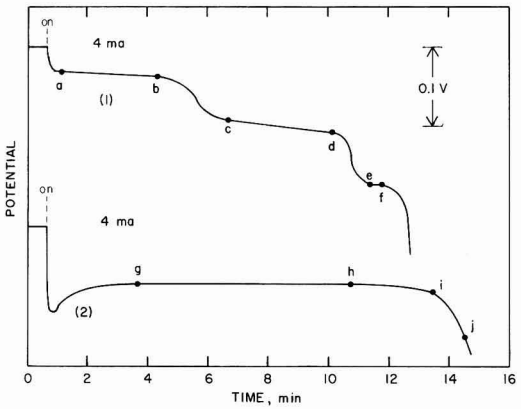

Fig. 2. Potential-time curves. The electrolyte was 0.1M H_2SO_4 (sat. with $PbSO_4$): curve 1, electrode consisting of a layer of β-PbO_2 (discharge capacity of 40 ma-min) on Pt support and layer of α-PbO_2 (capacity of 70 ma-min) on the β-PbO_2 surface, under a continuous discharge of 4 ma/electrode; curve 2, electrode consisting of a layer of α-PbO_2 (capacity of 40 ma-min) on Pt and a layer of β-PbO_2 (capacity of 60 ma-min) on the α-PbO_2 surface, under a continuous discharge current of 4 ma/electrode.

hi and the electrode allowed to recover before resuming discharge, the resulting curves for the growth and decay of polarization show rates and shapes characteristic of α-PbO_2 and not of β-PbO_2. If the electrode at point j was washed with 40% $NH_4C_2H_3O_2$, the electrode was rejuvenated and on subsequent discharge behaved like pure α-PbO_2. The potential minimum was least pronounced for the electrode having the smallest β-PbO_2 layer (30 ma-min capacity).

Electrodes consisting of a thin layer of β-PbO_2 (theoretical capacities varying from 40 to 70 ma-min) on Pt and a thin layer of α-PbO_2 (capacities varying from 30 to 120 ma-min) on the β-PbO_2 surface were also made. The α:β ratios varied from 0.75 to 2. These electrodes were discharged by currents varying from 2 to 5 ma/electrode. The discharge curves, for the most part, had characteristic shapes as shown by curve 1 of Fig. 2. Three distinct plateaus were observed. Initially (to point b) the discharge curves resembled that of pure α-PbO_2. Interrupting the current along line ab, allowing the electrode to recover, and then resuming discharge, resulted in decay and growth of polarization curves having the characteristics of pure α-PbO_2. Interruption, recovery, and resumption of discharge along the second plateau (line cd) resulted in curves that had characteristics between those of α- and β-PbO_2 (rate of growth and decay of polarization greater than for α-PbO_2 but less than for β-PbO_2). These rates increased from point c to d. The same treatment along the third plateau (line ef), yielded curves which had the characteristics of pure β-PbO_2 (no minimum was detected, but this might not be expected at the recorded sensitivity used).

One electrode gave a discharge curve differing from that of curve 1 of Fig. 2. For the electrode having the largest capacity of the external α-PbO_2 layer (120 ma-min), the curve had only one plateau and was no different from that of a pure α-PbO_2 electrode (see curve 2 of Fig. 1).

It had been suggested (3) that an expansion of the crystal lattice of β-PbO_2 early in discharge caused the minimum and the rise in the open-circuit potential, and that the lattice of α-PbO_2 did not undergo this expansion. Powder x-ray diffraction patterns of the oxide films were made for β-PbO_2 before and after the first discharge (point c and d in curve 3 of Fig. 1). Patterns were also before and after the first discharge of α-PbO_2. The β-PbO_2 patterns failed to reveal any appreciable shift in the lines which would indicate an expansion of the lattice. If the expansion does occur, it is too small to detect by this method.

Discussion

The studied discharge characteristics of the two modifications of PbO_2 in 0.1M H_2SO_4 show that the $PbSO_4$ produced on the discharge of α-PbO_2 remains as a tightly adhering film on the surface of the remaining undischarged α-PbO_2, and that produced on discharge of β-PbO_2 remains only in part on the surface and not as a film but as widely dispersed crystalline nuclei. This suggests that the discharge mechanism of the two forms may be quite different. The adherent $PbSO_4$ film on the α-PbO_2 electrode suggests that the Pb(II) reduction product reacts without leaving the electrode surface to form $PbSO_4$. The corresponding product in the reduction of β-PbO_2 passes into solution and then deposits on existing $PbSO_4$ crystals, only part of which are on the surface. Experiments in 4.4M H_2SO_4 electrolyte (9) seem to indicate that an adherent $PbSO_4$ film forms of both modifications on discharge. Although the discharge properties of PbO_2 electrodes in the more concentrated acid electrolytes and the conclusions drawn from these properties (9) were, for the most part, very different from those of this study in 0.1M H_2SO_4, these differences are not too surprising. A previous study of the discharge properties of β-PbO_2 as a function of H_2SO_4 concentration in the electrolyte (3) also revealed unexpected results at the higher acid concentrations. The magnitude of the overpotentials was at a minimum at about 0.1M H_2SO_4, and the rates of growth and decay of polarization were at a maximum at this value. No satisfactory explanation of this behavior has yet been found.

The discharge characteristics of the electrodes consisting of a thin layer of α-PbO_2 between the Pt surface and the β-PbO_2 layer indicate that the outer β-PbO_2 layer reacts first, and not until this layer has been nearly exhausted does the α-PbO_2 layer begin to react. This is in agreement with the conclusions drawn by Ikari, Yoshizawa, and Okada (9) for the discharge of a similar electrode in 4.4M H_2SO_4. These authors found, however, two distinct plateaus in the discharge curve, while only one plateau was observed under the conditions of this paper. They, also, found one minimum which preceded the first plateau. Rüetschi and Cahan (6) found two plateaus and two minima in the discharge curves of their two layer electrodes, which consisted of a layer of an α-PbO_2-β-PbO_2 mixture (4) between a

Pb or Pb alloy surface and a pure β-PbO_2 layer. They suggested that the α-PbO_2 probably discharged first. Although it is possible to argue that the modification having the higher electrode potential might discharge first at low current densities, that is not probable with the relatively large apparent current densities (0.1-1.0 ma/cm^2) used in all these investigations. Under these conditions the species, β-PbO_2, which is in more immediate contact with the electrolyte, will discharge first.

The discharge curves of the electrodes consisting of a thin layer of β-PbO_2 between the Pt surface and the thin outer layer of α-PbO_2 indicate that the α-PbO_2 alone starts to reduce first (initial plateau), followed by a "mixed" reduction of both forms (second plateau), and finally a reduction of the β-PbO_2 only (third plateau).

Acknowledgment

The author wishes to thank Dr. Warren C. Vosburgh, Department of Chemistry, Duke University, for his interest and suggestions concerning this research and preparation of this manuscript. He also wishes to thank Dr. J. C. Morrow, Department of Chemistry, University of North Carolina, who made the x-ray diffraction patterns.

This manuscript received Jan. 17, 1962; revised manuscript received March 14, 1962.

Any discussion of this paper will appear in a Discussion Section to be published in the June 1963 JOURNAL.

REFERENCES

1. W. H. Beck, R. Lind, and W. F. K. Wynne-Jones, *Trans. Faraday Soc.*, **50**, 147 (1950).
2. W. H. Beck, P. Jones, nd W. F. K. Wynne-Jones, *ibid.*, **50**, 1249 (1950).
3. H. B. Mark, Jr., and W. C. Vosburgh, *This Journal*, **108**, 615 (1961).
4. J. Burbank, *ibid.*, **104**, 693 (1957).
5. P. Rüetschi and B. D. Cahan, *ibid.*, **104**, 406 (1957).
6. P. Rüetschi and B. D. Cahan, *ibid.*, **105**, 369 (1958).
7. P. Rüetschi, R. T. Angstadt, and B. D. Cahan, *ibid.*, **106**, 547 (1959).
8. I. G. Kiselava and B. N. Kabanov, *Doklady Akad. Nauk SSSR*, **122**, 1042 (1958). *C. A.* **54**, 24014c (1960).
9. S. Ikari, S. Yoshizawa, and S. Okada, *J. Electrochem. Soc. Japan*, Overseas Ed., **27**, E223 (1959).
10. V. H. Dodson, *This Journal*, **108**, 406 (1961).
11. C. N. Reilley and W. G. Scribner, *Anal. Chem.*, **27**, 1210 (1955).
12. D. D. DeFord, Div. of Analytical Chemistry, 133rd Meeting, ACS, San Francisco, 1958.
13. G. L. Guettel, *Ind. Eng. Chem.*, Anal. Ed., **11**, 639 (1939).

Electrolytic Polarization Resulting from Longitudinal Current in Electrodes

Walter W. Harvey

Lincoln Laboratory,[1] Massachusetts Institute of Technology, Lexington, Massachusetts

Longitudinal current in a metal wire contacting an electrolyte leads to polarization of the interphase. If the variation in potential within the metal along the contact with the electrolyte is not negligibly small, *i.e.*, if the resistance or longitudinal current is sufficiently large, some portion of the current will be conducted through the electrolyte. That this must be so can be seen from the following argument. With no current flowing in the wire or in the electrolyte, the magnitude of the potential difference (p.d.) between the interior of the electrolyte and the interior of the wire will be the same over the entire length of the wire; measured with respect to a reference half-cell, this difference in potential is the "rest potential" of the given metal-electrolyte half-cell. If now a p.d. is impressed across the ends, causing current to flow through the wire, the result is that different parts of the wire will be at different potentials, so that the metal-electrolyte p.d. can equal the rest potential at only one position along the contact. It follows that electrolysis will take place, the current densities normally being greatest at the ends of the metal-electrolyte contact, where the anodic and cathodic overpotentials have their maximum values.[2] Similar considerations have been expressed before, particularly with reference to palladium wires containing hydrogen (1, 2); however, to the author's knowledge, the problem has not previously been analyzed quantitatively.

For the reasons indicated, the apportionment of current between wire and electrolyte will not be determined by the ratio of their resistances, as for a parallel arrangement of resistors, but (for a given wire) by the current density-overpotential characteristic of the given electrode material in the given electrolyte. Owing to polarization, the instantaneous current across the contact can be considerably greater than the steady value, so that the apparent resistance of an immersed wire from a-c measurements would be expected to decrease with increasing frequency (3). It goes without saying that the significant current density-overpotential characteristic is that pertaining to the conditions of the resistance measurement, *e.g.*, instantaneous or steady-state current densities for the d-c characteristic. It is equally clear that the desired characteristic would not be obtained using a fine wire electrode because of the anticipated nonuniform current density distribution.

Although we shall not be concerned here with mapping the paths of current flow in the electrolyte, it is reasonable to conclude that they extend to some small distance from the interface. Thus, in the immediate vicinity of the wire, the electric field in the electrolyte has a longitudinal component. If it is

[1] Operated with support from the U.S. Army, Navy, and Air Force.

[2] This statement requires modification if passivation effects are encountered.

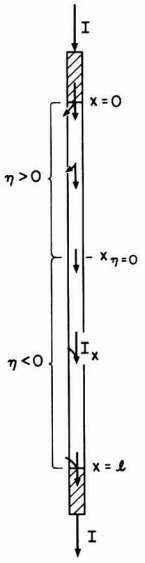

Fig. 1. Distribution of longitudinal current in a wire contacting an electrolyte.

true that the establishment of a potential gradient in a wire leads to current flow in the surrounding electrolyte, the converse must also be true. Accordingly, if a second wire is placed close to the wire carrying current, some current will flow in the second wire in addition to that flowing in the electrolyte. Apart from magnetic effects, therefore, an arrangement of closely situated parallel wires immersed in an electrolyte would be expected to exhibit coupling in a-c impedance measurements (4).

Derivation of the Potential Distribution

We treat the case of a uniform wire, a portion of whose surface contacts an electrolyte. The x-direction is taken parallel to the wire, and I_x denotes the longitudinal current in the wire. I_x varies with position along the wire-electrolyte contact, having a minimum value at the position of zero overpotential (see Fig. 1); in the pre-contact regions, $x < 0$ and $x > l$, I_x has the value I.

At points in the electrolyte sufficiently removed from the wire, the potential will be unaffected by longitudinal current in the wire. Thus, the p.d. between interior of the electrolyte and interior of the wire will vary as the potential $V(x)$ in the wire. That is,

$$\frac{d}{dx}\left(\phi_{\text{metal}} - \phi_{\text{electrolyte}}\right) = \frac{dV}{dx} \qquad [1]$$

The total metal-electrolyte p.d. appropriate to Eq. [1] is made up of a potential drop across the interphase plus any additional potential drop in the body of the electrolyte:

$$\phi_{\text{metal}} - \phi_{\text{electrolyte}} = \Delta\phi_{\text{interphase}} + \Delta\phi_{\text{electrolyte}} \qquad [2]$$

The electrolytic overpotential $\eta(x)$ is determined by the potential drop across the interphase; more particularly,

$$\frac{d}{dx}\left(\Delta\phi_{\text{interphase}}\right) = \frac{d\eta}{dx} \qquad [3]$$

Therefore, to the extent that $\Delta\phi_{\text{electrolyte}}$ is small in comparison to $\Delta\phi_{\text{interphase}}$, the gradients of potential and overpotential will be equal.

The potential gradient along the wire is

$$\frac{dV}{dx} = -\frac{\rho}{\pi r^2} I_x \qquad [4]$$

where ρ is the resistivity, and r the radius of the wire. We write the complete electrolytic current density-overpotential characteristic as $j = j(\eta)$, assigning positive values to j and η for anodic polarization. Then the integrated electrolytic current at position x is given by

$$i = 2\pi r \int_0^x j(\eta)\, dx \qquad [5]$$

whereupon I_x may be formulated as

$$I_x = I - 2\pi r \int_0^x j(\eta)\, dx \qquad [6]$$

and the potential gradient as

$$\frac{dV}{dx} = -\frac{\rho}{\pi r^2} I + \frac{2\rho}{r} \int_0^x j(\eta)\, dx \qquad [7]$$

According to our basic postulate, dV/dx may be set equal to $d\eta/dx$, so that on taking derivatives Eq. [7] becomes

$$\frac{d^2\eta}{dx^2} = \frac{2\rho}{r} \frac{d}{dx} \int_0^x j(\eta)\, dx \qquad [8]$$

from which we wish to obtain $\eta = \eta(x)$. Substituting $f(x)$ for $j\ (\eta)$, the derivative of the integral is simply $f(x)$, leading to

$$\frac{d^2\eta}{dx^2} - \frac{2\rho}{r} j(\eta) = 0 \qquad [9]$$

subject to the boundary conditions

$$\left.\frac{d\eta}{dx}\right)_{x=0} = \left.\frac{d\eta}{dx}\right)_{x=l} = -\frac{\rho I}{\pi r^2} \qquad [10]$$

A possible distribution of potential along the wire in accordance with Eq. [9] and conditions [10] is shown in Fig. 2. Identical considerations apply to a metal strip; the potential distribution for a thin strip is given by Eq. [9], with the radius r of the wire replaced by the thickness δ of the strip.

Unless $j(\eta)$ has a particularly simple form, it will not be possible to obtain an analytical solution to Eq. [9]. We illustrate the procedure for a linear characteristic $j(\eta) = b\eta$, such as often pertains at potentials not too far removed from the rest potential. It is evident that for a linear characteristic, η will be zero at $x = l/2$. The equation

$$\frac{d^2\eta}{dx^2} - \frac{2\rho}{r} b\eta = 0 \qquad [11]$$

obtained by substituting $j(\eta) = b\eta$ into Eq. [9] has the general solution

$$\eta = c_1 e^{\alpha x} + c_2 e^{-\alpha x} \qquad [12]$$

where

$$\alpha = (2\rho b/r)^{1/2} \qquad [13]$$

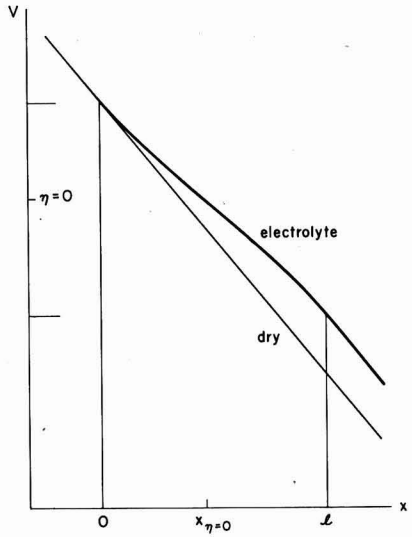

Fig. 2. Distribution of potential in a wire contacting an electrolyte

The constants c_1 and c_2 are evaluated from the boundary conditions [10] leading to the following analytical solution

$$\eta = \frac{\alpha I/b}{4\pi r \sinh \alpha l}\left[(e^{-\alpha l}-1)e^{\alpha x} + (e^{\alpha l}-1)e^{-\alpha x}\right] \quad [14]$$

Using this result, the current carried by the electrolyte is evaluable either as the total anodic current

$$i_+ = 2\pi r \int_0^{l/2} b\eta\, dx = I\left(1 - \operatorname{sech}\frac{\alpha l}{2}\right) \quad [15]$$

or the total cathodic current

$$i_- = 2\pi r \int_{l/2}^{l} b\eta\, dx \quad [16]$$

with, of course,

$$i_+ + i_- = 0 \quad [17]$$

For the general characteristic $j(\eta)$, the total electrolysis current is obtained from

$$i_+ = 2\pi r \int_0^{x_{\eta=0}} j(\eta)\, dx \quad [18]$$

Remarks

The distributions of potential and longitudinal current in an immersed metal wire through whose ends a current I is passed are seen to be determined by the radius and resistivity of the wire, the length of the contact with the electrolyte, and the current density-overpotential characteristic $j(\eta)$. The resistivity of the electrolyte does not enter explicitly since its influence is indirect, being confined to polarization effects which are included in the measured $j(\eta)$. The analysis on which the foregoing statements

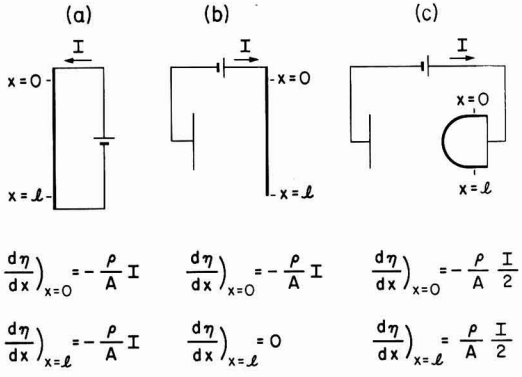

Fig. 3. Boundary conditions for (*a*) longitudinal current in an immersed wire, (*b*) a wire electrode with metallic contact at one end, (*c*) a wire electrode with metallic contacts at both ends. $A = \pi r^2$.

are based presupposes the condition $\Delta\phi_{\text{interphase}} >> \Delta\phi_{\text{electrolyte}}$. If this condition does not pertain in a practical case, details of the current flow in the electrolyte must be worked out. Even so, the method of treatment developed above should provide a useful approximation to the actual distributions of potential and current in the wire.

In most instances, the fraction of current conducted through the electrolyte will be small. For example, for a 10-cm length of 10-mil platinum wire and for a linear characteristic with $b = 100$ ma/v, i_+/I would be 0.002 according to Eq. [15], increasing roughly proportionally with b. However, for a very thin metal strip or film, or for a semiconductor, the fraction can be appreciable. For a 10-cm length of 0.00005-in. gold sheet and for the same $j(\eta)$ as in the previous example, the electrolytic current would be 5% of the total.

The basic Eq. [9] can be applied to other situations of interest including that of a wire electrode of the usual sort, with metallic contact at one end, or a wire electrode, possibly in the form of a wide loop, with metallic contacts at both ends. The three configurations which have been considered are compared in Fig. 3, where the appropriate boundary conditions are also to be found.

Manuscript received Nov. 30, 1961.

Any discussion of this paper will appear in a Discussion Section to be published in the June 1963 JOURNAL.

REFERENCES

1. C. A. Knorr and E. Schwartz, *Z. Elektrochem.*, **39**, 281 (1933).
2. See J. C. Barton and F. A. Lewis, *Trans. Faraday Soc.*, **58**, 103 (1962) for an account of recent work and references to the early literature.
3. G. M. Schmid and N. Hackerman, *This Journal*, **107**, 647 (1960).
4. G. M. Schmid and N. Hackerman, *ibid.*, **107**, 142 (1960).

The Anodic Dissolution of Nickel in Acetonitrile

Thomas C. Franklin and Charles R. Parsons[1]

Chemistry Department, Baylor University, Waco, Texas

Nickel normally occurs in solution as nickel(II). However, there are a number of complex compounds containing nickel(I) (1). Ni(I) has also been postulated as an intermediate in the electrodeposition of nickel (2) and anodic dissolution in aqueous systems (3). It has also been indicated that nickel dissolves anodically in acetonitrile to produce a mixture of nickel(I) and (II) (3). This is a report of a further investigation of the anodic dissolution of nickel in dimethylformamide and acetonitrile.

Experimental Method

Determination of oxidation number by weight loss of nickel.—The electrolysis cell was a 400 ml beaker containing a 100 ml porous porcelain cup as the anode compartment. The constant current was supplied by a regulated 500v d-c power supply and a series resistor. Most of the runs were for 1000 to 5000 sec with a current of approximately 0.1 amp and a current density of approximately 0.0004 amp/cm^2. The current was maintained constant by frequent manual adjustment. The cathode and anode were coils of 14 gauge nickel wire.

Fisher certified Reagent Grade acetonitrile and dimethylformamide were used as solvents. Tetramethylammonium chloride was used as an electrolyte in both the anode and cathode compartments.

Determination of nickel(II) concentration in solution.—In order to check on the possibility of nickel entering solution by a secondary process a colorimetric comparison was made between the amount of nickel(II) in solution and the amount of nickel(II) that would be expected in solution if the nickel had dissolved as nickel(II).

The standard curve for nickel(II) was prepared by dissolving 23 mg of dried reagent grade nickel chloride in 100 ml of acetonitrile. This was then diluted to form a series of standards and measured on a Klett Summerson colorimeter.

The anodic dissolution curves were obtained using an apparatus and procedure similar to that of Franklin and Roth (4) in which the anode compartment, the cell of a Klett Summerson colorimeter, was connected by an acetonitrile tetramethylammonium chloride bridge to the cathode compartment. A constant current of 0.0020 amp was passed (approximately 0.0002 amp/cm^2), and the colorimeter readings were taken at regular intervals. The cell was open to the atmosphere, but it was bubbled with nitrogen prior to and during the anodic dissolution.

Coulometric titration of nickel(I).—In order to determine if nickel(I) were actually present in solution, the solution was titrated coulometrically with iodine. It was very difficult to detect visually the iodine color in the solution already colored with nickel; therefore, the Klett-Summerson colorimeter was again used. Following an anodic dissolution run, potassium iodide was added to the solution. The colorimeter filter was changed from the red one used with nickel dissolution to a green one, and the colorimeter zero adjustment was changed to coincide with the reading before the filter change. The nickel anode was replaced with platinum wire and a current of 2.0 ma was passed. The colorimetric readings were recorded as a function of time.

Results and Analysis of Results

The experiments on the loss in weight of the nickel anode showed that in all experiments in acetonitrile

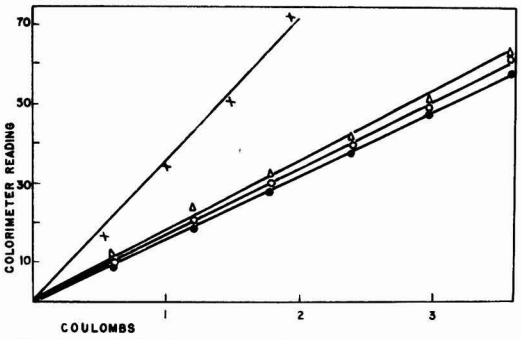

Fig. 1. Anodic dissolution of nickel in acetonitrile using a colorimetric coulometer: X, standardization curve of nickel (II) prepared from nickel (II) chloride; △, ○, ●, runs 1, 2, and 3 for the anodic dissolution of nickel in acetonitrile.

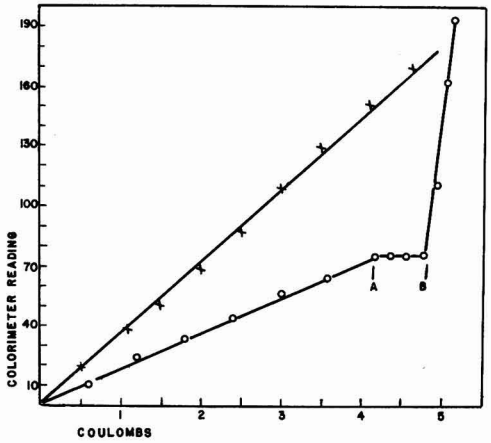

Fig. 2. Anodic dissolution of nickel in acetonitrile and coulometric titration of nickel (I) in a colorimetric coulometer: x, standardization curve of nickel (II) prepared from nickel (II) chloride; ○, anodic dissolution and titration curve for the titration of nickel (I).

[1] A student at La Vega Junior High School, Waco, Texas, at the time this work was done. He is now a student at Douglas MacArthur High School, San Antonio, Texas.

and dimethylformamide nickel dissolved with an oxidation number less than two. In dimethylformamide the average oxidation number for 5 runs was 1.66±0.12. For acetonitrile experiments the average oxidation number for twelve runs was 1.39±0.17.

Figure 1 shows typical data on the comparison of the nickel(II) concentration in solution as determined colorimetrically with that that would be in solution if the nickel had dissolved as nickel(II). As can be seen in all cases, there was less nickel(II) in solution than would be expected if nickel(II) were the only anodic product.

Figure 2 shows a typical run in which the nickel was anodically dissolved up to point A. Potassium iodide was then added, and the nickel anode was replaced with a platinum anode. As can be seen, the nickel(I) is titratable with the iodine generated, and the sudden break at B is the end point for this titration. The displacement of the anodic dissolution curve indicates that 2.0 coulombs of nickel dissolved as nickel(I). The titration indicates that 0.7 coulombs of nickel was present in solution as nickel(I). In all experiments the amount titrated was less than the colorimetric data indicated it should have been, probably because of air oxidation since the system was open to the air.

In summary, it has been shown that nickel dissolves anodically in acetonitrile and dimethylformamide containing tetramethylammonium chloride as a mixture of nickel(I) and nickel(II). The nickel(I) was shown to be stable enough in acetonitrile to be titrated with iodine.

Manuscript received Dec. 18, 1961; revised manuscript received Feb. 21, 1962.

Any discussion of this paper will appear in a Discussion Section to be published in the June 1963 JOURNAL.

REFERENCES

1. N. V. Sidgwick, "The Chemical Elements and Their Compounds," Vol. II, pp. 1429, 30, 52, Oxford at the Clarendon Press, (1950).
2. R. H. Sanborn and E. F. Orlemann, *J. Am. Chem. Soc.*, **78**, 4852 (1956).
3. T. C. Franklin and Jack Goodwyn, *This Journal*, **106**, 269 (1959).
4. T. C. Franklin and C. C. Roth, *Anal. Chem.*, **27**, 1197 (1955).

On the Crystallinity of GaAs Grown Horizontally in Quartz Boats

L. R. Weisberg, J. Blanc, and E. J. Stofko

RCA Laboratories, Radio Corporation of America, Princeton, New Jersey

While transparent fused quartz boats have been previously found to provide the highest purity GaAs grown by the horizontal Bridgman technique (1), the crystallinity of the GaAs has frequently been unsatisfactory. Therefore, a study has been carried out of factors affecting the crystalline quality of GaAs, such as boat treatment, arsenic pressure, furnace gradient, growth speed, melt temperature, impurities, and seeding. Over 50 crystals have been prepared, each roughly 9 cm long, and weighing 20g. Subsequent to growth, the crystals were examined for surface markings before and after "sand" blasting, and samples were removed for emission spectrographic analysis and Hall measurements. Several ingots that were essentially single crystals were x-ray analyzed for their axial orientation. Prior to growth, the transparent fused quartz boats were given either of two cleansing treatments: boats were either etched in HF acid for 10 min, or alternatively, sand blasted. In either case, the final treatment was an etch in 1:1 $HCl:HNO_3$ acid followed by extensive rinsing.

Two factors were observed to have a major effect on the crystallinity, namely, the boat treatment and the arsenic pressure. Concerning the former, crystals grown in HF treated boats generally had a poor crystal structure, with many small angle grain boundaries running through the crystal. However, crystals grown in sand blasted boats at growth speeds of 1.9 cm/hr were consistently of good quality. Visual observation of the ingot cross section showed that, without exception, ingots with good crystallinity wet the boat either not at all or to only a small degree. However, the absence of wetting proved to be only a necessary condition for good crystallinity and not a sufficient one, since many polycrystalline ingots were produced in HF treated boats when no wetting occurred. Furthermore, nucleation of new grains could not be correlated directly with places where wetting of the boat occurred. These results suggest that the crystallinity can be affected in part by a growth poison (2) which is introduced by the HF etching of the quartz boat. The effect of sand blasting the boat is both to prepare a more passive surface and also to reduce the contact area between the melt and the boat.

The second major growth factor was the arsenic pressure over the melt. A series of 22 GaAs crystals were grown with arsenic reservoir temperatures between 585° and 660°C, using growth speeds of either 1.3 or 1.9 cm/hr. When a reservoir temperature below 600°C was employed, the melt had a strong tendency to supercool, and the ingots were polycrystalline. As higher arsenic temperatures were used, the crystallinity continually improved; however, porosity began to occur, due to the escape of excess arsenic at the freezing interface. Porosity was encountered at 640°C using a growth speed of 1.3 cm/hr., and at 630°C using a growth speed of 1.9 cm/hr. However, the porosity does not destroy the crystallinity, since nearly single crystals of

GaAs have been prepared with an arsenic temperature of 640°C with a growth speed of 1.9 cm/hr. In general, an arsenic temperature of 625°-630°C is desirable for good crystallinity.

Only minor and inconsistent effects on the crystallinity were produced by most other growth factors such as variations in growth speed between 0.4 and 2 cm/hr, furnace temperature gradients between 5° and 24°C per cm across the freezing interface, and melt temperatures between 1250° and 1275°C. With respect to seeding experiments, it was observed first that there was no marked preferred growth direction for GaAs. Of ten unseeded single crystals, none had orientations close to the three principal crystallographic directions <001>, <011>, and <111>, and only four had orientations at all close to each other, clustering about the <013>. Twenty-one GaAs crystals were grown using seeds with either a <013>, <112>, or <011> orientation, but the seeding did not produce a significant improvement in the crystallinity.

No correlation could be observed between the crystallinity and the presence of any spectrographically detectable impurity in the as-grown ingots, which contained silicon, magnesium, copper, aluminum, and iron in quantities varying from 0.1 to 50 ppm in different crystals. Next, a series of crystals were grown, doped separately with either silicon, oxygen, carbon monoxide, water vapor, hydrogen, or copper. No noticeable effect on the crystallinity occurred for additions of up to 0.04 mg of oxygen, 0.8 mg of carbon monoxide, 0.03 mg of hydrogen, and 1 mg of copper. In two attempts, additions of 1 mg of silicon caused the melt to wet the boat appreciably, and the crystallinity was poor, indicating that the silicon acted differently when added in elemental form than when introduced due to reaction with the boat in an as-grown ingot where oxygen may be simultaneously introduced. Water vapor had the most pronounced effect. Two ingots, one doped with 56 mg and the other with 0.5 mg of water, adhered very badly to the boat resulting in very polycrystalline porous ingots containing cracks. In addition, the water vapor caused several grams of the GaAs ingot to be transported to the cooler end of the tube. This result implies that trace quantities of water vapor, perhaps due to the outgassing of the quartz ampoule, can be deleterious to the crystallinity of GaAs.

Acknowledgments

The authors are grateful to Mr. H. H. Whitaker for the spectrographic analyses, to Mr. G. Neighbor for the x-ray analyses, and to Mr. P. G. Herkart for important cooperation in some growth experiments. This research has been sponsored by the Electronics Research Directorate, Air Force Cambridge Research Laboratories, Office of Aerospace Research under Contract No. AF19(604)-6152.

Manuscript received Feb. 6, 1962; revised manuscript received March 23, 1962.

Any discussion of this paper will appear in a Discussion Section to be published in the June 1963 JOURNAL.

REFERENCES

1. L. R. Weisberg, F. D. Rosi, and P. G. Herkart, "Properties of Elemental and Compound Semiconductors," Metallurgical Society Conferences, Vol. 5, Interscience Publishers, Inc., New York (1960).
2. See, for example, G. W. Sears, *J. Chem. Phys.*, **29**, 979 (1958).

Epitaxial Silicon Thin Films

K. J. Miller, R. C. Manz, and M. J. Grieco

Bell Telephone Laboratories, Incorporated, Murray Hill, New Jersey

Study of silicon epitaxial film growth by the hydrogen reduction of silicon tetrachloride (1) has shown that constant deposition temperature affords a high degree of run-to-run thickness reproducibility. The process has been found to have a versatility especially useful for fabrication of grown junctions.

Hydrogen was bubbled through thermostated $SiCl_4$ and carried over an R. F. heated (111) oriented silicon sample in a quartz reaction chamber. If the reaction

$$SiCl_4(g) + 2H_2(g) \rightleftarrows Si(s) + 4HCl(g)$$

is assumed to be the idealized deposition reaction and reactants and products are in their standard states, calculations based on data in the literature (2) show that this reaction proceeds with the absorption of heat according to the equation

$$\Delta H_T^\circ(\text{cal.}) = 60.2\text{x}10^3 - 6.51T + 1.23\text{x}10^{-3}T^2 - 2.67\text{x}10^6T^{-1} \quad (298\text{-}1000^\circ\text{K})$$

The standard Gibbs free energy change, ΔG°, is favorable above about 1225°C. The curve obtained from the equation

$$\Delta G_T^\circ(\text{cal.}) = 60.2\text{x}10^3 + 15.0T\log T - 1.23\text{x}10^{-3}T^2 - 1.33\text{x}10^5T^{-1} - 85.9T \quad (289\text{-}1000^\circ\text{K})$$

was extrapolated beyond 1000°K. The flow conditions during epitaxial growth favor the reaction proceeding spontaneously at a lower temperature, however, because of the actual product and reactant activities, a, which are related to the free energy change, ΔG, by the equation

$$\Delta G = \Delta G^\circ + RT \ln \frac{a^4_{HCl}}{a_{SiCl_4}\, a_{H_2}{}^2}$$

Figure 1 shows the deposition reaction chamber. A Pt-10% Rh-Pt thermocouple sensing element provided a control voltage and was located in a well drilled in the susceptor on which samples were placed. The control temperature obtained from the thermocouple was held constant to $< \pm 1$°C. The temperature control apparatus was similar to that conventionally used for growing semiconductor single crystals from the melt and included a recorder-controller (Leeds and Northrup Co., Model S AZAR recorder and C.A.T. Control Unit) used with a 10 kw, 4 M.C., R. F. generator. Sample surface temperature was measured by an optical pyrometer through a right angle prism and a quartz optical

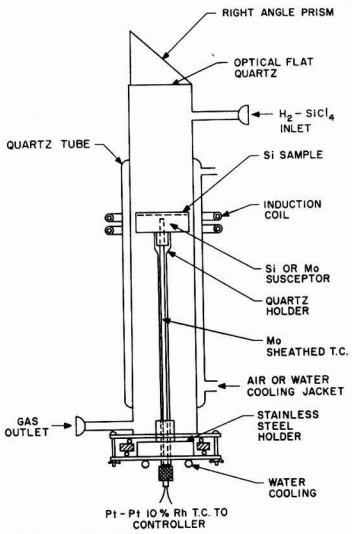

Fig. 1. Epitaxial silicon deposition reaction chamber

flat sealed to the top of the reaction chamber as seen in Fig. 1. Sample temperatures could be measured optically with a precision of ±3°C.

Films have been deposited with $SiCl_4$ concentrations of 1-2 mole % and with 1-3 l/min total hydrogen flows. Reaction chambers used have had inside diameters from 1 to 2 in. depending on sample size. Films up to 1¼ in. in diameter have been deposited in this apparatus using both silicon and molybdenum susceptors. When high resistivity silicon susceptors were used, infrared lamps were used initially to heat the silicon to increase R. F. coupling.

With ½ in. diameter substrates, a run-to-run control of film thickness as a function of time of deposition of approximately ±3% was obtained as compared with a ±15% reproducibility usually obtained for manual temperature control. For a sample temperature of 1200°C and a 2 l/min hydrogen flow through a 1 in. ID reaction chamber and with 1.3 mole % $SiCl_4$, the rate of deposition was 1.7 μ/min. At 1300°C the rate was found to be 2.1 μ/min. These deposition rates give $\Delta(\text{rate})/\Delta(\text{temp °C}) \cong 0.2\%/$°C. As an example, for a 5 min deposition at 1250°C, with a 1°C temperature difference from the control temperature, the film thickness difference should be 0.02μ from a 9.5μ predicted thickness.

Thicknesses measured interferometrically by angle-lapping-staining have been found to be uniform within measurement error across ½ in. diameter substrates. However, film smoothness has been found to vary across samples in proportion to the smoothness of the substrate material. For ½ in. diameter samples no center to edge temperature gradient was observed during epitaxial deposition. For 1¼ in. diameter samples heated on silicon susceptors, a 20°-25°C temperature gradient has usually been observed, which should contribute approximately 0.5μ to a film thickness variation for 10μ thick films. By angle-lapping-staining across 1¼ in. diameter samples, interference measurements have shown maximum deviations of ±0.5μ from 5-6μ mean thicknesses. When 1¼ in. diameter samples were heated on molybdenum susceptors, this temperature gradient was observed to be approximately 5°-10°C.

Higher temperature has been found to favor increased orientation of depositing silicon atoms. Epitaxial growth of silicon films with a high degree of crystalline perfection has been found to require a 1200°-1275°C temperature of deposition. Using the conditions outlined, films grown below 1050°C often are polycrystalline, while those films grown between 1050° and 1200°C generally have growth defects.

Water-free as well as oxygen-free hydrogen has been necessary to prevent the formation of oxide films on sample surfaces. The Deoxo Puridryer (obtained from Engelhard Industries, Inc.) and liquid nitrogen cold traps used have proven adequate to maintain the moisture level below 1 ppm. However, air as well as dust particles are introduced when samples are placed in the deposition apparatus. Sample surface defects sometimes observed are believed to be primarily caused by such contamination.

Doping of films to obtain desired resistivities has been accomplished by addition of PCl_3 to the $SiCl_4$. Film resistivity has been measured with a 4-point probe using films of the opposite conductivity type from the substrate and by capacitance^{-2} *vs.* reverse bias plots obtained from alloyed aluminum dot diodes fabricated on the films. Percentage variation of film resistivity across a sample has been found to be proportional to the nonuniformity of film thickness and to the magnitude of the film resistivity.

Reverse diode characteristics of some epitaxial film-substrate junctions have been studied. An example of an epitaxial film-substrate junction can be seen in Fig. 2a. The reverse I-V characteristics measured on 9 x 10 mil mesa etched diodes are shown in Fig. 2b. The n-type, 2 ohm-cm, film was 6μ thick and was deposited on a 1 ohm-cm, p-type silicon substrate. Measurements of capacitance^{-2} as a function of reverse voltage showed a linear relation for diodes and indicated that the interface was a step junction. The substrate in Fig. 2 was prepared for deposition by chemical polishing. The reverse current just before breakdown was less than 0.1 μa and the breakdown voltages of the diodes were found to agree with those usually obtained for step junction

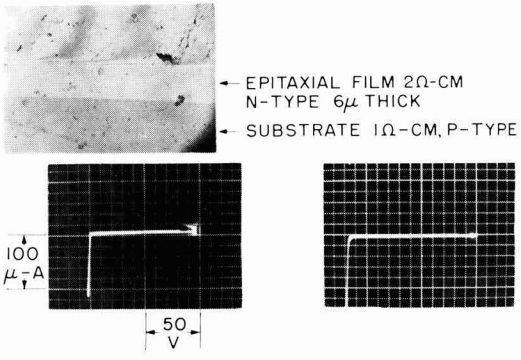

Fig. 2. a (top) Epitaxial film to substrate junction; Magnification, approximately 80X; b (bottom) reverse diode characteristics obtained for junction shown in a.

avalanche breakdown voltage as a function of resistivity.

Manuscript received Jan. 19, 1962. This paper was prepared for delivery before the Detroit Meeting, Oct. 1-6, 1961.

Any discussion of this paper will appear in a Discussion Section to be published in the June 1963 JOURNAL.

REFERENCES
1. H. C. Theuerer, *This Journal*, **108**, 649 (1961).
2. F. D. Rossini, D. D. Wagman, W. H. Evans, S. Levine, and I. Jaffe, U. S. Natl. Bur. Standard Circ. 500 (1952); K. K. Kelley, U. S. Bur. Mines Bull. 584 (1960); K. K. Kelley and E. G. King, *ibid.*, 592 (1961); D. R. Stull and G. C. Sinke, "Thermodynamic Properties of the Elements," Am. Chem. Soc., Washington, D. C. (1956).

Extent of Solid Solution in the GaSb-InSb System from Crystal Pulling Experiments

F. A. Trumbore, P. E. Freeland, and A. D. Mills

Bell Telephone Laboratories, Incorporated, Murray Hill, New Jersey

The literature contains a number of conflicting reports on the extent of solid solution in the GaSb-InSb pseudo-binary system. Reports of limited solid solubility (1-3) have been discredited by various workers (4-8) who showed that the system contains a complete series of homogeneous solid solutions. The latter workers used experimental techniques such as long term annealing of powders, slow directional freezing, and zone equalization. The purpose of the present paper is to report successful attempts to grow these solid solutions by the crystal pulling technique together with the results of x-ray measurements which are interpreted in terms of the phase diagram.

Experimental

Conventional rf induction heated crystal pulling machines (9) were used to pull ten GaSb-InSb samples under a hydrogen atmosphere at pull rates of 3-5 mm/hr and rotation rates of 140-144 rpm from alloy melts containing between 9 and 92 mole % InSb. Seed crystals of randomly oriented GaSb were used. In one case a crystal of GaSb-InSb solid solution grown in a previous run was used as a seed. Single crystals were often obtained, even when pulled from melts containing as much as 60 mole % InSb. The other samples usually contained large grains, and the x-ray powder patterns were quite sharp except for slight fuzziness in the case of crystals grown from melts containing about 70-80 mole % InSb. A number of the melts were doped with zinc or germanium, both of which acted as acceptors in the solid solutions. However, the concentrations of these dopants were negligible insofar as their effect on the x-ray results are concerned. X-ray powder patterns were taken with Straumanis-type Norelco cameras (114.6 mm diameter) using CuKα radiation. For five of the crystals the melt compositions were determined from weight loss measurements and were corrected for the composition of the grown material as calculated from the x-ray data. Weight losses, presumably due to evaporation of antimony, were only on the order of 0.1% or less. For the other five crystals, grown prior to the decision to study this system more extensively, the melt compositions were assumed to be weighed-in compositions. The uncertainty introduced by this assumption was small because the samples for x-ray analysis were taken from as near the seed as possible, and the size of the crystals was small compared to the total melt volume.

Results and Discussion

The results of the x-ray measurements are summarized in Table I together with the mole fraction of InSb in the melt, x^{L}_{InSb}. With the exception of three samples, as noted in Table I, the x-ray lines were essentially as sharp for the GaSb-InSb solid solutions as for the pure GaSb and InSb samples.

In order to obtain the compositions of the solid solutions from the measured lattice parameters it was first assumed that Vegard's law is valid for the GaSb-InSb system as indicated by Woolley and Smith (7). However, more recent work (10) indicates the presence of small deviations from Vegard's law. Accordingly, we have recalculated the alloy compositions by using the experimental x-ray data supplied by Woolley (10). While the calculated compositions of the InSb-rich solid solutions do not differ appreciably from the Vegard's law results there is a significant difference for the GaSb-rich alloys, at least in terms of x^{S}_{InSb}, the mole fraction of InSb in the solid solution. This is shown in Fig. 1 which is a plot of log k_{InSb} *vs.* x^{L}_{InSb} where k_{InSb} is the distribution coefficient defined by $k_{InSb} = x^{S}_{InSb}/$

Table I. Lattice constants of pulled GaSb-InSb solid solutions

Sample No.	x^{L}_{InSb}	Lattice constant, A
GaSb (pure)	—	6.095 ± 0.003*
5EP	0.088	6.100 ± 0.003
7EP	0.125	6.101 ± 0.003
15PF	0.248†	6.108 ± 0.003
16PF	0.422†	6.121 ± 0.003
10EP	0.605	6.138 ± 0.003
9PF	0.647	6.155 ± 0.003
12PF	0.717	6.167 ± 0.005**
17PF	0.814†	6.220 ± 0.005**
24PF	0.827†	6.245 ± 0.005**
27PF	0.918†	6.343 ± 0.003
InSb (pure)	—	6.479 ± 0.003*

* These values compare with the figures 6.095 and 6.478Å obtained for GaSb and InSb by Swanson *et al.* [NBS Circular 539, 6, 30 (1956); *ibid.*, 4, 73 (1955)].
** Slightly fuzzy lines.
† Melt compositions determined from weight loss measurements. Should be most reliable points.

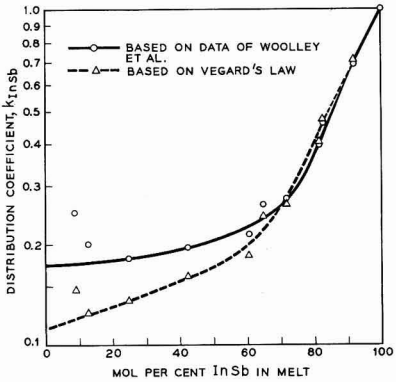

Fig. 1. Plot of log k_{InSb} as a function of x^{L}_{InSb} from the crystal pulling data. The dashed curve corresponds to the results if Vegard's law is used to calculate the alloy compositions from the x-ray data in Table I. The solid curve is derived from the x-ray data in Table I and Woolley and Smith's work on the variation of the lattice parameter with composition showing deviations from Vegard's law. In extrapolating k_{InSb} to $x^{L}_{InSb} = 0$ the points corresponding to samples No. 5EP and No. 7EP (Table I) were essentially neglected since the uncertainties in x^{S}_{InSb} were relatively large due to the small changes in lattice parameter compared to pure GaSb. The curves have also been drawn to favor those points obtained from the runs where weight loss measurements were made.

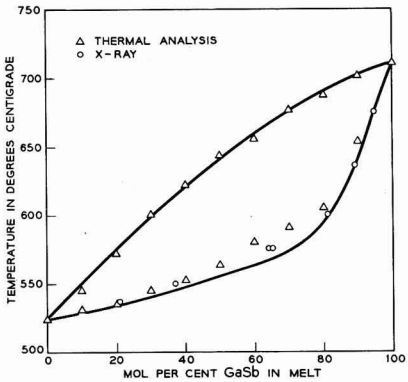

Fig. 2. GaSb-InSb phase diagram. The experimental points are those of Woolley and Smith. The liquidus curve has been drawn by the authors through these points. The solidus curve was calculated from the liquidus curve and distribution coefficient data obtained from the solid curve in Fig. 1.

x^{L}_{InSb}. The scatter in the points at the GaSb-rich end of the curve reflects the sensitivity of the calculation of x^{S}_{InSb} to slight errors in the lattice parameters and to the way we have drawn a curve to fit Woolley *et al.*'s x-ray data.

If the distribution coefficient data in Fig. 1 are equilibrium values, a knowledge of the GaSb-InSb liquidus curve would be sufficient to construct the equilibrium solidus curve for this system. Phase diagrams have been determined by Woolley and Smith (7) and Gorshkov and Goryunova (5). Although both diagrams indicate a complete series of homogeneous solid solutions, there are quantitative differences in the positions of the liquidus and solidus curves. (Some of the differences are due to the use of two different melting points for pure GaSb.) It appears that the work of Woolley and Smith is the more extensive and more reliable of the two sets of data, and we have plotted their experimental points, determined from x-ray data and from thermal analysis, in Fig. 2. The liquidus curve drawn through these points is our estimate of a reasonable curve considering the scatter of the data. The solidus curve in Fig. 2 was then calculated from the liquidus curve and the k_{InSb} data (Fig. 1), taking into account the reported departures from Vegard's law.

It is seen in Fig. 2 that the agreement between the calculated solidus curve and the experimental data of Woolley and Smith, especially the x-ray data, is relatively good. If one considers the latitude available in drawing the liquidus curve, the shallow solidus curve in the InSb-rich region where the importance of a slight error in temperature is magnified and the other possible sources of error in the present work and in that of Woolley *et al.* the agreement is probably within experimental error. Hence, it appears that the crystal pulling technique is capable of yielding equilibrium solid solubility data in systems of this type.

Conclusion

To the best of our knowledge this study represents the first application of the crystal pulling technique to the relatively complete coverage of a homogeneous alloy system of this type. The relative ease of growth and the short period of time involved (hours instead of days or months for some methods) indicates that more extensive application of the pulling technique to the study of phase diagrams would be profitable. Although a liquidus curve is necessary to obtain the complete phase diagram from crystal pulling data, a preliminary survey of a given system with the pulling method would serve to minimize confusion such as that caused by the erroneous reports of a miscibility gap in the GaSb-InSb system.

Acknowledgments

The authors gratefully acknowledge the assistance of E. M. Porbansky who grew the first GaSb-InSb crystals for this study and stimulating discussions with C. A. Burrus whose interest in these alloys led to the present work.

Manuscript received Feb. 5, 1962. This paper was prepared for delivery before the Los Angeles Meeting, May 6-10, 1962.

Any discussion of this paper will appear in a Discussion Section to be published in the June 1963 JOURNAL.

REFERENCES

1. W. Koster and B. Thoma, *Z. Metallkunde*, **46**, 293 (1955).
2. J. S. Blakemore, *Can. J. Phys.*, **35**, 91 (1957).
3. C. Kolm, S. A. Kulin, and B. L. Averbach, *Phys. Rev.*, **108**, 965 (1957).
4. N. A. Goryunova and N. N. Fedorova, *J. Tech. Phys. (USSR)*, **25**, 1339 (1955).
5. I. E. Gorshkov and N. A. Goryunova, *Zhur. neorg. khim.*, **3**, 668 (1958).
6. J. C. Woolley, B. A. Smith, and D. G. Lees, *Proc. Phys. Soc. London*, **69B**, 1339 (1956).

7. J. C. Woolley and B. A. Smith, *ibid.*, **72**, 214 (1958).
8. V. I. Ivanov-Omskii and B. T. Kolomiets, *Soviet Physics Solid State*, **1**, 834 (1959); *ibid.*, **2**, 363 (1960).
9. See M. Tanenbaum, in "Semiconductors," N. B. Hannay, Editor, Chap 3, Fig. 3.15 and 3.16. Reinhold Publishing Corp., New York (1959).
10. J. C. Woolley and C. M. Gillett, *J. Phys. Chem. Solids*, **17**, 34 (1960); also J. C. Woolley, Private communication.

Preparation of Small Samples of Ductile Titanium and Zirconium from the Isotopic Oxides by Iodide Refining

N. D. Veigel and J. M. Blocher, Jr.

Battelle Memorial Institute, Columbus, Ohio

To provide material for thin-foil work at the Argonne National Laboratory, 1-2g samples each of ductile titanium-46, -47, -48, -49, -50, and zirconium-90, -91, -92, and -94 in the form of 1-in. long rods were prepared by calcium reduction of the isotopic oxides[1] followed by two-step iodide refining. Iodide refining of titanium and zirconium is described by van Arkel (1). Information on calcium reduction of the oxides is given by Kubaschewski and Dench for TiO_2 (2) and by Lilliendahl, Gregory, and Wroughton for ZrO_2 (3).

The oxide was placed in a shallow molybdenum boat which straddled a bed of calcium chips in a horizontal cylindrical molybdenum tube provided with a tight-fitting cover. The oxide was reduced by exposure to calcium vapor overnight at 1000°C. After the resulting calcium oxide was leached out by water continuously neutralized with HCl, the crude metal powder was dried and treated again with calcium vapor for 5 hr at 1000°C. The resulting zirconium powder was heated to 900°C in vacuum to insure complete removal of excess calcium. In the case of titanium prepared similarly, it was necessary to heat the crude metal at 1300°C for 1 hr in vacuum to remove the excess calcium. Removal of the calcium is essential to prevent "tie up" of iodine as nonvolatile stable CaI_2 in subsequent iodide processing.

A small Pyrex glass van Arkel-de Boer bulb containing 0.5g of iodine and provided with two 1-in.-long 0.005-in. diameter tungsten filaments was used to refine the crude metal which was contained in the original molybdenum boat placed about 1 in. below the filaments. One filament was energized for transfer of the metal from the crude. When transfer to the first was complete (in about 4 hr), the second filament was energized and the first allowed to cool for the final transfer. A bulb (condensed TiI_4) temperature of about 135°C, a feed temperature of about 250°C, and a filament temperature of 1200°-1300°C were used for the titanium deposition. A bulb temperature of about 230°C, a feed temperature of about 300°C, and a filament temperature of 1200°-1300°C were used for zirconium deposition.

The effectiveness of the two-step refining is evident from the fact that the final products could be cold rolled directly to foil less than 0.025 mm thick while the products of the one-step process cracked in attempts to reach this thickness. The improved fabricability is consistent with the fact that hardness of the two-step products ranged from 71 to 150 KHN (50-g load), as compared with that of a previous single-step product which ranged from 250 to 350 KHN. To conserve the isotopic product it was desirable to measure hardness on the curved as-deposited surface of the crystal bar. Hence, the reported hardnesses are considered to be only indicative of the relative purity and are not directly comparable with hardness measured on flat surfaces. Hardness measurements taken on the as-deposited surface of a natural iodide titanium sample were 38% higher than those obtained on a sectioned and polished sample of the same material. The extent to which crystal orientation is a factor was not determined.

The relatively high contamination in the single-step process is attributed to a lower ratio of product weight to processing equipment surface than is normally encountered in iodide processing. The two-step process is believed to have resulted in intermediate gettering of the residual gaseous impurities in the processing bulb.

The ductility of the final product indicates low contamination by interstitial elements. The following Table compares spectrographic analyses of the one sample of titanium oxide and single-step refined titanium product for which analyses were obtained. The accuracy of the spectrographic procedure is reported to be ±50% at an impurity level

[1] Obtained from the Oak Ridge National Laboratory.

Table I. Spectrographic analysis (w/o) of titanium oxide and titanium prepared by calcium reduction and single-step iodide refining

	Si	Mg	W	Al	Cu	Ca	Zr	Fe	Mo	Sn	Ni
TiO_2	>0.1	0.03	N.D.	>0.1	0.001	0.05	0.03	0.01	0.005	0.003	<0.001
Deposited Ti as TiO_2	0.02	0.005	>0.1 (Core wire)	<0.03	0.001	0.01	<0.01	0.01	<0.001	0.003	0.002

of 0.0X w/o and ±100% at a level of 0.00X w/o.

Over-all recoveries of 70-90% of the isotopic zirconium and titanium were obtained.

Acknowledgment

The authors wish to thank Dr. Jan Yntema of Argonne National Laboratory for initiating this interesting work which was done under AEC Contract W-7405-eng-92.

Manuscript received Feb. 19, 1962.

Any discussion of this paper will appear in a Discussion Section to be published in the June 1963 JOURNAL.

REFERENCES

1. A. E. van Arkel "Reine Metalle," Julius Springer, Berlin (1939).
2. O. Kubaschewski and W. A. Dench, *J. Inst. Metals*, **82**, 87 (1953).
3. W. C. Lilliendahl, E. D. Gregory, and D. M. Wroughton, *This Journal*, **99**, 187, (1952).

A Transistorized 60 cps Sine Wave Commutator for Resistance and Potential Measurements

G. F. Pollnow[1] and Robert M. Kay

Research Division, Allis-Chalmers Manufacturing Company, Milwaukee, Wisconsin

The use of half-cell potentials in studying the nature of electrode processes is well known, and for processes at very low current densities there is usually no great experimental difficulty in making accurate measurements. However, at high current densities an error in the potential measurement is introduced by the large internal *IR* drop between the working electrodes. The *IR* drop between the reference electrode and the electrode of interest can be minimized by means of a Luggin capillary. In some systems the geometry of the cell precludes the use of a Luggin capillary; hence, a device to measure the potential of the electrode in its polarized state, but independent of the purely ohmic resistance, is desirable. A number of such mechanical and electronic current interrupters have been described in the literature (1-5), most of them operating on square waves and having the problems associated with generating such distortion-free, high-amplitude, and high-frequeincy wave forms. The present apparatus was designed primarily to obtain reliable, resistance-free terminal and half-cell potentials in connection with fuel cell research and development. In addition, the direct measurement of the ohmic voltage drop provides a convenient method of determining the resistance and the specific resistivity of the electrolyte in its working environment.

[1] Present address: Department of Chemistry, Wisconsin State College, Oshkosh, Wisconsin.

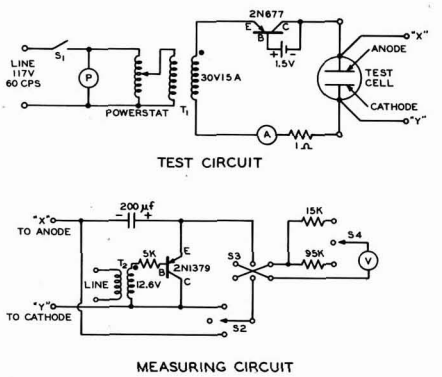

Fig. 1. Commutator circuit

Theory

The instrument described herein is a transistorized modification of a device reported by Kordesch and Marko (3) and is based on the same half-wave rectified 60 cps sine wave principle. The circuit shown in Fig. 1, however, possesses several advantages over the one previously mentioned. In particular, use of a power transistor with inverse bias in place of the diode rectifier reduces the external current at zero applied voltage from 60 ma to 25 μa when a 1.5v source of emf is under test. Second, the stability of the voltage measuring clamping circuit allows the direct measurement of the difference voltage, corresponding to the *IR* drop, to better than ± 1 mv. The bridge circuit employed by Kordesch and Marko requires zeroing before each measurement because of the aging of the bridge diodes employed and is not stable enough to measure the *IR* drop with the required precision.

Loading of the test cell is accomplished by means of the Powerstat controlled input to the transformer, T_1, whose output is rectified by the 2N677 power transistor. The bias supplied to the power transistor by the 1.5v dry cell keeps the current at zero in the load circuit until the input voltage from the transformer exceeds this voltage. Since no current is drained from the dry cell in operation, its life expectancy is sufficiently long to render uneconomic its replacement with an a-c rectifier. With the 2N677 power transistor mounted on a 3 x 4 x 1/16 in. copper heat sink, currents of 9-10 amp can be safely obtained. Greater currents can be obtained by decreasing the 1 ohm current limiting resistor and providing for the increased heat dissipation of the transistor.

Figure 2 shows the waveform of the current, I, through the cell, the voltage across the cell, V_b, the voltage across the capacitor, V_c, and the voltage across the clamping transistor, V_t, as a function of time.

As the current, I, is passed through the cell, the terminal voltage, V_b, decreases because of its inter-

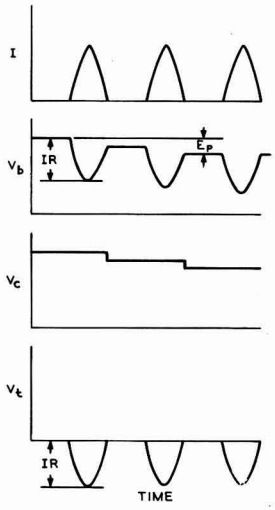

Fig. 2. Waveforms in the commutator circuit

nal ohmic resistance, R, and polarization voltage, E_p, as shown in Eq. [1]

$$V_b = E - IR - E_p \qquad [1]$$

The small filament transformer, T_2, supplies an alternating voltage to the base of the clamping transistor. When the base is negative, the emitter to collector path becomes a very low impedance. With a positive base voltage this path becomes essentially an open circuit. The voltage from T_2 is in phase with the voltage from T_1 so that the clamping transistor is conducting when the current through the test cell is zero. V_t then is zero, and the ohmic-free potential of the test cell in its polarized state is given by Eq. [2]

$$V_c = E - E_p \qquad [2]$$

On the other half cycle, current flows through the test cell and the clamping transistor becomes a very high impedance. V_c cannot change during this half cycle and so

$$V_t = E - E_p - IR - V_c = -IR \qquad [3]$$

This operation can be seen from the waveforms of Fig. 2. The open-circuit voltage E is obtained prior to loading of the cell.

In order to use the apparatus only for half-cell measurements with a calomel reference electrode, the capacitor should be reduced in size to 1-10 μf, and a high impedance voltmeter substituted for the built in meter. Half-cell measurements *vs.* a fiber type calomel electrode, with a microammeter in series, showed that even with the 200 μf capacitor the transient charging current did not exceed 20 μa and persisted for only a few seconds during the initial closing of the circuit. No permanent polarization of the calomel electrode was apparent, and once the capacitor was charged the current through the calomel electrode did not exceed 1 μa during further loading. A single pole, function selector switch, S_2, connects the internal voltmeter, V, across the capacitor, across the transistor, or permits opening the circuit to allow for an external high impedance voltmeter which for half-cell measurements is connected across the capacitor. In all cases, the four terminal method of voltage measurement is used to eliminate the IR drop due to the resistance of contacts and current carrying leads. The double-pole, double-throw switch, S_3, reverses the polarity of the 20,000 ohms/v voltmeter as required when the cell under test is changed from a source of emf to a pure resistive load. Connection of the clamping circuit leads to the test cell must be such that the correct polarity is maintained at all times on the electrolytic capacitor.

For cells having a small internal resistance a three-way range switch, S_4, to the voltmeter is provided, having positions of 0-1.0v, 0-5.0v, and one for an open circuit.

Experimental Results

A set of precision resistors were used to calibrate the commutator over the full range of the instrument. From the set of calibration curves shown in Fig. 3, it is apparent that the commutator is direct reading, well within the ±3% accuracy of the meters used to measure the current and the IR drop.

In order to demonstrate the equivalence of the commutator and the Luggin capillary when making half-cell measurements, a solution of 1M H_2SO_4: 2M CH_3OH, at 25 C° was subjected to the pulsed discharge of the commutator applied to two parallel, 1 in. by 1 in., electrodes placed 1 cm apart. Results are

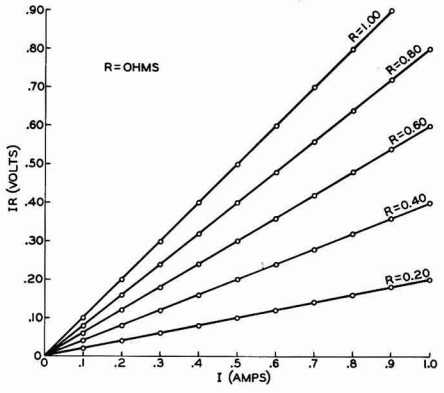

Fig. 3. Calibration of the commutator with a precision resistance box.

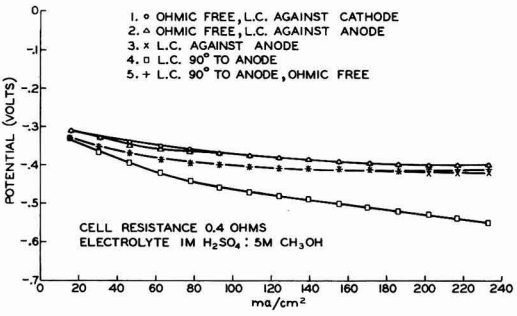

Fig. 4. Terminal and ohmic-free anode potentials vs. the saturated calomel electrode.

shown in Fig. 4. For curve 1, a Luggin capillary was first placed against the back side of the cathode while half-cell measurements, V_c, *vs.* a saturated calomel electrode were made with the VTVM across the capacitor as the current density was varied from 0 to 240 ma/cm^2. Next, the Luggin capillary was placed against the rear side of the anode and the foregoing procedure repeated to yield the data shown in curve 2.

The coincidence of curves 1 and 2 demonstrate that the half-cell potential measurements are, indeed, free of any ohmic component; however, their absolute accuracy is of course dependent on the rapidity with which the activation polarization decays.

Curves 3 and 5 demonstrate the equivalence of the Luggin capillary and the commutator with the capillary in the latter case turned through 90° away from the anode. With the Luggin capillary in this position, and the VTVM connected directly to the calomel electrode and the anode, curve 4 was obtained. It is interesting to note that the large *IR* drop shown here occurred even with the reference electrode behind the anode and clear of the field between the working electrodes. The small displacement of curves 3 and 5 from 1 and 2 is due to the change in geometry of the cell which occurred when the anode and cathode were interchanged with respect to the Luggin capillary; hence, curve 4 is to be compared to curves 3 and 5.

Conclusions

A 60 cps sine wave transistorized commutator has been constructed which measures directly, and displays on a meter, the internal ohmic *IR* drop and the ohmic-free terminal or half-cell voltage. Calibration of the instrument shows it to be direct reading within the ±3% accuracy of the meters employed. It has also been demonstrated that this device virtually eliminates the need for a Luggin capillary when making half-cell measurements on load, providing the decay time of the activation polarization is substantially less than 1/120 of a second.

Manuscript received Aug. 24, 1961; revised manuscript received Jan. 15, 1962.

Any discussion of this paper will appear in a Discussion Section to be published in the June 1963 JOURNAL.

REFERENCES

1. R. Glicksman and C. K. Morehouse, *This Journal*, **102**, 273 (1955).
2. R. A. Hickling, *Trans. Faraday Soc.*, **33**, 1540 (1937).
3. K. Kordesch and A. Marko, *This Journal*, **107**, 480 (1960).
4. W. Richeson and M. Eisenberg, *ibid.*, **107**, 642 (1960).
5. D. Staicopalous, E. Yeager, and J. Hovarka, *ibid.*, **98**, 68 (1951).

Brief Communication

Directional Thermal Expansion Coefficients of β-MnO_2

R. C. Bradt and J. S. Wiley

Research Division, Fansteel Metallurgical Corporation, North Chicago, Illinois

Directional thermal expansion coefficients of β-MnO_2 were determined over the range 25° to 500°C using high-temperature x-ray methods. This was accomplished by employing relationships between lattice constants and the angular shift of Bragg reflections (1). Thermal expansion coefficients obtained using x-ray techniques have been demonstrated to compare very favorably with those obtained by the more familiar dilatometric methods (2).

Samples were prepared by the thermal decomposition of manganous nitrate solution (J. T. Baker Reagent Grade) a well-established method of producing β-MnO_2 (3). Chemical analysis by total manganese and available oxygen determinations showed the sample to have the formula $MnO_{2.00}$ (0.04-0.09 H_2O). The samples were ground to pass a 200 mesh screen and the powder used to make an ether slurry which was painted on a platinum high-temperature sample holder for x-ray observation.

Using a G. E. Model XRD-5 diffractometer, and Fe-$K_{\alpha 1}$ radiation, observations were made in air from room temperature to 500°C, where decomposition to Mn_2O_3 prevented further data accumulation. Except for the initial observation, where total decomposition occurred, the heating and cooling observations agreed quite favorably. Data were treated using the least squares method. Figures 1 and 2 show the results.

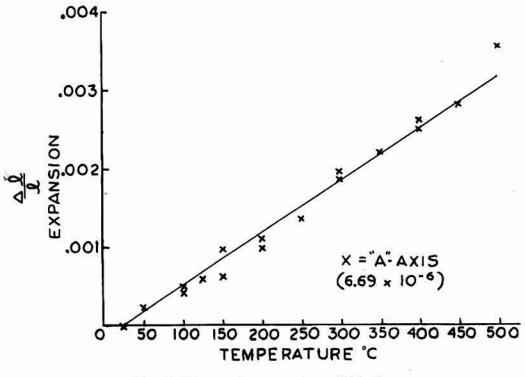

Fig. 1. Thermal expansion of MnO_2

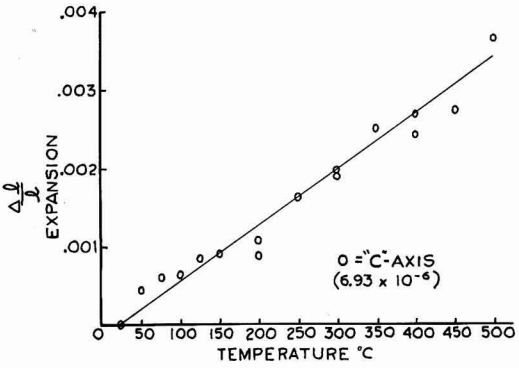

Fig. 2. Thermal expansion of MnO_2

The measurements showed that the tetragonal unit cell of β-MnO_2 has a thermal expansion coefficient of 6.69 x 10^{-6} cm/cm-°C along the "a"-axis and 6.93 x 10^{-6} cm/cm-°C along the "c"-axis over the temperature range of 25°-500°C.

Manuscript received Feb. 19, 1962.

Any discussion of this paper will appear in a Discussion Section to be published in the June 1963 JOURNAL.

REFERENCES

1. Gunji Shinoda, *Mem. Coll. Sci. Kyoto Imp. Univ.*, Series A, **16**, 193 (1933).
2. William J. Campbell, Stephan Stecura, and Clark Grain, *Report of Investigation 5738*, U. S. Dept. of the Int., Bureau of Mines (1961).
3. T. E. Moore, M. Ellis, P. W. Selwood, *J. Am. Chem. Soc.*, **72**, 856 (1950).

FUTURE MEETINGS OF
The Electrochemical Society

★ ★ ★

Boston, Mass., September 16, 17, 18, 19, and 20, 1962

Headquarters at the Statler-Hilton Hotel
Sessions will be scheduled on
Batteries (General Sessions on primary and secondary batteries, and fuel cells), Battery—Theoretical Electrochemistry Joint Symposium on Porous Electrodes, Corrosion, Corrosion—Electronics Joint Symposium on Phenomena at Interfaces, Electrodeposition (including a Symposium on Alloy Electrodeposition), Electrodeposition—Electronics Joint Symposium on Electrochemical Processes for Semiconductor Devices, Electronics—Semiconductors (including a Symposium on Semiconductor Phenomena), Electrothermics and Metallurgy (including a Symposium on Hot Pressing), Electrothermics and Metallurgy—Corrosion Joint Symposium on High-Temperature Corrosion

★ ★ ★

Pittsburgh, Pa., April 14, 15, 16, 17, and 18, 1963

Headquarters at the Penn Sheraton Hotel
Sessions probably will be scheduled on
Electric Insulation, Electronics (including Luminescence and Semiconductors), Electrothermics and Metallurgy, Industrial Electrolytics, and Theoretical Electrochemistry

★ ★ ★

New York, N. Y., September 29, 30, and October 1, 2, and 3, 1963

Headquarters at the New Yorker Hotel

★ ★ ★

Toronto, Ont., Canada, May 3, 4, 5, 6, and 7, 1964

Headquarters at the Royal York Hotel

★ ★ ★

Washington, D. C., October 11, 12, 13, 14, and 15, 1964

Headquarters at the Sheraton-Park Hotel

Papers are now being solicited for the meeting to be held in Pittsburgh, Pa., April 14, 15, 16, 17, and 18, 1963. Triplicate copies of each abstract *(not exceeding 75 words in length)* are due at Society Headquarters, 30 East 42 St., New York 17, N. Y., *not later than December 14, 1962* in order to be included in the program. *Please indicate on abstract for which Division's symposium the paper is to be scheduled, and underline the name of the author who will present the paper.* No paper will be placed on the program unless one of the authors, or a qualified person designated by the authors, has agreed to present it in person. An author who wishes his paper considered for publication in the JOURNAL should send triplicate copies of the manuscript to the Managing Editor of the JOURNAL, 30 East 42 St., New York 17, N. Y.

Presentation of a paper at a technical meeting of the Society does not guarantee publication in the JOURNAL. However, all papers so presented become the property of The Electrochemical Society, and may not be published elsewhere, either in whole or in part, unless permission for release is requested of and granted by the Editor. Papers already published elsewhere, or submitted for publication elsewhere, are not acceptable for oral presentation except on invitation by a Divisional program Chairman.

Scientific *Versus* Humanistic Thought

Presidential Address[1]

Henry B. Linford[2]

A year and a half ago in Houston, when I last gave a general address to this Society,[3] I spent my time talking about the situation in the secondary schools, devoting the bulk of that discussion to the inadequacy of the preparation of the large majority of our primary and secondary school teachers. This evening, I wish to continue my discussion of education. However, I will here spend my time not on teacher preparation but on the proper distribution of content of the curriculum. Furthermore, I will be talking about the college and university education level, rather than the primary and secondary school level.

The colleges and universities have open to the young graduate of our secondary schools the possibility of entering a liberal arts college, either an independent institution or a liberal arts college within the framework of a university. Also, there is the possibility of direct admission to a professional school, such as engineering, agriculture, home economics, *etc.* A term which I have just used more than likely needs more defining in order that we do not get caught up in an argument in semantics. I am referring to the term "liberal arts." The dictionary says that liberal arts comprises the arts, natural sciences, social sciences, and humanities. Students graduating from such a college are supposed to be prepared for a well-rounded, useful life in our modern civilization. There are, as a result, many professional schools that require a liberal arts background for admission; some of these are the law, medical, graduate business, journalism, and architectural schools. As a matter of fact, there are many that feel that, in the case of engineering, the student should have a complete four years of a liberal arts background before entering into the professional training. However, in this case, it has not been the custom to emphasize liberal arts to this extent. On the other hand, as I develop my thesis this evening you will see that, even though an independent liberal arts degree usually is not obtained, the trend in engineering education is toward more humanities and less of the so-called professional courses. There is no question that, regardless of the type of work a person intends to enter into, the need for a very strong foundation in the liberal arts in both the natural sciences and the humanities and social sciences is absolutely necessary. Herein lies my story for this evening. I am afraid that the feeling is not mutual. In other words, those working in the sciences see the need for a strong background in the humanities. I wish it also were true that those in the humanities realized the need for a strong foundation in the sciences.

To make a rough comparison as to load requirements in the two areas, I have reviewed the programs now required for graduation by three branches of Columbia University, realizing that this is not necessarily typical but certainly is indicative of the situation. Columbia College, the undergraduate liberal arts college for men, requires that 12% of the total points required for graduation be in the natural sciences and mathematics, 20% in humanities (in which, for this purpose, I have included English and languages), and 11% in the social sciences. Barnard College, the undergraduate liberal arts college for women, requires a minimum of 8% in natural sciences and mathematics, 15% in the humanities, and about 5% in the social sciences. These percentages do not add up to 100% since there are a great many free electives, and also point requirements, in the chosen major. Columbia Engineering School, on the other hand, requires 41% of the courses in natural sciences and mathematics, 22% in the humanities and social sciences lumped together, and 37% in the professional courses.

We have electives in the engineering program; however, they are not what you might call free electives. In other words, of this 22% which I have lumped together in humanities, English, languages, and social sciences, many are listed in the program as nontechnical electives and must be selected from these fields. Now, if we go back and summarize, we see that the Columbia Engineering School requires as high a percentage of the total point load to be in the nontechnical area, humanities, English, languages, and social sciences, as does Barnard College. And I might point out that this means a considerably higher total point load in these areas, since Barnard graduates the student with a minimum of 120 points, while the engineering program adds up to 142 points. In the case of Columbia College, the minimum percentages are higher in these areas but, again, the point load is not far from the same because of the fact that the College does not require as many points for graduation as the Engineering School. This is an interesting situation, where the engineers require nearly as much of the humanities, social sciences, and English as does a liberal arts college.

However, the counterpart is far from true. You will notice that 12% and 8% have been mentioned as the minimum amount of natural sciences and mathematics in the two liberal arts colleges. This does not even tell the entire story. Most of the science and mathematics departments have two types of courses, the service course and the course for the majors. Thus, the typical liberal arts student who is taking the usual two courses that are required will take the elementary introductory course which usually is taught on a strictly nonmathematical basis and, in essence, should be considered not a course in chemistry but a course *about* chemistry, or not a course in physics but a course *about* physics. This leaves us with a high percentage of our total population woefully unprepared in the field of science.

Why has this situation been allowed to develop? I am afraid it is because people will follow the path of least resistance. We have here, I believe, a situation that stems back to our elementary school system. About a year and a half ago, the American Mathematical Association went on record as favoring a much stronger preparation in

[1] Delivered at the Los Angeles Meeting, May 8, 1962.

[2] Professor of Chemical Engineering, Columbia University, New York City.

[3] Acheson Medal Address, October 11, 1960 [*see This Journal*, **108**, 7C (1961)].

mathematics for primary school teachers. They pointed out that in their day-to-day teaching the teachers will be devoting about 1/4 to 1/3 of their time to mathematics. The Association was making a plea for a higher proportion of the course work in the teacher-training program to be taken in mathematics. Too high a percentage of the teachers do not take any mathematics courses in college. One reason given for the plea was that a teacher who is insecure in the field and is just trying to keep ahead of the class is a teacher who will instill fear of the subject in the students. I believe that, by greatly increasing the competence of the teachers in the field of mathematics, we could dispel the fear of mathematics in our young people. This would allow us to start applying mathematics at a much earlier age and would, therefore, allow the two courses that are typically required in the liberal arts program to be taught on a firm mathematical basis, so that the student would have a real appreciation for the scientific approach at the time of graduation from the liberal arts college, regardless of his major.

Returning to the matter of special service courses, you don't find English departments giving English literature courses as watered-down service courses. You don't find the social science departments giving such courses as sociology at two levels. Why, then, should we countenance slovenly educational procedures when we are dealing with the natural sciences? Is it because we want to graduate a group of young people, and put the stamp of the university on them, knowing full well that their education has been only partly completed? I do not think this is a real intent but, in effect, this is what has been done and what is being done. What I am pleading for here is the application of uniform rules right across the board in liberal arts.

The matter of the technical competence of the general public has been the subject of considerable controversy of late. Sir Charles P. Snow of England has written very strongly on this point. As a matter of fact, he maintains that a person who does not understand the second law of thermodynamics is no more educated than one who has not read Shakespeare. This may be an exaggeration—but I am guilty of the same thing myself since I like to make a point by exaggeration. At the same time, there is a need for the general public to be aware of science so as to be able to think using scientific methods.

In this regard, I would like to quote from a recent speech by Dean Ralph A. Morgen of the School of Graduate Studies of Stevens Institute of Technology. He said, "If a person does not understand what he reads on the front page of the daily newspaper, he is uneducated." He further said, "Every person should know enough physics, chemistry, and biology to understand everything pertaining to those subjects appearing in his newspaper. Each specialist is going to have to know how to talk to the other man. If we can't talk among ourselves, how are we going to be able to talk between nations?"

A very serious aspect of this situation was brought forcefully to mind a few years back. I had for years commuted to New York City in a "car pool" and, each morning as I waited for the car to drive up, I would sit in the living room. At that time, Dave Garroway was "M.C.-ing" a morning television show of news, weather, and interviews. This particular morning, fortunately, the car pool was a little bit late. Mr. Garroway was interviewing one of our U. S. Senators. The Senator was chairman of a committee to study the needs of legislation regarding the use of outer space. I might add that this was soon after the first Russian Sputnik was launched and, as I remember it, we had just sent our first satellite into orbit. This, also, was about the time of the U-2 incident. The Senator described the problem thusly: "If you own a piece of property, you of course control the air just above the land, but you do not have to go up many hundred feet before you have lost your legal claim to that air space. However, the Federal Government does control the use of this air space, but there must be some point at which even the Federal Government loses control." With Sputniks flying overhead, was Russia violating our air space? This question has not been brought up in reality. The Senator said that, in studying the problem, it was very difficult to determine exactly where you would say the Government had lost dominion. He added that very likely this point would be specified as the place where gravity of the earth no longer exerted any pull! I might say that Mr. Garroway tried very desperately, three times, to get the Senator to revise the statement, making some technical sense out of it, but, no, it was obvious that the Senator, who was responsible for legislation in this area, did not realize that the Sputniks were in free fall and had no conception as to what free fall meant. I am positive that the concept that the force of gravity never drops to zero was the furthest thing from his mind. To me, this is a frightening situation. It is one that we will have to live with until we are able to convince the nonscientist that he should not consider himself educated as long as he cannot understand science.

There obviously are two sides to this question and, in this regard, I wish to quote from a recent article printed in the *New York Times Magazine Section*. The article was written by a professor of philosophy at Yale. The title is " 'Hamlet' *vs.* the Laws of Thermodynamics." The subhead line is "In this Scientific Age, is it More Science We Need? Or, as this Author Contends, Are the Humanities Still Indispensable to the Educated Man and Citizen?" He tears to pieces Sir Charles P. Snow's little book "The Two Cultures," contending that a humanistic education is superior to a scientific education, superior to it in preparation of the individual for living and working in our current society. If I might quote a bit from the aforementioned article, I think that I will be able to make my point. It said, "Well, what is the sort of thinking we shall have to do? It is the thinking necessary to be a good citizen, the good neighbor, the good father or mother of a family, the competent man of affairs, the supporter of sound causes generally, the person with sensitive allergies for political hocum, specious advertising, religious superstition, class and race tension, and lopsided partisanship in all its fifty-seven varieties.

"In this kind of thinking the difficulties are less logical than psychological. The main one is to stick to the path of reasonableness through a fog of passion, pride, and prejudice, to thread one's way through a thicket of likes and dislikes, callow enthusiasms, dubious authorities, and distorting complexes.

"Now the thinking of physical science is not this kind of thinking, nor does practice in its clear air necessarily help us much in the murky ways of common life. The physical laboratory is disinfected of emotion; among its equations are no personal equations; its atmosphere is air-conditioned to exclude the mist and miasma that surround us in the house and on the street. The scientist seeking to verify or amend Ohm's law may have to struggle against his own slowness and thickness of wit, but he does not noticeably have to struggle with superstitution. Ohm's law is either true or false; emotionally it does not matter which; why be hot about it."

If I may skip a little bit, and we go on and pick up the thought, we see that he continued, "The best training in objectivity lies in fields where there is some temptation to subjectivity, just as the best training in clearness of thought lies in those fields where clearness has to be

achieved by you and is not waiting for you ready-made. That is the difficulty with mathematics as an educational discipline. I admire, at a great distance, the skill of the mathematician in manipulating his symbols according to his recondite rules, just as I admire the astonishing gift of young Bobby Fischer for manipulating the men on a chess board. But, I confess to some disquietude when I learn how much of this sort of 'thinking' can be done more surely and swiftly, by machines." I think that this philosopher has indicated quite clearly that he does not appreciate the scientific method. He is looking at it from a distance and, I might add, from an uneducated distance, from which all he sees is the finished product, the finished product of the thinking of the scientist. Does he think that science developed without superstition? Surely he knows history better than this. Does he think that science and scientific experimentation are without human frailty? The human factor enters into all but a very few of our scientific developments. And, then, the closing comment that the mathematical thinking is now being done by machines is the final proof of his own incomplete education of exactly the type that I have been discussing this evening. Anyone familiar with machine calculations knows that machines only follow directions and are capable only of doing just what they are told to do. It is a shame that such individuals as the author of the above-quoted article currently are responsible for the training of our young people, and apparently with the support of the others with like training.

We should stop and ask ourselves, why are we interested in education? What purpose should education serve? The purist would have nothing taught that could be used directly. However, I think that all are agreed that education should fit an individual to live in our modern civilization. Granted, at the time that our university system was being born, scientific knowledge was in very ill repute, scientists were for the most part alchemists or their counterpart, and it was not until the beginning of the 19th Century that it became a part of our educational program. I know that Columbia University started as Kings College in 1754, but it was not until 1864 that the School of Mines was started, and it was in this school that physics, chemistry, geology, and all of the engineering first got its start in the university. I am sure that this background is one of the real reasons for the down-grading of science, and the feeling that the scientific method is inferior to the humanistic method. However, whether we want it or not, we are living in a scientific age. And, if we want our children to end up ignorant of what is going on about them, then we can continue to foster the programs of the past. Isn't it better that we prepare ourselves for this (scientific) way of life even from the point of view of just day-to-day living. If our average population had a moderate amount of scientific background, many of the fraudulent devices and chemicals that now are being sold, and sold at a good profit, with government blessings in this country could not even get a foothold.

I am speaking of the celebrated case of the battery additive. I call it a scandal because it was pure fraud. How could it be perpetrated?—simply because our politicians are ignorant of science. As a result, they are subject to pressures which they cannot withstand because they don't know enough. These pressures are exerted by small businessmen who are attempting to hoodwink the public and make a nefarious dollar. The case of special corrosion prevention devices, I think, is worthy of note in the same regard. Allow me to read from the advertising brochure of one such company: "The ——— Water Conditioner is the first important application of nuclear physics principles to the effective treatment of water to combat scale and corrosion. It prevents scale and corrosion by imparting added energy to the atoms of the water solution. This energy changes the outer orbit electrons of the atoms of dissolved minerals and salts so that the molecules which the atoms form cannot build scale but are kept in suspension within the system or are precipitated as a drainable mud. The added energy at the same time establishes a uniform electrolytic potential within the system and stops corrosion.

"In actual operation, the water that flows through the Conditioner is passed through a series of alternating fields of static energy. The effect is to cause an intramolecular disruption, at the same time adding kinetic energy to the electrons in the outer orbits of the atoms.

"Construction.—The ——— Water Conditioner is built in two (2) sections.

"A. Dispersing Cell.

"The dispersing cell contains the 'Perma-Core,' a kinetic energy generator made of a patented metal of extreme density whose energy shows itself in alternating fields of unusual magnetic intensity.

"The 'Perma-Core' is a permanent well of static energy. This energy force modifies the structure of the molecules of minerals and salts in the water as described above.

"The 'Perma-Core' requires neither supervision nor control and is practically everlasting. It needs no regeneration. There are no moving parts.

"B. Homogenizing Chamber.

"The homogenizing or mixing chamber is an alloy casting containing a core against which the flow of water is directed in such a way that the water is tumbled upon itself to produce a homogeneous energy distribution within the molecules of the solution."

In that short bit, there is more scientific double talk than you can shake a stick at. I do not think it needs any further discussion than to say that a metallic casting which acts as a kinetic energy generator, but is everlasting, needing no supervision and no regeneration, is obviously a fraud. Yet, this company is in business. I maintain that, if our average American citizen had only a moderate scientific background, such frauds as this would never even have been attempted. It would be difficult to attain this level of competence on the part of the general public since, apparently from time immemorial, we have been gullible. Our only hope is to raise the intellectual scientific competence of the general public. In this same regard, it should be pointed out that one of the most difficult tasks a teacher has is to dispel from the student's mind the thought that "just because it is in print it must be right." It is this feeling that these companies that I have just been talking about are working on. They feel that if they produce these brochures they will get to believe them, and soon the general public will get to believe them. How else could they be printed?

Our real hope for the future of this country is the development of a citizenry capable of clear, concise thinking. I know of no better medium for teaching such thinking than the physical sciences with a mathematical basis. A better appreciation for the scientific method of thinking, rather than a detailed knowledge of science, is what I would instill in the liberal arts student. We must, however, make sure that the education be complete and see to it that we not only have a good mathematical science background but also that we continue to instill the humanities in the hopes that man can continue to grow, develop, and eventually learn to live peacefully with his neighbor.

WARNING

The deadline, July 31, for receipt of articles for the first two issues of the new magazine of the Society to be named

ELECTROCHEMICAL TECHNOLOGY

is rapidly approaching.

Authors who wish to have their papers considered for these issues should send their manuscripts (three copies, double-spaced) promptly to

The Editor
ELECTROCHEMICAL TECHNOLOGY
The Electrochemical Society, Inc.
30 East 42 Street
New York 17, N. Y.

in accordance with the notice on page 168C of this issue.

Papers also are needed for subsequent issues. Act now and enjoy the unique distinction of becoming one of the first-volume authors.

Charles L. Faust Selected 1962 Acheson Medalist

Charles L. Faust, head of the Electrochemical Engineering Division of Battelle Memorial Institute, Columbus, Ohio, has been chosen as the 17th recipient of the Edward Goodrich Acheson Medal and Prize of The Electrochemical Society. Presentation of the award will be made at the banquet to be held during the 122nd Meeting of the Society in Boston, Mass., at the Statler-Hilton Hotel, September 16-20, 1962.

The award, a gold medal and $1000 prize, is made every two years for conspicuous "contribution to the advancement of the objects, purposes, or activities" of the Society.

Dr. Faust attended Washington University, receiving his B.S. degree in chemical engineering in 1930 and his M.S. degree in chemistry in 1931. He received the Ph.D. degree in chemical engineering from the University of Minnesota in 1934. In that same year, he joined Battelle Memorial Institute as a research technologist carrying on studies in electrochemistry; he has been head of the Electrochemical Engineering Division since 1945. An originator of many concepts, he has inspired his colleagues in the initiation and development of new and sound ideas. Both the creativity and effective following through on ideas, which have been characteristic of his leadership, have served to make him a key figure in the growth of electrochemical research at the Institute.

In the field of research, Dr. Faust has built up an imposing record of accomplishment. The studies in which he has participated and which he has directed have contributed both to basic knowledge and to industrial progress. His broad research interest encompass electrorefining; electrowinning; electrolysis; electroforming; electroplating; electropolishing and electroshaping; battery technology; aqueous, fused, and organic electrolytes; and other electroprocesses. He has led in the pioneering development of commercial processes for the electrodeposition of alloys, electropolishing, and electroshaping.

Charles L. Faust

Among studies relating to basic problems should be listed the research on the mechanisms by which hydrogen enters metals. Recently, too, Dr. Faust has been responsible for recognizing and disclosing the significance of metal surface properties and characteristics in metallurgical processes. Through the years, he and his colleagues have utilized new and often unconventional methods for electroplating metals which were previously impossible to plate.

The practical effectiveness of his research is demonstrated by the 135 patents that bear his name. The prodigious activity disclosed by his record of patents is also reflected in Dr. Faust's writings. He has been author and coauthor of more than 60 articles and papers and has contributed chapters to eight technical books.

Dr. Faust's interests also include editorial duties. He served as Associate Editor of the ECS monograph "Modern Electroplating" and is also a member of the Editorial Staff for the edition now being revised. He was Associate Editor of "Electroplating Engineering Handbook" in 1955 and of the *Monthly Review* of the American Electroplaters' Society (later *Plating*) in 1942-1949. At present, he is Section Editor for *Chemical Abstracts*, Electrochemistry, Section 4. Also, at present he is Chairman of the ECS Publication Committee.

During and since World War II, Dr. Faust served almost continuously on the War Metallurgy Committee. He also served on committees of the Materials Advisory Board of the National Academy of Sciences as a member of Panels on Selenium, Gun Liner Materials, and the New Processes for Machining and Grinding. Recently, he also served as research referee for the National Academy of Sciences, National Research Council Committee Advisory to the Office of Ordnance Research for the Army. He was among those who received the Manhattan special award authorized by the War Department in recognition of individual contribution to the atomic bomb program, awarded in 1946. In 1961, Dr. Faust received the Scientific Achievement Award of the American Electroplaters' Society, which is their highest honor.

Dr. Faust's many years of service (since 1938) to The Electrochemical Society, in many capacities, reflect an exceptionally high degree of dedication and devotion to its welfare. He was President in 1950-1951 and Vice-President in 1947-1949. He also served as Chairman of the Electrodeposition Division in 1942, member of the Board of Directors as Manager 1943-1945, member of the Publication Committee in 1944, member of the Ways and Means Committee 1946-1959 (Chairman in 1951), Acheson Award Committee (Chairman 1946), Nominating Committee (Chairman 1958), and Honors and Awards Committee (Chairman 1960). He was General Chairman of the Columbus Conventions of 1948 and 1959. From 1960 to the present, he has been Chairman of the Publication Committee, which currently is directing the Society's expanded publication program.

Boston Meeting of The Electrochemical Society, September 16-20, 1962

Skyline of the Charles River—From the first warm days of spring, the Charles River is a mecca for small sailing craft, Harvard "shells," and a few yachts of considerable size. From Cambridge, across the Charles, this "Student's View" highlights the contrast of Boston, "City of Yesterday and Tomorrow." The modern John Hancock Mutual Life Insurance Co. Building towers above early 19th Century church steeples of the Back Bay.

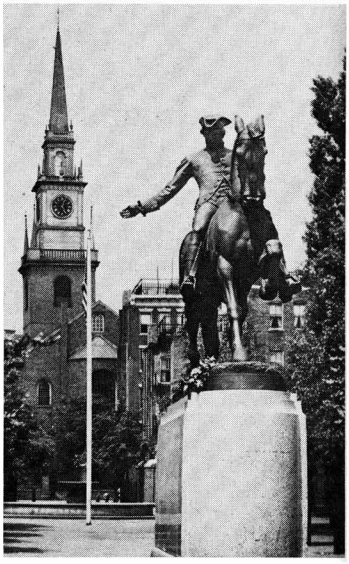

Paul Revere Mall—A statue of Paul Revere graces the small park known as Paul Revere Mall. The historic Old North Church, Boston's oldest church edifice, is in the background. It was in the steeple of this church that the lanterns were hung to signal the start of Paul Revere's famous Ride.

From September 16 through September 20, the Fall Meeting of The Electrochemical Society will be held in Boston, Mass., at the Statler-Hilton Hotel under the General Chairmanship of Horace H. Homer. Other Committee Chairman are:

H. H. Homer

Paul T. Woodberry—Hotel Arrangements, Emerson H. Newton—Entertainment, Frank C. Benner—Plant Trips, Richard A. Peak—Registration, Mrs. Harry C. Gatos—Ladies' Program, Charles W. Jerome—Vice-Chairman, Charles Levy—Treasurer, Paul L. Raymond—Secretary.

Some of the high lights of the meeting will include the real old New England Clam Bake to be held Wednesday, September 19, at historic Plymouth, Mass. This is a must for anyone who has never participated in such a gourmet's treat, and will be an affair never to be forgotten. High light of the Ladies' Program will be a guided tour conducted at the Museum of Fine Arts, showing historic and cultural sights of greater Boston, climaxed by a private luncheon at the Museum itself. Plant trips of the larger industrial and research communities, including Western Electric in North Andover, Avco Research & Development in Wilmington, and High Voltage Engineering in Burlington, have been arranged. Others will be added to the program by convention time.

On Tuesday evening, September 18, there will be a Reception and Banquet in honor of Dr. Charles L. Faust, the recipient of the Society's 1962 Edward Goodrich Acheson Gold Medal and Prize. Dr. Faust will deliver the Acheson Medal Address. Another speaker will be Dr. Gordon S. Brown, Dean of Engineering at Massachusetts Institute of Technology, who will talk on the problems of education.

There is no finer climate anywhere in the world than in New England during the month of September. Here the days are crisp and bright, the weather is sparkling, and the nights are pleasant and cool. Boston abounds with thousands of points of interest, historically, culturally, educationally, and technically. It is the birthplace of liberty, and has many historic shrines and points of interest. The famous Freedom Trail provides an opportunity to view many of the historic sights in and around Boston, including Boston Common, the State House, Park Street Church, Kings Chapel, the birthplace of Benjamin Franklin, The Boston Massacre, Old Faneuil Hall, Paul Revere House, The Old North Church, Old Ironsides, Bunker Hill Monument, and many others. In addition, the suburbs of Boston provide additional historic shrines in places such as Plymouth, Salem, Marblehead, Cambridge, Lexington and Concord, Rockport, Gloucester, Sudbury, and many, many others.

Boston is famous for sea food. First, as the country's largest fish-shipping port, it can choose the "best of the catch" that the cold flavor-heightened North Atlantic waters yield. Second, by making use of the old-fashioned Yankee cooking and "handed-down" recipes, Boston restaurants have developed many

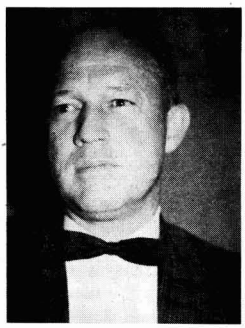
P. T. Woodberry

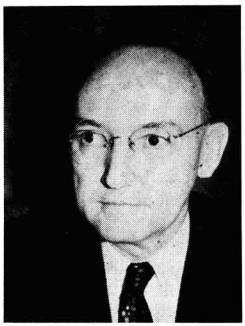
E. H. Newton

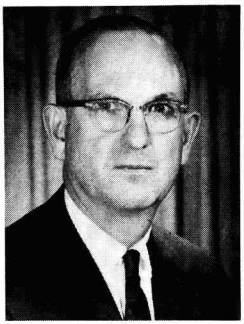
F. C. Benner

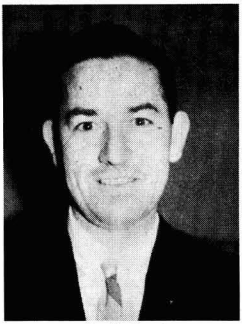
R. A. Peak


Mrs. H. C. Gatos


C. W. Jerome

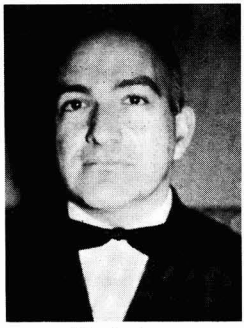
Charles Levy

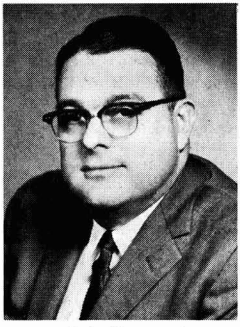
P. L. Raymond

distinctive and taste-thrilling ways of preparing lobster, shellfish, and saltwater fish dishes.

Boston is also one of the cultural centers of America, with its 200 universities, colleges, and schools, including Boston University, Harvard, Massachusetts Institute of Technology, Boston College, Radcliffe, Wellesley, Tufts University, the New England Conservatory of Music, Northeastern University, Massachusetts School of Art. In addition, there is the Boston Public Library, Symphony Hall, home of the world-renowned Boston Symphony Orchestra. The Boston Museum of Fine Arts will be the center of one of the activities for the ladies.

On the lighter side, Boston has several summer stock theaters which will be concluding their programs during the week of the convention. In addition, there is ample evening entertainment at many hotels and night clubs. All in all, between the convention and Boston's congenial hospitality, the September meeting is bound to be one you will never forget.

The complete program for the Boston Meeting, including general information and 75-word abstracts of papers to be presented at the technical sessions, will be be published in the August issue of the JOURNAL.

Manuscripts and Abstracts for Spring 1963 Meeting

Papers are now being solicited for the Spring Meeting of the Society, to be held at the Penn Sheraton Hotel in Pittsburgh, Pa., April 14, 15, 16, 17, and 18, 1963. Technical sessions probably will be scheduled on: Electric Insulation, Electronics (including Luminescence and Semiconductors), Electrothermics and Metallurgy, Industrial Electrolytics, and Theoretical Electrochemistry.

To be considered for this meeting, triplicate copies of abstracts (*not exceeding 75 words in length*) must be received at Society Headquarters, 30 East 42 St., New York 17, N. Y., *not later than December 14, 1962. Please indicate on abstract for which Division's symposium the paper is to be scheduled, and underline the name of the author who will present the paper.* No paper will be placed on the program unless one of the authors, or a qualified person designated by the authors, has agreed to present it in person. An author who wishes his paper considered for publication in the JOURNAL should send triplicate copies of the manuscript to the Managing Editor of the JOURNAL, 30 East 42 St., New York 17, N. Y.

Presentation of a paper at a technical meeting of the Society does not guarantee publication in the JOURNAL. However, all papers so presented become the property of The Electrochemical Society, and may not be published elsewhere, either in whole or in part, unless permission for release is requested of and granted by the Editor. Papers already published elsewhere, or submitted for publication elsewhere, are not acceptable for oral presentation except on invitation by a Divisional program Chairman.

Annual Report of the Board of Directors, April 1, 1961-March 31, 1962

(Presented at Society Business Meeting, Los Angeles, May 7, 1962)

Your Board of Directors has the following matters of special interest to bring to the attention of members at this time.

New Magazine

There long has been a generally recognized need for the publication of a new magazine covering electroprocesses in areas of engineering, technology, design, economics, and appropriate reviews. The Publication Committee has studied this matter in a comprehensive manner and the Board of Directors approved of its recommendation that such a magazine be published on a bimonthly basis beginning in 1963. It will be changed to a monthly periodical as soon as sufficient papers are received to justify such a move.

It is felt that this new magazine will complement the present JOURNAL and will enable the Society to offer a more comprehensive publication program and thus contribute to its future growth and development. A. C. Loonam will serve as Editor and Natalie T. Michalski as Managing Editor.

Extended Abstract Booklets

On recommendation of the Publication Committee, the Board of Directors also approved of publishing Extended Abstract Booklets of papers presented each year at our two National Meetings. These booklets will contain abstracts of 500-1000 words each. It is expected that this program will be instituted at our 1963 Spring Meeting.

Publication Committee

In view of its expanded activities, the personnel of our Publication Committee has been enlarged and appropriate amendments to our Bylaws have been approved by the Board of Directors to provide for its increased activities.

Technical Committee

The appointment of a Technical Committee has been provided for by appropriate amendments to our Bylaws. It is apparent from a survey made that there is need for consultation and coordination of effort on the part of our various Divisions in planning future symposia at our National Meetings.

The personnel of the Committee will be composed of the Chairmen of our various Divisions, the Secretary, and one of our Vice-Presidents who will act as Chairman of the Committee. Periodic meetings will be held when future symposia will be considered and, where there is a mutuality of interest evidenced, joint Divisional sponsorship will ensue. It is hoped in this way to make our National Meetings of greater interest and value.

F. M. Becket Memorial Award

Revised Rules for the F. M. Becket Memorial Award were approved and the first award of this nature will be made this year [*see* Division News, May 1962 JOURNAL, pg. 135C].

Summer Fellowship Awards

On recommendation of the Honors and Awards Committee, the Board again approved of the awarding of three Summer Fellowship Awards for 1962. [Details will appear in a later issue of the JOURNAL.]

Model Bylaws for Divisions

On the recommendation of a special committee, a draft of Model Bylaws for Divisions was approved. Previously, the draft of Model Bylaws for Local Sections was also approved.

Guide for Division and Section Awards

Similarly, on recommendation of the Honors and Awards Committee, the Board approved of a Guide for Division and Section Awards which it is felt will be helpful to all concerned.

1961 Palladium Medal Award

On recommendation of the Palladium Medal Award Committee, the 1961 Palladium Medal was awarded to Professor H. H. Uhlig at our Detroit Meeting.

Prize Essay Contest

An effort was made to determine whether interest could be revived in the Prize Essay Contest which was initiated some years ago. Our renewed efforts in this regard still indicate a lack of interest.

Voting by Proxy by Board Members

Advice of counsel reveals that Article VI, Section 6, of the Constitution, which permits members of the Board of Directors to appoint proxies to represent them at Board Meetings, is unconstitutional because of a prohibition against this practice in the Membership Corporations Law of State of New York. Accordingly, this provision in our Constitution is being eliminated.

Papers Solicited for New ECS Magazine to be Published in 1963

As announced in the February issue of the JOURNAL (page 37C), The Electrochemical Society will publish a new magazine to be named **Electrochemical Technology.** The first issue will be published in January-February 1963. Initially, the new publication will be issued bimonthly. It will become a monthly publication as soon as enough papers are received to justify such a step.

Electrochemical Technology will cover electroprocesses in areas of technology, engineering, design, devices, economics, and appropriate reviews. The same review procedures which apply to the present JOURNAL will also obtain with regard to the new magazine.

A. C. Loonam, Editor, is now soliciting papers for publication in **Electrochemical Technology.** All members and others concerned, who are engaged in the applied areas of electroprocesses, who can submit papers on timely subjects are urged to do so as soon as possible.

Triplicate copies of each manuscript, prepared in accordance with the Instructions to Authors of Papers published on pp. 131C-132C of the May JOURNAL, should be submitted to the Editor, **Electrochemical Technology,** The Electrochemical Society, Inc., **30 East 42 St., New York 17, N. Y.**

Manuscripts so submitted become the property of The Electrochemical Society and may not be published elsewhere, in whole or in part, unless permission is requested of and granted by the Editor.

Second International Conference on Passivity

The Second International Conference on Passivity will be held in Canada during the first week of September 1962. Papers presented at this meeting will be published in a special additional issue of the JOURNAL.

New Society Offices

In view of our expanded publication program and increased activity in other areas, the staff at our National Office is being expanded and new office space has been leased at 30 East 42 St., New York, for our new Society Headquarters. We hope that as many members as possible will visit our new offices when they come to New York.

Henry B. Linford, *President*

Annual Report of the Secretary, April 1, 1961-March 31, 1962

(Presented at Society Business Meeting, Los Angeles, May 7, 1962)

It is a pleasure to review the progress which has been made by your Society for the past fiscal year ending March 31, 1962.

Membership

The membership of the Society is at an all-time high of 3443 members. This compares with the previous year's total of 3333 and shows a net increase of 110.

Patron and Sustaining Memberships

Corporate support in the form of Sustaining Memberships showed a net increase of 4, which totals 149 as of March 31, 1962. Patron Memberships remain the same at 5.

Journal of the Society

The JOURNAL continues to experience continued growth, and budget appropriations are adequate to provide funds for the prompt printing of all papers which have passed our review procedures and have been accepted for publication.

Monographs and Special Publications

During the year, the publication of "Electrode Processes," covering papers presented at our Philadelphia Meeting, and the monograph "Metal Iodides and Iodide Metals" came off the press. Others previously approved, and now in various stages of publication, include: "Primary Batteries," "Alkaline Storage Batteries," "Ultrafine Particles," "Iron Ores," "Rhenium," "Modern Electroplating," and "High-Temperature Technology."

In lieu of publishing a complete new edition of the "Corrosion Handbook," it has been decided that it will be more practical to publish separate volumes on various aspects of corrosion. Twelve or more such books are contemplated.

F. M. Becket Memorial Award

Robert E. Johnson of the Montana School of Mines has been selected as the first recipient of the F. M. Becket Memorial Award [*see* Division News, May 1962 JOURNAL, pg. 135C]. Arrangements have been made with Dr. Carl Wagner of the Max-Planck-Institut für Physikalische Chemie, Göttingen, Germany, for Mr. Johnson to continue his studies there during the summer of 1962. This is a biennial award.

Summer Fellowship Awards

During the summer of 1961, the Society made three Summer Fellowship Awards in the amount of $800 each. The recipients were: Ronald L. Brubaker, Princeton University (Edward Weston Fellowship); Robert E. Visco, University of Illinois; Michael J. Schaer, Oregon State University. These students were selected from institutions in the East, Midwest, and Pacific Coast.

The awards will be made again during the summer of 1962, and one will be designated as the Edward Weston Summer Fellowship and another the Colin Garfield Fink Summer Fellowship.

These awards are made possible from income from investments in the Society's Consolidated Fellowship Fund and Edward Weston Fellowship Fund.

Honorary Members

By action of the Board of Directors, Oliver W. Storey and Stanislaus Skowronski have been elected Honorary Members of the Society.

Young Author's Prize

A. C. Makrides was selected as the Young Author's Prize Winner for 1960 in recognition of his paper "Dissolution of Iron in Sulfuric Acid and Ferric Sulfate Solutions" which was published in the November 1960 issue of the JOURNAL.

The winner of the 1961 prize will be announced at our Banquet on Tuesday evening, May 8. [Details will appear in a later issue of the JOURNAL.]

Francis Mills Turner Memorial Award

This award for 1960 was shared by R. E. Meyer and P. C. Milner: R. E. Meyer for his paper "Cathodic Processes on Passive Zirconium" which appeared in the October 1960 JOURNAL, and P. C. Milner for his paper "Interpretation of Measurements of Potential Decay on Open Circuit" which appeared in the April 1960 JOURNAL.

The winner of the 1961 award will be announced at our Banquet on Tuesday evening, May 8. [Details will appear in a later issue of the JOURNAL.]

Constitutional Amendments

Amendments to the Constitution of the Society, which were presented in detail and approved at our last Annual Meeting, were ratified by mail vote of the membership as required by our procedures. There were 1038 valid ballots cast as follows: Article VI—Approved 1036, Disapproved 2, Total 1038; Article VII—Approved 1002, Disapproved 35, No Vote 1, Total 1038; Article X—Approved 1022, Disapproved 16, Total 1038.

Ivor E. Campbell, *Secretary*

Notice to Members and Subscribers

(Re Changes of Address)

To insure receipt of each issue of the JOURNAL, please be sure to give us your old address, as well as your new one, when you move. Our records are filed by states and cities, not by individual names. The Post Office does not forward magazines.

We should have this information *by the 16th of the month* to avoid delays in receipt of the next issue.

Financial Statement of The Electrochemical Society, Inc.

Statement of Income and Expenses
April 1, 1961-March 30, 1962

	Budget	General Fund	Society Reserve Fund
Income			
Membership Dues	$ 55,700	$ 61,462.02	
Patron and Sustaining Memberships	25,500	24,102.50	
Reprints	5,000	5,159.22	
Nonmember Journal Subscriptions	34,000	44,546.40	
Office Sale Journal and Publications	500	754.66	
Advertising	9,000	8,743.63	
Bound Volumes	3,000	2,311.00	
Conventions	16,900	15,193.77	
Interest Earned on General Funds	800	1,076.73	
	$150,400	$163,349.93	
Nonmember Journal Subscriptions	5,100		$ 5,956.20
Nonmember Convention Registration Fees	3,400		2,646.00
Monograph Royalties	3,000		2,516.44
Income From Investments	4,000		6,341.21
	15,500	17,459.85	$ 17,459.85
	$165,900	$180,809.78	
Expenses			
Print and Mail Journal	$ 60,000	$ 59,510.05	
Salaries	65,500	63,232.12	
Rent	5,400	5,400.00	
Postage, Supplies, and Miscellaneous	8,000	9,434.21	
Bound Volumes	3,000	4,055.03	
Local Sections and Divisions	2,000	1,623.00	
Membership Directory	600	1,165.40	
Young Author's Prize	100	100.00	
New York Office Travel	3,000	1,440.21	
Presidential Office Fund	2,000	1,595.35	
Conventions: Program Booklets	2,000	2,231.09	
Materials, Supplies, and Postage	1,000	2,369.30	
	$152,600	$152,155.76	
Contingency Fund — 1% Estimated Income	1,500		
	$154,100		
Excess Income Over Expenses General Fund	—3,700	11,194.17	
Income Credited to Society Reserve Fund	15,500	17,459.85	
Total Excess Income Over Expenses	$ 11,800	$ 28,654.02	

Balance Sheet at March 30, 1962
Statement of Assets

Cash		
Chemical Bank New York Trust Company		
Electronics Division Monograph Fund	$ 587.97	
Corrosion Division Monograph Fund	1,953.43	
Electrodeposition Division Monograph Fund	1,161.19	
Electrothermics & Metallurgy Division Monograph Fund	534.48	
Theoretical Division Monograph Fund	2,191.95	
New Capital Equipment Fund	915.98	
Colin Garfield Fink Fellowship Fund	1,818.02	
Consolidated Fellowship Fund	1,601.98	
Society Reserve Fund	14,883.46	
General Fund	26,879.93	$ 52,528.39
Petty Cash Fund	36.20	
Excelsior Savings Bank— General Fund	9,706.32	
Greenwich Savings Bank— General Fund	9,299.86	
Chase Manhattan Bank Savings Account— General Fund	18,784.00	
First National City Bank Savings Account— General Fund	10,190.19	48,016.57
		$100,544.96
Investments		
Edward Goodrich Acheson Fund Securities	$ 40,114.25	
Savings Account	1,896.74	42,010.99
F. M. Becket Memorial Award Fund Securities	$ 21,941.50	
Savings Account	1,436.07	23,377.57
Consolidated Fellowship Fund Securities		44,312.75
Colin Fink Fellowship Fund Securities		3,386.29
Joseph W. Richards Memorial Fund Savings Bank Account		861.67
Edward Weston Fellowship Fund Securities	16,281.78	

Manufacturers Hanover Bank	525.83	16,807.61	
General Portfolio of Investments			
Corrosion Division:			
Corrosion Handbook	19,935.88		
Other Equity	260.00		
Electrodeposition Division	1,000.00		
Electrothermics & Metallurgy Division	4,000.00		
Society Reserve Fund	144,007.05	169,202.93	299,959.81

Other Assets

Convention Advance		1,000.00	
Accounts Receivable		4,255.90	
Furniture and Fixtures	13,450.00		
Less Reserve for Depreciation	1,048.86	12,407.14	
Inventory		4,489.70	
Rent Prepaid		1,241.67	23,388.41
			$423,893.18

Statement of Liabilities and Surpluses

Liabilities

Unearned Income (10-Year Index)	$ 4,978.76	
Accounts Payable	101.35	
Overseas Subscriptions Payable (DBG—Faraday)	1,642.70	
Life Memberships	2,154.80	
Federal and State Taxes Withheld	2,097.56	$ 10,975.17

Surpluses

Special Funds			
Edward Goodrich Acheson Fund	42,010.99		
F. M. Becket Memorial Award Fund	23,377.57		
Consolidated Fellowship Fund	45,914.73		
Colin Fink Fellowship Fund	5,204.31		
Joseph W. Richards Memorial Fund	861.67		
Edward Weston Fellowship Fund	16,807.61	134,176.88	
Division Monograph Funds			
Corrosion	22,149.31		
Electrodeposition	2,161.19		
Electronics	587.97		
Electrothermics & Metallurgy	5,534.48		
Less Iron Ores Advance	1,000.00	4,534.48	
Theoretical		2,191.95	31,624.90
Society Reserve Fund			
Surplus		141,430.66	
Net Income Received		17,459.85	158,890.51
General Fund			
Surplus		76,261.04	
Increase in Asset Values		1,219.01	
		77,480.05	
Less Advances:			
Electro Organic Chemistry	500.00		
Technology of Columbium	456.80		
Vacuum Metallurgy	58.94		
High Temperature Technology	185.37		
Modern Electroplating	163.37	1,364.48	
		76,115.57	
New Capital Equipment		915.98	
Excess Income Over Expenses		11,194.17	88,225.72 412,918.01
			$423,893.18

General Portfolio of Investments

Value of Securities 3/31/61		$152,341.63
Securities Purchased	$ 24,169.66	
Dividend Shares	1,807.97	
Interest Earned	222.71	26,200.34
		$178,541.97
Securities Sold	12,100.63	
Securities Transferred to Fink Fellowship Fund	1,638.43	13,739.06
		$164,802.91
Increase in Value of Securities 3/30/62		4,400.02
FUND VALUE 3/30/62		$169,202.93

Society Reserve Fund

Equity Value in General Portfolio 3/31/61		$127,145.75
Additional Investments:		
*Dividend Shares	1,807.97	
New Purchases	24,169.66	
*Interest Earned	222.71	26,200.34
		$153,346.09

Less:		
Securities Sold	12,100.63	
Securities Transferred to Fink Fellowship Fund	1,638.43	13,739.06
		$139,607.03
Increased Value Securities 3/30/62		4,400.02
Equity Value in General Portfolio 3/30/62		$144,007.05
Bank Credit Balance 3/31/61	11,523.32	
*Cash Dividends	4,310.53	
*Convention Registration Fees	2,646.00	
*Journal Subscriptions	5,956.20	
*Monograph Royalties	2,516.44	15,429.17
	26,952.49	
Securities Sold	12,100.63	
	39,053.12	
Securities Purchased	24,169.66	
Bank Credit Balance 3/30/62		14,883.46
FUND VALUE 3/30/62		$158,890.51

*Total Income from Sources Indicated $17,459.85

General Fund Surplus

Surplus 3/31/61		$ 76,261.04
Increases		
Value Inventory 3/30/62	916.30	
Value Accounts Receivable 3/30/62	1,232.03	
Furniture and Fixture Replacements	332.59	2,480.92
		78,741.96
Decreases		
New Capital Equipment Appropriation	600.00	
Reserve For Depreciation Furniture & Fixtures	661.91	1,261.91
		77,480.05
Less Monograph Advances		1,364.48
		76,115.57
New Capital Equipment		915.98
Excess Income Over Expenses General Fund		11,194.17
VALUE 3/30/62		$ 88,225.72

Division Monograph Funds

Corrosion Division

Equity Value in General Portfolio 3/31/61		$ 20,195.88
Bank Credit Balance 3/31/61	1,770.80	
Monograph Royalties	1,622.47	3,393.27
Corrosion Research Council Contribution	784.50	
Palladium Medal Award Expenses	189.32	
Prize Essay Content	466.02	1,439.84
Bank Credit Balance 3/30/62		1,953.43
FUND VALUE 3/30/62		$ 22,149.31

Electrodeposition Division

Equity Value General Portfolio 3/31/61		$ 1,000.00
Bank Credit Balance 3/31/61	1,600.05	
Symposium Expense	400.00	
Royalty Refund	2.56	
Mailing Expense	36.30	438.86
Bank Credit Balance 3/30/62		1,161.19
FUND VALUE 3/30/62		$ 2,161.19

Electronics Division

Bank Credit Balance 3/31/61	$ 427.29	
Monograph Royalties	160.68	
FUND VALUE 3/30/62		$ 587.97

Electrothermics and Metallurgy Division

Equity Value in General Portfolio 3/31/61		$ 4,000.00
Bank Credit Balance 3/31/61	1,529.82	
Monograph Royalties	134.44	
	1,664.26	
Mailing Expense	129.78	
	1,534.48	
Advance for Iron Ores Monograph	1,000.00	
Bank Credit Balance 3/30/62		534.48
FUND VALUE 3/30/62		$ 4,534.48

Theoretical Electrochemistry Division

Bank Credit Balance 3/31/61	1,858.97	
Monograph Royalties	878.87	$ 2,737.84
Modern Instrumentation Symposium Expense		545.89
FUND VALUE 3/30/62		$ 2,191.95

Special Funds

Edward Goodrich Acheson Fund

Value Securities 3/31/61	38,739.01	
Securities Sold	1,151.02	
	37,587.99	
Securities Purchased	1,834.39	
	39,422.38	
Increased Value 3/30/62	691.87	
Value Securities 3/30/62		$ 40,114.25
Savings Account Balance 3/31/61	913.40	
Dividends from Investments	1,579.49	
Interest Earned	50.72	
Expense Refund	36.50	

Securities Sold	1,151.02	
	3,751.13	
Securities Purchased	1,834.39	
Bank Balance 3/30/62		1,896.74
FUND VALUE 3/30/62		$ 42,010.99

Joseph W. Richards Memorial Fund

Savings Account Balance 3/31/61	829.75	
Interest Earned	31.92	
FUND VALUE 3/30/62		$ 861.67

F. M. Becket Memorial Award Fund

Value Securities 3/31/61			$ 20,926.56
Additional Securities Purchased			26.39
			20,952.95
Increased Value 3/30/62			988.55
			21,941.50
Savings Account Balance 3/31/61		1,264.39	
Interest Earned		42.36	
Cash Dividends		600.98	
		1,907.73	
Award Expenses	445.27		
Securities Purchased	26.39	471.66	
Savings Account Balance			1,436.07
FUND VALUE 3/30/62			$ 23,377.57

Consolidated Fellowship Fund

Value Securities 3/31/61	45,027.36	
Less Value Securities 3/30/62	714.61	
Value Securities 3/30/62		44,312.75
Bank Credit Balance 3/31/61	832.23	
Cash Dividends	2,769.75	
	3,601.98	
Summer Fellowship Awards	2,000.00	
Bank Credit Balance 3/30/62		1,601.98
FUND VALUE 3/30/62		$ 45,914.73

Colin Garfield Fink Fellowship Fund

Value Securities 3/31/61		$ 730.00
Donation of Securities	1,620.37	
Transferred from Society Reserve Fund	1,638.43	
Dividend Shares	102.13	3,360.93
		4,090.93
Less Value Securities 3/30/62		704.64
Value Securities 3/30/62		3,386.29
Bank Credit Balance 3/31/61	273.75	
Cash Donations	1,510.21	
Cash Dividends	35.86	
	1,819.82	
Less Transfer Tax	1.80	
Bank Credit Balance 3/30/62		1,818.02
FUND VALUE 3/30/62		$ 5,204.31

Edward Weston Fellowship Fund

Value Securities 3/31/61		$15,670.46
Increased Value Securities 3/30/62		611.32
Value of Securities 3/30/62		$ 16,281.78
Checking Account Balance 3/31/61	524.77	
Dividends on Investments	534.39	
	1,059.16	
Weston Summer Fellowship Award	533.33	
Checking Account Balance 3/30/62		525.83
FUND VALUE 3/30/62		$ 16,807.61

Certificate of Audit

I have examined the balance sheet and statement of income and expenses of The Electrochemical Society, Incorporated, for the period April 1, 1961 to March 30, 1962. My examination was made in accordance with generally accepted auditing standards and, accordingly, included such tests of the accounting records as were considered necessary.

In my opinion, the balance sheet and statement of income and expenses present fairly the financial position of The Electrochemical Society, Incorporated, at March 30, 1962, in conformity with generally accepted accounting principles applied on a basis consistent with that of the preceding year.

(Signed) N. W. Marinelli, *Auditor*

December 1962 Discussion Section

A Discussion Section, covering papers published in the January-June 1962 JOURNALS, is scheduled for publication in the December 1962 issue. Any discussion which did not reach the Editor in time for inclusion in the June 1962 Discussion Section will be included in the December 1962 issue.

Those who plan to contribute remarks for this Discussion Section should submit their comments or questions in triplicate to the Managing Editor of the JOURNAL, 30 East 42 St., New York 17, N. Y. *not later than September 3, 1962.* All discussion will be forwarded to the author(s) for reply before being printed in the JOURNAL.

Symposium on Stress Corrosion of Metals Rescheduled for March 1963

The Corrosion Division Symposium on Stress Corrosion of Metals originally planned for the 1963 Fall Meeting of The Electrochemical Society, as announced in the April, May, and June JOURNALS, has been rescheduled and will be held in conjunction with the Second International Congress on Metallic Corrosion in New York City, March 11-15, 1963.

Subjects suggested for this symposium are: classical stress corrosion; hydrogen embrittlement as a factor in stress-corrosion cracking; brittle fracture as affected by environmental conditions; and the application of modern concepts of solid-state physics to stress corrosion.

Papers giving data to support or disprove one of the current theories of the mechanism of stress-corrosion cracking would be considered under the classification of classical stress corrosion. Papers merely summarizing data on a particular alloy or group of alloys are not considered to have a place in the symposium.

Inasmuch as results of center or edge notch tests on very high-strength alloys are reported to be highly sensitive to the test environment, the Chairmen feel that papers giving results and particularly suggested mechanisms for these phenomena should be included.

Metal physics is an increasingly important field and papers in which the modern concepts of solid-state physics are applied to the theory would be desirable.

Titles of proposed papers should be submitted as soon as possible to one of the Co-Chairmen: E. H. Phelps, Applied Research Lab., U. S. Steel Corp., Monroeville, Pa., and Hugh L. Logan, National Bureau of Standards, Washington, D. C. Abstracts of about 1000 words and containing up to four figures are due October 31 and the completed papers at the time of the Conference.

Personals

Adolf Goetzberger has been given new duties in the Research and Development Section of Clevite/Shockley Transistor in Palo Alto, Calif. Dr. Goetzberger, who has been a member of the Shockley Senior Research Staff for three years, has been appointed manager of research and development with the responsibility for the scientific and technical work of that department. He joined Shockley in 1958, coming from Munich, West Germany, where he had been a member of the Siemens and Halske semiconductor group.

R. Scott Modjeska has been elevated to the position of research director in physical sciences at Cinch Manufacturing Co. in Chicago, Ill. His research activities include vacuum metallurgy, electrodeposition, extractive metallurgy, corrosion, physical metallurgy, thin films, and semiconductor and rectifier materials. Prior to joining Cinch, he was technical director of Scientific Control Labs., Inc.

John L. Sprague has been elected a senior vice-president of the Sprague Electric Co., North Adams, Mass., and became co-director of the firm's engineering laboratories as of June 1. A director of the company since March of this year, Dr. Sprague most recently has been head of the Transistor Research Dept. of Sprague Electric's research laboratories.

William J. Holian

It is with the deepest regret that the Society announces the death of William J. Holian, Assistant Secretary of The Electrochemical Society from 1948 to 1955. Mr. Holian, who had been ailing for many years, died suddenly at his home in Stamford, Conn., on April 23, 1962.

Mr. Holian, who was experienced in office management, was appointed Assistant Secretary by the Board of Directors in September 1948. He was in charge of the Society's National Office, working closely with the Secretary (Henry B. Linford) on all matters of business. He continued in this capacity until the fall of 1954, when illness necessitated that he curtail some of his duties, and which culminated in his official resignation from the Society in June 1955.

He is survived by his wife, Alma.

Cleveland F. Nixon

Cleveland F. Nixon, head of the electrochemistry department of the General Motors Research Laboratories in Warren, Mich., died at his home of a heart attack on May 4, 1962. He was 60 years old.

Mr. Nixon was born on May 4, 1901 in Philadelphia, Pa. He was graduated in 1923 from the University of Wisconsin with a B. S. degree in chemical engineering.

For six years, he was employed in the laboratory of Western Electric Clock Co., Peru, Ill., and, in 1929, he joined the staff of the General Motors Ternstedt Division as a plating engineer. He was director of process development at Ternstedt at the time of his transfer to the GM Research Labs. in January 1952 to head the electrochemical department, which was engaged in research and development of plating and the electrochemical generation of electrical energy.

Mr. Nixon was active in many technical societies. He had been a member of The Electrochemical Society since 1923, and also held memberships in the American Electroplater's Society, the American Society for Testing Materials, the Society of Automotive Engineers, the American Chemical Society, and the American Society for Metals.

He was the author of many technical papers on plating and plating processes for which he received several awards.

Mr. Nixon is survived by his wife, Charlotte, four sons, a daughter, and a sister.

Book Reviews

Biochemical Mechanisms, by Lloyd L. Ingraham. Published by John Wiley & Sons, Inc., New York, 1962. 108 pages; $5.75.

This book is a valuable attempt to apply the general mechanistic principles of inorganic and organic chemistry to reactions of importance in the field of biochemistry. It is timely and has the virtue of brevity. It includes short but excellent reviews of atomic orbitals, bonding, ligand field theory, transition states, "high energy" bonds, and other topics, in addition to a discussion of the application of these principles to biochemically important reactions. As the author points out, many of the mechanisms are highly speculative. However, this approach to an understanding of enzyme mechanisms should prove to be a stimulus for further experimental studies.

The book is well written, containing excellent diagrams and formula

representation. It is recommended highly both for the biochemist who would relate his reactions to mechanistic theory, as well as to the nonbiochemist who would understand the nature of reactions which take place in the living cell. The appearance of this book emphasizes the most important principle of modern biochemistry—that the reactions which take place in the living cell may be explained in terms of the basic laws of chemistry.

Abraham Mazur
New York Hospital
Cornell Medical School

Interfacial Phenomena, by J. T. Davies and E. K. Rideal. Published by Academic Press, Inc., New York, 1961. 474 pages; $14.00.

This volume should be of value in all branches of physical science dealing with heterogeneous systems. One should not necessarily look at this compendium as pertinent only to colloid systems, *i.e.*, where the particle size range is 50-5000Å or where the interfacial area between phases is very large compared to that if the phase (s) is not in a state of dispersion. Rather, any study involving phase boundaries could be benefited by "Interfacial Phenomena" with its coverage of general topics of the interface in terms of physical and electrical forces, electrokinetics, adsorption, monolayers, physical and electrical transport, and chemical and physical reactions. Thus, the text applies to problems in electrostatics or electroconductivity at boundaries, to mass transfer as in evaporation, dissolution, precipitation, condensation, diffusion across boundaries and along boundaries, and to energy transfer (heat) through boundaries where "stationary" films have so great an influence.

Two chapters, some 160 pages, are devoted to electrical phenomena. They represent a good up-to-date review of this ambiguous subject. The treatment, being both from the static and dynamic viewpoints, goes well into theory with supporting thermodynamics, mathematics, and experimental results. The various electrical potential concepts are discussed, and explanations of interfacial phenomena are given in terms of them. From an electrokinetic viewpoint, the subjects of surface conductance, electro-osmosis, streaming potentials, streaming currents, electrophoresis, and fall (velocity) potentials are well handled.

In the same vein, the text includes up-to-date comprehensive reviews of interfacial tension considerations —surface energy, cohesion and adhesion, spreading, and contact angles, *etc.;* adsorption processes—energy, kinetics, relation to interfacial tension, *etc.;* monolayers—surface pressure, surface viscosity, *etc.;* dispersions; and adhesion. Appreciable space is given to discussions on experimentation in these subjects.

The bibliographies associated with each subject, being comprehensive and including key works, provide avenues for further study. Despite the great number of references, the book shows little evidence of mere listings of investigators' findings. Rather, a spectrum of subject matter, much of which was not available in one treatise before, is now presented on a pretty-well-integrated basis.

Generally speaking, "Interfacial Phenomena" is a good book to have in the library or as part of one's personal collection. Besides its usefulness to chemists, it should be worth while for chemical engineers and biologists. It is equally valuable in industrial and academic laboratories, to the researcher and the instructor.

Max Bender
Fairleigh Dickinson University

Announcements from Publishers

"Superconductive Devices," by John W. Bremer. McGraw-Hill Electronic Sciences Series. Published by McGraw-Hill Book Co., New York, 1962. 179 pages, plus index; $8.00.

"Standard X-Ray Diffraction Powder Patterns," by Howard E. Swanson, Marlene C. Morris, Roger Stinchfield, and Eloise H. Evans. National Bureau of Standards Monograph 25, Section 1, issued March 9, 1962; 56 pages; 40 cents. Order from the Superintendent of Documents, U. S. Government Printing Office, Washington 25, D. C.

New Products

Fluoborates for High-Speed Electroplating. New fluoborates of copper, lead, tin, zinc, iron, nickel, and cadmium have been developed for high-speed electroplating and electroforming. Developed and proven "in the field" to meet exacting customer specifications, these new baths are based on certain excellent properties of fluoboric acid, which had been difficult to use until recently.

A price schedule is contained in the "Guide to Fluoborate Plating" available from Meaker Co., Nutley, N. J.

Bright Barrel Zinc Plating Process. Hanson-Van Winkle-Munning Co. has announced the availability of ZINCALUME "B," an inexpensive, high-quality barrel zinc electroplating process that meets today's demands for bright zinc deposits at low cost. It is an easy-to-dissolve powder and is compatible with most other proprietary barrel zinc

Brief Communications

The JOURNAL accepts short technical reports having unusual importance or timely interest, where speed of publication is a consideration. The communication may summarize results of important research justifying announcement before such time as a more detailed manuscript can be published. Consideration also will be given to reports of significant unfinished research which the author cannot pursue further, but the results of which are of potential use to others. Comments on papers already published in the JOURNAL should be reserved for the Discussion Section published biannually.

Submit communications in triplicate, typewritten double-spaced, to the Editor, Journal of The Electrochemical Society, 30 East 42 St., New York 17, N. Y.

addition agents. Bright deposits are produced directly from the bath.

For additional information and samples of parts plated with ZINC-ALUME "B," write to Hanson-Van Winkle-Munning Co., Matawan, N. J.

Carbon Electrodes for Fuel Cells. Development of a new series of carbon electrodes for fuel cells has been announced by Pure Carbon Co., Inc. The new series, covering 20 different grades and offering a wide range of physical properties, including median pore diameters from 0.3 to 18μ, and surface areas from 0.1 to 600-plus sq m/g, is a result of Pure Carbon's continuing research to aid fuel cell manufacturers.

For complete information, contact Pure Carbon Co., Inc., 411 Hall Ave., St. Marys, Pa.

Literature from Industry

MACro Polish-3P, a new chemical polishing process that produces a smooth, semibright finish on Zamak No. 3 zinc diecast alloys, is described in Product Data Sheet No. 69, available from MacDermid Inc., Waterbury, Conn.

The product produces a uniform finish that is an excellent base for electroplating or other applications where a smooth surface is required. Buffing often can be eliminated before copper, nickel, and chromium plating.

Metex Acid Salt M-629, a new method of stripping decorative chrome from nickel that enables the operator to maintain an active nickel surface and rechrome after rinsing without additional treatment, is described in Product Data Sheet No. 43B-1, available from MacDermid Inc., Waterbury, Conn.

The product is a safe, easy-to-handle dry powder that strips chrome by immersion only.

Advertiser's Index

The Electrochemical Society

Patron Members

Aluminum Co. of Canada, Ltd.,
Montreal, Que., Canada
International Nickel Co., Inc.,
New York, N. Y.
Olin Mathieson Chemical Corp.,
Chemicals Div., Industrial Chemicals
Development Dept., Niagara Falls, N. Y.
Union Carbide Corp.
Divisions:
National Carbon Co., New York, N. Y.
Union Carbide Consumer Products Co.,
New York, N. Y
Union Carbide Metals Co.,
New York, N. Y.
Westinghouse Electric Corp., Pittsburgh, Pa.

Sustaining Members

Air Reduction Co., Inc., New York, N. Y.
Ajax Electro Metallurgical Corp.,
Philadelphia, Pa.
Allen-Bradley Co., Milwaukee, Wis.
Allied Chemical Corp.
Solvay Process Div., Syracuse, N. Y.
General Chemical Div., Morristown, N. J.
Alloy Steel Products Co., Inc., Linden, N. J.
Aluminum Co. of America,
New Kensington, Pa.
American Metal Climax, Inc.,
New York, N. Y.
American Potash & Chemical Corp.,
Los Angeles, Calif. (2 memberships)
American Smelting and Refining Co.,
South Plainfield, N. J.
American Zinc Co. of Illinois,
East St. Louis, Ill.
American Zinc, Lead & Smelting Co.,
St. Louis, Mo. (2 memberships)
American Zinc Oxide Co., Columbus, Ohio
M. Ames Chemical Works, Inc.,
Glens Falls, N. Y.
Armco Steel Corp., Middletown, Ohio
Basic Inc., Maple Grove, Ohio
Bell Telephone Laboratories, Inc.,
New York, N. Y. (2 memberships)
Bethlehem Steel Co., Bethlehem, Pa.
(2 memberships)
Boeing Airplane Co., Seattle, Wash.
Burgess Battery Co., Freeport, Ill.
(4 memberships)
Canadian Industries Ltd., Montreal,
Que., Canada
Carborundum Co., Niagara Falls, N. Y.
Catalyst Research Corp., Baltimore, Md.
Consolidated Mining & Smelting Co. of
Canada, Ltd., Trail, B. C., Canada
(2 memberships)
Continental Can Co., Inc., Chicago, Ill.
Cooper Metallurgical Associates, Cleveland,
Ohio
Corning Glass Works, Corning, N. Y.
Diamond Alkali Co., Painesville, Ohio
Dow Chemical Co., Midland, Mich.
Wilbur B. Driver Co., Newark, N. J.
(2 memberships)
E. I. du Pont de Nemours & Co., Inc.,
Wilmington, Del.
Eagle-Picher Co., Chemical and Metals Div.,
Joplin, Mo.
Eastman Kodak Co., Rochester, N. Y.
Thomas A. Edison Research Laboratory, Div.
of McGraw-Edison Co., West Orange, N. J.
Electric Auto-Lite Co., Toledo, Ohio
C & D Div., Conshohocken, Pa.
Electric Storage Battery Co., Yardley, Pa.
Engelhard Industries, Inc., Newark, N. J.
(2 memberships)
The Eppley Laboratory, Inc., Newport, R. I.
(2 memberships)
Exmet Corp., Tuckahoe, N. Y.
Fairchild Semiconductor Corp., Palo Alto,
Calif.
Food Machinery & Chemical Corp.
Becco Chemical Div., Buffalo, N. Y.
Westvaco Chlor-Alkali Div., South
Charleston, W. Va.
Foote Mineral Co., Exton, Pa.
Ford Motor Co., Dearborn, Mich.
General Electric Co., Schenectady, N. Y.
Chemistry & Chemical Engineering
Component, General Engineering
Laboratory
Chemistry Research Dept.
General Physics Research Dept.
Metallurgy & Ceramics Research Dept.
Aircraft Accessory Turbine Dept.,
West Lynn, Mass.
General Instrument Corp., Newark, N. J.
General Motors Corp.
Allison Div., Indianapolis, Ind.
Delco-Remy Div., Anderson, Ind.
Guide Lamp Div., Anderson, Ind.
Research Laboratories Div., Warren, Mich.
General Telephone & Electronics
Laboratories Inc., Bayside, N. Y.
(2 memberships)
Gillette Safety Razor Co., Boston, Mass.
Globe-Union, Inc., Milwaukee, Wis.
B. F. Goodrich Chemical Co.,
Cleveland, Ohio

(Sustaining Members cont'd)

Gould-National Batteries, Inc., Minneapolis, Minn.
Great Lakes Carbon Corp., New York, N. Y.
Hanson-Van Winkle-Munning Co., Matawan, N. J. (2 memberships)
Harshaw Chemical Co., Cleveland, Ohio (2 memberships)
Hercules Powder Co., Wilmington, Del.
Hill Cross Co., Inc., West New York, N. J.
Hoffman Electronics Corp., Semiconductor Div., El Monte, Calif. (2 memberships)
Hooker Chemical Corp., Niagara Falls, N. Y. (3 memberships)
HP Associates, Palo Alto, Calif.
Hughes Research Laboratories, Div. of Hughes Aircraft Co., Malibu, Calif.
International Business Machines Corp., New York, N. Y.
International Minerals & Chemical Corp., Skokie, Ill.
ITT Federal Laboratories, Div. of International Telephone & Telegraph Corp., Nutley, N. J.
Jones & Laughlin Steel Corp., Pittsburgh, Pa.
K. W. Battery Co., Skokie, Ill.
Kaiser Aluminum & Chemical Corp.
Div. of Chemical Research, Permanente, Calif.
Div. of Metallurgical Research, Spokane, Wash.
Kawecki Chemical Co., Boyertown, Pa.
Kennecott Copper Corp., New York, N. Y.
Leesona Moos Laboratories, Div. of Leesona Corp., Jamaica, N. Y.
Libbey-Owens-Ford Glass Co., Toledo, Ohio
Lockheed Aircraft Corp., Missiles & Space Div., Sunnyvale, Calif.
Mallinckrodt Chemical Works, St. Louis, Mo.
P. R. Mallory & Co., Indianapolis, Ind.
Merck & Co., Inc., Rahway, N. J.
Metal & Thermit Corp., Detroit, Mich.
Miles Chemical Co., Div. of Miles Laboratories, Inc., Elkhart, Ind.
Minneapolis-Honeywell Regulator Co., Minneapolis, Minn.
Minnesota Mining & Manufacturing Co., St. Paul, Minn.
Monsanto Chemical Co., St. Louis, Mo.
Motorola, Inc., Chicago, Ill.
National Cash Register Co., Dayton, Ohio
National Lead Co., New York, N. Y.
National Research Corp., Cambridge, Mass.
National Steel Corp., Weirton, W. Va.
North American Aviation, Inc., Rocketdyne Div., Canoga Park, Calif.
Northern Electric Co., Montreal, Que., Canada
Norton Co., Worcester, Mass.
Ovitron Corp., Long Island City, N. Y.
Owens-Illinois Glass Co., Toledo, Ohio
Peerless Roll Leaf Co., Inc., Union City, N. J.
Pennsalt Chemicals Corp., Philadelphia, Pa.
Phelps Dodge Refining Corp., Maspeth, N. Y.
Philco Corp., Research Div., Blue Bell, Pa.
Philips Laboratories, Inc., Irvington-on-Hudson, N. Y.
Pittsburgh Plate Glass Co., Chemical Div., Pittsburgh, Pa.
Potash Co. of America, Carlsbad, N. Mex.
The Pure Oil Co., Research Center, Crystal Lake, Ill.
Radio Corp. of America
Tube Div., Harrison, N. J.
RCA Victor Record Div., Indianapolis, Ind.
Ray-O-Vac Co., Madison, Wis.
Raytheon Co., Waltham, Mass.
Remington Rand, Div. of Sperry Rand Corp., New York, N. Y.
Reynolds Metals Co., Richmond, Va.
Rheem Semiconductor Corp., Mountain View, Calif.
Schering Corp., Bloomfield, N. J.
Shawinigan Chemicals Ltd., Montreal, Que., Canada
Socony Mobil Oil Co., Inc., Dallas, Texas
Speer Carbon Co.
International Graphite & Electrode Div., St. Marys, Pa.
Sprague Electric Co., North Adams, Mass.
Stackpole Carbon Co., St. Marys, Pa.
Stauffer Chemical Co., New York, N. Y.
Tennessee Products & Chemical Corp., Nashville, Tenn.
Texas Instruments, Inc., Dallas, Texas
Metals and Controls Corp., Attleboro, Mass.
Three Point One Four Corp., Yonkers, N. Y.
Titanium Metals Corp. of America, Henderson, Nev.
Tung-Sol Electric Inc., Newark, N. J.
Udylite Corp., Detroit, Mich. (4 memberships)
United States Borax & Chemical Corp., Los Angeles, Calif.
Universal-Cyclops Steel Corp., Bridgeville, Pa.
Upjohn Co., Kalamazoo, Mich.
U. S. Steel Corp., Pittsburgh, Pa.
Victor Chemical Works, Chicago, Ill.
Western Electric Co., Inc., Chicago, Ill.
Wyandotte Chemicals Corp., Wyandotte, Mich.
Yardney Electric Corp., New York, N. Y.